Distribution, transport and fate of major herbicides and their metabolites. November 1993

Chesters, Gordon et al.
Madison, Wisconsin: Water Resources Center, University of Wisconsin-Madison, November 1993

Final Report to

THE WISCONSIN DEPARTMENT OF AGRICULTURE, TRADE AND CONSUMER PROTECTION

Contract 91-01/AGA9779/AGB6933

and

THE WATER RESOURCES CENTER

Contract 101-4 A-34-9454

DISTRIBUTION, TRANSPORT AND FATE OF MAJOR HERBICIDES AND THEIR METABOLITES

by

Gordon Chesters
Jonathan Levy
Harry W. Read
Daniel P. Gustafson

Water Resources Center, University of Wisconsin-Madison, 1975 Willow Drive, Madison, WI 53706

November 1993

Mention of trade names or commercial products does not constitute their endorsement by the Water Resources Center or by the State of Wisconsin.

The final report is a compendium of five articles. Articles I, II and V were submitted to the *Journal of Contaminant Hydrology*, III and IV to *Water Resources Research*.

TABLE OF CONTENTS

LIST OF TABLES

LIST OF FIGURES

Page v
image missing/
not available

I. Distribution, Sources and Fate of Atrazine in a Sandy-till Aquifer

ABSTRACT

A field study was initiated around an atrazine-contaminated private dairy-farm well to investigate sources and extent of contamination from atrazine and its metabolites in the shallow glacial till aquifer and to relate the distribution of the contaminants to the ground-water flow system. Area landuse is dairy farming with typical rotations of corn and alfalfa; soils are predominantly silt loams. The shallow groundwater system is dominated by downward vertical hydraulic gradients and water from the till aquifer discharges to the bedrock aquifer. Where downward gradients exist it is possible to predict travel time (TT) and mean horizontal distance travelled (MHD) to various monitoring wells. The MHDs to many wells are small, and atrazine residue concentrations result from pesticide application and handling nearby. According to the Darcy TT estimates, once water reaches the water table, it takes decades to reach some of the deeper wells. Tritium-interpreted ages suggest that at least part of the water at contaminated wells is > 7 yr old even in wells screened near the water table. Such long travel times indicate that responses of groundwater quality to atrazine-use restrictions will be slow.

The distribution of contamination signaled both point and nonpoint-source contamination. For atrazine and three atrazine metabolites, there were widespread detections mostly < 0.5 $\mu g\ L^{-1}$ (ppb), with highest concentrations occurring near areas of pesticide handling. If results at this site are representative of other areas in Wisconsin, the 1992 inclusion of the chlorinated metabolites in Wisconsin's groundwater standards for atrazine will lead to many more violations of those standards and increased regulatory action. Concentrations of atrazine and desethylated atrazine in water from monitoring wells decreased with increased TTs to those wells. There was no increase with TT of desethylated atrazine concentrations relative to the parent compound, indicating that while both compounds are undergoing dissipation, degradation of atrazine to desethylated atrazine is not a major dissipation pathway in groundwater. There is some evidence of increased desisopropylated atrazine and diamino-chloro-*s*-triazine concentrations relative to atrazine and desethylated atrazine concentrations with increased TT suggesting that some microbial degradation may be occurring in groundwater. Other dissipation pathways include hydrolysis to hydroxyatrazine (which is more strongly sorbed than the chlorinated metabolites), irreversible sorption, mechanical dispersion, and chemical diffusion.

INTRODUCTION

Large-scale groundwater quality surveys by the Wisconsin Department of Agriculture, Trade and Consumer Protection (WDATCP) have found widespread contamination of private drinking water wells by atrazine residues (LeMasters and Doyle, 1989). In Wisconsin, U.S.A. little site-specific atrazine research has been performed outside such areas with coarse-textured soils as the lower Wisconsin River valley and the sand plains of central Wisconsin. This 2.5-yr study was initiated in June 1989 to investigate and characterize the distribution of atrazine parent compound and its metabolites (together

referred to as atrazine residues) in the shallow groundwater overlying a bedrock aquifer. Three atrazine metabolites were given regulatory significance in 1992 when they were included in Wisconsin's groundwater standards for atrazine. When the sum of the concentrations of the four compounds (compounds 1, 2, 3 and 4 in Fig. 1 and Table 1) exceeds the enforcement standard (ES) of 3.0 ppb or the preventive action limit (PAL) of 0.3 ppb various regulatory actions are triggered. If data from this study site are typical, the inclusion of metabolites in the groundwater standards has serious implications for regulating atrazine use.

A site was selected in the vicinity of a private well which, at that time, had the highest measured groundwater concentration of atrazine in Dane County, Wisconsin, U.S.A. By observing spatial and temporal patterns of atrazine residue concentrations in the shallow aquifer, an attempt was made to determine whether the contamination is mainly due to point or nonpoint sources. This study also attempts to relate the distribution of atrazine residues to the site hydrogeology and address the implications those relationships have for determining the fate of atrazine residues in groundwater and for regulating atrazine use.

Atrazine [2-chloro-4-ethylamino-6-isopropylamino-*s*-triazine] was introduced in 1953 and has been the most widely used herbicide in Wisconsin and the United States (Wehtje et al., 1984). In Wisconsin it is used primarily to control annual broadleaf and grassy weeds in corn and sweet corn. In 1985, it was applied to 77% of all Wisconsin corn fields, but by 1990 its use had declined to 56% (Wisconsin Agricultural Statistics Service, 1991). In the environment, atrazine is transformed by chemical and biological means; degradation products and pathways are shown in Fig. 1 and Table 1.

Chemical degradation of atrazine occurs by hydrolysis to hydroxyatrazine (Table 1, compound 5) in which the chloro substituent is nucleophilically replaced by a hydroxyl group. Based on the small differences between atrazine degradation rates in sterile and nonsterile soils, chemical degradation of atrazine appears to be the dominant, but not sole transformation mechanism (Chesters et al., 1988; Junk

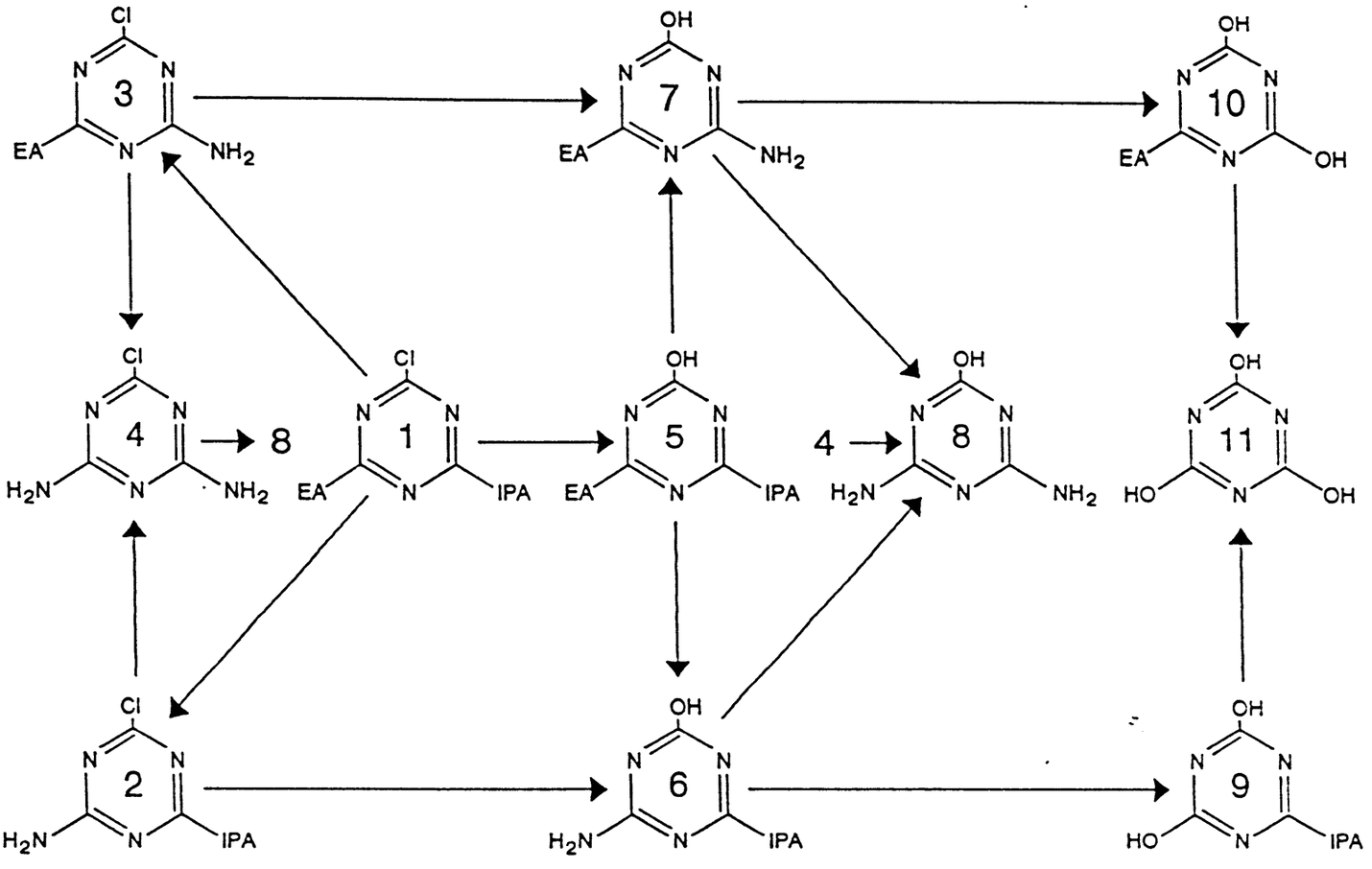

EA = ethylamino: $C_2 H_5 NH$

IPA = isopropylamino: $(CH_3)_2 CHNH$

Fig. 1. Degradation pathways of atrazine (1) and its metabolites (2 - 11).

TABLE 1

Atrazine and metabolites found in soils

*Compound code**	*Chemical name*	*Common name*
1	2-Chloro-4-ethylamino-6-isopropylamino-*s*-triazine	Atrazine
2	2-Chloro-4-amino-6-isopropylamino-*s*-triazine	Desethylated atrazine
3	2-Chloro-4-ethylamino-6-amino-*s*-triazine	Desisopropylated atrazine
4	2-Chloro-4,-6-diamino-*s*-triazine	Diamino-chloro-*s*-triazine
5	2-Hydroxy-4-ethylamino-6-isopropylamino-*s*-triazine	Hydroxyatrazine
6	2-Hydroxy-4-amino-6-isopropylamino-*s*-triazine	Desethylated hydroxyatrazine
7	2-Hydroxy-4-ethylamino-6-amino-*s*-triazine	Desisopropylated hydroxyatrazine
8	2-Hydroxy-4,6-diamino-*s*-triazine	Diamino-hydroxy-*s*-triazine
9	2,4-Dihydroxy-6-isopropylamino-*s*-triazine	
10	2,6-Dihydroxy-4-ethylamino-*s*-triazine	
11	2,4,6-Trihydroxy-*s*-triazine	Cyanuric Acid

* Refers to compounds in Fig. 1.

et al., 1984; Saltzman and Mingelgrin, 1984; Armstrong et al., 1967; Harris, 1967). Hydroxyatrazine was not included in the proposed new standard because the Wisconsin Department of Health and Social Services determined that it presents a lesser human health risk than the chlorinated metabolites (Anderson et al., 1990).

In the presence of microorganisms, atrazine is transformed by desalkylation at one or both alkylamino groups. Removal of the ethyl group, the isopropyl group or both results in the formation of

desethylated atrazine (DEAT), desisopropylated atrazine (DIAT) or diamino-chloro-*s*-triazine (DIAM) (Fig. 1, Table 1, compounds 2, 3 and 4). Atrazine and the three chlorinated metabolites are thought to pose a similar risk to human health (Anderson et al., 1990) and it is these compounds that have been included in Wisconsin's groundwater standards for atrazine. The chlorinated metabolites can also undergo hydrolysis to form less phytotoxic compounds (Fig. 1, Table 1, compounds 6, 7 and 8).

Atrazine has been detected in groundwater in 13 states, usually at concentrations below 2 ppb (Isensee et al., 1990) and contamination is thought to originate most often from normal field use. Contamination is prominent in areas with shallow depths to groundwater and coarse-textured soils, planted in continuous corn and undergoing heavy irrigation. Evidence is accumulating, however, that atrazine leaching also occurs in finer-textured soils (Hall and Hartwig, 1978; Pionke and Glotfelty, 1989; LeMasters and Doyle, 1989), partially by transport through macropores (Isensee et al., 1990, 1988; Starr and Glotfelty, 1990).

Atrazine in groundwater might result from its long use history and slow movement to groundwater with little degradation occurring once the residues have been leached beyond the biologically active root zone. In Wisconsin, atrazine has been detected in groundwater beneath fields that probably serve as the source area even though atrazine has not been applied for at least 2 yr (McGrath, 1991). It was detected in soil from fields in Maryland where it had not been applied in 2 or 3 yr (Isensee et al., 1990).

While there have been numerous studies on leaching of atrazine, studies examining the behavior of atrazine metabolites are more limited. Their relative mobilities have been investigated by comparing leaching patterns and relative sorption coefficients (Bowman, 1990; Brouwer et al., 1990; Schiavon, 1988a, 1988b; Best and Weber, 1974; Armstrong and Chesters, 1968; and Green et al., 1968). The order of mobility expected from the sorption and leaching experiments is DEAT > DIAM > DIAT ≥ atrazine > hydroxyatrazine. Because of its high sorbability, hydroxyatrazine is unlikely to be detected

in groundwater, and should appear in highest concentrations in the surface soils.

The area selected for study is 4.1 km^2 encompassing parts of three dairy farms near the Village of Waunakee in south-central Wisconsin (Fig. 2) and has features typical of glaciated Dane County. Soils are medium-textured, predominantly Plano, Ringwood, St. Charles and Dodge silt loams. They are generally deep, well to moderately well drained, nearly level to sloping on glaciated uplands, have high fertility and available water capacity and moderate permeability (Glocker and Patzer, 1978). Organic matter contents range from 2.0 to 5.8% in the first 30 cm, typically decreasing to < 1.0% by 120 cm.

FIELD METHODS

Fifty-five groundwater sampling points were installed at 25 locations (Fig. 3). Nested piezometers and multilevel samplers were used to measure water quality with depth. Multilevel samplers (K1 to K4) were drilled using air-rotary techniques and 15- to 20-cm diameter augers. During drilling, material was sampled at intervals for stratigraphic description using a 7.6-cm O.D. steam-cleaned split spoon equipped with polycarbonate liners in 15-cm segments. Each bore sample was used to determine grain-size, pH and organic matter content. The multilevel sampling assemblies were installed approximately 9.1 m into ground water. The assemblies consist of a 3.2-cm I.D. flush-threaded PVC pipe with a 0.30-m-long screen surrounded by seven polypropylene sampling tubes (0.95-cm I.D.). The tubes terminate below the water table at intervals of 0.91 or 1.5 m. At the end of each tube is a 7.6-cm-long screen of Style 3401 Typar® spunbonded polypropylene. The assembly was sand-packed to about 0.61 m above the water table and sealed with bentonite. Due to the small volumes of the polypropylene tubes and low recharge rates at K1 and K2, sampling for atrazine analysis at these wells was impractical, but the PVC wells were used for measuring potentiometric levels and sampling. K3 and K4 were fully functional multilevel sampling wells.

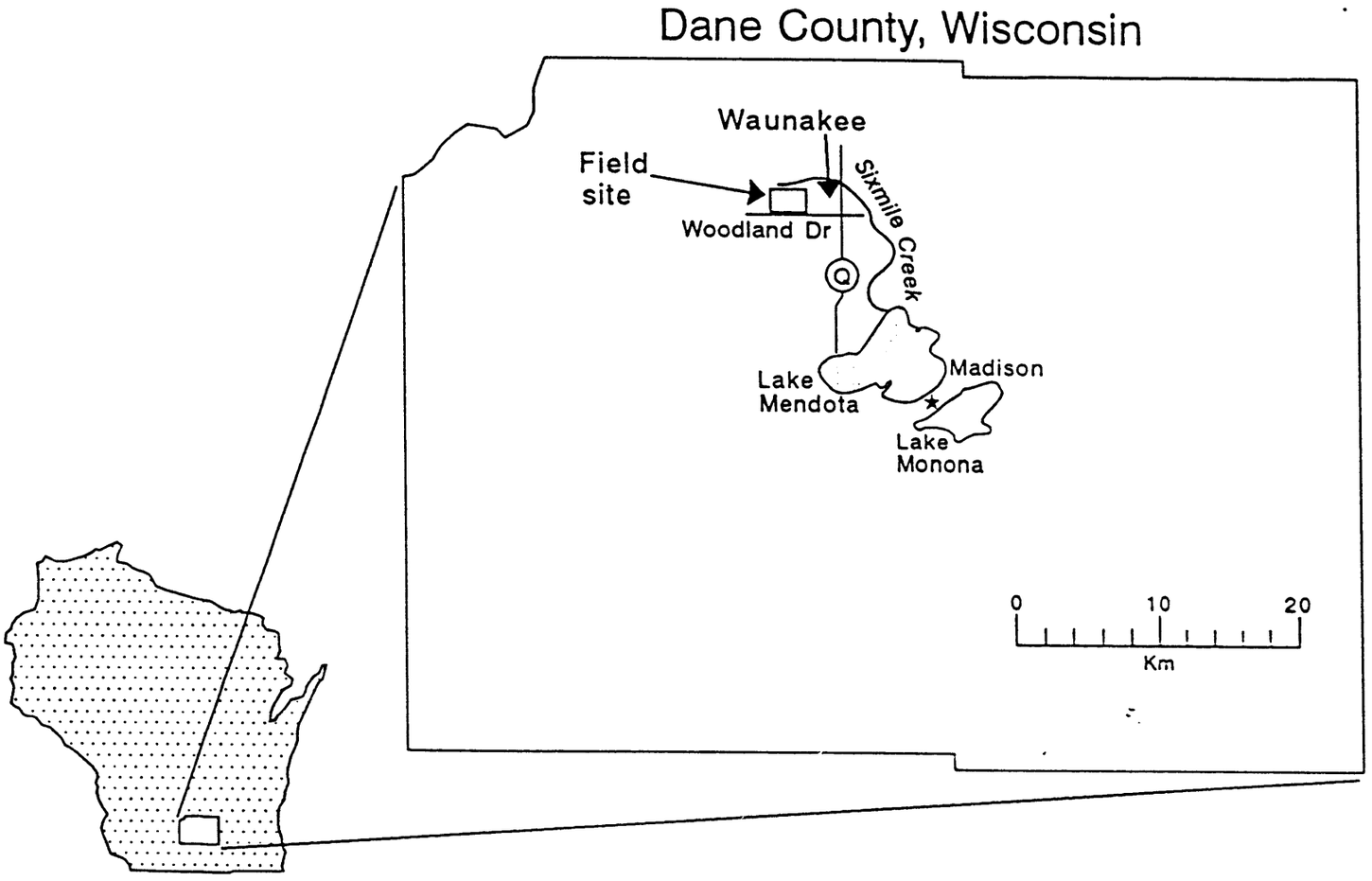

Fig. 2. Field site location.

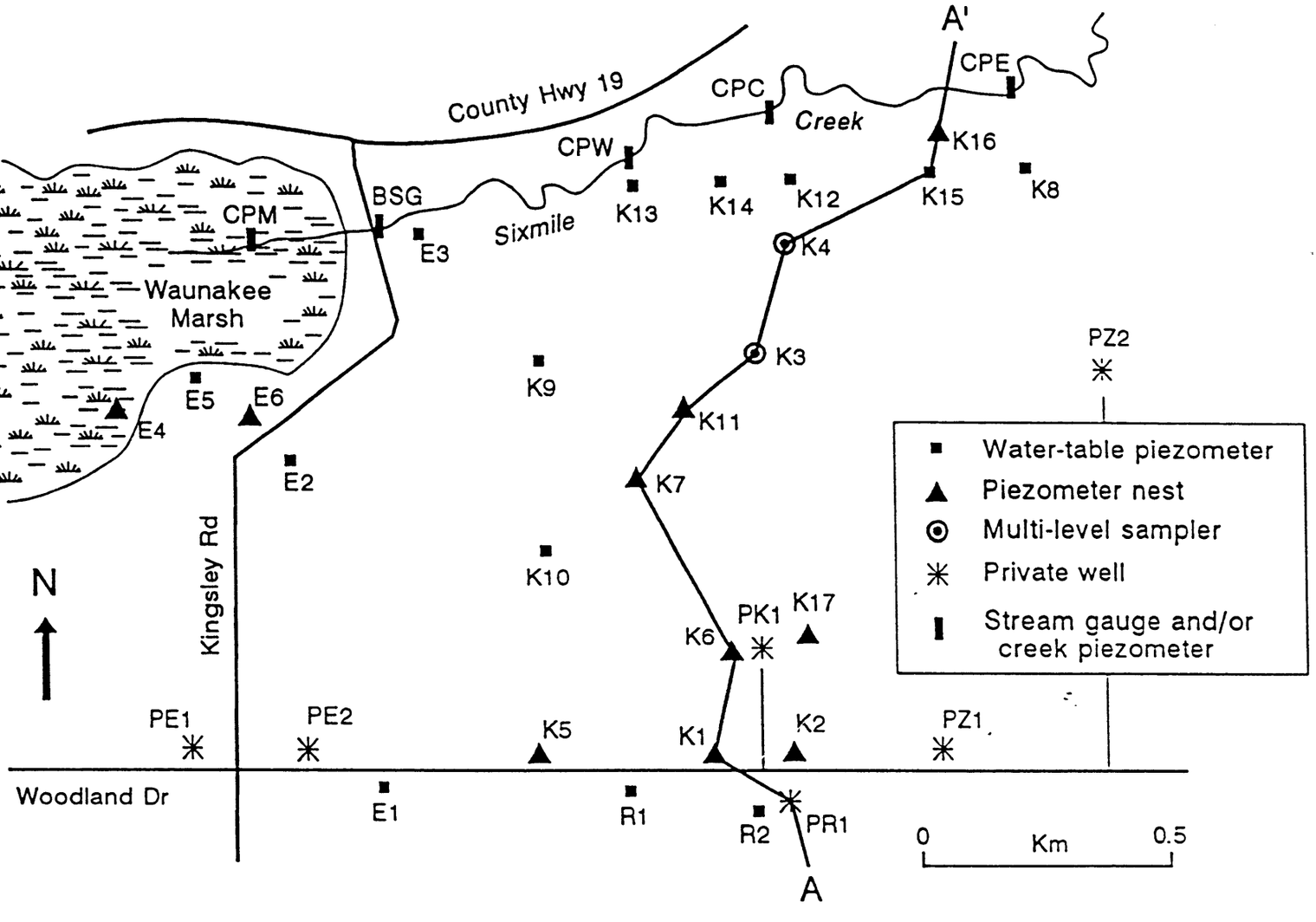

Fig. 3. Monitoring area with well locations. The transect A-A' corresponds to the geologic cross section shown in Figs. 5 and 7.

Twenty-two water-table wells were installed, nine of which were nested with either one, two or three other piezometers screened deeper in the ground-water system. Most boreholes were drilled with 11-cm, solid-stem augers. Screens were sand-packed unless the natural material collapsed above the top of the screen. Holes were sealed with bentonite to within 0.6 m of the ground surface. Most wells are 5.1-cm I.D. flush-threaded PVC with 1.5-m-long screens intersecting the water table. Where depth to ground water is < 2.1 m, holes were hand-augured and 1.3-cm I.D. water-table wells with 1.5-m-long screens were installed. During well installation, drilling samples were peeled from the augers at 1.5-m intervals, characterized and analyzed for grain-size, organic matter content, and pH. Geology was also investigated by interpretation of private well logs and previously existing geologic maps. In two locations, depth to bedrock was determined by shallow seismic refraction techniques.

Nested pairs of polypropylene piezometers (0.95-cm I.D.) with 10-cm screens (style 3401 Typar® spunbonded polypropylene) were installed at four locations in Sixmile Creek and Waunakee Marsh -- CPM, CPW, CPC, and CPE (Fig. 3) -- to determine whether ground water is moving to or from the creek. Piezometers were installed by pounding steel pipe with a loose fitting plug on the bottom into the creek bed. The polypropylene tubing was inserted through the pipe and the pipe was recovered, leaving the tubing in place. Creek bottom sediment collapsed around the tubing and anchored the piezometer.

Well elevations were surveyed relative to a common datum. Water-table elevations, potentiometric heads and hydraulic gradients were measured at least monthly at most wells and weekly at many wells throughout most of the study period. Approximately 217 private well drilling logs indicating depth to water at the time of well installation were used in conjunction with U.S. Geological Survey topographic maps to determine regional potentiometric surface elevation. In addition, in September 1991, depth to water was measured in 11 private wells within a 23 km^2 area surrounding the field site. Well elevations were determined either by surveying or with a barometric altimeter. The 11 potentiometric surface elevations provided greater detail surrounding the study site and confirmed the

validity of the larger map prepared using well logs.

Wells and multilevel ports were sampled monthly or bimonthly (in winter) from October 1989 to June 1992. Water was also sampled at least twice from five private wells and analyzed for atrazine residues. A peristaltic pump and dedicated tubing were used for sampling multilevel ports at K3 and K4 and at the 1.3-cm I.D. wells. Sampling of the 5.1- and 3.2-cm I.D. wells was conducted with stainless steel bailers. The multilevel-port dedicated tubing was flushed with *in situ* water before sampling. All other sampling equipment was rinsed with distilled water between each use. Most wells recharge slowly enough to be bailed dry and sampled later. Some wells had to be sampled the following day to allow enough time for recharge. Four well volumes were purged before sampling from wells that could not be bailed dry to ensure the sample was characteristic of the aquifer. A submersible teflon bladder pump was used to remove 4 well volumes from two deeper wells that recharged quickly. Samples were collected in 1 L amber glass bottles and kept cold for transport to the laboratory where they remained refrigerated until extraction, usually within 7 days of sampling. Occasionally, rinse blanks were collected by passing distilled water through sampling equipment after routine sampling and cleaning. At least one blank was collected for each type of sampling equipment used after the equipment was exposed to the wells known to be the most contaminated. Analysis of blanks indicated that no detectable cross contamination from sampling occurred.

ANALYTICAL METHODS FOR ATRAZINE RESIDUE DETERMINATION

Atrazine residues in groundwater samples were determined by extraction followed by chromatographic analysis. Methods through February 1992 allowed acceptable quantification of only atrazine and DEAT (Table 1, compounds 1 and 2). New methods used from April through June 1992 allowed quantification of DIAT and DIAM (Table 1, compounds 3 and 4).

From October 1989 through December 1990, organic compounds were extracted by passing 500

mL portions of the groundwater samples through solid-phase extraction (SPE) tubes packed with 0.5 g of n-octadecylated (C_{18}) silica particles (Method 1). Hydrophobic contaminants partition from water to the bonded organic phase. Atrazine and some of its metabolites are retained by the columns and are eluded by passing methanol through the SPE cartridge, achieving extraction, concentration and cleanup in one step. The methanol extract is usually suitable for direct analysis by gas chromatography (GC) and high performance liquid chromatography (HPLC). HPLC was used as the primary analytical method; GC served as confirmatory analysis.

The HPLC separation method employed a 15-cm long column packed with silica bonded to both n-octyl (C_8) and cation exchange functional groups, a mobile phase of methanol and water buffered with phosphate (50 mM, pH 6.7) and an ultraviolet detector. The column packing facilitates separation based on both the hydrophobic and weak base characteristics of triazines. GC analysis was accomplished on a 10-m capillary column with an electron capture detector. GC analysis was not performed for every sampling round.

In 1991, sample fortification and recovery experiments indicated that extraction efficiency for DEAT is improved (from about 50 to >90%) by addition of 50 g L^{-1} NaCl to the samples prior to extraction and by using SPE cartridges containing 1 g instead of 0.5 g of packing material (Method 2).

By using a longer (25 cm) column and a gradient elution procedure, a better HPLC separation was achieved, allowing quantification of DIAT and DIAM. Also, a new extraction method developed by Ciba-Geigy Corp. (Ciba-Geigy, 1992) was adopted (Method 3). In Method 3, 500 mL portions of groundwater were buffered at pH 8 with phosphate, extracted twice with ethyl acetate and twice with dichloromethane. The extracts were evaporated to dryness and the residues resuspended in 1 mL of methanol rather than 0.5 mL of acetone, as prescribed in the Ciba-Geigy method. This extract was then analyzed by HPLC, as described earlier. The only other modifications of the Ciba-Geigy protocol were that the final volume was 1 mL not 0.5 mL, and the final solvent was methanol, not acetone. The

procedure improved extraction efficiency of DIAT (to about 85%) and DIAM (to about 60%).

Concentration trends and averages over the entire study period are of interest. The three extraction methods were therefore compared so that all concentrations could be standardized to equivalent concentrations as if one extraction method was used. Duplicate sets of samples were analyzed using Methods 1 and 2 and Methods 2 and 3. Regression analyses were performed on the data so that Method 1 and 3 concentrations could be expressed in equivalent Method 2 concentrations. Details of the regression analyses are provided in Levy (1993).

ASSESSING RELIABILITY OF ANALYTICAL METHODS

The uncertainty involved in the reporting of an atrazine or DEAT concentration was investigated in detail for analytical Method 2 using analysis of variance (ANOVA). The ANOVA was based on sampling of only two wells since such a detailed analysis was too costly to perform at all the wells. It was assumed that the variances and the breakdown of variances for these wells would be representative of all wells. The ANOVA was designed to quantify the variances associated with sampling (σ_S^2), extraction (σ_E^2) and HPLC analysis (σ_H^2). Seven successive 2-L samples were taken from the wells and split into two 1-L subsamples. Each subsample underwent extraction and was twice analyzed by HPLC. The variance of the mean concentration when sampling is carried out at this detail is:

$$\frac{\sigma_S^2}{7} + \frac{\sigma_E^2}{14} + \frac{\sigma_H^2}{28} \qquad (1)$$

allowing estimation of the component variances. Under normal conditions, only one 1-L sample is taken from each well, only one extraction is performed and two HPLC analyses are run. Extrapolating the component variances to the normal sampling case, the variance for an estimation of the mean concentration is:

$$\sigma_S^2 + \sigma_E^2 + \frac{\sigma_H^2}{2} \qquad (2)$$

Some concentrations reported are averages over time from a single well. The variance of a mean concentration from n independent samples taken at a well over time (assumes no autocorrelation) is:

$$\frac{\sigma_S^2}{n} + \frac{\sigma_E^2}{n} + \frac{\sigma_H^2}{2n} \qquad (3)$$

The ANOVA results and the confidence intervals for a regular well sampling are presented in Table 2. The 95% confidence interval for concentration estimated from a typical (single) sampling is calculated using the sample mean ($\bar{X}$) concentration, the variance of the mean from Table 2, and 12 degrees of freedom (Snedecor and Cochran, 1980). The confidence intervals based on the combined-well ANOVAs are the best intervals to quantify the uncertainty of a measured concentration at any well. Those intervals should be kept in mind while interpreting the atrazine residue data. The ANOVAs indicate that the sampling and analytical methodology is reasonably sensitive and reproducible.

TABLE 2

ANOVA results for atrazine residue analyses of water from wells K6.B and K3.1

Compound	*Estimated* σ_S^2 *(ppb²)*	*Estimated* σ_E^2 *(ppb²)*	*Estimated* σ_H^2 *(ppb²)*	*Estimated Variance of the Mean* (ppb²)*	*95% Confidence Interval (ppb)*
Atrazine	0.00259	0.00259	0.00131	0.00584	$\bar{X} \pm 0.167$
DEAT	0	0	0.0230	0.0115	$\bar{X} \pm 0.234$

* This variance is for a typical sampling consisting of 1 sample, 1 extraction and duplicate HPLC runs.

SITE HYDROGEOLOGY

The shallow aquifer is in sandy glacial till, part of the Horicon Formation of undifferentiated Quaternary deposits laid down by the Green Bay Lobe of the Laurentide ice sheet during late Wisconsin time (13,000 to 19,000 yr ago) (Mickelson et al., 1984). The deposits are yellow-brown calcareous gravelly sandy loam or loamy sand. Pebbles and cobbles were found up to 20 cm in diameter. No bedding planes were observed in split-spoon cores. Typical till grain-size distribution is 65 to 75% sand, 15 to 30% silt, and 1 to 15% clay. Lenses of sandier material (as high as 97% at 2.5 m below ground surface) were observed. The sand lenses are glacial outwash deposits and were found only above the water table. Hydraulic conductivity data (discussed later) indicate, however, that sand lenses also exist below the water table. The connectedness and lateral extent of the outwash is unknown. Mickelson (1983) identifies more glacial outwash along Sixmile Creek on the northern border of the site. Some samples contained higher silt and clay contents than are typical for the Horicon till which may indicate clay lenses or a deeper soil column at these locations.

Till thickness ranges from 4.6 to 30 m. Underlying the till through most of the area is Cambrian sandstone, containing dolomite and shale (Cline, 1965; Ostrom, 1967). Underlying the Cambrian sandstones is Precambrian rhyolite, granite and basalt. Average thickness of the Cambrian sandstone is 210 m. In the study area are two drumlins aligned southwest-northeast (Mickelson and McCartney, 1979). The larger one rises > 308 m above mean sea level (msl) and is topped with 6.1 to 7.6 m of soil and till over Prairie du Chien Group dolomite. It is the only place in the monitoring area where Ordovician Prairie du Chien bedrock remains.

The potentiometric surface maps indicate a regional groundwater divide located 5 to 7 km northwest of the field site which separates groundwater flowing east and south into the Yahara River basin and north and west to the Wisconsin River. Regional flow through the bedrock aquifer in the study area is southeasterly with a gradient of 0.0033.

Water-table mapping based on monitoring wells indicates a local, shallow flow system of a more complex nature, affected by surface topography, drainage features, recharge patterns and variations in hydraulic conductivity. Representative water-table maps are shown for April 1991 and January 1992 (Fig. 4). Standing surface water from ditches draining barnyards at the two adjacent farms is responsible for the high water table to the east of well K2. Water-table maps show a horizontal groundwater-flow divide through the study area, corresponding roughly to a surface divide. Water recharges the groundwater throughout most of the study area as indicated by downward gradients at piezometer nests; vertical gradients are much greater than horizontal gradients over most of the study area. Fig. 5 shows an August 1991 isopotential diagram along a north-south cross section A-A' (transect shown in Fig. 3). While the horizontal component of flow north and west of the water-table divide is initially towards Sixmile Creek, the flow direction is predominantly downward and the horizontal direction eventually reverses with depth to join the southerly regional flow. Upward groundwater gradients are found near and in Sixmile Creek and Waunakee Marsh, indicative of groundwater discharge areas. Based on the equipotential contours (Fig. 5) and measured groundwater seepage rates into Sixmile Creek, the discharge area to Sixmile Creek may extend only 100 to 150 m to each side.

Annual water-level fluctuations were from 1 to 2 m with greater fluctuations at the water table. Vertical hydraulic gradients are generally greatest when water-table elevations are highest. Potentiometric heads deeper in the till aquifer generally respond less to recharge events than do shallower heads. The response to recharge events in the upper aquifer accounts for the differences seen in the water-table configurations during the year (Fig. 4). Horizontal gradients are also affected by seasonal recharge and water-table fluctuations and tend to increase during periods of high water table.

Hydraulic conductivities of the Horicon till were measured using piezometer rising- and falling-head slug tests (Bouwer and Rice, 1976). For piezometers screened at the water table the rising tests are more accurate (Bouwer, 1989) and were used exclusively to calculate hydraulic conductivity. For other

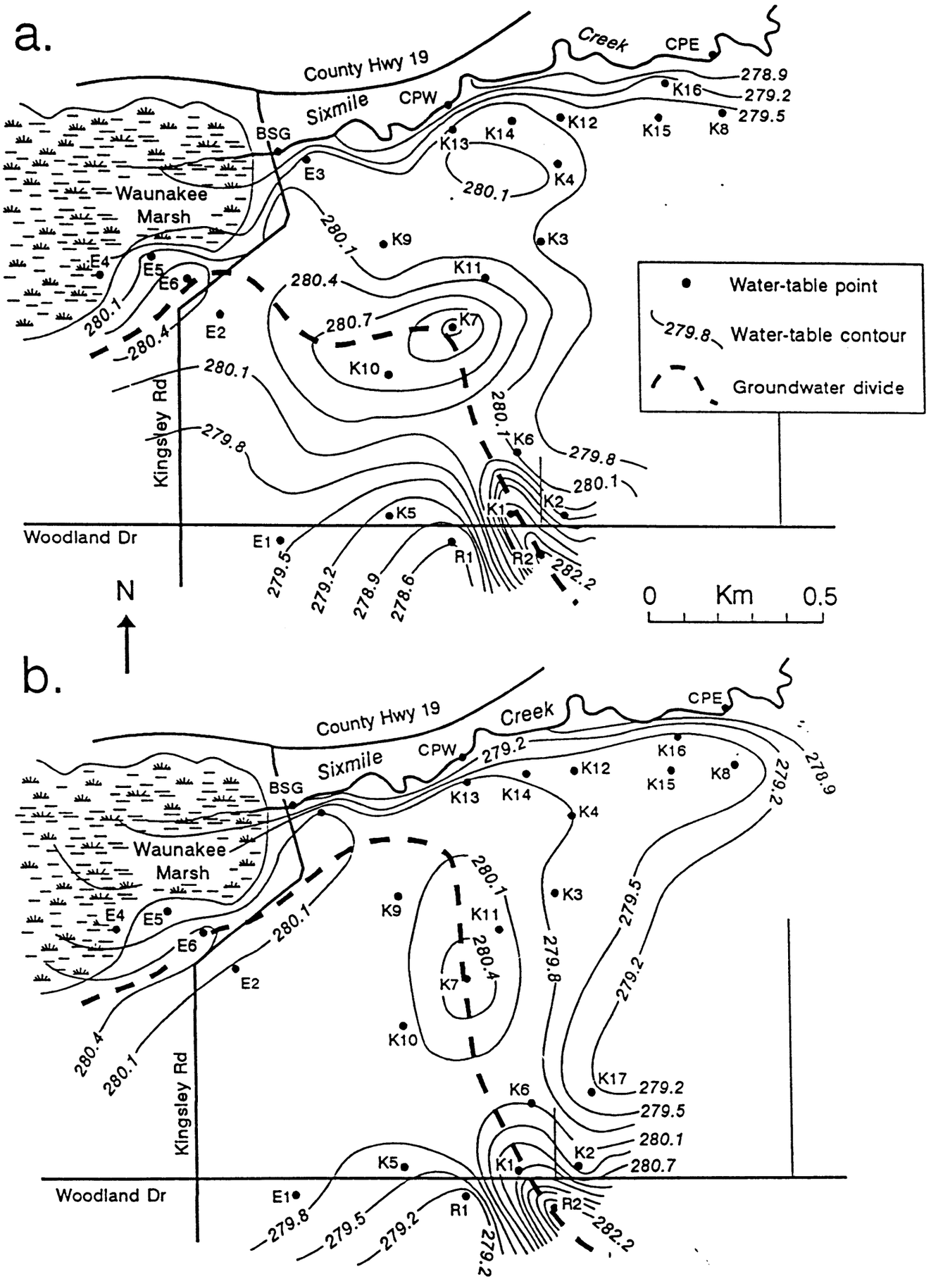

Fig. 4. Water-table elevations in m above msl on (a) 4/22/91 and (b) 1/9/92. Contour interval is 0.3 m.

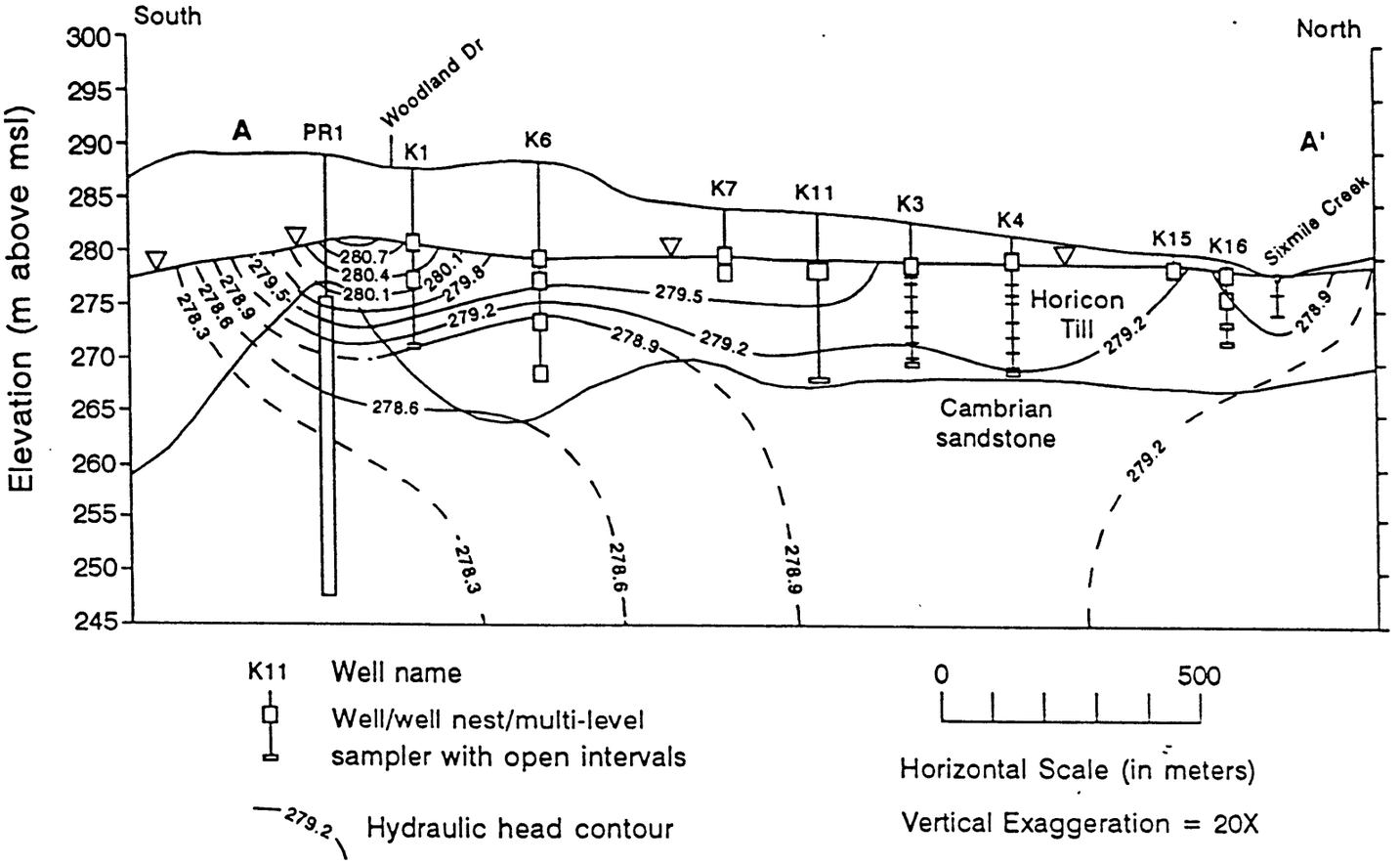

Fig. 5. Hydraulic head on 8/5/91 along transect A-A' (Fig. 3). Contour interval is 0.3 m. Dashed contours indicate increased uncertainty.

piezometers, falling- and rising-test results were examined for reliability based on the straight-line fit of plots of log water displacement with time, and the better test was used. When both tests were satisfactory, the geometric mean was used. Hydraulic conductivity was approximately log-normally distributed with a range of 1.2×10^{-6} to 2.4×10^{-2} cm sec^{-1}; the geometric mean was 1.2×10^{-4} with a 95% confidence interval of 6.7×10^{-5} to 2.3×10^{-4} cm sec^{-1}.

Downward hydraulic gradients at piezometer nests K1, K2, K3, K4, K6, K7 and K11 indicate that vertical flow dominates over much of the field area. It therefore becomes important to estimate vertical hydraulic conductivities based on the measured horizontal hydraulic conductivity and a horizontal to vertical hydraulic conductivity anisotropy ratio (K_h:K_v). Estimates of K_h:K_v can be obtained from analyses of time-drawdown curves from aquifer pumping tests. Although no pumping tests were performed at this site, Rayne (1993) performed 2 pumping tests in the Horicon Formation at a site 22 km to the southeast. Time-drawdown data were analyzed to estimate likely K_h:K_v values. Analyses were performed with a computer program, Aqtesolv (Duffield and Rumbaugh, 1989), according to the method for delayed yield in unconfined aquifers with partially penetrating pumping and observation wells (Neuman, 1975). The analyses also produce estimates of aquifer specific yield (S_y). The K_h:K_v estimates for 19 observation wells were distributed approximately log-normally with a geometric mean of 2.8 and a 95% confidence interval between 1.7 and 4.6. The S_y data are approximately log-normal and have a geometric mean of 0.11 with a 95% confidence interval of 0.084 to 0.15.

GROUNDWATER VELOCITIES, TRAVEL TIMES AND MEAN HORIZONTAL DISTANCES TRAVELED TO MONITORING WELLS

As derived from Darcy's law, average linear groundwater velocity ($\bar{v}$) is expressed as:

$$\bar{v} = -\frac{K}{n_e}\frac{\partial h}{\partial l} \qquad (4)$$

where K is hydraulic conductivity (cm sec^{-1}); n_e is effective porosity (unitless); and $\partial h/\partial l$ is the hydraulic gradient (unitless) (Freeze and Cherry, 1979). Gradients and horizontal hydraulic conductivities were measured in the field. The n_e estimate of the till aquifer was based on the S_y estimates. Since S_y is likely a minimum estimate of n_e, an n_e value of 0.15 was assumed. The relatively low value reflects the poorly sorted nature of the till. Although this value is based on S_y data from another field site, its uncertainty is probably still less than that of hydraulic conductivity calculated from slug tests.

Where downward gradients dominate, groundwater travel paths to monitoring wells are assumed to be simple curves originating at the water table near the well. Groundwater travel times from the water table to the middle of the piezometer screen were calculated for each piezometer within a piezometer nest where downward gradients dominate using the measured vertical hydraulic gradients averaged over the study period. Hydraulic conductivities measured by slug tests were assumed to represent K_h, which was divided by $K_h:K_v = 2.8$ to obtain K_v. To compute a groundwater velocity for an interval between two wells, an effective hydraulic conductivity was estimated based on individual slug test data at the two wells. If the velocity $v(x)$ at every point along an interval from x_1 to x_2 were known, the travel time (TT) would be:

$$TT = \int_{x_1}^{x_2} \frac{1}{v(x)}\, dx \qquad (5)$$

where $v(x)$ depends linearly on K(x), the hydraulic conductivity at each point x (Eq. 4). Hydraulic gradient and porosity were assumed constant over the interval. The effective velocity (V_e) for that interval is:

$$V_e = \frac{x_2 - x_1}{\int_{x_1}^{x_2} \frac{1}{v(x)}\, dx} \tag{6}$$

Estimates of K(x) (and $v(x)$) were based on the assumption of log-normality of hydraulic conductivity and that logs of conductivities (and velocities) varied linearly from x_1 to x_2:

$$\ln[v(x)] = \frac{\ln[v(x_2)] - \ln[v(x_1)]}{x_2 - x_1}\, x + \frac{x_2 \ln[v(x_1)] - x_1 \ln[v(x_2)]}{x_2 - x_1} \tag{7}$$

or:

$$v(x) = \exp\left[\frac{\ln[v(x_2)] - \ln[v(x_1)]}{x_2 - x_1}\, x + \frac{x_2 \ln[v(x_1)] - x_1 \ln[v(x_2)]}{x_2 - x_1}\right] \tag{8}$$

Substituting Eq. 7 into Eq. 5:

$$V_e = \frac{v(x_1)v(x_2)\ (\ln[v(x_1)] - \ln[v(x_2)])}{v(x_1) - v(x_2)} \tag{9}$$

and V_e falls between the harmonic and geometric means of $v(x_1)$ and $v(x_2)$.

V_e was also evaluated numerically using a computer spreadsheet program with the distance between well screen pairs divided into 0.003-m intervals. A velocity was calculated for each interval using geometric interpolation between the measured values at the well screens; the residence time of a hypothetical groundwater particle in each interval was calculated. Total travel time between well screens was the sum of the individual residence times and V_e was the total distance divided by the total time. Numerical and analytical solutions corresponded.

Estimated travel time (TT) was used in conjunction with an estimate of horizontal groundwater velocity

to calculate the mean horizontal distance traveled (MHD) by groundwater reaching each piezometer. The average horizontal hydraulic gradients at the water table (between the well nest in question and the nearest upgradient well nest) were used to calculate the horizontal groundwater velocity.

Many sources of uncertainty are involved in the calculations. Slug tests measure hydraulic conductivity in smaller areas around a well screen than aquifer pumping tests. Depending on aquifer heterogeneity, the values used may not apply to areas far from and between well screens. Hydraulic gradients may vary locally in ways that can only be clarified with a denser well network. The anisotropy ratio and porosity are estimated based on few data. Nonetheless, the velocity estimates and resultant TTs and MHDs represent the best estimates possible with the existing well-monitoring network. Calculations were made for each well nest where the average vertical hydraulic gradient was downward -- at K1, K2, K3, K4, K5, K6, K7 and K11 (Table 3). For other monitoring wells TT and MHD predictions are more difficult; since the flow paths have a greater horizontal component, the origins are farther from the wells where less information is available regarding gradients and conductivities. The horizontal distances shown in Table 3 indicate that the MHD for each well is small and the water quality of the wells reflects the land use and farm practices in the immediate vicinity. Since K7 is near a water-table divide and has no upgradient wells, the MHD is not given.

To some extent, TT estimates can be verified with measurement of tritium (^3H) concentrations in groundwater. Atmospheric testing of nuclear weapons beginning about 1952 resulted in elevated concentrations of atmospheric ^3H peaking around 1963 and steadily declining since. The short ^3H half-life of 12.3 yr makes ^3H a good indicator of recent groundwater recharge and relative groundwater age (Bradbury, 1991). If the ^3H concentration of groundwater is $<$ 0.2 tritium units (TU), the water is $>$ 50-yr old and has undergone substantial ^3H decay (Hendry, 1988); if it is 0.2 to 2.0 TU, the water probably recharged before 1952, but $<$ 50-yr ago; if it is 2.0 to 10 TU, recharge probably occurred between 1952 and 1960; if it is $>$ 100 TU, recharge probably occurred between 1960 and 1966; and if

TABLE 3

Predicted water travel time (TT) and mean horizontal distance traveled (MHD) to monitoring wells

Well	*Depth to groundwater (m)*	*Depth below water table (m)*	*TT from water table (yr)*	*MHD (m)*
K1.C	6.56	0.30	0.84	0.26
K1.B	6.56	3.29	4.7	2.8
K1.Main	6.56	9.41	5.2	3.5
K2.B	7.73	0.51	0.45	1.1
K2.Main	7.73	4.20	8.9	9.3
K3.B	4.18	0.59	0.11	0.24
K3.Main	4.18	9.60	1.1	3.9
K4.B	2.37	0.37	3.8	0.091
K4.Main	2.37	10.52	24	2.6
K5.C	8.45	0.21	1.8	1.9
K5.B	8.45	1.35	9.4	12
K5.A	8.45	3.73	20	34
K6.D	9.17	0.35	0.17	0.18
K6.A	9.17	2.15	0.63	1.1
K6.B	9.17	6.08	0.75	1.8
K6.C	9.17	11.32	1.2	5.1
K7.A	4.26	0.55	2.8	NC*
K7.B	4.26	1.86	4.7	NC
K11.A	4.37	0.74	1.6	0.16
K11.B	4.34	1.29	2.8	0.28
K11.C	4.37	11.65	9.8	2.4

* NC is not calculated due to the absence of upgradient wells.

it is 10 to 100 TU, recharge was probably after 1966, but might have been just before the peak period of 1960 to 1966. To make more precise estimates of groundwater age, ^3H levels in groundwater have been matched to a curve of local, historic atmospheric ^3H corrected for radioactive decay (Bradbury, 1991). Such a curve was generated for a nearby basin (McGrath, 1991). Most ^3H levels correspond to more than one age and must be interpreted cautiously. The ages reflect the time since the water entered the subsurface as opposed to the Darcy-estimated TTs which reflect only residence time in the saturated zone. Groundwater dating with ^3H assumes that minimal mixing of old and young groundwater occurs.

Samples for ^3H analysis were taken from 10 wells at 5 locations in the monitoring area and were analyzed at the University of Waterloo, Ontario, Canada (Table 4). The Darcy TT estimates are shown for comparison. All wells contained water of 17 to 54 TU, indicating minimum ages of 7 to 19 yr. Interpreted water ages at well nest K6 and multilevel sampler K3 (where strong downward hydraulic gradients are present) are obtained by accepting the minimum age at the shallowest point and assigning appropriate older ages from the ^3H curve of McGrath (1991) to deeper points. Water from K11.C is apparently older than water from the other wells sampled.

TABLE 4

Results and interpretations of ^3H analyses

Well	Sampling Date	Depth below water table (m)	^3H amount (TU)	Minimum age (yr)	Interpreted age (yr)	Darcy TT estimate (yr)
K3.1	9/12/90	1.23	29.4 ± 2.2	8.5	8.5	0.22
K3.4	9/12/90	4.59	34.9 ± 2.5	9.0	9.0	0.69
K3-Main	9/12/90	9.61	28.3 ± 2.2	8.5	9.5	1.1
K6.A	9/12/90	2.15	17.3 ± 1.5	7.0	7.0	0.63
K6.B	9/12/90	6.08	36.0 ± 2.6	9.0	9.0	0.75
K6.C	9/12/90	11.3	32.6 ± 2.3	9.0	12.0	1.2
K11.C	4/15/91	11.6	53.6 ± 3.6	19.0	19.0	9.8
K16.C	4/15/91	7.44	33.1 ± 2.3	10.0	10.0	NC*1
K16.D	4/15/91	0.765	20.3 ± 1.5	8.0	8.0	NC*1
PK1*2	4/15/91	? to 33	24.3 ± 1.8	9.0	9.0	NC*3

*1 Not calculated due to lack of downward hydraulic gradient.
*2 PK1 is a private well with known bottom elevation, but unknown open interval.
*3 Not calculated due to unknown open interval.

Major discrepancies exist between the Darcy TT and ^3H age estimates at K3 and K6. Uncertainty inherent in both methods may be responsible for some or all of the inconsistency. Two other explanations may also contribute: 1. the ^3H ages include time of transport through the unsaturated zone

while the Darcy TTs do not -- linear regression of the ^3H ages against the Darcy TTs indicate that discrepancies are resolved by assuming that water drains through the unsaturated-zone at about 1 m yr^{-1} (Levy, 1993); and 2. there is mixing of older and newer water. It is possible that a given sample contains mostly newer water and small amounts of older water. For example, if 90% of a sample from K6.C was 2 yr old water (as predicted with the Darcy estimate) with 10 TU and 10% was water that had recharged in 1966 but had been held up in low conductivity lenses in either the saturated or the unsaturated zones, the resulting sample might have as much as 24 TU and seem to be 8 yr old. If 10% of the water recharged in 1971, the interpreted age would be 7 yr. Water at any well could be a mixture of many different ages. In a heterogeneous system, the quick responses of hydrographs and even hydraulic conductivity measurements are biased to reflect zones and paths of higher conductivity. However the discrepancies are explained, the ^3H concentrations indicate that at least some water from every sample recharged before or during 1983 and at least some of the water at most wells is older than the Darcy estimated residence times indicate. Based on the minimum ^3H content of 17 TU all the water sampled is < 25 yr old.

The vertical flow paths and estimated groundwater velocities suggest that although the till has a lower permeability than the underlying bedrock, contamination may still reach the bedrock aquifer. Since this movement may take decades, atrazine residue concentrations measured in private wells today may have resulted from pesticide-use practices that have been discontinued due to regulatory or voluntary changes in management practices.

ATRAZINE RESIDUE CONCENTRATIONS AND DISTRIBUTION

From October 1989 through February 1992, only atrazine and DEAT were found in quantifiable amounts because of the extraction techniques used. As of April 1992, a new extraction method allowed more accurate determination of DIAT and DIAM concentrations. The DIAT and DIAM data obtained

from those analyses are described separately.

Although concentrations at individual wells varied with time, the variability from well to well was greater than the variability over time. ANOVAs were performed comparing the variabilities (autocorrelations were ignored). For both compounds, differences between wells were highly significant compared to the variability over time at $p < 0.001$. The greater well to well variability compared to variability over time and the lack of observable temporal trends mean that average concentrations over time at each sampling point are good indicators of the extent of contamination at those aquifer locations and the distribution of those averages is the best representation of contaminant distribution during the study period. HPLC data for each sampling location averaged over the study period are shown in Table 5. To compute averages, non-detections were treated as 0 ppb. The DEAT concentrations are modified to correct for the lower molecular weight of the metabolite. In this way, the concentration of DEAT shown is equal to the concentration of its parent compound before degradation and the ratio of modified DEAT to atrazine concentrations is the same as the ratio of their molar concentrations. The DEAT:atrazine ratio (DAR) is shown in Table 5 and is the ratio of average concentrations over the study period. Results from private bedrock wells are also shown. At some time, atrazine was detected at some depth at 22 of 25 locations monitored with single or nested piezometers and at 5 of 6 private wells in the monitoring area. DEAT in groundwater was as widespread as atrazine, also occurring at 21 of 25 locations monitored (all depths included) and 5 of 6 private wells. At 42 of the 59 individual monitoring piezometers and multilevel sampling ports, average concentrations of DEAT exceeded those of the parent compound (average DAR > 1). The average DAR was < 1 at 12 of the 59 wells and ports, and neither compound was ever detected at 5 of the 59 wells and ports. The number of sampling points (including private wells) with atrazine plus DEAT concentrations that exceed Wisconsin's PAL and ES for total atrazine residues is shown in Table 6. The distribution of atrazine and DEAT concentrations are also shown individually to indicate their relative impact and the impact of including DEAT in groundwater

TABLE 5

Time-averaged HPLC results from October 1989 through June 1992

Well	Number of Samples	Depth to WT[*1] (m)	Mid-screen Depth Below WT (m)	Atrazine Conc. (ppb)	Modified DEAT[*2] (ppb)	Total (ppb)	DAR[*3]
K1.C	4	6.69	-0.26	0.58	0.42	1.00	0.74
K1.B	14	6.74	3.18	0.07	0.66	0.72	9.74
K1.MAIN	17	6.69	9.30	0.22	0.89	1.11	4.0
K2.B	11	7.77	0.24	0.00	0.00	0.00	NC[*4]
K2.MAIN	18	7.84	4.18	0.05	0.07	0.13	1.34
K3.B	9	4.19	0.42	0.50	1.97	2.43	3.96
K3.1	17	4.10	1.26	1.09	3.23	4.32	2.95
K3.2	18	4.10	2.18	0.95	2.97	3.82	3.03
K3.3	18	4.10	3.09	0.94	2.76	3.71	2.94
K3.4	17	4.10	4.61	0.52	1.64	2.16	3.16
K3.5	17	4.10	6.14	0.26	0.99	1.25	3.86
K3.6	17	4.10	7.66	0.19	0.89	1.09	4.69
K3.7	17	4.10	9.19	0.27	0.97	1.24	3.66
K3.MAIN	16	4.10	9.62	0.23	0.82	1.06	3.51
K4.B	9	2.41	-0.03	0.57	0.75	1.31	1.32
K4.1	17	2.34	2.15	0.13	0.70	0.83	5.46
K4.2	17	2.34	3.07	0.12	0.78	0.90	6.72
K4.3	17	2.34	3.98	0.09	0.68	0.77	7.84
K4.4	17	2.34	5.51	0.14	0.62	0.76	4.4
K4.5	17	2.34	7.03	0.09	0.64	0.73	6.9
K4.6	17	2.34	8.56	0.16	0.75	0.91	4.74
K4.7	17	2.34	10.08	0.07	0.64	0.71	9.33
K4.MAIN	16	2.34	10.52	0.08	0.59	0.67	7.39
K5.C	3	8.42	-0.35	0.00	0.00	0.00	NC
K5.B	13	8.46	1.34	0.00	0.01	0.01	NC
K5.A	14	8.49	3.72	0.00	0.00	0.00	NC
K6.D	8	9.43	-0.34	1.50	1.44	2.94	0.96
K6.A	15	9.43	1.88	2.68	2.77	5.46	1.03
K6.B	14	9.43	5.81	1.09	0.72	1.81	0.66
K6.C	13	9.43	11.04	0.59	0.45	1.04	0.76
K7.A	12	4.27	0.26	0.19	0.56	0.75	2.97
K7.B	8	4.27	1.84	0.09	0.64	0.73	7.27
K8	14	4.53	0.63	0.01	0.29	0.30	26.29
K9	15	12.73	1.01	0.11	0.41	0.52	3.79
K10	15	6.45	0.44	0.26	0.18	0.44	0.71
K11.A	7	4.37	0.74	0.00	0.65	0.65	1.27
K11.B	8	4.37	1.27	0.04	0.47	0.52	11.03
K11.C	7	4.37	11.64	0.15	0.19	0.34	1.27

TABLE 5

Continued

Well	Number of Samples	Depth to WT (m)	Mid-screen Depth Below WT (m)	Atrazine Conc. (ppb)	Modified DEAT (ppb)	Total (ppb)	DAR
K12	11	1.26	0.13	0.32	0.66	0.98	2.08
K13	11	1.59	-0.15	0.21	0.93	1.14	4.52
K14	2	2.11	-0.51	0.24	0.00	0.24	0.00
K15	10	1.21	0.55	0.08	0.10	0.18	1.16
K16.D	6	0.52	0.85	0.00	0.14	0.16	5.70
K16.A	7	0.57	3.08	0.16	0.55	0.71	3.37
K16.B	6	0.57	5.57	0.10	0.37	0.42	3.91
K16.C	7	0.59	7.53	0.02	0.27	0.29	13.67
K17.A	4	12.4	1.15	0.91	1.16	2.07	1.28
K17.B	4	12.5	2.60	0.41	0.97	1.38	2.34
K17.C	3	12.5	5.32	0.51	1.12	1.63	2.19
R01	3	9.90	-0.06	0.02	0.00	0.02	0.00
R02	6	5.16	1.23	0.43	0.34	0.77	0.80
E01	9	9.71	0.68	0.08	0.06	0.14	0.79
E02	7	7.23	0.76	0.04	0.00	0.04	0.00
E03	7	0.74	0.81	0.00	0.07	0.07	0.00
E04	2	0.01	2.16	0.00	0.00	0.00	NC
E05	3	1.45	0.35	0.17	0.17	0.34	0.97
E06.A	9	0.83	1.45	0.02	0.00	0.02	0.00
E06.B	7	0.83	2.90	0.00	0.00	0.00	NC
PK1[*5]	18	-	-	1.01	1.44	2.45	1.43
PE1	3	-	-	0.04	0.00	0.04	0.00
PE2	3	-	-	0.07	0.11	0.18	1.52
PR1	2	-	-	0.46	0.26	0.72	0.58
PZ1	3	-	-	0.07	0.40	0.47	5.70
PZ2	3	-	-	0.16	0.51	0.68	3.13
Sixmile Creek	4	-	-	0.00	0.00	0.00	NC
CPW2[*6]	1	-	-	0.07	0.26	0.33	3.78

[*1] WT is water table.

[*2] Modified DEAT is DEAT concentration corrected to reflect the higher molecular weight of parent atrazine.

[*3] DAR is the modified metabolite:atrazine ratio.

[*4] NC indicates the DAR cannot be computed due to residue concentrations less than the detection limit.

[*5] P signifies a domestic well.

[*6] CPW2 is the deeper creek piezometer at CPW.

TABLE 6

Summary of atrazine and DEAT average concentrations at 35 sampling locations indicating number of violations of Wisconsin's PAL (0.3 ppb) and ES (3.0 ppb)

	Number of Samples Based on Non-modified Averages		
Concentration	*Atra*	*DEAT*	*Total*
No Detect:	8	10	5
>0, <0.3 ppb:	39	15	14
>0.3, <3.0 ppb:	18	40	42
> 3.0 ppb:	0	0	4

standards. DEAT concentrations used in Table 6 were not modified since that adjustment is not made by state regulatory agencies.

Horizontal distributions of average atrazine and DEAT concentrations near the water table are presented in Figs. 6a and b. The maps show isopleths at 0.5 ppb contour intervals from 0.5 to 2.5 ppb and also the 0.25 ppb isopleth. The data were averaged over the study period (Table 5). At each location, all wells and sampling ports between the water table and 4 m below the water table were included to provide a more representative picture of contamination since the highest concentrations were often below the water table. Concentrations from different wells at each location within 4 m of the water table are averaged according to screen length and distance between screens. Since the concentration variability is probably large compared to well density, caution should be employed in interpreting the maps, especially in predicting concentrations between wells. The maps simply visually summarize average concentration data. Fig. 6a indicates that contamination by atrazine residues at low concentrations (e.g., < 0.5 ppb) is widespread. Contamination by DEAT is even more widespread than that by atrazine. The widespread, low-level contamination probably results from low-level nonpoint source contamination over much of the area and, therefore, the contamination distribution is related to

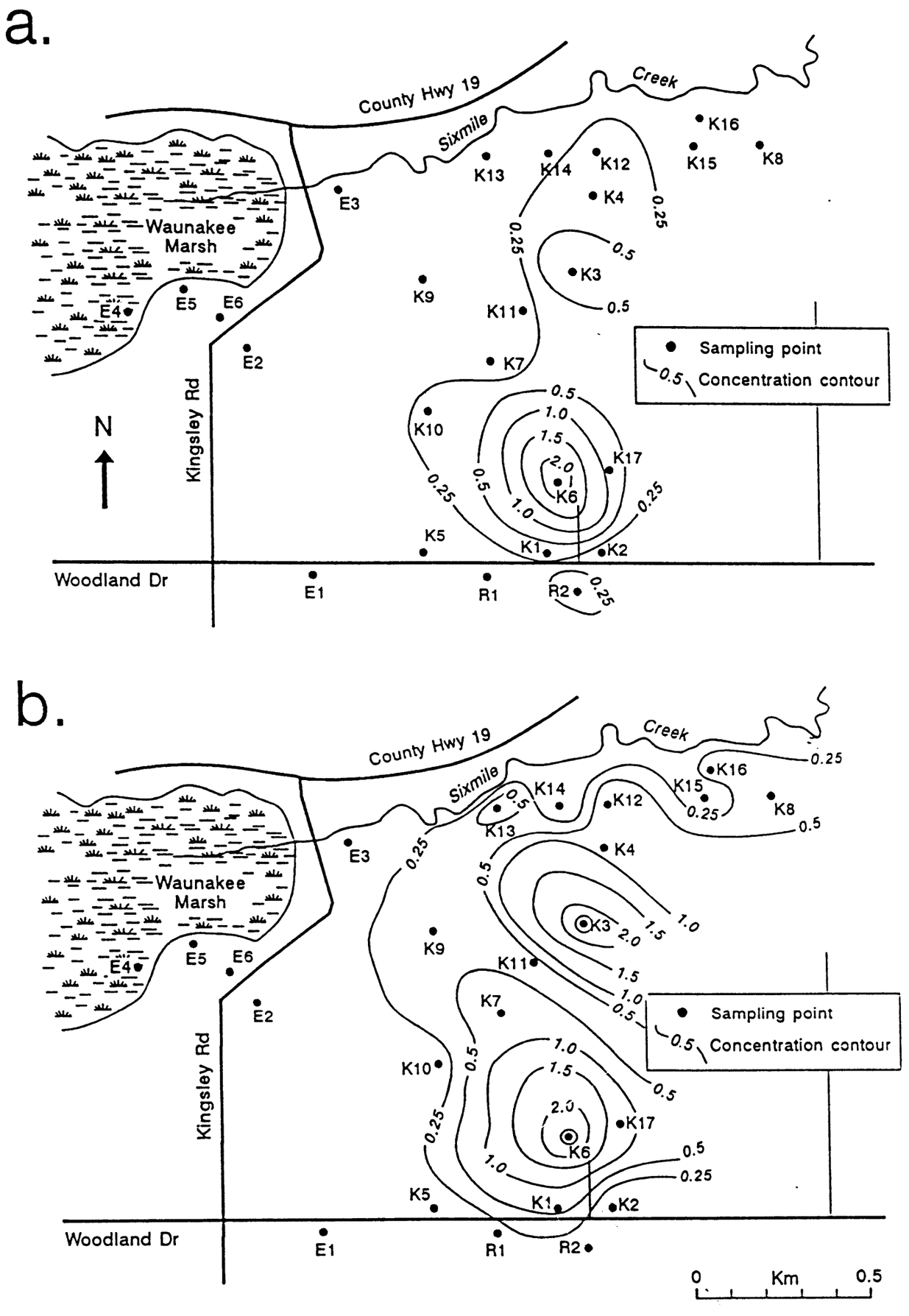

Fig. 6. Average concentrations (ppb) of (a) atrazine and (b) DEAT from 0 to 4 m below the water table. Contour interval is 0.5 ppb. The 0.25 ppb contour is also included.

land use. Wells K5, K10 and K9 lie along a property boundary where the farmer to the west has not applied atrazine since at least 1987. Vertical contamination distribution along the transect A-A' from Fig. 3 is shown in Fig. 7; concentrations from R2 and K12, lying near A-A', were used in the profiles.

Throughout the study period, highest atrazine and DEAT concentrations were at well site K6 (Figs. 6 and 7). Concentrations at the two deepest wells (K6.B and K6.C) indicate decreasing contamination with depth; however, concentrations at K6.A, screened 0.9 to 2.4 m below the water table, were usually higher than at K6.D, screened at the water table. Average atrazine plus DEAT concentration at K6.A was 5.5 ppb, well in excess of the Wisconsin ES. Concentrations of atrazine relative to DEAT were high at K6, resulting in some of the lowest DAR values observed; averages for the nested wells were 0.66 to 1.03. The low DARs may be due to the nature of the source and/or time of transport to the water table. K6 is located near an equipment shed and the main pesticide mixing/loading area. The proximity of K6 to pesticide handling areas suggests that the high concentrations might have resulted from minor accidental spills and may reflect point-source origins. The residue distributions (Figs. 6 and 7) dramatize the possible point-source contamination at K6. Lower DAR values are expected to be associated with point-source contamination if the contaminants enter the aquifer through a natural or artificial conduit or are somehow driven to the water table so that they bypass the soil microorganisms that desethylate atrazine (Adams and Thurman, 1991; Perry, 1990). Point-source contamination by atrazine at high concentrations might also decrease soil microbial populations, and lower DAR values. However, Perry (1990) reported DARs < 0.04 in a shallow aquifer believed to be contaminated by point sources, far lower than those found at K6. Low average DARs were also found at R2, located near standing water from barnyard runoff which perhaps accelerated leaching of atrazine residues through the soil. Low DARs were consistently found at K10, near snowmelt ponds. However, just as much ponding occurs at K7 where DAR values are higher. Low DARs might indicate point sources and/or accelerated leaching due to ponding, but those factors fail to explain all the variability.

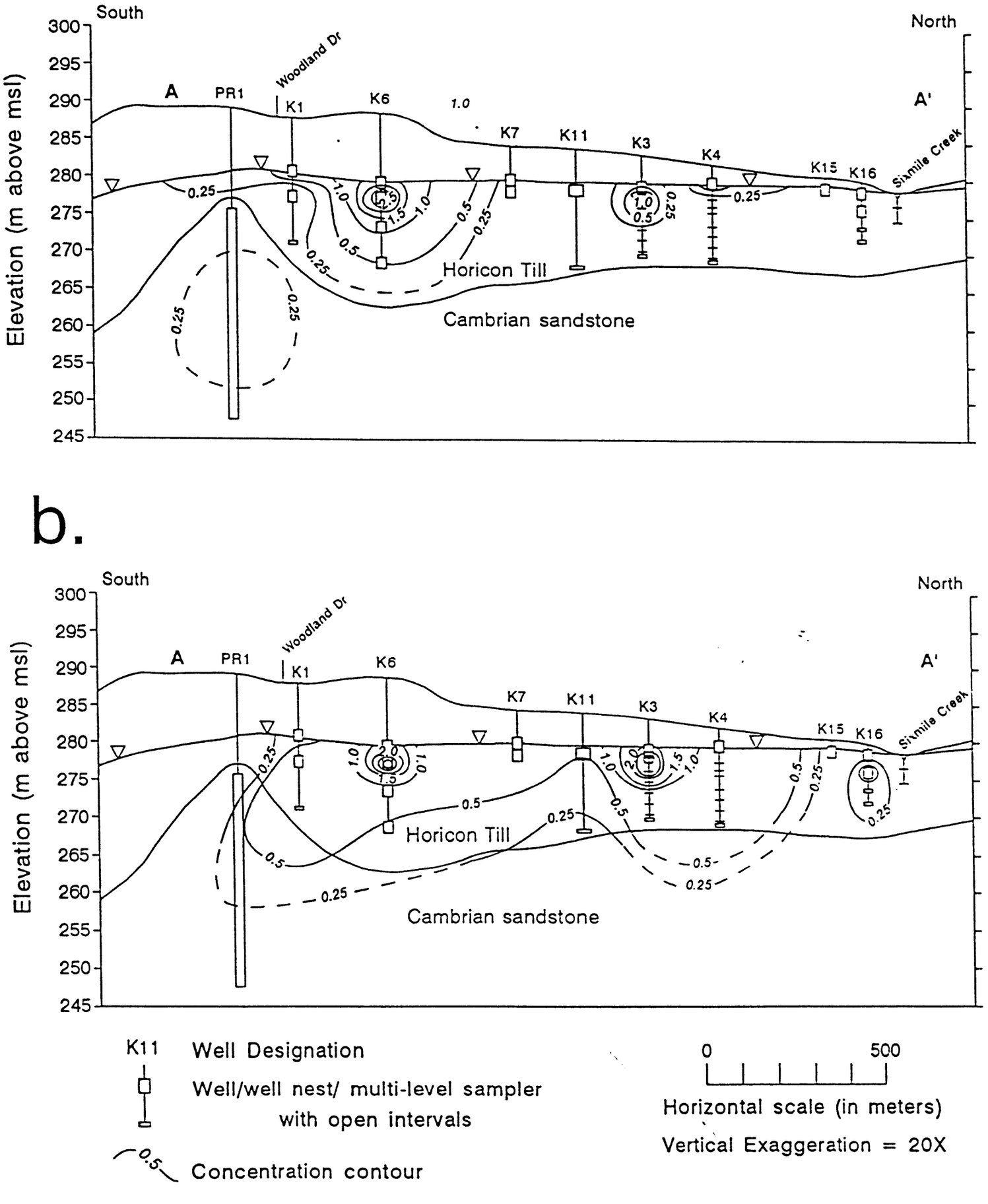

Fig. 7. Average concentrations (ppb) of (a) atrazine and (b) DEAT along transect A-A' (Fig. 3). Contour interval is 0.5 ppb. The 0.25 ppb contour is also included. Dashed contours indicate increased uncertainty.

After K6, highest atrazine and DEAT concentrations were found at multilevel sampling well K3 which is not near a pesticide handling area. Concentrations at K3 tend to peak 0.9 to 3.4 m below the water table and then decrease with depth. Concentrations of DEAT are consistently higher than those of atrazine at all depths. The DARs at K3 are substantially higher than at K6, possibly representing a difference between point- and nonpoint-source contamination. Average DARs at K3 ranged from 3.0 to 4.7. Concentrations at multilevel well K4 (about 200 m north of K3) are generally lower than at K3 and show no concentration trend with depth. Residue concentrations were higher, however, in the adjacent water-table well than in any of the multilevel ports.

Although contamination at K6 is likely to be due in part to point sources, residue concentrations as high as those at K6 may result from normal field applications. A 2-m thick uniformly contaminated plume with a total residue concentration of 10 ppb (i.e., contamination more severe than at K6) would result from 3.0×10^{-6} kg m^{-2} atrazine residues leaching to the water table and spreading uniformly through a medium with a porosity of 0.15. At the normal atrazine application rate of 2.0 kg ha^{-1} a.i. (before recent atrazine-use restrictions), this amount of contamination would result if only 1.5% of applied atrazine leached to groundwater. Very little atrazine is needed for the PAL (0.3 ppb) to be violated. An average yearly recharge of 20 cm would need to leach only 0.03% of applied atrazine at 2 kg ha^{-1} a.i. to create a uniform plume with a concentration of 0.3 ppb and a thickness of 1.33 m at a porosity of 0.15.

Due to the inclusion of DIAT and DIAM data, the April, May and June 1992 sampling results give a more complete picture of groundwater contamination by atrazine residues. Averaged April, May and June 1992 concentrations for DIAT and DIAM are presented in Table 7. Concentrations of atrazine and DEAT are also shown for comparison along with total residue concentrations. Since only one analytical method is represented (Method 3), atrazine and DEAT concentrations in Table 7 are not standardized to equivalent Method 2 concentrations as was done earlier. The reported concentrations

TABLE 7

Average April, May and June 1992 sampling\analysis results

Well	Number of Samples	ATRA[*2] Avg (ppb)	Mod. DEAT[*3] Avg (ppb)	Mod. DIAT[*4] Avg (ppb)	Mod. DIAM[*5] Avg (ppb)	Total[*6] Avg (ppb)	Mod. Total[*7] Avg (ppb)	DEAT: ATRA	DIAT: ATRA	DIAM: OTHERS[*8]
K3.B	3	0.66	1.58	0.29	0.79	2.79	3.31	2.4	0.44	0.31
K3.1	3	1.61	2.13	0.23	0.71	4.12	4.67	1.3	0.14	0.18
K3.2	3	1.17	2.07	0.29	0.67	3.65	4.20	1.8	0.25	0.19
K3.3	3	1.10	1.99	0.17	0.65	3.40	3.90	1.8	0.15	0.20
K3.4	3	0.49	1.18	0.19	0.52	2.03	2.39	2.4	0.40	0.28
K3.5	3	0.58	0.94	0.18	0.60	1.95	2.30	1.6	0.31	0.35
K3.6	3	0.47	0.84	0.29	0.65	1.86	2.24	1.8	0.61	0.41
K3.7	2	1.03	1.28	0.37	0.63	2.86	3.30	1.2	0.36	0.24
K3.M	3	0.49	0.92	0.36	0.68	2.04	2.45	1.9	0.74	0.38
K4.B	3	0.45	0.58	2.24	3.53	5.14	6.80	1.3	5.0	1.1
K6.D	3	1.22	0.84	1.99	2.58	5.28	6.62	0.69	1.6	0.64
K6.A	3	2.27	1.33	2.42	2.95	7.37	8.97	0.59	1.1	0.49
K6.B	2	1.29	0.62	0.37	0.33	2.34	2.59	0.48	0.29	0.14
K6.C	2	1.11	0.70	1.53	2.19	4.43	5.53	0.63	1.4	0.66
K7.A	3	0.31	0.49	0.52	0.40	1.42	1.72	1.6	1.7	0.30
K7.B	3	0.56	0.54	0.34	0.26	1.47	1.69	1.0	0.60	0.18
K8	1	0.00	0.10	0.55	0.31	0.74	0.96	NC[*9]	NC	0.48
K9	1	0.34	0.62	0.62	0.49	1.71	2.07	1.8	1.8	0.31
K10	1	0.27	0.10	0.24	0.16	0.66	0.77	0.38	0.87	0.27
K11.B	3	0.15	0.67	0.80	2.73	3.22	5.93	0.39	0.47	0.85
K11.C	3	0.89	0.59	0.88	2.51	3.81	4.87	0.66	0.99	1.1
K12	2	0.68	0.40	0.62	1.96	2.84	3.64	0.59	0.91	1.2
K15	3	0.08	0.03	0.30	0.09	0.41	0.51	0.41	3.6	0.21
K16.D	3	0.34	0.18	0.18	0.09	0.70	0.78	0.54	0.53	0.13
K16.A	3	0.37	0.60	0.30	1.01	1.81	2.27	1.6	0.81	0.80
K16.B	2	0.28	0.52	0.24	0.78	1.45	1.81	1.9	0.88	0.75
K16.C	3	0.14	0.38	0.44	0.26	0.99	1.21	2.7	3.2	0.28
K17.A	3	1.44	1.00	0.67	0.98	3.50	4.08	0.69	0.46	0.32
K17.B	3	0.58	0.94	0.36	0.68	2.13	2.55	1.6	0.62	0.36
K17.C	2	0.80	1.05	0.40	0.68	2.50	2.93	1.3	0.50	0.30

TABLE 7

Continued

Well	Number of Samples	ATRA Avg (ppb)	Mod. DEAT Avg (ppb)	Mod. DIAT Avg (ppb)	Mod. DIAM Avg (ppb)	Total Avg (ppb)	Mod. Total Avg (ppb)	DEAT: ATRA	DIAT: ATRA	DIAM: OTHERS
E1	2	0.49	0.19	0.21	0.02	0.83	0.90	0.39	0.42	0.03
E2	1	0.22	0.02	0.55	0.00	0.68	0.79	0.10	2.5	0.00
R1	1	0.12	0.02	0.40	0.00	0.46	0.54	0.19	3.3	0.00
R2	2	0.78	1.21	0.47	0.81	2.75	3.26	1.6	0.60	0.33
PK1	3	1.35	1.31	0.75	0.66	3.54	4.07	1.0	0.55	0.19

*1 Modified metabolite concentration is corrected to reflect the higher molecular weight of parent atrazine.
*2 ATRA is parent atrazine.
*3 DEAT is desethylated atrazine.
*4 DIAT is desisopropylated atrazine.
*5 DIAM is diamino-chloro-s-triazine.
*6 This total is with non-modified metabolite concentrations as used by regulatory agencies.
*7 This total is with modified metabolite concentrations.
*8 Others indicates the sum of atrazine, DEAT and DIAT.
*9 NC indicates the ratio cannot be computed because atrazine concentrations were below the detection limit.

of all residues and their totals were determined by the same method. To achieve a manageable workload, the number of sampled wells in 1992 was reduced from previous years; wells that consistently indicated little or no atrazine contamination were not sampled. The metabolite concentrations have again been modified to correct for their lower molecular weights. As with atrazine and DEAT, detects of DIAT and DIAM are widespread and their inclusion greatly increases the number of violations of the Wisconsin groundwater standard. Table 8 presents the number of violations each compound would cause individually and combined. These numbers are based on non-modified concentrations since Wisconsin regulatory agencies make no such adjustment. Water from none of the sampled wells contained total chlorinated atrazine residue concentrations < the 0.3 ppb PAL. Comparing Tables 6 and 8 clearly

indicates that the inclusion of DIAT and DIAM greatly increases the number of violations at this site. As was true for atrazine and DEAT, variability was greater across sampling points than over time for DIAT and DIAM. The differences between wells were significant at $p < 0.001$.

TABLE 8

Summary of April through June 1992 atrazine residue concentrations at 35 monitoring wells indicating number of violations of Wisconsin's PAL (0.3 ppb) and ES (3.0 ppb)

	Number of Samples Based on Non-modified Averages				
Concentration	*Atra*	*DEAT*	*DIAT*	*DIAM*	*Total*
No Detect:	1	0	0	2	0
>0, <0.3 ppb:	7	7	17	9	0
>0.3, <3.0 ppb:	27	28	18	24	24
> 3.0 ppb:	0	0	0	0	11

Concentrations of DIAT and DIAM are relatively high at wells K6.D and K6.C, where atrazine and DEAT concentrations are highest. However, the second highest and highest concentrations of DIAT and DIAM, respectively were found at the water table at K4 (K4.B) where atrazine and DEAT concentrations were not particularly high. High DIAM concentrations were also found in water sampled from K6.C, K11.B, K11.C, K12 and K16.A, where concentrations of atrazine and DEAT are generally much lower. Ratios of each metabolite to its parent compound(s) are shown in Table 7. The concentration of DIAM is compared to the sum of atrazine, DEAT, and DIAT since it can be formed by degradation of any of these compounds. DIAT and DIAM can also be formed by degradation of other triazine herbicides (e.g. cyanazine and simazine), however, no other triazine use was reported in the area.

RELATIONSHIP OF ATRAZINE RESIDUE CONCENTRATIONS TO GROUNDWATER TRAVEL TIMES

Procedure

The total residence time of residues in groundwater should be related to overall pesticide residue concentrations and possibly the ratio of metabolites to parent compound concentrations. The longer the residence time, the greater the opportunity for residue degradation and dilution through dispersion. Due to sorption, pesticide residues move through the aquifer more slowly than water, but assuming the aquifer is relatively homogeneous with respect to sorption of atrazine residues, travel times for atrazine residues would be proportional to groundwater travel time with the constant of proportionality equal to the retardation factor, which, in turn, depends on the degree of residue sorption.

Correlation and regression analyses were performed to explore the relationships of measured atrazine residue concentrations and the ratio of metabolite to parent concentrations (DAR) to groundwater travel-time (TT) estimates. Based on the assumption of homogeneity of sorption and retardation, it seems reasonable that for each compound, the TTs provide good relative estimates of residue travel time. Relationships of the concentrations and ratios from single sampling periods to TTs were explored, but of particular interest were average concentrations of atrazine and DEAT and their ratios. Averages were calculated with standardization to extraction Method 2 as described earlier. The time-averaged concentrations are assumed to characterize the contamination at a sampling point better than any one measured concentration and conceptually represents a steady-state concentration assuming a constant contaminant input at the water table. Average concentrations were regressed against TT estimates for the monitoring wells at which a given concentration was measured. Relationships of average concentrations to the depth to groundwater at the monitoring well and to the depth below water table of the well screen were also examined. It was thought that the depth to groundwater might reflect the time of transport through the unsaturated zone. Correlation and regression analyses were also performed on the natural logs of the average concentrations, DARs, TTs, depths to groundwater, and depths below

water table to determine whether logarithmic models provide better fits. When logarithmic regression models were used, non-detections had to be represented by something other than 0. The sampling, extraction and HPLC variances for the ANOVA presented in Table 2 were employed with Eq. 3 to estimate a 95% confidence interval for any well with an average concentration of 0 ppb. The 95% confidence interval was based on the number of samples taken from the well, one extraction/sample and two HPLC runs/extraction. The upper limit of the 95% confidence interval represents the highest concentration likely to be misinterpreted as a nondetect. Regression analyses were performed using this upper limit and one-half and one-fourth of this limit. Results were similar in all cases; the reported results were all obtained using one-half the upper 95% confidence interval limit. Well K2.B was a frequent outlier in the analyses and was excluded on the basis that the water chemistry results indicate the water comes from perennially-ponded surface water just to the east of the well. Sources of contamination at K2.B are therefore qualitatively different from the other wells. Also, the multilevel sampling ports at K4 all yielded very similar atrazine residue concentrations as well as similar estimated TTs. The relationship may be genuine, but the K4 samples formed an influential clump in the regressions. To reduce this influence, only the shallowest and the deepest sampling points were used in the regression analyses. The results with and without the other seven sampling points were similar.

Atrazine and DEAT Regression Results

No significant correlation was found between depth of a well below the water table and the concentration at the well. However, average atrazine residue concentrations at specific wells were negatively correlated with estimated TTs to those wells, implying that concentrations decrease with increased residence time in the aquifer. For atrazine, correlation coefficients of concentrations from individual sampling rounds (beginning with April 1990 when there were enough wells to observe a reasonable correlation) ranged from -0.26 to -0.50. Log-log correlations between concentration and TT

were generally better. Except for one positive (but insignificant) correlation, correlation coefficients (r) ranged from -0.027 (also insignificant) to -0.84 (highly significant). The correlation coefficient between the logs of average atrazine concentrations (Avg. ATRA, in ppb) and logs of the TTs (in days) was -0.73. The regression equation describing this relationship is:

$$\ln(Avg.\ ATRA) = 3.1 - 0.72 \ln(TT), \quad R^2 = 0.54 \text{ on } 25 \text{ } df \tag{10}$$

where df is degrees of freedom for the regression equation. As indicated by the low R^2 value, TT does not account for all variability in concentrations, but the relationship is significant at $p < 0.001$. The log-log regression model (Fig. 8a) provided a better fit than either the semi-log or linear model. When depth to groundwater or depth below water table were added to the equation in either the log or linear form, the regression was not significantly improved.

Average DEAT concentrations were negatively correlated with TT estimates. The regression model describing this relationship was:

$$\ln(Avg.\ DEAT) = 3.5 - 0.64 \ln(TT), \qquad 25 \text{ } df \tag{11}$$

The R^2-value is not shown because a weighted least squares regression was used with weights equal to the inverse squared ln(TT) values. The weighted regression method was used to remove heteroscedasticity from regression errors (Chatterjee and Price, 1977). The regression model (Fig. 8b) is significant at $p < 0.001$. Two wells had standardized residuals > 2, but neither was a statistical outlier using a conservative Bonferroni test procedure (Berry and Lindgren, 1990). Neither the slope nor the intercept for this relationship was significantly different from the atrazine-TT relationship. Depth to groundwater (DTG in m) was not significantly correlated with average DEAT concentrations (Avg. DEAT), but when added to the regression model, the model was significantly improved:

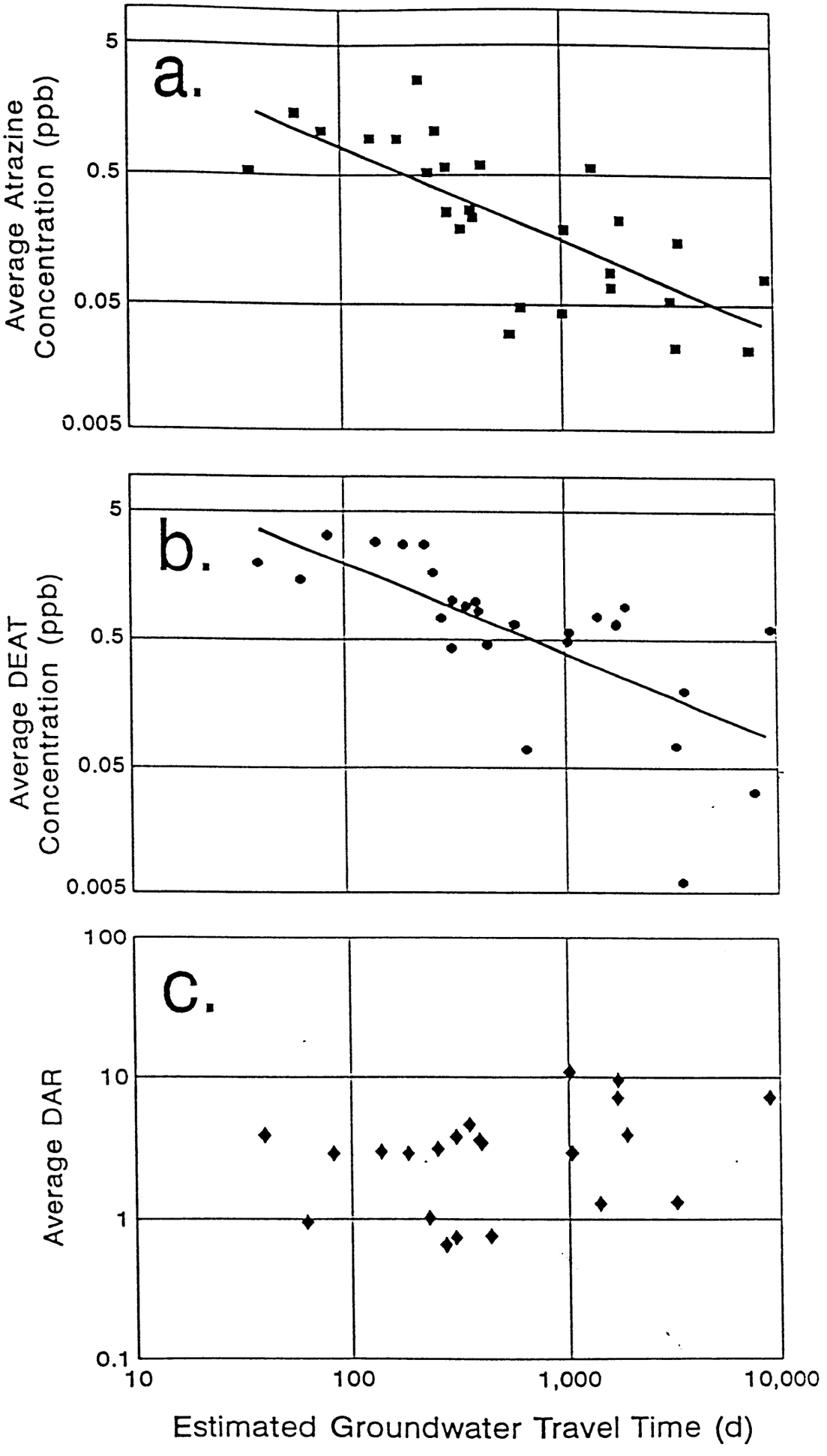

Fig. 8. Average (a) atrazine concentration, (b) DEAT concentration (in ppb) and (c) DEAT:atrazine concentration ratio (DAR) versus estimated groundwater travel times to various monitoring wells. Concentrations and ratios represent averages from October 1989 through June 1992.

$$\ln(Avg.\ DEAT) = 8.3 - 0.71 \ln(TT) - 1.5 \ln(DTG), \quad R^2 = 0.64 \text{ on } 24 \text{ } df \qquad (12)$$

The DTG term was significant at $p=0.001$; TT was significant at $p<0.001$. The full regression model was significant at $p<0.001$ and there were no statistical outliers. The model suggests that DEAT concentrations decrease with time spent in the unsaturated and saturated zones.

As aquifer travel time increases, one might expect the DAR to increase as atrazine is degraded to DEAT. However, no significant relationships between DAR and TT or DTG were observed (Fig. 8c). The lack of such a relationship implies that little or no degradation of atrazine to DEAT occurs in the aquifer. Most of the degradation probably occurs in the unsaturated zone, especially in the soil-root zone where organic matter contents and microbial populations are highest.

The regression models indicate that atrazine and metabolite concentrations decrease with time in the aquifer at similar rates. Dissipation pathways for both compounds include hydrolysis and irreversible sorption, dilution due to dispersion and chemical diffusion and microbial degradation to DIAM. Degradation to DIAT is an additional degradation pathway for atrazine.

DIAT and DIAM Regression Results: April through June 1992

Analyses of only three sampling rounds (April, May and June 1992, Table 6) have been completed with methodology allowing determination of DIAT and DIAM concentrations. Although less reliable than using average concentrations over a longer period, regression analyses performed with average concentrations from these three sampling rounds were used so that an insight could be gained into how DIAT and DIAM concentrations change with time spent in the subsurface.

No significant relationship could be found between DIAT, DIAM or total residue concentrations and estimated TTs (Figs. 9a,b). Some evidence exists, however, that the average ratio of DIAT:atrazine increases slightly with estimated aquifer TT:

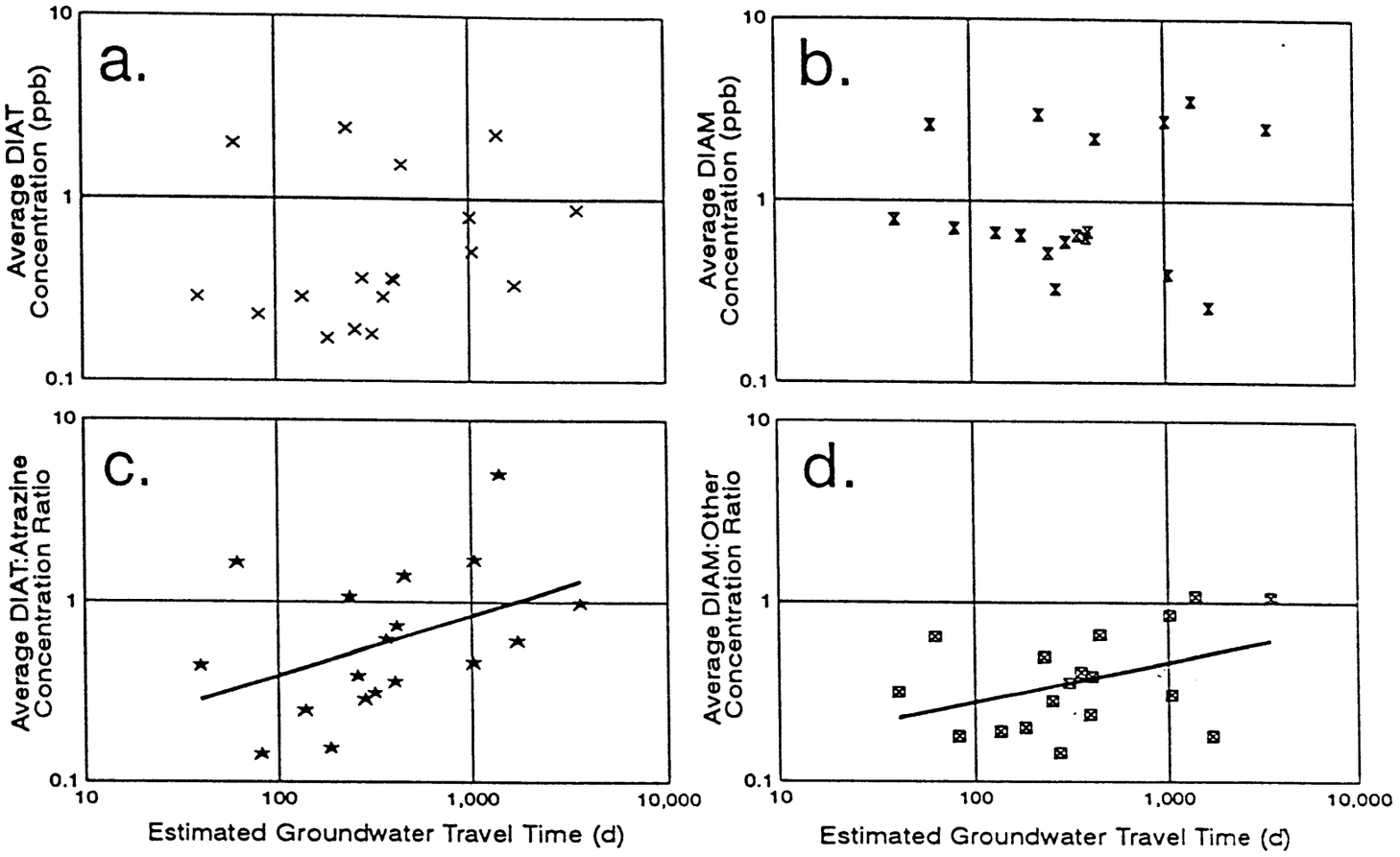

Fig. 9. Average (a) DIAT concentration, (b) DIAM concentration (in ppb), (c) DIAM:atrazine concentration ratio and (d) ratio of DIAM concentration to the sum of the other atrazine residue concentrations versus estimated groundwater travel times to various monitoring wells. Concentrations and ratios represent averages from April through June 1992.

$$\ln(DAR2) = -3.0 + 0.45 \ln(TT), \quad R^2 = 0.21 \text{ on } 16 \text{ df} \tag{13}$$

where DAR2 is the indicated ratio. This relationship is significant at p=0.032 and is shown in Fig. 9c.

The average DIAM concentration was compared to the sum of its possible parents -- atrazine, DEAT and DIAT. There is very weak evidence to suggest that the DIAM concentration increases with TT relative to the other chlorinated compounds:

$$\ln(DAR3) = -2.5 + 0.26 \ln(TT), \quad R^2 = 0.13 \text{ on } 16 \text{ df} \tag{14}$$

where DAR3 is indicated ratio. The regression model is significant at p=0.076 and is shown in Fig. 9d. In this case, the linear model provided the better fit:

$$DAR3 = 0.29 + 0.00021 \ln(TT), \quad R^2 = 0.35 \text{ on } 16 \text{ df} \tag{15}$$

significant at p=0.007. One well (K11.B) was removed from the analysis as an outlier. The ratios of the DIAM concentration to the other three compounds were also examined individually. Of the three ratios, the one with the strongest relationship to TT was DIAM:DEAT:

$$DIAM{:}DEAT = 0.92 + 0.0011 \ln(TT), \quad R^2 = 0.23 \text{ on } 16 \text{ df} \tag{16}$$

significant at p=0.025.

More sampling rounds would be needed to establish average concentrations and determine with greater certainty whether such relationships are valid. However, there is weak evidence that microbial degradation to DIAT and DIAM accounts for some of the dissipation of atrazine and DEAT in groundwater. The fact that DIAT and DIAM concentrations do not appear to dissipate with TT perhaps implies that they might be forming and dissipating in groundwater at similar rates.

SUMMARY AND CONCLUSIONS

Atrazine contamination was originally discovered in water from private well PK1 as part of the WDATCP Grade A Dairy Farm Well Water Quality Survey (LeMasters and Doyle, 1989). The Waunakee field study was initiated in the area around that well to investigate sources and extent of atrazine residue contamination in the shallow glacial till aquifer.

Local flow in the Horicon till is complex with a water-table configuration reflecting local ponding and recharge patterns and variations in hydraulic conductivities. Most of the field area is dominated by downward vertical hydraulic gradients, so that much of the water in the till aquifer discharges to the bedrock aquifer below. Where downward gradients exist, the TTs and MHDs to various monitoring wells can be estimated analytically, using interpolative methods to incorporate some of the measured variation in hydraulic conductivity.

Although atrazine residues are widespread through much of the study area, concentrations are highest at K6, near PK1. The high concentrations and low concentration ratio of DEAT:atrazine relative to most of the other wells may be indicative of point-source contamination, especially since K6 is the well closest to the pesticide handling area. Whatever is responsible for the high concentrations at K6 is probably also responsible for the contamination at K17 and at PK1. As high as the atrazine residue concentrations are at K6, they could still conceivably result from normal field application and leaching.

Although some evidence of point-source pollution exists, most groundwater residues probably result from normal field applications; atrazine plus DEAT concentrations are generally < 1.0 ppb, with DAR-values generally > 1, although 1992 detections of DIAT and DIAM indicate the contamination problem is more severe. The new ES and PAL of 3.0 and 0.3 ppb, which include atrazine and three chlorinated metabolites, have dramatically increased the number of groundwater standards violations.

The relationships between estimated groundwater travel times and atrazine residue concentrations give some insight into atrazine fate in the aquifer. Atrazine and DEAT concentrations decrease with time

spent in the aquifer. Since DEAT concentrations do not increase relative to the parent compound, no evidence exists that atrazine degradation to DEAT is occurring in groundwater. Other dissipation pathways must account for decreases of both compounds. Preliminary analyses from 1992 indicate that concentrations of DIAT and DIAM might increase with aquifer travel time relative to their parent compounds and that some microbial degradation is occurring.

The age of the water and residues at some monitoring wells (as much as 24 yr, not accounting for sorption), and the apparently slow dissipation rates of atrazine residues in groundwater, imply that the beneficial impacts of such regulatory action as atrazine-use prohibition may not be observed for many years. Even if atrazine input to groundwater were to cease completely, it might still be years or decades before groundwater concentrations dissipate to levels below those of regulatory concern. DIAT and DIAM might prove to cause more difficult contamination problems since their concentrations do not seem to decrease with estimated travel time as do concentrations of atrazine and DEAT. In a future paper, the general relationships described here for atrazine and DEAT will be incorporated into contaminant transport computer models to help quantify their expected persistence at various aquifer locations and depths and assess the long-term threat to drinking water.

REFERENCES

Adams, C.D. and Thurman, E.M., 1991. Formation and transport of desethylatrazine in the soil and vadose zone. J. Environ. Qual., 20:540-547.

Anderson, H.A., Goldring, J.M. and Knobeloch, L.M., 1990. Draft public health related groundwater standards-cycle 4. Summary of Scientific support documentation for NR 140.10, Wisconsin Department of Health and Social Services, Division of Health, Madison, WI, 108 pp.

Armstrong, D.E., Chesters, G. and Harris, R.F., 1967. Atrazine hydrolysis in soil. Soil Sci. Soc. of Amer. Proc., 31:61-66.

Armstrong, D.E. and Chesters, G., 1968. Adsorption catalyzed chemical hydrolysis of atrazine. Environ. Sci. and Technol., 2:683-689.

Best, J.A. and Weber, J.E., 1974. Disappearance of s-triazines as affected by soil pH using a balance

sheet approach. Weed Sci., 22:364-373.

Berry, D.A. and Lindgren, B.W., 1990. Statistics: Theory and Methods. Brooks/Cole Publishing Co., Pacific Grove, CA.

Bouwer, H., 1989. The Bouwer and Rice slug test -- an update. Ground Water, 27:304-309.

Bouwer, H. and Rice, R.C., 1976. A slug test for determining hydraulic conductivity of unconfined aquifers with completely or partially penetrating wells. Water Resour. Res., 12:423-428.

Bowman, B.T., 1990. Mobility and persistence of alachlor, atrazine and metolachlor in Plainfield sand, and atrazine and isazofos in Honeywood silt loam, using field lysimeters. Environ. Toxicol. and Chem., 9:453-461.

Bradbury, K.R., 1991. Tritium as an indicator of ground-water age in central Wisconsin. Ground Water, 29:398-404.

Brouwer, W.W.M., Boesten, J.J.T.I. and Siegers, W.G., 1990. Adsorption of transformation products of atrazine by soil. Weed Sci., 30:123-128.

Chatterjee, S. and Price, B., 1977. Regression Analysis by Example. John Wiley and Sons, New York, NY.

Chesters, G., Alhajjar, B.J., Fathulla, R.N. and Simsiman, G.V., 1988. Degradation and transport of alachlor, metolachlor and atrazine in soils and aquifer material. Quarterly Report submitted to the WDNR, Water Resources Center, Madison, WI, 22 pp.

Ciba-Geigy, 1992. Analytical method no. AG567. Ciba-Geigy Agricultural Division, Residue Chemistry Dept., Greensboro, NC, 40 pp.

Cline, D.R., 1965. Geology and ground-water resources of Dane County, Wisconsin. Geological Survey Water-Supply Paper 1779-U, United States Government Printing Office, Washington, DC, 64 pp.

Duffield, G.M. and Rumbaugh, J.O., III, 1989. AQTESOLV: aquifer test solver, version 1.00. Geraghty & Miller, Inc., Reston, VA, 135 pp.

Freeze, R.A. and Cherry, J.A., 1979. Groundwater. Prentice-Hall, Inc., Englewood Cliffs, NJ, 604 pp.

Glocker, C.L. and Patzer, R.A., 1978. Soil survey of Dane County. Wisconsin, U.S. Department of Agriculture, Soil Conservation Service and the University of Wisconsin, Madison, WI, 193 pp.

Green, R.E., Yamane, V.K. and Obien, S.R., 1968. Transport of atrazine in a latosolic soil in relation to adsorption, degradation, and soil water variables. Trans. Ninth Inter. Congress of Soil Sci., Adelaide, Australia, 1:195-204.

Hall, J.K. and Hartwig, N.L., 1978. Atrazine mobility in two soils under conventional tillage. J. Environ. Qual., 7:63-68.

Harris, C.I., 1967. Fate of 2-chloro-*s*-triazine herbicides in soil. J. Agric. Food Chem., 15:157-162.

Hendry, M.J., 1988. Do isotopes have a place in ground-water studies? Ground Water, 26:410-415.

Isensee, A.R., Helling, C.S., Gish, T.J., Kearney, P.C., Coffman, C.B. and Zhuang, W., 1988. Groundwater residues of atrazine, alachlor, and cyanazine under no-tillage practices. Chemosphere, 17:165-174.

Isensee, A.R., Nash, R.G. and Helling, C.S., 1990. Effect of conventional vs. no-tillage on pesticide leaching to shallow groundwater. J. Environ. Qual., 19:434-440.

Junk, G., Richard, J. and Dahm, P., 1984. Degradation of pesticides in controlled water-soil systems. In: R. Krueger and J. Seiber (Editors), Treatment and Disposal of Pesticide Wastes, American Chemical Society, Washington, DC, pp. 38-67

LeMasters, G. and Doyle, D.J., 1989. Grade A dairy farm well water quality survey. Wisconsin Department of Agriculture, Trade and Consumer Protection/Wisconsin Agricultural Statistics Service, Madison, WI, 36 pp.

Levy, J., 1993. A field and modeling study of atrazine transport and fate in groundwater. Ph.D. Dissertation, Land Resources Program, Institute for Environmental Studies, University of Wisconsin-Madison, Madison, WI, 561 pp.

McGrath, R., 1991. Investigation of atrazine contamination in bedrock aquifers, western Dane County, Wisconsin. M.S. Thesis, Department of Geology and Geophysics, University of Wisconsin-Madison, Madison, WI, 218 pp.

Mickelson, D.M. and McCartney, M.C., 1979. Map of the glacial geology of Dane County, Wisconsin. University of Wisconsin-Extension and the Wisconsin Geological and Natural History Survey, Madison, WI.

Mickelson, D.M. 1983. A guide to the glacial landscapes of Dane County, Wisconsin. Field Trip Guide Book 6, Wisconsin Geological and Natural History Survey, Madison, WI. 53 pp.

Mickelson, D.M., Clayton L., Baker, R.W., Mode, W.N. and Schneider, A.F., 1984. Pleistocene stratigraphic units of Wisconsin. Miscellaneous paper 84-1, Wisconsin Geological and Natural History Survey, Madison, WI, 15 pp.

Neuman, S.P., 1975. Analysis of pumping test data from anisotropic unconfined aquifers considering delayed gravity response. Water Resour. Res., 11:329-342.

Ostrom, M.E., 1967. Paleozoic stratagraphic nomenclature for Wisconsin. Info. Circ. No. 8, Wisconsin Geological and Natural History Survey, Madison, WI, 5 pp.

Perry, C.A., 1990. Source, extent and degradation of herbicides in a shallow aquifer near Hesston, Kansas. U.S. Geol. Surv. Water-Resources Invest. Rep. 90-4019, U.S. Gov. Print. Office, Washington, DC, 24 pp.

Pionke, H.B. and Glotfelty, D.E., 1989. Nature and extent of groundwater contamination by pesticides

in an agricultural watershed. Water Res., 23:1031-1037.

Rayne, T., 1993. Variability of hydraulic conductivity in a sandy till: the effect of scale and method. Ph.D. Dissertation, Department of Geology and Geophysics, University of Wisconsin-Madison, Madison, WI, 134 pp.

Saltzman, S. and Mingelgrin, U., 1984. Nonbiological degradation of pesticides in the unsaturated zone. In: B. Yaron, G. Dagan and J. Goldschmidt (Editors), Between Soil Surface and Groundwater, Springer-Verlag, Berlin, pp. 153-161.

Schiavon, M., 1988a. Studies of the leaching of atrazine, of its chlorinated derivatives, and of hydroxyatrazine from soil using 14C ring-labeled compounds under outdoor conditions. Ecotoxicol. Environ. Safety, 15:46-54.

Schiavon, M., 1988b. Studies of the movement and the formation of bound residues of atrazine, of its chlorinated derivatives, and of hydroxyatrazine in soil using ^{14}C ring-labeled compounds under outdoor conditions. Ecotoxicol. Environ. Safety, 15:55-61.

Snedecor, G.W. and Cochran, W.G., 1980. Statistical Methods. The Iowa State University Press, Ames, IA, 507 pp.

Starr, J.L. and Glotfelty, D.E., 1990. Atrazine and bromide movement through a silt loam soil. J. Environ. Qual., 19:552-558.

Wehtje, G., Mielke, L.N., Leavitt, J.R.C. and Schepers, J.S., 1984. Leaching of atrazine in the root zone of an alluvial soil in Nebraska. J. Environ. Qual., 13:507-513.

Wisconsin Agricultural Statistics Service, 1991. Pesticide use: Wisconsin 1991. Wisconsin Agricultural Statistics Service, Madison, WI, 31 pp.

II. Simulation of Atrazine and Metabolite Transport and Fate in a Sandy-till Aquifer

ABSTRACT

A one-dimensional contaminant transport model was developed in FORTRAN incorporating major chemical processes and allowing variable groundwater velocity and dispersion along the simulated flow path. The flow paths correspond to those predicted as part of a 2.5-yr field study of the distribution of atrazine and its metabolites in groundwater. Flow paths are predominantly downward at piezometer nests where vertical hydraulic gradients dominate. Simulations of atrazine and desethylated atrazine transport and fate at individual piezometer nests are made with groundwater velocity profiles incorporating measured variation of hydraulic conductivity from piezometer to piezometer and assuming a logarithmic interpolation of hydraulic conductivity between piezometers. Regression equations were developed, based on an extensive literature review, to estimate acceptable sorption and dispersivity coefficients for the transport model. The one-dimensional simulations were calibrated using the concentration/travel-time relationships established previously for atrazine and desethylated atrazine. The calibration procedure provides estimates of atrazine and desethylated atrazine degradation rates in groundwater, thereby allowing an assessment of the impact of long-term residue leaching on groundwater quality and establishing possible rates of residue dissipation if residue movement to groundwater ceased.

INTRODUCTION

Atrazine [2-chloro-4-ethylamino-6-isopropylamino-*s*-triazine] was registered for use on corn in Wisconsin in 1960 and in 1990 was still the most widely used herbicide on corn and the second most widely used on sweet corn (Wisconsin Agricultural Statistics Service, 1991). As of 1989 atrazine accounted for 12% of all U.S. pesticide use with applications of 34 to 41 million kg yr^{-1} (Belluck et al., 1991).

Detection of atrazine in U.S. groundwater occurs 10 to 20 times more frequently than any other pesticide and has been detected in 25 states. Most detections have occurred in groundwater underlying coarse-textured soils, although evidence is accumulating that atrazine leaching also occurs in medium- and fine-textured soils. Based on a statewide survey, the Wisconsin Department of Agriculture, Trade and Consumer Protection determined with 95% confidence that 9 to 15% of the state's private farm wells contained atrazine-contaminated water. Contamination occurred under a variety of geological and pedological conditions (LeMasters and Doyle, 1989).

Atrazine is considered a "possible human carcinogen" based on the incidence of mammary tumors in female rats. The U.S. EPA estimates that at 3 ppb, consumption of drinking water poses a lifetime cancer risk of 1 in 100,000 (Belluck et al., 1991). In 1992, Wisconsin included three chlorinated metabolites of atrazine (desethylated atrazine or DEAT, desisopropylated atrazine or DIAT and diamino-chloro-*s*-triazine or DIAM) in the state's groundwater standards for atrazine after concluding that their biological effects from exposure were similar to those of atrazine. The frequency of violations of these groundwater standards drives Wisconsin's regulatory action.

A 2.5-yr field study was conducted in a 4.1 km^2 area of Dane County, Wisconsin, U.S.A. to investigate the distribution of atrazine and its metabolites in a shallow sandy-till aquifer (part of the Horicon formation) overlain by silt loam soils and underlain by a Cambrian sandstone aquifer from which area residents get their water (Levy et al., 1993). At eight piezometer nests, downward hydraulic gradients dominated horizontal gradients. At those nests, groundwater-flow paths to individual wells were predicted to originate at the water table near the well nest. Estimates of groundwater travel times (TTs) along those paths were estimated and ranged from 2 mo to 24 yr. Concentrations of atrazine residues and ratios of metabolites to parent compound at individual monitoring wells were compared to the estimated TTs. Time-averaged concentrations of atrazine and DEAT decreased with increases in estimated TT, indicating dissipation of both compounds in the aquifer. The concentration ratio of DEAT:atrazine did not increase with estimated TT suggesting that while DEAT might form rapidly in near-surface soils (Muir and Baker, 1978; Frank and Sirons, 1985) atrazine degradation to DEAT is not a major process in the sandy-till aquifer. Concentrations of DIAT and DIAM were not significantly related to aquifer TT, but ratios of DIAT and DIAM to the concentrations of the parent compounds increased with increased TT. These relationships were weak but suggested that some degradation of atrazine to DIAT and possibly of DEAT and atrazine to DIAM is occurring in groundwater. These degradation pathways at least partially explain the observed dissipation of atrazine and DEAT with time

spent in the aquifer (Levy et al., 1993).

The analytical and numerical estimates of travel paths and times made by Levy et al. (1993) applied to groundwater movement only and encompassed only the advective component of atrazine residue transport. Dispersion and chemical reactions were not incorporated. Together with advection, these processes control the threat that residues present to groundwater quality. The transport and fate of atrazine and DEAT is simulated herein using a one-dimensional computer model to recreate and explain the previously established relationships. Such a model calibration addresses the question as to whether those relationships can be explained with reasonable estimates of chemical transport parameters. In addition, the model-calibration process can be used to make estimates of the model parameters with perhaps the greatest associated uncertainty: the atrazine and DEAT degradation rates. Calibrated model-parameter values can help predict the long-term impact of groundwater contamination by atrazine.

CONCEPTUAL MODEL, GOVERNING EQUATION AND NUMERICAL APPROACH

A one-dimensional model was developed to simulate flow and transport at individual piezometer nests where downward hydraulic gradients were dominant. Since flow is predominantly downward, the model's entry point represents the water table and its exit is some point below the bottom of the deepest piezometer. Included in the model are advection, dispersion, sorption and degradation of sorbed and dissolved phases. The model numerically solves the one-dimensional mass balance advection-dispersion equation:

$$n\frac{\partial C}{\partial t} + \rho\frac{\partial \bar{C}}{\partial t} = nD\frac{\partial^2 C}{\partial x^2} - nv\frac{\partial C}{\partial x} - nk_1 C - \rho k_2 \bar{C} \qquad (17)$$

where C and $\bar{C}$ are concentrations in the dissolved and sorbed phases ($\mu g\ mL^{-1}$ and $\mu g\ g^{-1}$), n is aquifer porosity (unitless), ρ is aquifer bulk density ($g\ cm^{-3}$), D is the coefficient of hydrodynamic dispersion ($cm^2\ sec^{-1}$) and is the sum of mechanical dispersion and molecular diffusion (d_f), v is average linear

groundwater velocity (cm sec^{-1}) and k_1 and k_2 are pseudo first-order degradation rates for dissolved and sorbed phases (sec^{-1}). Mechanical dispersion (for one dimension) is v times the effective longitudinal dispersivity, A_l (in cm), of the medium. Freeze and Cherry (1979) suggest a molecular diffusion coefficient for major ions in coarse-grained unconsolidated materials of $1x10^{-6}$ to $2x10^{-5}$ cm^2 sec^{-1} at 25°C. A value of $1x10^{-5}$ cm^2 sec^{-1} for atrazine was assumed for the model. In all model runs, the diffusion coefficient has a negligible role. $\bar{C}$ is eliminated from Eq. 17 by incorporating equilibrium sorption conditions relating C and $\bar{C}$. The Freundlich isotherm is used most often to describe atrazine sorption:

$$\bar{C} = K_f C^a \tag{18}$$

and therefore:

$$\frac{\partial \bar{C}}{\partial t} = aK_f C^{a-1} \frac{\partial C}{\partial t} \tag{19}$$

where K_f and a are empirical constants. Sorption causes an apparent retardation in the solute relative to groundwater. Using a Freundlich isotherm and equilibrium conditions, the retardation factor (R_f) is related to K_f, a and the concentration, C, of the compound:

$$R_f = 1 + \frac{\rho}{n} a K_f C^{a-1} \tag{20}$$

Making the substitution in Eqs. 18 and 19, and dividing the equation by the retardation factor given in Eq. 20, Eq. 17 reduces to:

$$\frac{\partial C}{\partial t} = \frac{(A_l v + d_f)}{R_f} \frac{\partial^2 C}{\partial x^2} - \frac{v}{R_f} \frac{\partial C}{\partial x} - \frac{k_1}{R_f} C - \frac{\rho}{n} \frac{k_2}{R_f} K_f C^a \tag{21}$$

Eq. 21 was solved with finite-difference methods using a forward-in-time, centered-in-space,

Crank-Nicolson approach (Huyakorn and Pinder, 1983). The two-step iterative predictor-corrector method was used to handle the C^{a-1} term (Eq. 20) and the C^a term (Eq. 21). The entry boundary representing the water table was modeled as a third-type boundary in which the solute flux across the boundary is specified as vC_0, where C_0 is the constant solute concentration in water just outside the model boundary. This boundary condition simulated incoming recharge at a constant concentration. At the exit, a second-type boundary was simulated in which the concentration gradient is 0. Detailed description of the finite difference approximations of the governing equations used in the model are presented in Levy (1993, Appendix H).

Since one purpose of the modeling was to explain the relationships of atrazine and DEAT concentrations to estimated TTs, the groundwater flow was simulated in such a way as to mimic the analytical approach taken to estimate TTs to the monitoring wells (Levy et al., 1993). In that approach, K_v values and, therefore, vertical velocities were calculated at individual piezometers; velocities between piezometers were interpolated assuming a smooth geometric progression. A similar approach was used in the numerical model, but using only two specified velocities. The velocities at the first and last model cells are specified and velocities at all other cells are geometrically interpolated. The velocity within a cell is constant in space and time. For most model runs, 500 cells ranging in length from 0.006 to 0.03 m were used, making the differences in velocity from cell to cell too small to handle numerically. Therefore, the model domain was divided into a user-specified number of velocity zones (usually 50 of thickness 0.3 m), each with constant velocity, and the velocity interpolation applied to the zones rather than the cells. For those piezometer nests with only two slug test K measurements, the velocity fields generated in the analytical and numerical models are nearly identical. For nests with more than two K measurements, first and last cell velocities were chosen so that the effective velocity to the deepest piezometer was equal in both cases. The mechanical component of the dispersion coefficient, $A_l v$, also varies between velocity zones according to v. The model domain is homogenous with respect to ρ

(estimated as 1.6 g cm^{-3}), n, A_l, K_f, a, k_1 and k_2. For simplicity, the porosity (n) and effective porosity (n_e) are assumed equal. The Fortran code is described in Levy (1993, Appendix H).

CHEMICAL TRANSPORT PARAMETER ESTIMATION

Dispersivity

Hydrodynamic dispersion is the mixing process by which solutes spread out relative to the path expected from the average velocity, causing solute dilution. The advective component of dispersion is proportional to the groundwater velocity and is caused by tortuosity, variability of velocities and variability of pore sizes at the microscopic scale (Freeze and Cherry, 1979). Since these causes are properties of the porous medium they are classically incorporated in a constant defined as dispersivity. In actuality, however, dispersivity has an apparent scale dependence in which field-observed dispersion coefficients are orders of magnitude greater than those from laboratory column studies (Gelhar and Axness, 1983). The scale dependence has been explained deterministically by assuming aquifer stratification (Molz et al., 1983), fractal geometry (Wheatcraft and Tyler, 1988) and/or hydraulic conductivity (K) heterogeneity (Gelhar and Axness, 1983). To estimate an appropriate dispersivity for the Horicon till at the scale of interest, two independent methods are undertaken.

Gelhar and Axness (1983) provide a method for estimating the effective or macroscale dispersivity tensor (A_{ij}) based on a statistical description of the log K field given a variety of field conditions. For the simplest case of a statistically isotropic (log K correlation scale, λ, is the same in all directions), unstratified medium in which microdispersivity lengths are small compared to λ, effective dispersivity in the direction of flow (A_{11}) is related to log K variance (σ_f^2) and λ:

$$A_{11} = \sigma_f^2 \lambda / \gamma^2 \qquad (22)$$

where γ is a flow factor which for the isotropic case equals $1 + \sigma_f^2/6$. Since the model in this chapter

is one-dimensional, only A_{11} is of interest. Given the sparsity of the field data, Eq. 22 is used to produce only a general approximation of effective dispersivity. The one-dimensional model simulates transport at individual piezometer nests at a scale of $\leq$ 12 m. Variograms were made using hydraulic conductivity data from all wells and piezometer nests (Levy, 1993), but most of the constituent data pairs are between, not within nests. Therefore, the variogram applies to a much larger scale than the one of interest. Using only the 31 pairs of ln K values from piezometers within the same nest, σ_f^2 is estimated to be 2.6. However, there is an insufficient number of points for constructing a variogram. Rayne (1993) installed many piezometers in the Horicon till at two different field sites. Slug tests were performed at 25 and 26 locations at the two sites, with a maximum three-dimensional separation distance of 12 m. Combining the sites (but only considering pairs of measurements from within the same site) allows construction of a variogram with 625 pairs (Fig. 10). The variogram does not yield a precise estimate of λ, but a value of 2.5 to 6 m seems reasonable. (Fig. 10 includes a possible spherical variogram model.) The population σ_f^2 is estimated to be 0.52. Applying these values to Eq. 22 gives an effective dispersivity of between 1.1 and 2.6 m.

A second method of estimating an appropriate effective dispersivity is to base the estimate on previous studies. To do this effectively, it is important to determine which study sites have controlling features similar to those at the study site. Gelhar et al. (1992) provide a table of dispersivity measurements for 59 different field sites including many site characteristics; they assigned a rank of high, intermediate or low reliability to each field measurement. Using only those dispersivities from the table ranked with high or intermediate reliability regression analyses were performed to investigate relationships between site characteristics and reported dispersivities (Levy, 1993). The regression analysis indicated that longitudinal macrodispersivity (A_l, equivalent to A_{11} in the Gelhar and Axness, (1983) analysis) increases with increasing scale and the range of measured K values and decreasing effective porosity (n_e). That dispersivity increases with increasing scale has already been discussed. The relationship to the range

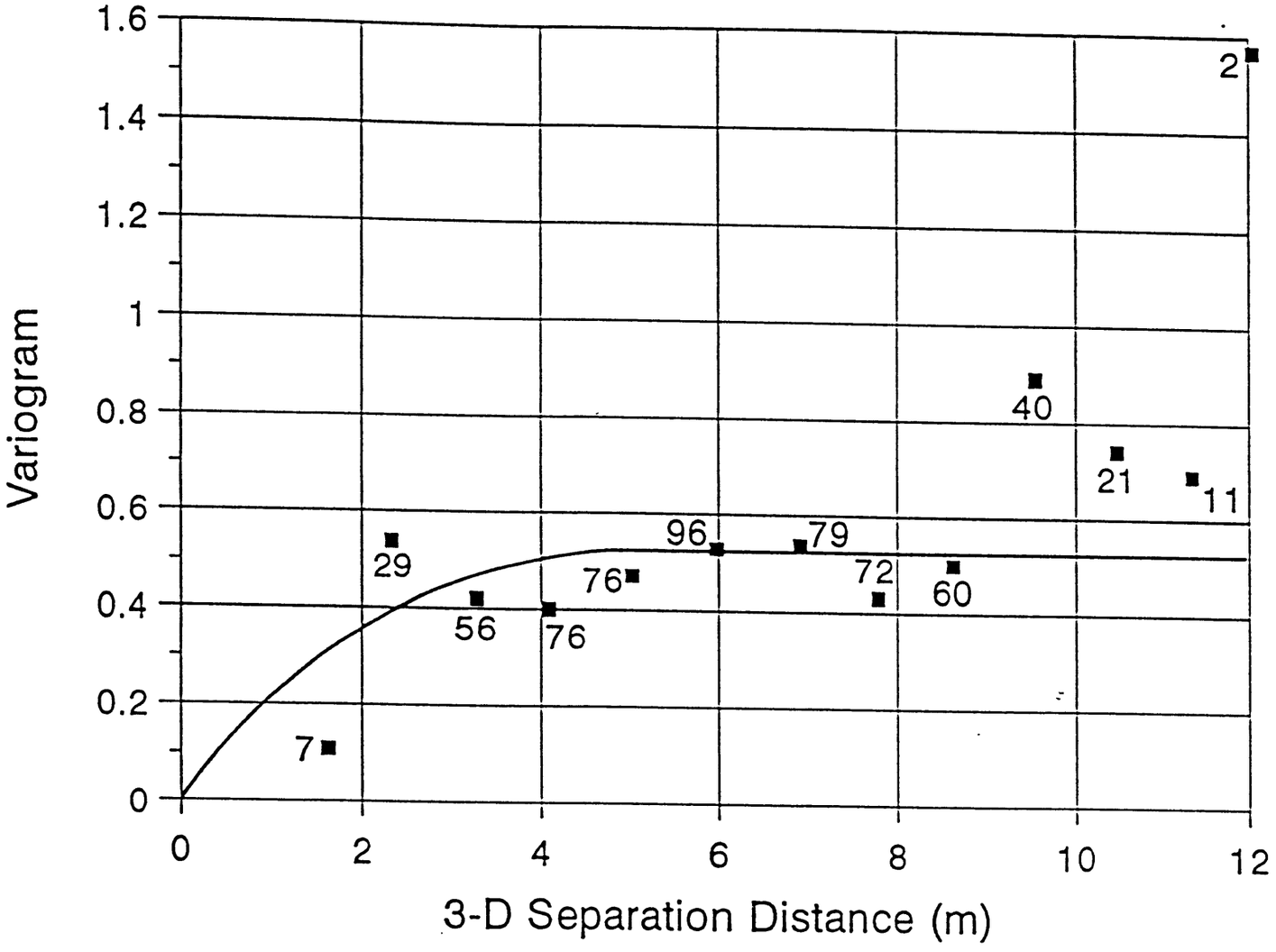

Fig. 10. Variogram of natural log, Horicon till hydraulic conductivity. Data are from Rayne (1993). Distances are three-dimensional separation distances. A possible spherical variogram model is shown. Values next to the points indicate the number of pairs used.

of measured K values makes sense since the larger the K range the larger the σ_f^2. Poorly sorted material can be expected to have smaller n_e values and increased dispersivity due to increased microscopic flow tortuosity and variable velocities. Many regression models were explored with untransformed and log-transformed parameter values; the one that best described the above relationships is:

$$\ln(A_l) = -0.37 + 0.027(K\ Range) - 9.0(n_e) + 0.55\ \ln(Scale),\quad R^2 = 0.69\ on\ 9\ df \qquad (23)$$

where df is degrees of freedom for the regression equation, and K Range is the maximum K:minimum K. K Range, n_e and ln(scale) are significant at p=0.046, 0.014 and 0.025, respectively. The full regression model is significant at p=0.003. The geometric mean of K Range values from individual well nests was 10.2; n_e was estimated at 0.15 (Levy et al., 1993). The maximum scale of interest is 20 m, corresponding to a large saturated till thickness. Using these values in Eq. 23 yields A_l = 1.4 m. Removing K Range from the regression model allowed inclusion of data from many more experiments. Although the new model has a lower R^2 value, it has many more degrees of freedom, resulting in decreased prediction uncertainty:

$$\ln(A_l) = -0.73 - 6.1(n_e) + 0.66\ \ln(Scale) \qquad R^2 = 0.45\ on\ 21\ df \qquad (24)$$

In this model n_e and ln(scale) are significant at p=0.015 and 0.001 and the full model is significant at p=0.001. Based on Eq. 24, A_l = 1.4 m. There is still great uncertainty associated with this estimate based on the uncertainty of the regression model and the parameter values used in the model. Although uncertain, the regression model predictions agree closely with the estimate using Eq. 22 and data from Rayne (1993) and was assumed to be a reasonable estimate.

Sorption Coefficients

Multiple regression analyses were employed to choose appropriate model sorption coefficients.

Through an exhaustive literature search of atrazine and metabolite laboratory soil-sorption experiments, a table was compiled with sorption coefficients and certain soil characteristics (Levy, 1993 -- Appendix I). The characteristics included organic matter (OM) and clay contents and aquifer pH, all factors related to atrazine sorption and measurable at the field site. The multiple regression analyses were intended to provide not only reasonable coefficients for this study, but as general equations that could be applied to a broad range of conditions and locations. For that reason, cation exchange capacity (CEC) was included even though it was not measured at the site. However, it was not an important variable. The table (Levy, 1993 -- Table I-1) includes data from 35 investigations, some of which measured Freundlich coefficients, K_f and a, and some measured a linear coefficient K_d assuming that a = 1. K_f and K_d values have been combined in the regression analyses with the assumption that had the experimenters measured the exponent, it would have been 1 and, therefore, the K_d values are actually the K_f values. The units of all measurements were considered the same even though the units for K_f vary according to the Freundlich exponent. Three of the 35 studies measured sorption coefficients for one or more atrazine metabolites. Those data allow comparison of atrazine and metabolite sorbability.

Regressions were performed on a subset of data considered more representative of the Horicon till. That subset excluded organic soils (peats and mucks) and those soils with clay contents > 27 %: clays, silty clays, sandy clays, clay loams and silty clay loams. Sorption increases with increasing OM and clay contents and decreasing pH. The best regression model is:

$$K_f = 1.3 + 0.57(OM) + 0.039(\%Clay) - 0.19(pH), \quad R^2 = 0.66 \text{ on } 104 \text{ } df \qquad (25)$$

OM and clay contents and pH were significant at $p<0.001$, $p=0.006$ and $p=0.031$, respectively. The full model was significant at $p<0.001$. Based on the borehole sample analyses (Levy, 1993 -- Appendix C), the average OM and clay contents and pH for the till are 0.19%, 8.27% and 7.23% yielding an average K_f of 0.37.

The Freundlich exponent for the atrazine sorption isotherm was determined in 15 laboratory investigations. In the subset of mineral soils with clay content < 27%, the mean value is 0.89 with a 95% confidence interval between 0.87 and 0.92.

Based on seven comparisons on the same soils, the sorption coefficient for DEAT was proportional to that for atrazine:

$$K_f\ DEAT = 0.091 + 0.35(K_f\ Atra) \qquad R^2 = 0.86\ on\ 5\ df \tag{26}$$

significant at p=0.002. The intercept of in Eq. 26 is not significantly different from 0 (p=0.41). When the regression is forced through the origin, the relationship is:

$$K_f\ DEAT = 0.39(K_f\ Atra) \tag{27}$$

significant at p<0.001. Using a paired-experiment analysis and a significance level of p=0.05 (Snedecor and Cochran, 1980), the Freundlich exponent for atrazine was not significantly different from that for DEAT. The average DEAT exponent was 0.87.

Degradation Rate

As with sorption, a literature search of atrazine degradation laboratory experiments was used to compile a table of pseudo first-order degradation rates and the characteristics of the media from which the degradation rates were derived (Levy, 1993 -- Table I-3). In most of these experiments, degradation rates were based on the disappearance rate of atrazine and no effort was made to distinguish between rates of individual metabolite formation. Multiple regression analyses were employed to quantify the relationships between atrazine degradation and soil characteristics so that appropriate transport model pseudo first-order degradation rates could be selected given the characteristics from the Horicon till. The characteristics included OM and clay contents, pH and temperature. Data from all 21 experiments

indicate that the atrazine degradation rate (k in day^{-1}) increases with decreasing pH and increasing temperature (T in °C) within the ranges of pH and T used:

$$\ln(k) = -3.2 - 0.33(pH) + 0.031(T); \qquad R^2 = 0.15 \text{ on } 78 \text{ } df \tag{28}$$

The coefficients for pH and T are significant at $p=0.003$ and $p=0.011$, respectively and the full model is significant at $p=0.001$. The low R^2 value indicates that most of the variability remains unaccounted for. On the subset of mineral soils with clay content < 27%, k was significantly related only to T, and the relationship had an intercept not significantly different from 0. When forced through the origin and weighted with the inverse of the squared temperatures to remove heteroscedasticity (Chatterjee and Price, 1977), the regression model is:

$$k = 0.00061(T) \tag{29}$$

significant at $p<0.001$. The average pH of borehole samples is 8.27 and the average groundwater temperature at the field site is 9.9°C. These values yield a degradation rate of 0.0039 and 0.0060 day^{-1} for Eqs. 28 and 29, respectively; the degradation rates correspond to half-lives of 178 and 115 days.

The sorption and degradation experiments were almost all conducted on unsaturated surface soils. For sorption, the extrapolation of the regression models to deeper aquifer material is assumed to be reasonable because the factors most affecting sorption are accounted for. For degradation, however, the microbial population is a variable rarely measured in laboratory experiments, not measured at the field site and not accounted for in the regression models. Since the microbial population is likely related to depth and degree of saturation, extrapolation of Eqs. 28 and 29 is not reasonable. Evidence suggests that the atrazine degradation rate in deeper and saturated media may be much slower than indicated by the regression models. Perry (1990), Sinclair and Lee (1992) and Weidner (1974) suggest an atrazine half-life in groundwater of 1,000 days or much greater, corresponding to a degradation rate of < 0.00069

day^{-1}. The degradation rate is therefore initially left unspecified and is used as a calibration parameter in the one-dimensional transport model.

Sorption can catalyze chemical hydrolysis of atrazine while inhibiting microbial degradation (Armstrong and Chesters, 1968). The sorbed and dissolved phases are, therefore, likely to have different degradation rates. However, because little information exists regarding differences between those rates, they are modeled as equal. Keeping both processes in the model is useful, nonetheless, as it allows determination of their relative impact on model results.

MODEL CALIBRATION AND RESULTS

As established in Levy et al. (1993) and quantified by regression equations, average atrazine and DEAT concentrations at the monitoring wells decrease with estimated groundwater travel times (TTs) to those wells:

$$\ln(Avg.\ ATRA) = 3.1 - 0.72 \ln(TT), \quad R^2 = 0.54 \text{ on } 25 \text{ df} \tag{30}$$

$$\ln(Avg.\ DEAT) = 3.5 - 0.64 \ln(TT), \quad 25 \text{ df} \tag{31}$$

Both regression models are significant at $p < 0.001$, even though the R^2 value in Eq. 30 indicates that TT does not account for all variability in concentrations. The R^2-value for Eq. 31 is not shown because a weighted least squares regression was used with weights equal to the inverse squared ln(TT) values. The weighted regression method was used to remove heteroscedasticity from regression errors (Chatterjee and Price, 1977).

The dissipation with time indicated by Eqs. 30 and 31 can be explained by chemical and microbial degradation. Assuming long-term, steady-state leaching of atrazine residues, dissipation through degradation implies that the measured concentrations have reached steady-state and will not get bigger

with time. Water from sampling points with long associated TTs will, on average, always have low concentrations. On the other hand, if little or no degradation is occurring in the aquifer, the decrease in concentrations with time can still be explained by assuming that the main part of the contaminant front has yet to arrive at the more distant (in a time sense) points. Low concentrations could result from the arrival of the dispersive head of the front. This situation implies that concentrations throughout the system will continue to increase with atrazine use and that over time, concentrations in deeper private wells will increase to the levels presently found in shallow monitoring wells. Establishing reasonable model parameters that explain the concentration-TT relationships is crucial to predicting the long-term threat of atrazine residues to area groundwater.

Model calibration pertains to atrazine and DEAT only. Similar modeling of the other metabolites requires more relevant laboratory and field data and is left for future work. The objective of the model calibration is not to match atrazine simulated and measured concentrations exactly at individual piezometer nests, but rather to find realistic model parameters that recreate the general relationships between concentration and estimated TTs represented by Eqs. 30 and 31. All model parameters except velocity are held constant from piezometer nest to piezometer nest and within nests. Matching the general relationship provides a way of investigating under what conditions the velocity differences between the piezometer nests adequately explain the range and distribution of concentrations measured in the field. Even the atrazine and DEAT input concentrations are held constant during this exercise. It is assumed that atrazine is being leached to the water table at the same rate everywhere and over time. The calibration objective is to use the regression-derived sorption and dispersion coefficients and find input concentrations and degradation rates that yield distributions of long-term atrazine and DEAT concentrations that relate to groundwater velocities in the same way that the measured concentrations were previously shown to do.

Calibration is a trial-and-error process in which the model is run for each piezometer nest for a

simulated period of 35 yr, approximating the length of time of atrazine use. The simulated concentrations at the end of 35 yr are noted for each piezometer. To compare their distribution with measured concentrations, the simulated concentrations are treated as if they were real. The analysis of concentrations versus the estimated TTs is then repeated with the simulated concentrations plotted against estimated TTs. Simulated concentrations < 0.01 ppb would actually be unmeasurable and are treated as analytically not detected. Just as was done for measured concentrations, substitutions are made for the nondetected values based on the analytical uncertainty (Levy et al., 1993). The model is considered calibrated when the simulated concentrations yield a relationship to estimated TTs similar to the relationships in Eqs. 30 and 31. The simulated concentrations are not random data, so formal regression analyses do not apply. However, for the purpose of deciding when the concentration-travel time relationships are similar enough, the best-fit slope and intercept using the simulated concentrations are compared with those from Eqs. 30 and 31. The model is considered calibrated when the best-fit slope and intercept from the simulated concentrations are within two standard deviations of the regressed slopes and intercepts from Eqs. 30 and 31.

Many unsuccessful efforts were made to match the concentration-TT relationships with no degradation by adjusting sorption coefficients, dispersivity and input concentrations within reasonable ranges. Some degradation was necessary to make a match. With sorption coefficients and dispersivity back to the regression-based values, the calibration criteria are met for atrazine when the input concentration at the water table is 1.6 ppb and the degradation rate in the dissolved and sorbed phase is 0.00035 day^{-1}. Such a degradation rate corresponds to a half-life of 1,980 days. The comparison of the relationships of the measured and simulated atrazine concentrations to estimated groundwater travel times is shown in Fig. 11a; best-fit regression lines also are shown. The regression line through the measured concentrations is represented by Eq. 30. The deviations of the simulated concentrations from a smooth curve result from differences in simulated velocity fields between piezometer nests. If the simulated

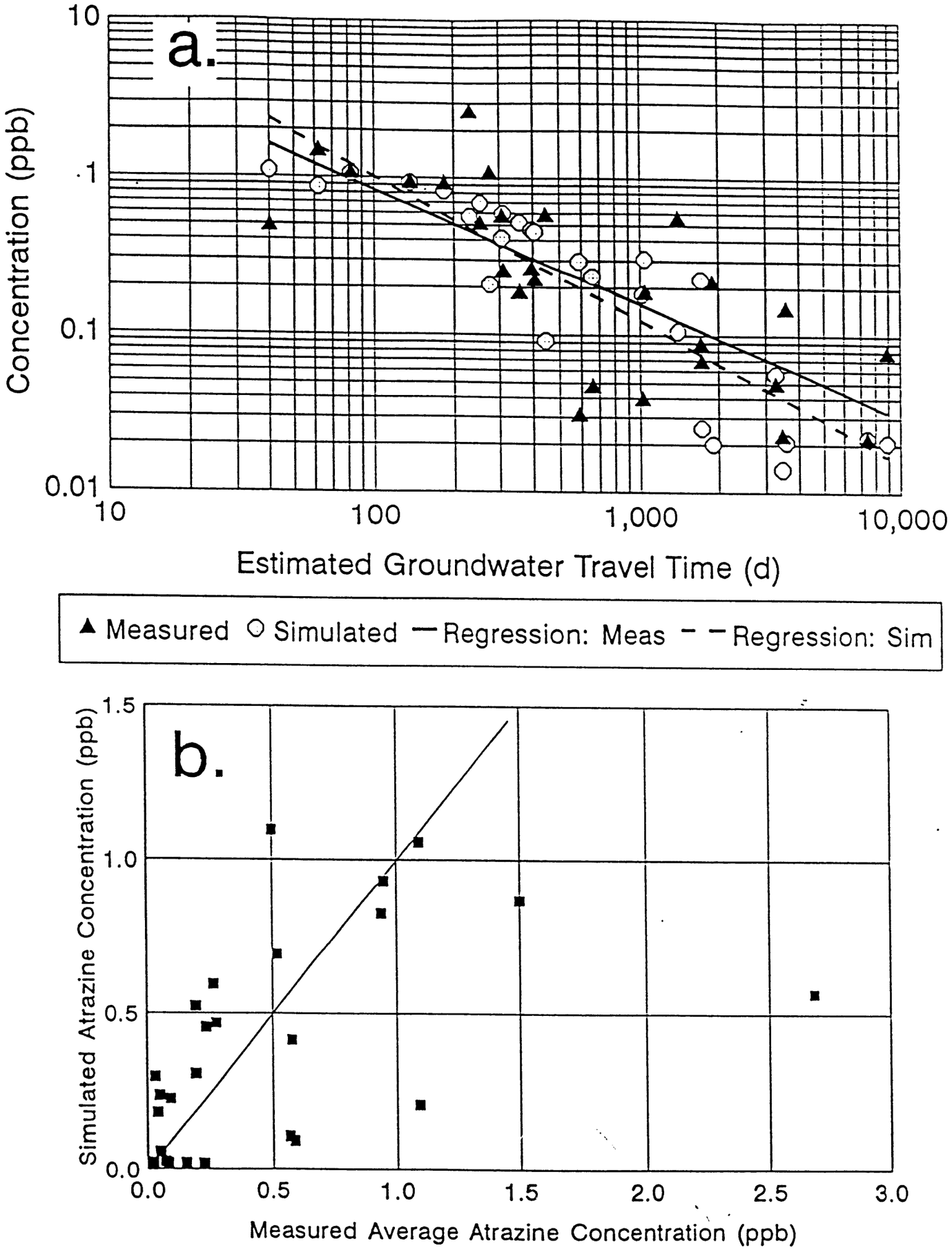

Fig. 11. Comparison of (a) relationships of the simulated and measured atrazine concentrations to analytically-estimated groundwater travel times and (b) comparison of simulated and measured concentrations at individual piezometers.

concentrations < 0.01 ppb were plotted, it would be clear that the linear log-log model is inappropriate. The simulated concentrations drop more rapidly at longer travel times than does the linear log-log model. It is possible that if smaller concentrations were detectable, the linear log-log model for the measured concentrations would prove equally inadequate.

Fig. 11b compares simulated and measured concentrations at individual piezometers and demonstrates that this kind of match was not the calibration goal. The line indicating a perfect match is shown for comparison. There is general agreement of concentrations, with the exception of one outlier corresponding to well K6.A where the average measured concentration is much higher than the simulated one. The lack of agreement at K6.A exemplifies the problem of individual matches. Given the modeling conditions of a steady-state, homogeneous input at the water table, a higher concentration at K6.A than at the shallower piezometer K6.D cannot be simulated. To match individual piezometer concentrations, the input concentrations and timings at the water table would have to be different at each piezometer nest. Such a calibration is purely academic without knowing input histories at each location and goes beyond the purposes of this exercise.

The implications of the calibrated model parameter values are exemplified by breakthrough curves at piezometers K6 and K5 (Fig. 12) where groundwater velocities are among the fastest and slowest simulated. These nests were chosen as examples because their measured concentrations were among the highest and lowest observed, respectively. In these simulations, input to the water table was stopped completely after 35 yr to explore how fast concentrations at different depths will dissipate. Due to degradation, steady-state concentrations at all piezometers are reached within approximately 20 yr after the start of the input at the water table, indicating that concentrations at deeper wells are not expected to rise as time goes by. The wells in which a steady-state concentration is not reached in 20 yr are those with such long associated travel times that the predicted concentrations after 35 yr are < 0.01 ppb. Differences in simulated concentrations between piezometers of similar depths are due solely to the

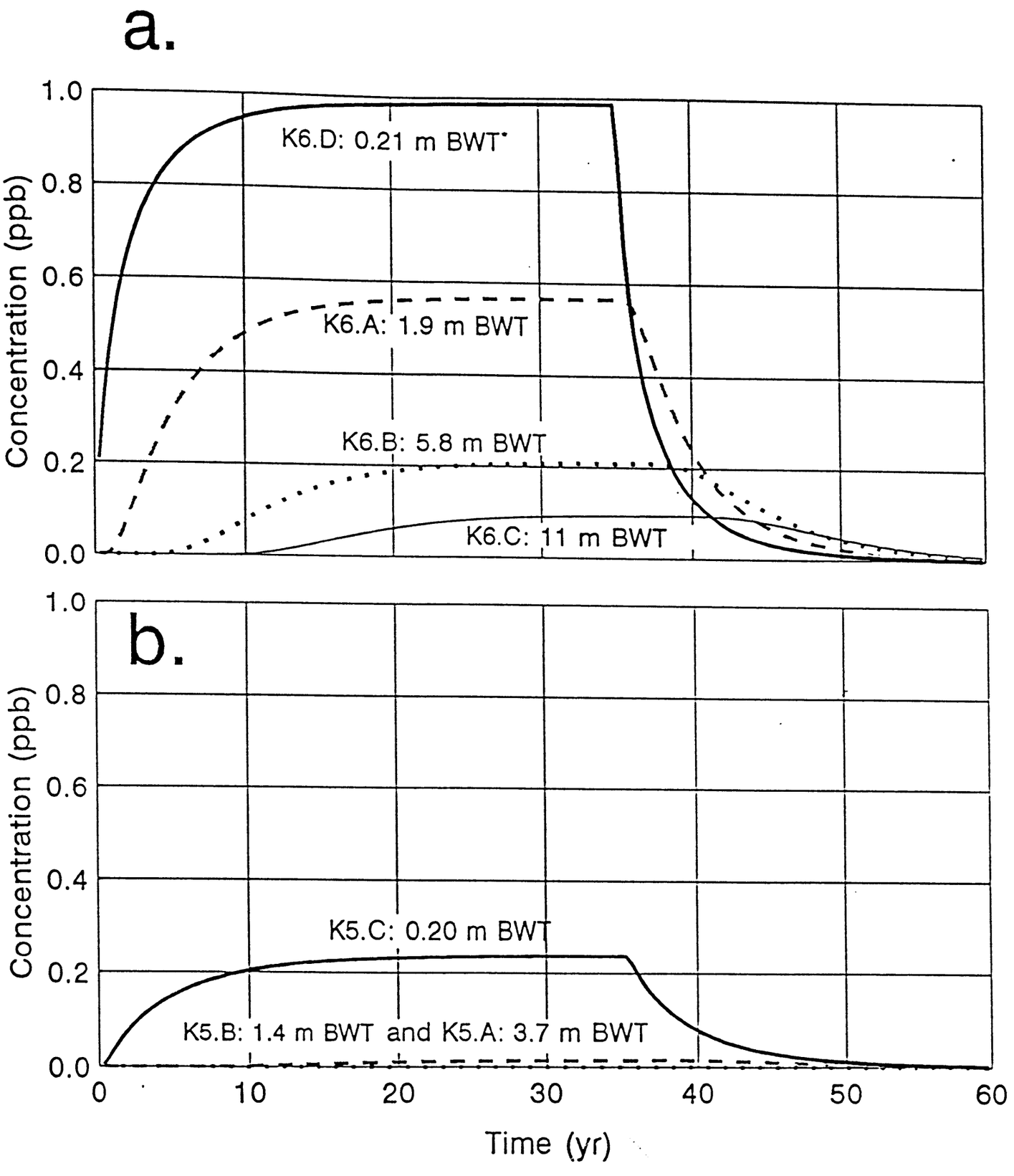

*BWT is below the water table

Fig. 12. Simulated atrazine concentrations (ppb) at piezometer nests (a) K6 and (b) K5 given 35 yr of recharge contaminated with 3.0 ppb atrazine followed by a cut off of the source.

velocity differences at each nest. When input to the water table stops, concentrations dissipate most quickly at the shallower wells due to advection. Because degradation is slow, concentrations would still be measurable in most piezometers even 10 yr after input stops. Concentrations at deeper piezometers, where concentrations are initially lowest, dissipate very slowly. For example, K6.B and K6.C concentrations drop to half their steady-state concentrations in 10 and 15 yr, respectively. For the simulations at all individual piezometers, the times for concentrations to decrease to half their steady-state values ranged from 1.5 to 36 yr and averaged 9 yr.

DEAT has a lower average sorption coefficient than atrazine and yet shows a similar relationship of concentration to estimated groundwater travel time. For simulated DEAT concentrations to match the relationship given a smaller K_f value, a higher input concentration and/or degradation rate is required. A higher degradation rate implies that although DEAT is more mobile and DEAT contamination is more widespread than that of atrazine, it may not pose as great a long-term risk. The same method of calibration of the one-dimensional transport model as that used for atrazine was performed with respect to DEAT. The input concentration and dissolved and sorbed phase degradation rates were manipulated until simulated concentrations had a relationship to estimated TTs that was similar to the relationship in Eq. 31. Using a K_f value of 0.14 and an exponent of 0.87, the calibrated input concentration and degradation rate are 2.8 ppb and 0.00055 day^{-1}, corresponding to a half-life of 1,260 d. The relationship match is shown in Fig. 13a; the regression line through the measured values is the one represented by Eq. 31. The match at individual piezometers (not the calibration goal) is shown in Fig. 13b with the line of equality for comparison. The set of points with the highest measured concentrations represent the four shallowest piezometers at one of the multilevel-sampling units. The simulated DEAT breakthrough curves for piezometers in nests K6 and K5 using the calibrated model parameters are shown in Fig. 14. (Note the scale for piezometer nest K6 is twice as large as that for K5.) Compared to atrazine (Fig. 12), steady state concentrations for DEAT are higher and reached as much as 10 yr sooner. Dissipation of

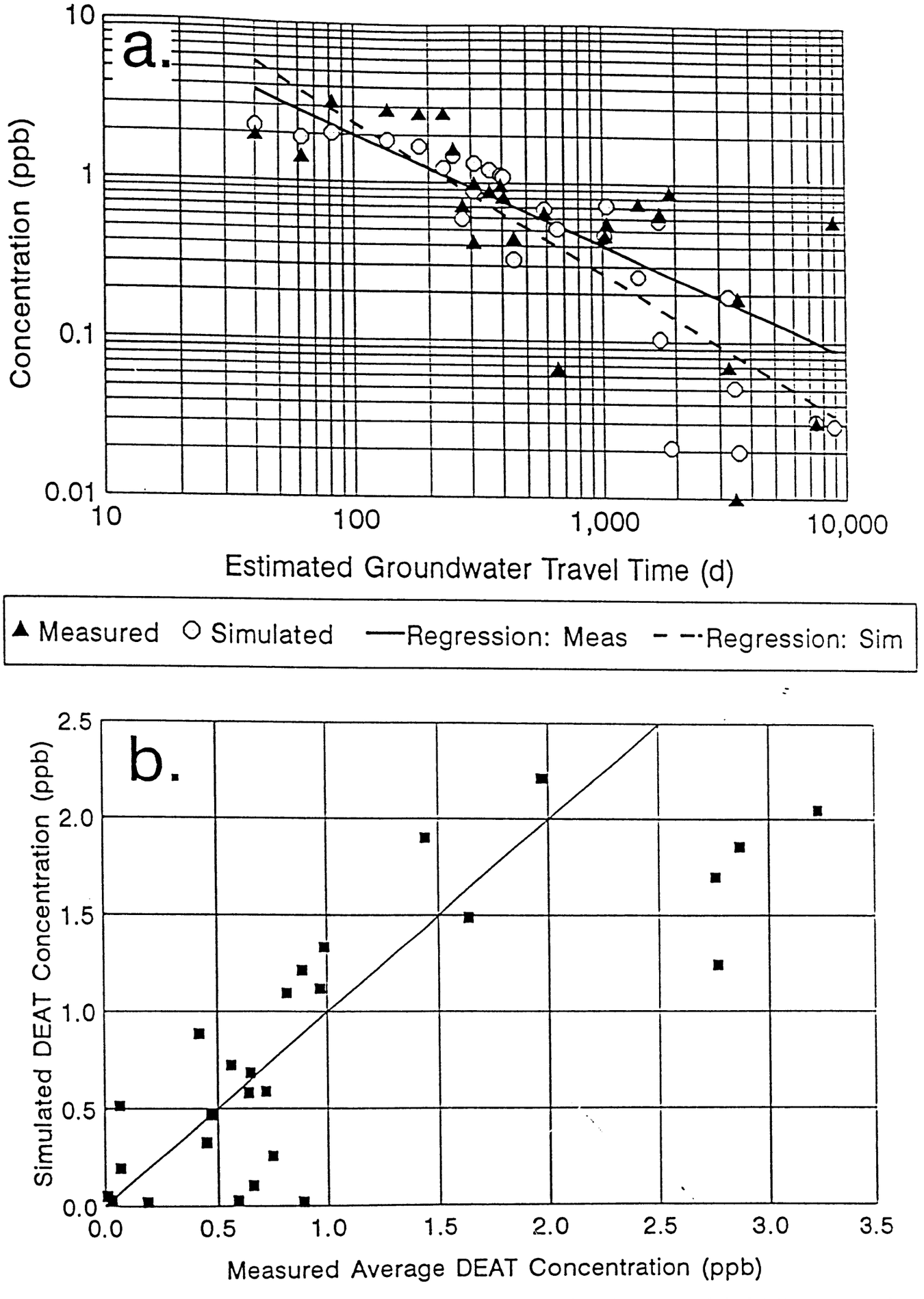

Fig. 13. Comparison of (a) relationships of the simulated and measured DEAT concentrations to analytically-estimated groundwater travel times and (b) comparison of simulated and measured concentrations at individual piezometers.

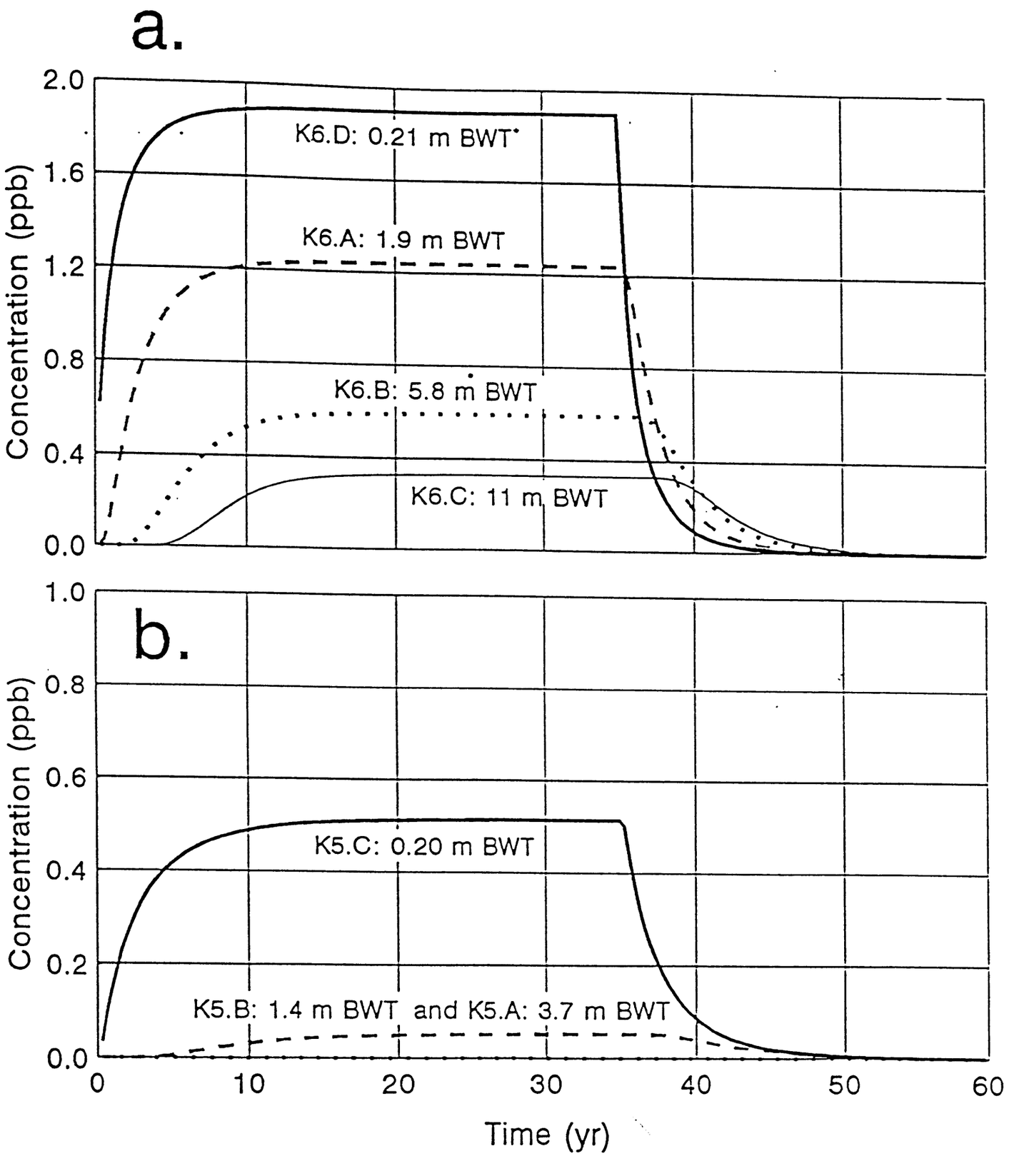

*BWT is below the water table

Fig. 14. Simulated DEAT concentrations (ppb) at piezometer nests (a) K6 and (b) K5 given 35 yr of recharge contaminated with 3.0 ppb DEAT followed by a cut off of the source.

DEAT concentrations after input to the water table stops occurs more quickly than dissipation of simulated atrazine concentrations; for all simulations, the times for concentrations to decrease to half their steady-state values ranged from 0.81 to 22 yr with an average of 5.4 yr.

Due to a deficiency of model input information for DIAT and DIAM, their fate and transport are not simulated. However, the lack of evidence of DIAT and DIAM dissipation with groundwater travel time indicates that of all atrazine residues, those compounds may pose the greatest long-term risk to area drinking water (Levy et al., 1993).

The calibrated atrazine and DEAT parameter values are not unique. With nine variables -- A_l, v, d_f, K_f, a, k_1, k_2, ρ and n -- it is probable that another set of values could produce a match at least as good as the one presented here. Still, the model used the literature-based best estimates of sorption and dispersivity and the calibrated input concentrations and degradation rates are reasonable values. Elsewhere we will use the parameter values in a three-dimensional transport model along with their inherent uncertainty to make model predictions with quantifiable uncertainties.

SUMMARY AND CONCLUSIONS

Relationships exist between average atrazine concentrations at piezometers within nests where downward hydraulic gradients exist and groundwater travel times to those piezometers have been estimated. A one-dimensional chemical transport model was developed to simulate atrazine and DEAT movement and fate at the piezometer nests to determine what reasonable parameter values explain those relationships. The transport model includes the processes of sorption using a Freundlich isotherm and degradation of both the dissolved and sorbed phases assuming pseudo first-order kinetics. Given an entry and an exit groundwater velocity, the model uses a geometric interpolation to calculate velocities at all interior model cells. The variable velocity model was used to mimic the way in which groundwater travel times to piezometers were estimated analytically (Levy et al., 1993).

Sorption coefficients and effective dispersivity estimates were based on multiple regression analyses of literature data from other groundwater studies and laboratory experiments. Variables were found that were related to sorption coefficients and dispersivity, regression models were formulated and measured field values from the study site were entered into those models to make predictions for reasonable transport model parameter values. Degradation rates and input concentrations were left as calibration parameters.

The model was run for each piezometer nest and corresponding velocity field. It was calibrated by choosing input concentrations and degradation rates that produced a set of simulated concentrations with a relationship to groundwater travel times similar to the ones established for atrazine and DEAT. Since input histories at each piezometer nest are unknown, no effort was made to match individual piezometer concentrations with their simulated counterparts. The calibrated atrazine input concentration and degradation rate were 1.6 ppb and 0.00035 day^{-1}, corresponding to a half-life of 1,980 days. For DEAT, the calibrated input concentration and degradation rate were 2.8 ppb and 0.00055 day^{-1}, corresponding to a half-life of 1,260 days. Even with these slow degradation rates, given a constant long-term source at the water table, non-negligible concentrations at all piezometers reach a steady-state condition within about 20 yr. Assuming the simulated degradation rate is a reasonable estimate of the true value, concentrations at deeper piezometers and bedrock wells are not expected to increase substantially over time due to continued atrazine use. DIAT and DIAM do not seem to dissipate with aquifer travel time (Levy et al., 1993) and may prove to be greater long-term threats to area drinking water quality. However, the slow atrazine and DEAT degradation rates result in long dissipation times even after all input to the water table has stopped. Atrazine and metabolite detections and groundwater-standard violations in water from private farm wells are widespread in Wisconsin. As of 1993, in response to the violations, The Wisconsin Department of Agriculture, Trade and Consumer Protection has placed about 32,000 ha in Atrazine Management Areas, where maximum application rates of atrazine

are reduced, and over 500,000 ha in Atrazine Prohibition Areas, where atrazine use is not allowed. The simulations discussed here indicate that even in an atrazine prohibition area, in which, optimistically (a best-case scenario), all leaching through the unsaturated zone stops, it may take more than 10 yr before concentrations at deeper wells drop to half of what they were during the period of atrazine use. A provision of the Wisconsin's atrazine legislation (AG 30, Wisconsin Administrative Code) calls for a review of the atrazine provisions in 1996 by evaluating the success of atrazine rules in attaining and maintaining compliance with the groundwater standards. Regulators and legislators need to consider that in many pedologic and geologic settings, 2 to 5 yr may not be sufficient to make an accurate assessment of the long-term effects of altered atrazine application rates or prohibition.

REFERENCES

Armstrong, D.E. and Chesters, G., 1968. Adsorption catalyzed chemical hydrolysis of atrazine. Environ. Sci. and Technol., 2:683-689.

Belluck, D.A., Benjamin, S.L. and Dawson, T., 1991. Groundwater contamination by atrazine and its metabolites: risk assessment, policy, and legal implications. In: J.R.L. Somasundaram, and J.R. Coats (Editors), Pesticide transformation products: fate and significance in the environment, ACS Symp. Ser. 459. American Chemical Society, Washington, D.C., pp. 254-273.

Chatterjee, S. and Price, B., 1977. Regression analysis by example. John Wiley and Sons, New York, NY.

Freeze, R.A. and Cherry, J.A., 1979. Groundwater. Prentice-Hall, Inc., Englewood Cliffs, NJ, 604 pp.

Gelhar, L.W. and Axness, C.L., 1983. Three-dimensional stochastic analysis of macrodispersion in aquifers. Water Resour. Res., 19:161-180.

Gelhar, L. W., Welty, C. and Rehfeldt, K.R., 1992. A critical review of data on field-scale dispersion in aquifers. Water Resour. Res., 28(7):1955-1974.

Huyakorn, P.S. and Pinder, G.F., 1983. Computational methods in subsurface flow. Academic Press, Inc., Orlando, FL.

LeMasters, G. and Doyle, D.J., 1989. Grade A dairy farm well water quality survey. Wisconsin Department of Agriculture, Trade and Consumer Protection/Wisconsin Agricultural Statistics Service, Madison, WI, 36 pp.

Levy, J., 1993. A field and modeling study of atrazine transport and fate in groundwater. Ph.D. Dissertation, Land Resources Program, Institute for Environmental Studies, University of Wisconsin-Madison, Madison, WI, 561 pp.

Levy, J., Chesters, G., Read, H.W. and Gustafson, D.P., 1993. Distribution, sources and fate of atrazine in groundwater: a field study. J. Contam. Hydrol. 00: 000-000.

Molz, F.J., Guven, O. and Melville, J.G., 1983. An examination of scale-dependent dispersion coefficients. Ground Water, 21:715-725.

Perry, C.A., 1990. Source, extent and degradation of herbicides in a shallow aquifer near Hesston, Kansas. U.S. Geol. Surv. Water-Resources Invest. Rep. 90-4019, U.S. Gov. Print. Office, Washington, DC, 24 pp.

Rayne, T., 1993. Variability of hydraulic conductivity in a sandy till: the effect of scale and method. Ph.D. Dissertation, Department of Geology and Geophysics, University of Wisconsin-Madison, Madison, WI, 134 pp.

Sinclair, J.L. and Lee, T.R., 1992. Biodegradation of atrazine in subsurface environments. EPA/600/S-92/001. Environmental Research Brief. U.S. Environmental Protection Agency, 8 pp.

Weidner, C.W., 1974. Degradation in groundwater and mobility of herbicides. M.S. Thesis. University of Nebraska, Lincoln, NE, 69 pp.

Wheatcraft, S.W. and Tyler, S.W., 1988. An explanation of scale-dependent dispersivity in heterogeneous aquifers using concepts of fractal geometry. Water Resour. Res., 24:566-578.

Wisconsin Agricultural Statistics Service, 1991. Pesticide use: Wisconsin 1991. Wisconsin Agricultural Statistics Service, Madison, WI, 31 pp.

III. Simulation of Groundwater Flow with the use of Geostatistical Methods for Model Calibration

ABSTRACT

A 33-month field study was conducted on a 4.1 km^2 site in a dairy-farming area in Wisconsin, U.S.A., to evaluate the sources and distribution of the herbicide atrazine and its metabolites in groundwater and to relate contaminant distribution to the groundwater-flow system. As a first step toward this objective, the groundwater-flow system was simulated in three dimensions. A method is developed by which calibration targets are statistically determined before beginning the calibration process. The method includes quantification of uncertainty. Geostatistics and kriging play a central role in development of calibration targets. Sensitivity analyses demonstrate how improvements in calibration of one target are made at the expense of worsening calibration of other targets. Using pre-determined calibration targets guides the selection of the best set of calibration parameters.

INTRODUCTION

A field investigation was conducted at a 4.1 km^2 site in south-central Wisconsin, U.S.A., to study the sources and distribution of atrazine and its metabolites in a shallow sandy-till aquifer overlying a sandstone aquifer which serves as a local source of drinking water. One objective was to relate contaminant distribution to the groundwater-flow field. The relationships between atrazine and metabolite concentrations and the groundwater-flow system are described in Levy et al. (1993). They provide insight into atrazine and metabolite degradation processes and rates and were incorporated into one-dimensional contaminant transport simulations at individual piezometer-nest sites to predict the long-term impact of atrazine use on groundwater quality (Levy and Chesters, 1993). For similar predictions at the field scale, three-dimensional modeling is necessary to incorporate the spatial variability of depth to bedrock and account for the hydrologic effects of local surface water bodies. One component of a three-dimensional contaminant-transport modeling effort is the three-dimensional simulation of groundwater flow. In this paper, a methodology is discussed for establishing calibration targets for calibration of the flow model.

A flow model must accurately reproduce field-measured hydraulic heads and flows. Ideally,

calibration should be accomplished by finding a set of parameter values, boundary conditions and stresses so that the simulated heads and fluxes match the field-measured values within a preestablished range of error (Anderson and Woessner, 1992). The calibration value and its associated uncertainty is defined as the calibration target (Anderson and Woessner, 1992). Establishing calibration targets before beginning the calibration process is rarely done and depends on quantification of the uncertainty associated with the measured values.

In this paper, sources of calibration-value uncertainty are discussed and methods are proposed for their quantification. Forward (trial-and-error) calibration of the flow model is performed for the field site and the goodness-of-fit of the calibration is examined in terms of the predetermined calibration targets.

SITE HYDROGEOLOGY AND CONCEPTUAL MODEL

The groundwater-flow model was based on a conceptual model of the hydrogeologic system developed from the geologic and hydrogeologic information described in Levy et al. (1993). Monitoring wells were installed at 25 locations and included water-table wells, piezometer nests, piezometers installed through a creek bed and multilevel samplers (Fig. 15). The geology in the study area consists of two hydrostratigraphic units (Fig. 16). The upper unit, a sandy till, is part of the Horicon Formation of undifferentiated Quaternary deposits. No bedding planes were observed in split-spoon samples. Typical grain-size distribution is 65 to 75% sand, 15 to 30% silt and 1 to 15% clay. Pebbles and cobbles were found up to 20 cm in diameter. Within the monitoring area, till thickness ranges from < 7 m overlying a bedrock drumlin to > 40 m overlying a bedrock valley near Waunakee Marsh. Throughout most of the monitored area, bedrock comprises various Cambrian sandstones containing dolomite and shale (Cline, 1965; Ostrom, 1967). The sandstone aquifer extends to the Precambrian bedrock surface at about 47 m above mean sea level (msl), a thickness of 190 to 235 m.

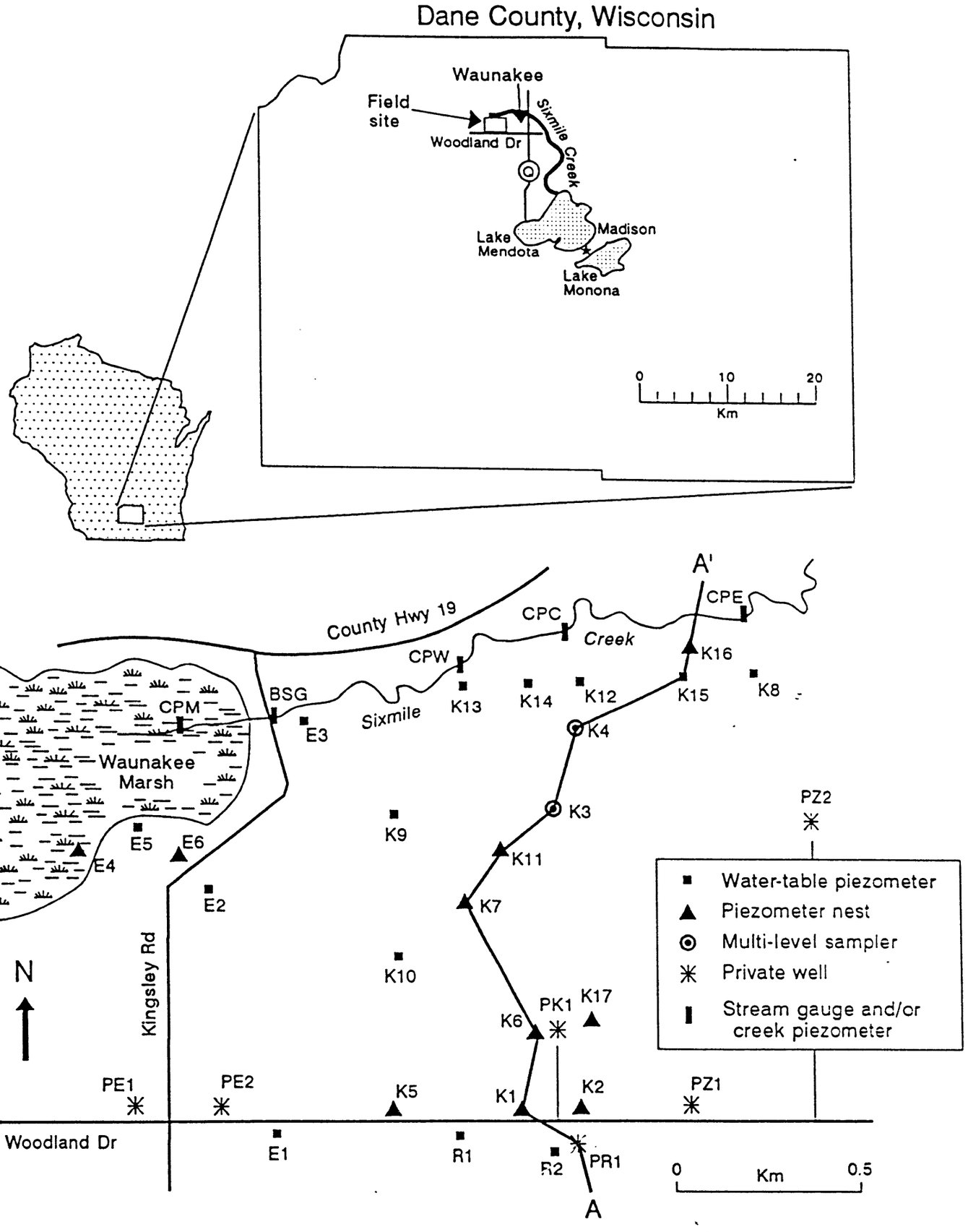

Fig. 15. Monitoring area and well locations. The transect A-A' corresponds to the geologic cross section shown in Fig. 2.

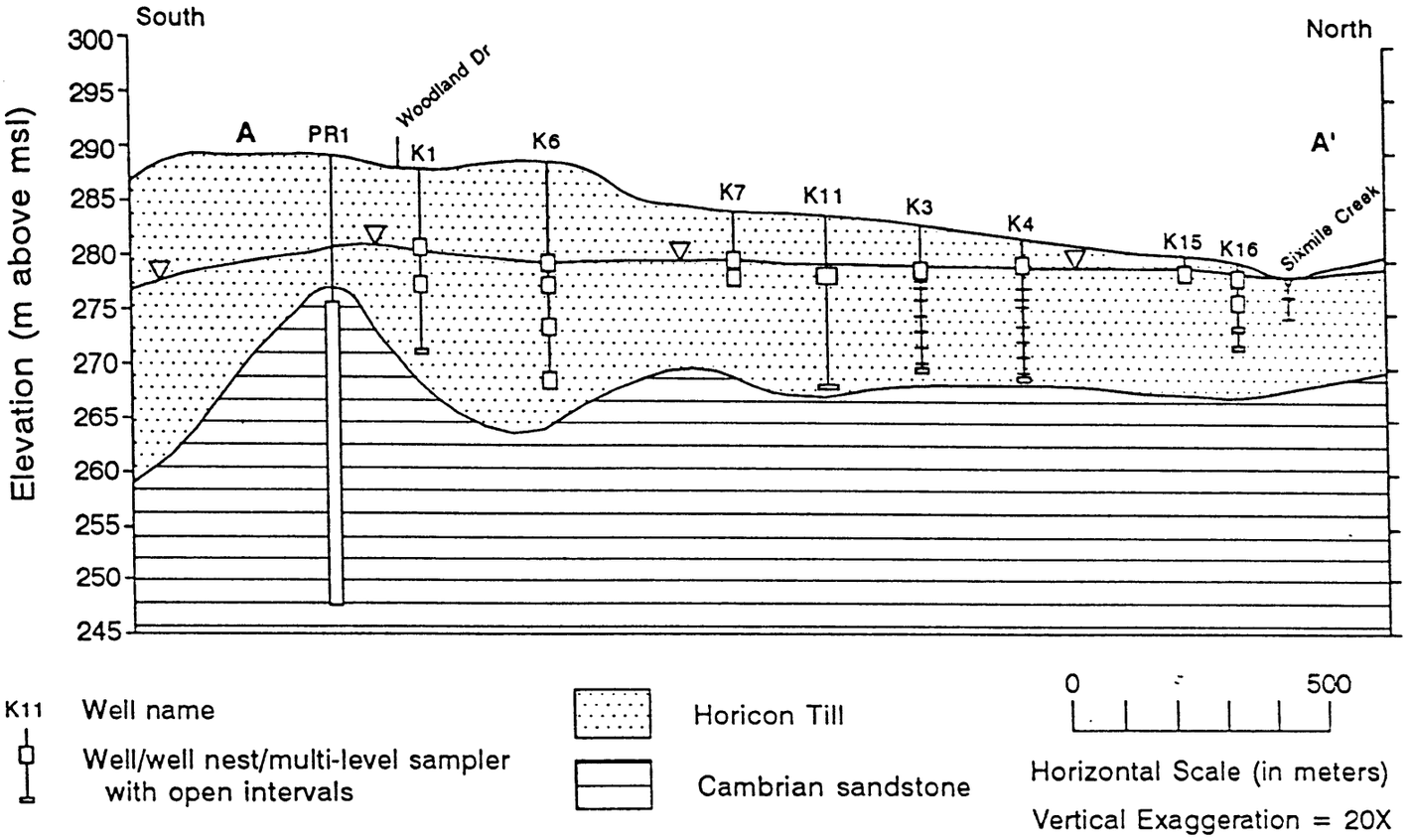

Fig. 16. Generalized geology along cross section A-A' (transect shown in Fig. 15).

Potentiometric surface maps constructed with 217 private well-drilling logs and 11 private-well head measurements indicate a regional groundwater divide located 5 to 7 km northwest of the study area separating groundwater flowing east and south into the Yahara River basin and north and west to the Wisconsin River. Regional flow through the bedrock aquifer in the monitoring area is southeasterly with a gradient of 0.0033. Lake Mendota and associated creeks and marshes 6 to 7 km to the southeast are the likely discharge areas for the regional flow system.

Water-table mapping based on monitoring wells indicates a complex, shallow flow system affected by surface topography, drainage features, recharge patterns and variations in hydraulic conductivity. In areas of bedrock highs, the water table is in the sandstone and the sandstone aquifer is unconfined. Representative water-table and cross sectional potentiometric-surface maps are shown for August 1991 (Fig. 17). Water recharges most of the study area as indicated by downward gradients at most piezometer nests; vertical hydraulic gradients are much greater than horizontal gradients over most of the study area (Fig. 17b). Upward hydraulic gradients are found near and in Sixmile Creek and Waunakee Marsh, which act as groundwater discharge areas. Based on the equipotential contours (Fig. 17b) and measured groundwater seepage rates into Sixmile Creek, the discharge area to Sixmile Creek and Waunakee Marsh extends only 100 to 150 m to each side. Within that area, water from the till discharges into the surface-water bodies. It is unlikely that Sixmile Creek, Waunakee Marsh or Dorn Creek (1.6 km to the south of Woodland Drive) are hydrologic boundaries to regional flow within the sandstone.

Statistical information regarding hydraulic conductivities and fluxes played an integral part in model calibration and are therefore presented here. Hydraulic conductivity of the till aquifer was measured with piezometer slug tests (Bouwer and Rice, 1976). Conductivities were distributed approximately log-normally with a mean of 1.2×10^{-4} cm/sec and a 95% confidence interval of 6.7×10^{-5} to 2.3×10^{-4} cm/sec. Bedrock hydraulic conductivities were calculated based on specific capacity data

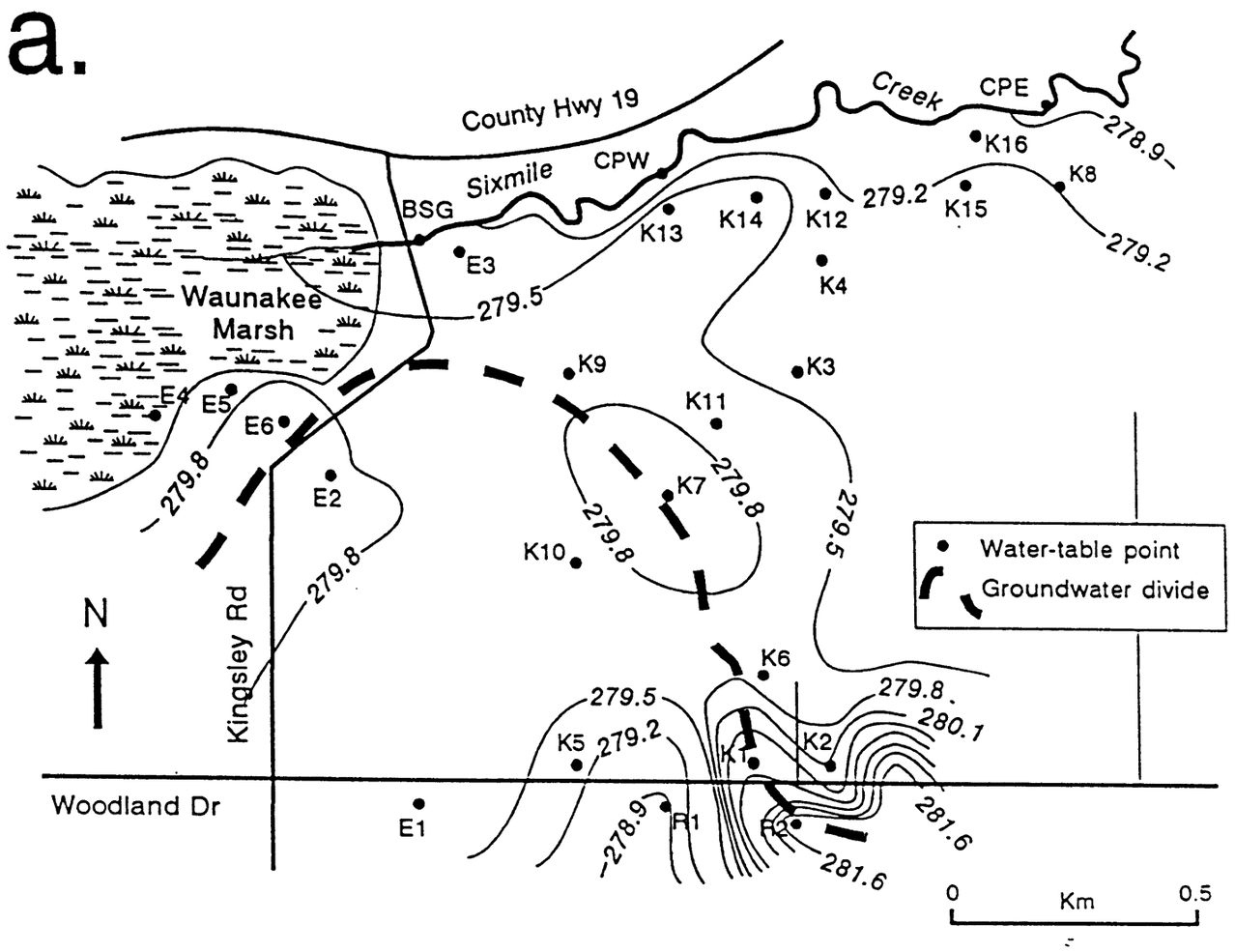

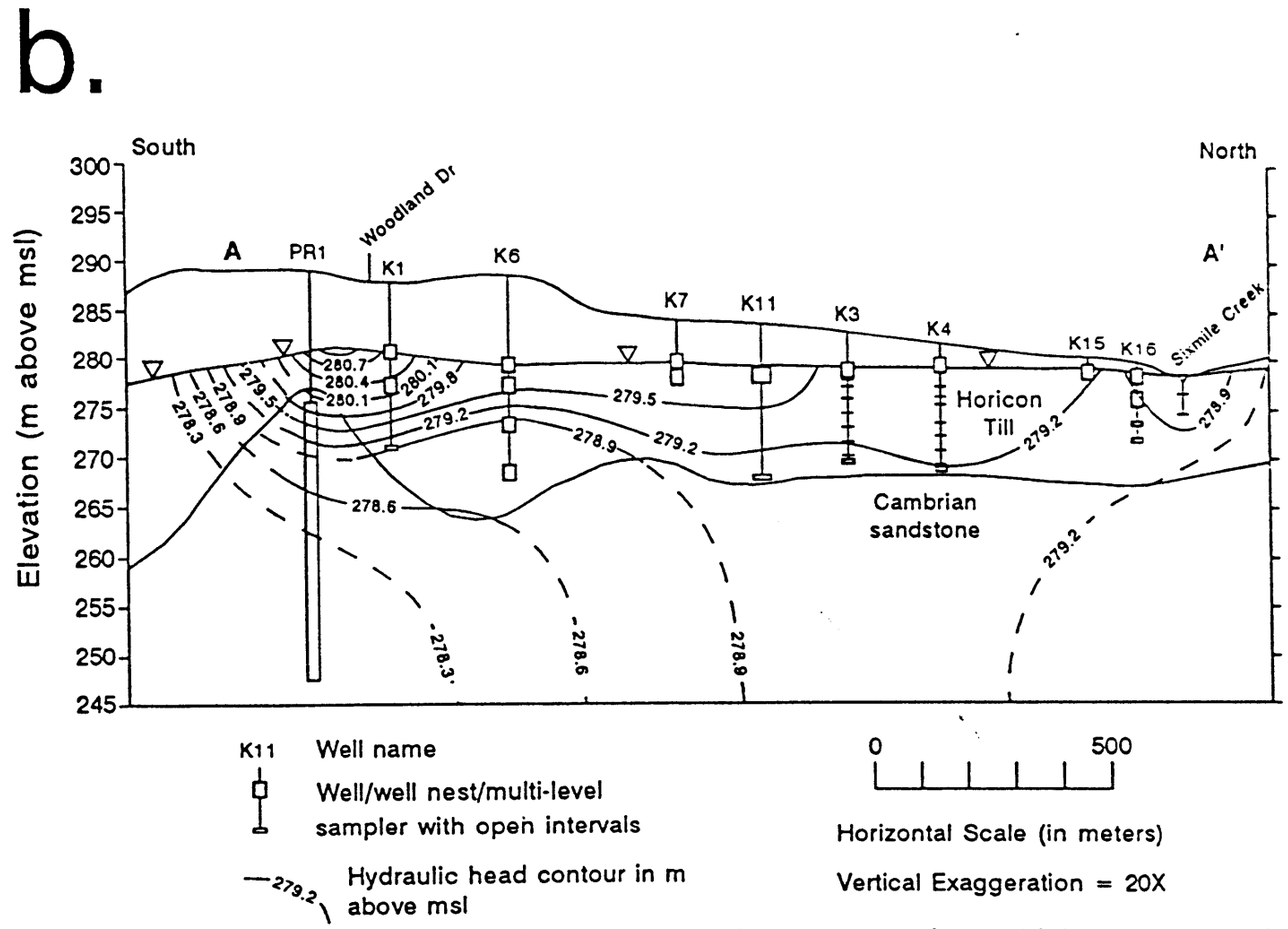

Fig. 17. a) Water-table elevations and b) hydraulic head along cross section A-A' (transect shown in Fig. 1) in August 1991. Contour interval is 0.3 m. Dashed contours indicate greater uncertainty.

from private well logs using the computer program TGUESS (Bradbury and Rothschild, 1985). Bedrock conductivities were log-normally distributed with a mean of 3.5×10^{-3} cm/sec and a 95% confidence interval of 2.5×10^{-3} to 4.9×10^{-3} cm/sec. Vertical hydraulic conductivities (K_v) were determined from the measured horizontal hydraulic conductivity (K_h) and an assumed horizontal to vertical hydraulic conductivity anisotropy ratio (K_h:K_v). Estimates of K_h:K_v can be obtained from analyses of time-drawdown curves from aquifer pumping tests. No pumping tests were performed at this site, but Rayne (1993) performed two pumping tests in the Horicon Formation at a site 22 km to the southeast. Time-drawdown data from those tests were analyzed to estimate K_h:K_v values at this site. Analyses were performed with a computer program, AQTESOLV (Duffield and Rumbaugh, 1989), according to the method for delayed yield in unconfined aquifers with partially penetrating pumping and observation wells (Neuman, 1975). The K_h:K_v estimates for 19 observation wells were distributed approximately log-normally with a geometric mean of 2.8 and a 95% confidence interval between 1.7 and 4.6.

Recharge is likely to be spatially variable due to surface drainage and ponding patterns. No irrigation is used in the area. Three municipal wells finished in the Cambrian sandstone serve the village of Waunakee, about 2 km east of the monitoring area. There are seven private wells within the monitoring area, two serving private residents and five serving dairy farms.

FLOW MODEL DESCRIPTION AND INITIAL PARAMETER-VALUE SELECTION

The groundwater flow system was modeled under steady-state conditions with MODFLOW (McDonald and Harbaugh, 1984), the modular three-dimensional groundwater flow model developed by the U.S. Geological Survey (USGS). The steady-state assumption was appropriate given the objective of simulating long-term atrazine residue movement. The system is not heavily stressed by municipal pumping and drawdown and it is assumed that flow conditions have not substantially changed since the advent of atrazine use. The modeling was intended to address questions concerning atrazine transport

across such distances as the water table to the bedrock surface or to private wells. Groundwater velocities are slow enough that flow across these distances takes years to decades. Therefore, although hydraulic heads and gradients fluctuate seasonally, these fluctuations are probably less important than average heads and gradients over a period of years. Target heads were based on measured heads averaged over the study period and pumping and recharge rates were assumed constant and estimated based on averaged values.

The model area and boundaries are shown in Fig. 18. Although only two hydrostratigraphic units are represented, the modeled saturated thickness is divided into six continuous layers to ensure enough detail to simulate vertical groundwater flow. The bottom of Layer 6 corresponded to the Cambrian sandstone-Precambrian bedrock contact.

The model area is divided into 50 columns and 31 rows so that each layer has a total of 1,550 cells. Grid spacing is finest within the monitoring area, where cells are squares of 61.0 m on a side. Cell lengths and widths gradually increase from the monitoring area to the model boundaries so that the largest cells are squares of 305 m on a side. Water-table elevations across the model area vary from about 286.5 to 271.3 m above msl.

Model boundaries ideally coincide with regional hydrologic boundaries, but in this case, the model area would have had to stretch from the regional groundwater divide to the northwest of the study area to Lake Mendota to the southeast. Alternative boundaries were chosen in order to simulate flow in the study area in sufficient detail (Fig. 18). The southwest corner of the model area coincides with a regional potentiometric surface high determined by regional mapping. Streamlines were inferred emanating from this high toward Waunakee Marsh to the north and Dorn Creek to the east. The streamlines were modeled as no-flow boundaries in all layers. The southeastern model boundary consists of the 271.2 m equipotential contour that connects Dorn and Sixmile Creeks and was modeled as a specified-head boundary in all active layers.

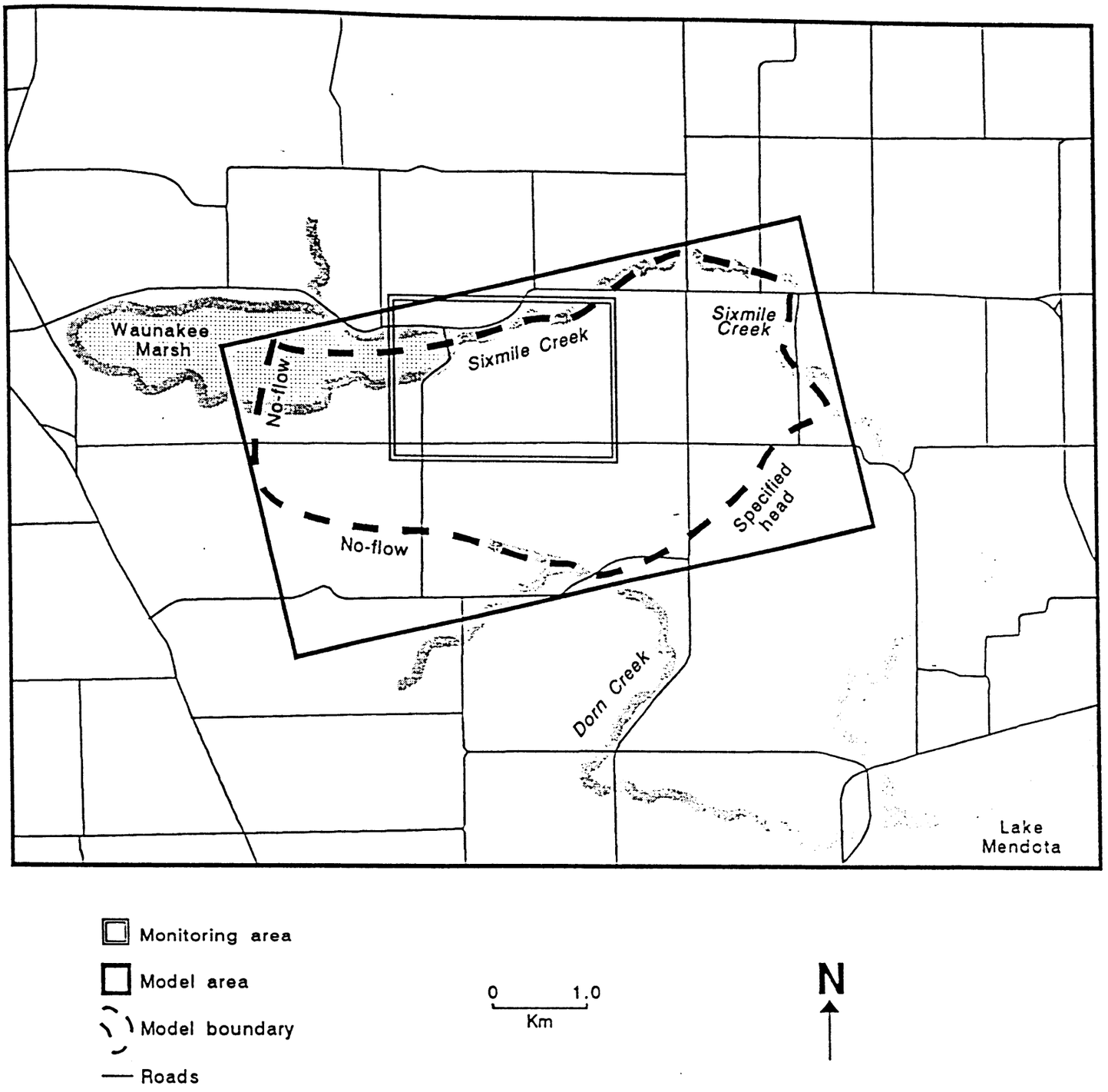

Fig. 18. Model area with model boundaries and monitoring area.

Waunakee Marsh and Sixmile Creek form the northern model boundary (Fig. 18) and Sixmile Creek forms most of the eastern boundary. The marsh and creek were modeled as head-dependent boundaries using MODFLOW's river package. Sediment conductivity estimates were based on slug tests and seepage meter measurements (Levy, 1993). The mean creek bed hydraulic conductivity was 4.2×10^{-5} cm/sec with a 95% confidence interval of 3.4×10^{-6} to 5.2×10^{-4} cm/sec. Only relatively shallow water close to the creek and marsh discharge to those bodies. Deeper water moves downward joining the regional groundwater flow. Therefore, underflow into and out of the model area occurs at a certain depth below the creek and marsh. To simulate this condition, cells two or more layers below the creek and boundary marsh cells were simulated as specified-head boundaries. Dorn Creek forms part of the southern model boundary (Fig. 18) and was modeled in the same way as Sixmile Creek.

Horizontal hydraulic conductivity (K_h) model values for the sandstone aquifer were based on specific capacity data from 234 private wells. Kriging was used to interpolate values between wells. Kriging of all hydraulic conductivities was performed on log-transformed data assuming stationarity and using the geostatistical package Geo-Eas, version 1.2.1 (Englund and Sparks, 1991). Kriging parameters were based on variogram analysis. No trends in hydraulic conductivity were observed within the kriged regions.

Hydraulic conductivity assignments for the model cells within the Horicon till were based on slug test in monitoring wells. An attempt was made to treat the different till layers separately, i.e., make use of any data available on the vertical distribution of measured K. There were insufficient data to calculate a variogram. Kriging was based on an assumed spherical model using a nugget of 0, a sill equal to the global variance and a range chosen so that the model area affected by an individual value would consist of the cell in which the well is located and the adjacent cells. Because little information was available for each layer, simple rather than ordinary kriging was used so that a kriged estimation tends toward population rather than the local mean as the distance from sample locations increases (Englund and

Sparks, 1991).

Vertical hydraulic conductivity (K_v) was calculated for every active cell using the assigned K_h values divided by K_h:K_v, initially estimated as 2.8 for the till. Because the sandstone units are likely to have more horizontal bedding planes than the till, bedrock K_h:K_v was initially set at 5.6, twice that of the till.

No field data were available for estimating average recharge rates to groundwater. The spatial distribution of appropriate recharge rates was estimated using a method described by Stoertz and Bradbury (1989). The model is run with specified heads at the water table and fluxes across the water table are calculated. The resulting distribution of fluxes was used as a guide for assigning relative recharge rates. In addition to this numerical approach, higher recharge rates were assigned to areas where surface ponding was noted during snowmelt and after a heavy rainfall period in 1991. Most of the modeled area corresponds to initial recharge rates of 5.6 or 18.9 cm/yr. Limited areas were initially modeled with recharge rates up to 67 cm/yr for areas of severe ponding.

Of the three Waunakee municipal wells, only one falls in the active model area. It was modeled with a pumping rate of 1,100 m^3/d based on the average rate from January 1990 through December 1991 (Brockner, 1992). Seven private wells also were simulated. Private well pumping rates were based on an average of 0.13 m^3/day/cow for dairy farms and 0.19 m^3/day/person (Birge, 1993; Harkin, 1993).

MODEL CALIBRATION TARGETS AND SOURCES OF UNCERTAINTY

Calibration was performed by adjusting the initial K_h, K_v and recharge values and model boundary conditions until the model approximates field-measured values of head and flow. Since steady-state conditions were simulated, the calibration values were time-averaged field measurements when such data were available; single measurements were assumed to represent steady-state conditions. Calibration values consisted of bedrock heads based on private-well drilling logs and head measurements, water-table

elevations within the monitoring area measured from October 1989 through February 1992 and flux into Sixmile Creek based on seepage metering. Since the rate of vertical groundwater flow was of key importance to the modeling effort, the shallow vertical hydraulic gradients within the monitoring area served as a fourth type of calibration value. The gradients were also measured at piezometer nests from October 1989 through February 1992. For each type of calibration value in this modeling effort, the types of uncertainty are described and quantified.

Water-table Elevations within the Monitoring Area

Uncertainty associated with the water-table calibration values are of three types: measurement and averaging error, temporal uncertainty and spatial uncertainty.

Measurement error accounts for the least uncertainty. Water-table elevations were determined by measuring the distance from the top of the well casing to groundwater in wells screened at or just below the water table. The casing elevations were surveyed relative to a nearby road-intersection. The intersection elevation was read from a USGS topographic map and is probably accurate to within 1 m. Water-table elevations relative to this datum are less important than the elevations relative to each other, which were measured with much greater accuracy. Surveying was performed to the closest 0.003 m checked by ending a survey run at the point of origin. If large elevation discrepancies were found at the close of a survey loop, the loop was repeated. Maximum error of the relative casing elevations from one end of the monitoring area to the other is estimated as 0.03 m and about 0.006 m for wells in close proximity. Depth to water was measured by electric tape to the nearest 0.006 m. Time-averaged water-table elevations were determined graphically using hydrographs for each water-table well. The hydrographs were drawn assuming a smooth curve through discrete measurements. The average was visually chosen by finding the elevation equally dividing the area under and above the hydrograph curve. Time-averaging over the study period was judged to be accurate to within at least 0.15 m. The combined

maximum measurement and averaging error for a water-table estimate at a well relative to other wells is about ± 0.18 m.

Temporal uncertainty stems from the fact that a 2-year average water-table elevation may not represent a longer-term, steady-state average. To quantify temporal variability, long-term water-level records are needed. The two wells closest to the monitoring area with long water-level records are USGS wells DN-1136 and DN-441, domestic wells finished in the Cambrian sandstone. Water-level elevations were measured monthly by the USGS (Fig. 19). For comparison, the water-table elevation for monitoring well K3.B is shown. DN-1136 and DN-441 lie approximately 11 km SW and 14 km ENE of the monitoring area. For this analysis, long-term water-table fluctuations were assumed to be similar to those in these bedrock wells. (In actuality, water-table fluctuations are usually greater than deeper fluctuations. The variances calculated in this analysis may therefore be underestimations.) The uncertainty in an estimate of a long-term mean based on one or more observations depends on the variance of the population of observations over a long-term period. To estimate that variance, time-series analysis (Cryer, 1986) was performed on the DN-441 record. Although DN-1136 was closer to the field site, the DN-441 record is 32 years long, 21 years more than the DN-1136 record (Fig. 19). The statistical software package Minitab (Ryan et al., 1985) was used to fit a variety of time-series models (Cryer, 1986). The best-fit model was an auto-regressive three-parameter model in which the head at a given time (h_t) is estimated from the three previous head measurements:

$$h_t = \phi_1 h_{t-1} + \phi_2 h_{t-2} + \phi_3 h_{t-3} + \epsilon_t \qquad (32)$$

The ϕ terms are the model-fitting parameters and ϵ is the error term. The estimated values for ϕ_1, ϕ_2 and ϕ_3 were 0.968, -0.114 and 0.121. The values were used in the Yule-Walker equations (Cryer, 1986; Eqs. 4.33 and 4.34) to solve for γ_0, the estimated variance of a head observation. The variance (Var) of a mean head ($\bar{h}$) estimated from n observations depends on γ_0 and the covariances (Cov) between all

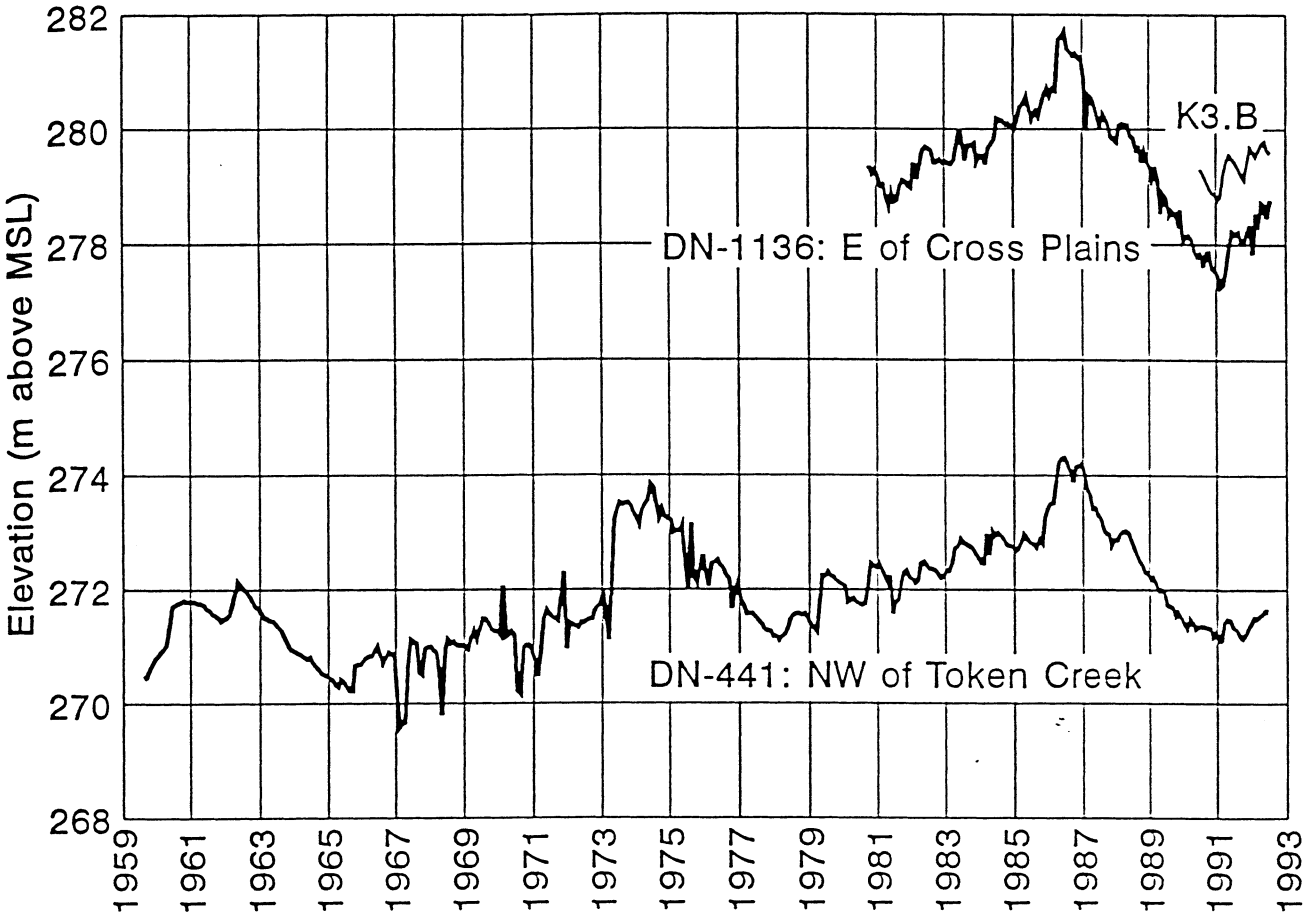

Fig. 19. Long-term hydraulic head data at two wells finished in Cambrian sandstone. Data collected by the U.S. Geological Survey, Madison, WI. Water-table heads at piezometer K3 shown for comparison.

combinations of two observations for $i \neq j$:

$$Var(\bar{h}) = \left[\frac{1}{n}\right]^2 \left[\sum_{1}^{n} \gamma_0 + \sum_{i \neq j}^{n} \sum_{j}^{n} Cov(h_i,h_j)\right] \quad (33)$$

The covariances, in turn, depend on γ_0 and empirical parameters calculated by the Yule-Walker equations. To estimate the variance of a mean over a 2-year period, the variance based on 24 monthly observations at DN-441 was calculated. Estimates of γ_0 and $Var(\bar{h})$ for 24 observations are 1.0 m^2 and 0.84 m^2. Accounting for the uncertainty in estimating a long-term average from observations over a 2-year period, the 95% confidence interval for a mean water-table elevation from a 2-year average is approximately $\bar{h} \pm 1.9$ m. The interval could be even larger considering that water-table fluctuations are typically larger than those from deeper wells such as DN-441.

Spatial uncertainty of water-table calibration values is caused by interpolation of measured values to model nodes and the fact that point measurements at monitoring wells are used to estimate average water-table elevations in model cells, with areas of 61x61 m^2. Kriging is a method of encompassing and quantifying both sources of uncertainty by interpolating between point measurements and providing estimate variances for whole kriging cells designed to conform to model cells. The closer a node is to measured points, the smaller is the variance of its kriged-estimate. For kriging-grid cells that encompass measured points, the smaller the cell dimensions, the smaller the variance of the estimate. Kriging parameters are based on model-fitting for the parameter variogram. When data for variogram-model fitting are scare, a conservative approach is to use the likely minimum nugget and sill and the maximum range. Such a selection results in the smallest variances of the kriging estimates, thereby forcing a more accurate calibration.

Time-averaged water-table elevations from 30 locations were roughly normally distributed with no large-scale trends across the monitoring area. A data set of 30 observations is relatively small, and

this allows only an approximate variogram-model fitting. The variogram and possible model are presented in Fig. 20. The nugget was assumed to be 0 and the sill set at 0.41 m^2, based on the global variance of the data. The range appears to be < 240 m and so a range of 240 m was selected. The time-averaged water-table elevations were kriged with a grid spacing and alignment coinciding with the flow-model grid in the monitoring area. For model cells encompassing monitoring wells, kriging-estimate standard deviations (σ_k, square root of the kriging variance) ranged from 0.19 to 0.32 m and averaged 0.25 m. The head differences between the measured and kriged values reflect the smoothing resulting from kriging and ranged from -0.37 to 0.45 m; the average absolute difference was 0.08 m. The 95% confidence interval for each kriging estimate is approximately the estimated value $\pm$ 2 σ_k. Considering only cells with monitoring wells, the average σ_k of 0.25 m yields an average 95% confidence interval range of $\pm$ 0.5 m. The average σ_k for all kriged cells roughly covering the monitoring area (i.e., not just cells with water-table wells) was 0.57 m.

Spatial variability of head values is also caused by aquifer heterogeneity. Model cells represent average aquifer properties within the cell, but the model does not account for small-scale heterogeneities that can influence field-measured heads. Gelhar (1986) has discussed the effect of hydraulic conductivity variability on head variability. He assumed that hydraulic conductivity (log-normally distributed) and head are stationary random processes to show that variations in head are forced by the variation in the logarithm of hydraulic conductivity (ln K). For steady-state flow in a statistically isotropic medium (i.e., ln K correlation lengths are independent of direction) the head variance (σ_h^2) is:

$$\sigma_h^2 = \frac{1}{3} J^2 \sigma_f^2 \lambda^2 \qquad (34)$$

where J is mean hydraulic gradient, σ_f^2 is the variance of ln K and λ is the correlation length for ln K. The analysis is valid only where mean conditions of J, h and ln K vary slowly in space relative to correlation scales. The variability accounted for by aquifer heterogeneity is some of the same variability

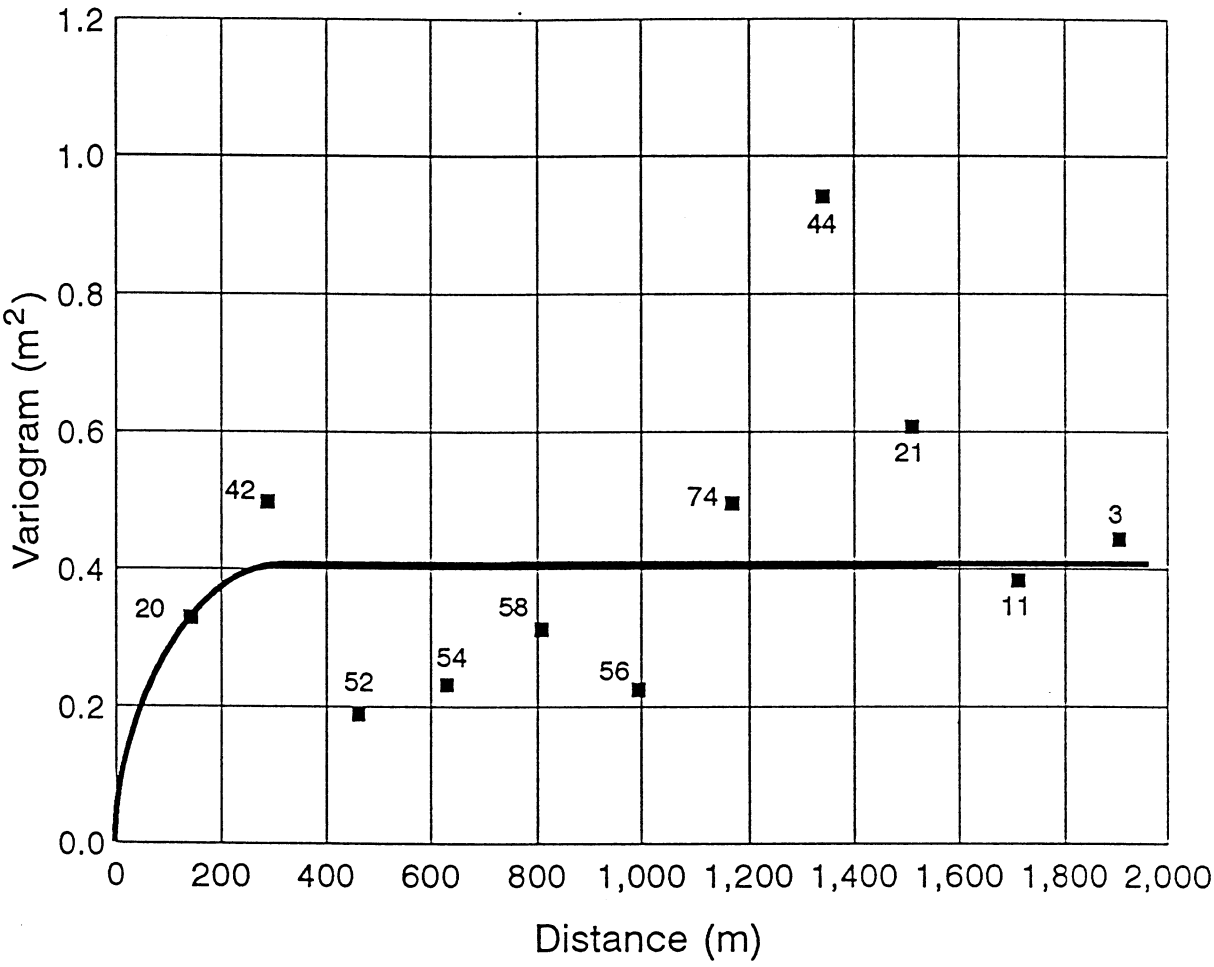

Fig. 20. Variogram of time-averaged water-table heads measured at monitoring piezometers. Spherical model is shown. Values next to the points indicate the number of pairs used.

accounted for by kriging, i.e., the effect of extrapolating point measurements to represent conditions in model cells. Quantification of variability should be similar for both analyses, and a comparison is presented. Accurate estimates of λ are possible only with a large number of monitoring wells and K measurements. Assuming isotropy, three-dimensional ln K variograms based on slug test data from monitoring wells in the till aquifer were constructed (Fig. 21). The 30 observations accounting for the first variogram point are from pairs of piezometers in the same nest with an average separation distance of 5.3 m. The variogram lacks sufficient structure to approximate a model, but the range appears to be $<$ 200 m. Assuming the average estimated σ_k from the kriging of cells with monitoring points is a reasonable approximation of σ_h in Eq. 34, λ can be solved for using Eq. 34 to determine if the value is reasonable in comparison with the variogram (Fig. 21). Average σ_k was 0.25 m, yielding an estimated σ_h^2 of 0.063 m^2. The average J is approximately 0.0035 across the monitoring area, and slug test-based σ_f^2 for monitoring wells is 3.31. These values yield a λ of 68 m, a value not inconsistent with the ln K variogram (Fig. 21).

If the estimated variances stemming from temporal, spatial and measurement uncertainties are independent, they can be summed to produce a total variance of the calibration-value estimate. If the measurement error range of $\pm$ 0.18 m represents a 95% confidence interval, it is equivalent to a variance of 0.0081 m^2. Added to the 0.84 and 0.063 m^2 variances caused by temporal and kriging-based, spatial uncertainty, total variance of a water-table calibration value at a model cell is 0.91 m^2, yielding a 95% confidence interval range of $\pm$ 1.9 m to be used as a calibration target. Such a range, however, accounts for a large part of the total water-table elevation differences across the monitoring area (Fig. 17). A much stricter calibration approach is to eliminate temporal uncertainty by assuming that the whether or not the individual 2-year average water-table elevations represent steady-state conditions, gradients resulting from their relative elevations do, in fact, represent steady-state. It was also assumed that the smoothing and interpolation resulting from kriging would tend to encompass any small measurement or

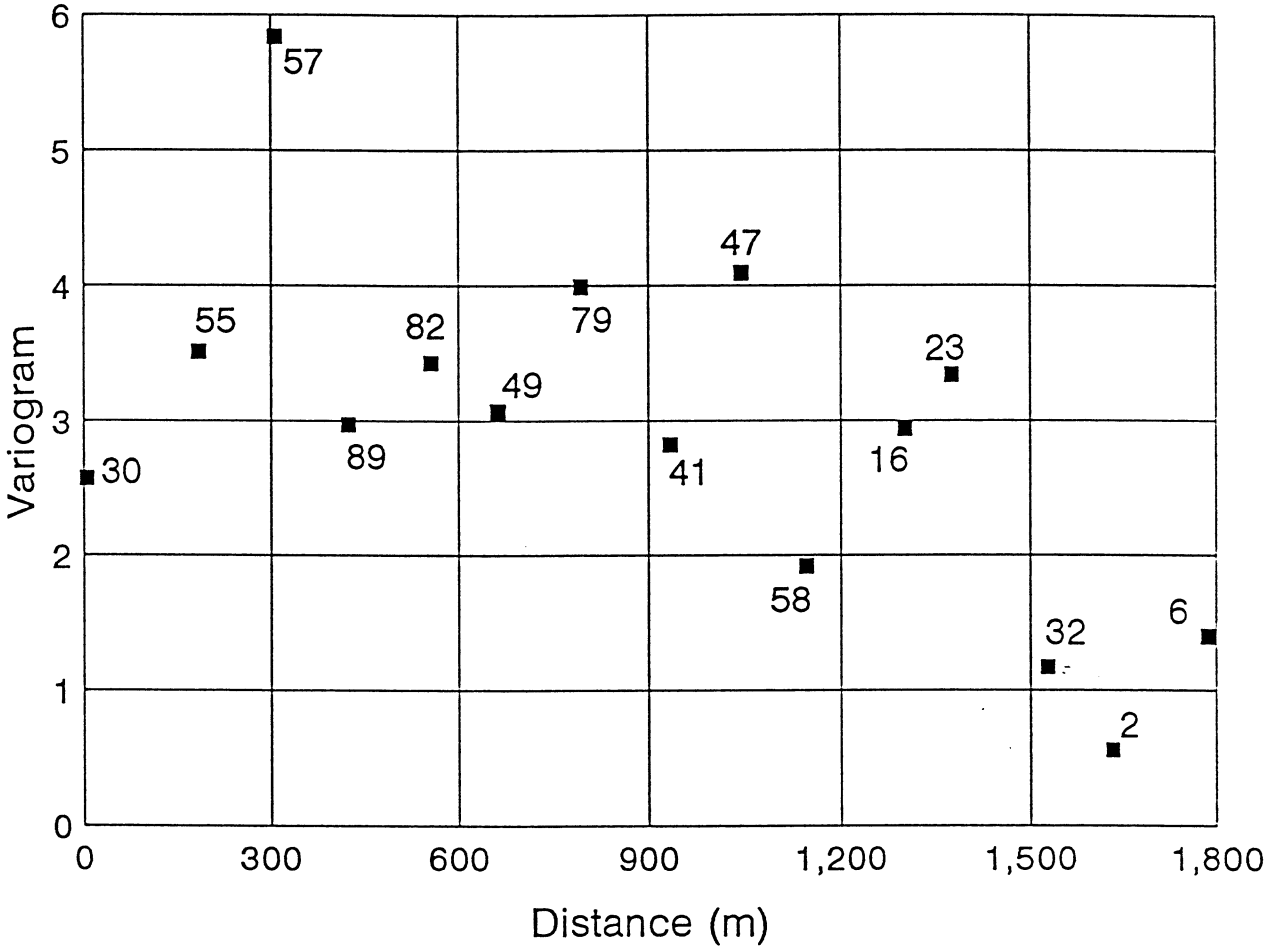

Fig. 21. Variogram of natural log till hydraulic conductivity. Distances are three-dimensional separation distances. Values next to the points indicate the number of pairs used.

averaging errors. In the end, the 95% confidence intervals estimated by kriging were used as conservative (i.e., strict) calibration targets for the water-table elevations in model cells with monitoring wells.

Kriging provides estimates of the calibration values and σ_k values for every model cell, and these values could be used as calibration targets too. The kriged surface, however, does not accurately incorporate land surface and surface water information. Hence, less faith should be placed in the kriged surface farther from the monitoring wells. Consequently, only the kriged estimates and σ_k-values of cells with monitoring wells were used as calibration targets.

Bedrock Hydraulic Heads

Uncertainty in determining bedrock head calibration values is also caused by measurement error and temporal and spatial effects. Bedrock head estimates are based on depth-to-water measurements at 11 private wells within a 23 km^2 area surrounding the monitoring area and 217 drilling logs within a 240 km^2 area incorporating the model area. The estimates are accurate to about 1.5 m. Unlike water-table elevations in monitoring wells, bedrock heads estimated from private-well drilling logs are based on depth-to-water measurements, each taken at a different time over the last 40 to 50 years. Kriging of bedrock heads averages information spatially and temporally and was therefore used to quantify total uncertainty. Two neighboring wells may have very different estimated heads because they were measured at different times. Increased uncertainty caused by both temporal variability and measurement errors, is incorporated into the variogram model, and subsequently results in higher σ_k-values.

Kriging was performed for a 95 km^2 area encompassing the model area and 143 bedrock head values. Variogram and visual analyses of the contoured-head surface revealed a trend of generally decreasing head from northwest to southeast. Such a trend gives a false impression of increasing variances with distance, up to the maximum distance possible within the kriging region. To construct

a representative variogram model, first such trends are removed and then a variogram is constructed for the deviations of individual observations from the trend surface. Kriging was used to establish the trend by subdividing the area and obtaining an average head in each subregion. The whole area was first kriged with a grid spacing of 3 km using a variogram model with a range of 10.6 km resulting in 20 subregions, each with an averaged head value. Deviations from the appropriate subregion averages were calculated for each head measurement within or close to the model area and a variogram was constructed (Fig. 22). The visually-determined "best-fit" model was a spherical variogram with a nugget, sill and range of 7.0 m^2, 9.3 m^2 and 1,680 m, respectively; the parameters were then used to krige the original head values. A kriging grid cell size of 122 m was used to approximate the average MODFLOW cell size. Unlike the water-table elevations, the kriged bedrock potentiometric surface represents the best estimate of the head distribution throughout the modeling area, and there was no reason to put greater trust in a hand-contoured surface than the kriged surface. Kriging, therefore, produced calibration values throughout the model area, not just at cells containing private well measurements. A computer code was written that paired each MODFLOW cell center with the closest kriging-grid cell center. Each MODFLOW cell was assigned the kriged estimate and σ_k of its paired kriging grid cell to serve as the MODFLOW cell's calibration target. The 30 private wells in the model area have open intervals whose centers fall in model Layers 2 through 6, most often in Layer 3. Model Layer 3 heads were originally compared to kriged heads during calibration, but within the monitoring area much of Layer 3 is till, not bedrock. Layer 4 is modeled as till only in the easternmost part of the monitoring area and was therefore chosen as the layer whose heads would be compared against kriged calibration targets. Model calibration with respect to bedrock heads is based on simulated heads in Layer 4 being within 2 σ_k -- roughly the 95% confidence interval -- of the kriged bedrock head value. For all 1,312 Layer-4 active model cells, the σ_k-values range from 1.59 to 2.77 m and average 2.27 m. The average σ_k in cells with measured points is 1.85 m. For those cells, the absolute differences between the kriged and measured heads range

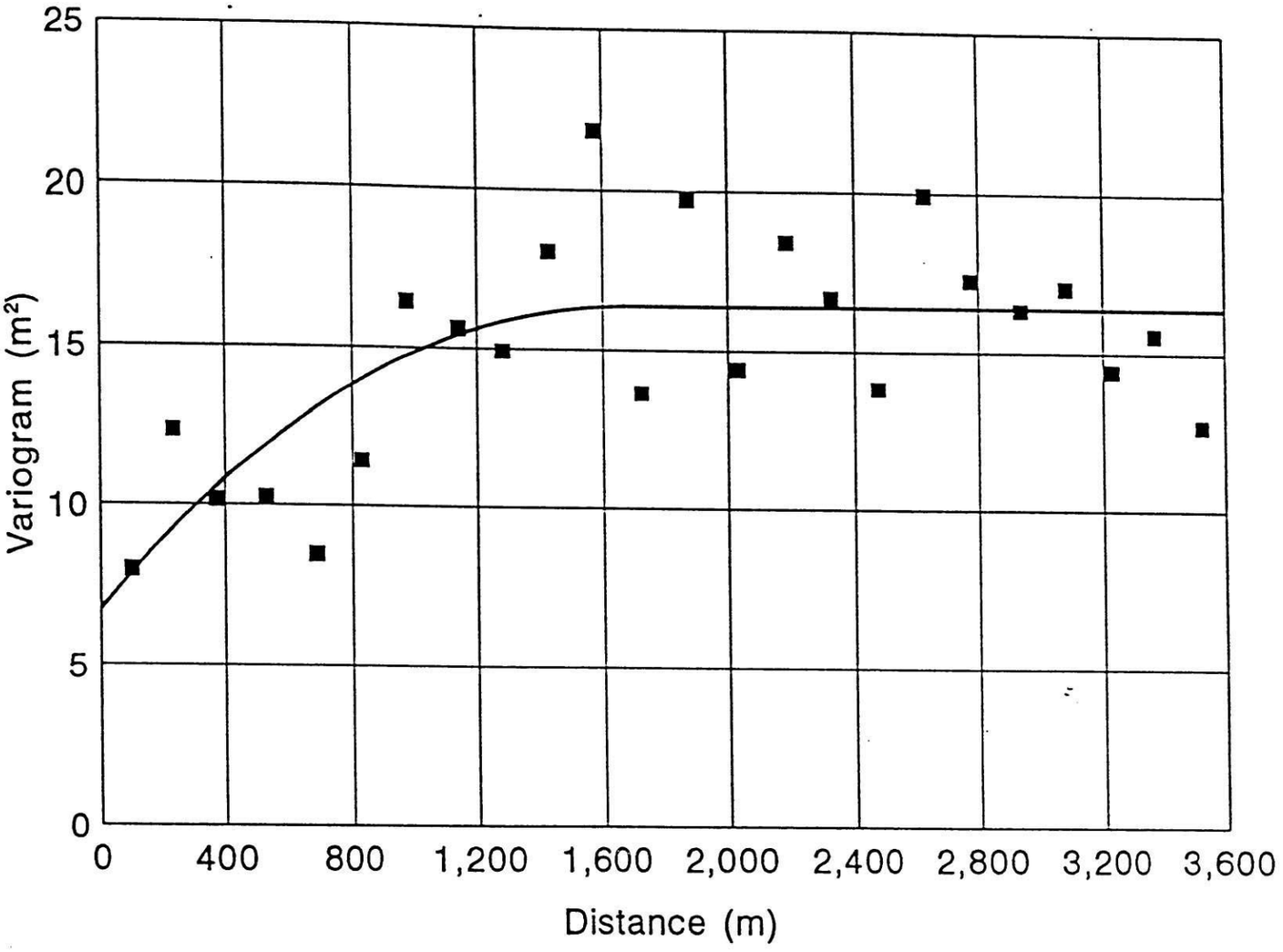

Fig. 22. Variogram of the deviations from sub-region average hydraulic head at nearby private wells. Spherical model is shown.

from 0 to 4.35 m and averaged 1.70 m. Large discrepancies between the kriged and measured head reflect the smoothing that results from kriging as well as the effect of scaling up from point measurements to kriging grid cells.

Specified-head elevations along the model boundaries in Layers 3, 4, 5 and 6 were originally based on the hand-contoured bedrock head surface. To be consistent with using kriged heads as calibration targets, the constant head values were adjusted to reflect the kriged values. Specified bedrock-head values were kept consistent with specified-head elevations in the overlying creek surface so that inappropriate gradients and fluxes would not occur.

Vertical Gradients

Calibrating to water-table elevations ensures that realistic horizontal hydraulic gradients and consequently realistic horizontal groundwater velocities are simulated. Because vertical groundwater flow is so important in this situation, calibrating the model to match vertical hydraulic gradients is necessary. Since piezometers rarely extended into model Layer 3, calibration was based on the simulated vertical gradients between model Layers 1 and 2. Following the procedure used for water-table elevations, vertical gradients at each piezometer nest were time-averaged from October 1989 through February 1992. If there were more than two piezometers in a nest, the two that most closely reflected the middle of model Layers 1 and 2 at that cell were selected. At four nests, piezometers did not extend into Layer 2. There the measured vertical gradient was assumed to extend deeper and represent the gradient between Layers 1 and 2. The monitoring area was kriged using the 16 average gradients and a kriging grid coincident with the MODFLOW grid in the monitoring area to produce estimates of the vertical gradient throughout that area. Kriging parameters were based on variogram analyses, but variogram structure is highly questionable given so few data. The variogram (Fig. 23) was fitted using a spherical model with a nugget and sill of 0 and 0.014 (unitless) and a range of 640 m. The sill is based on global variance.

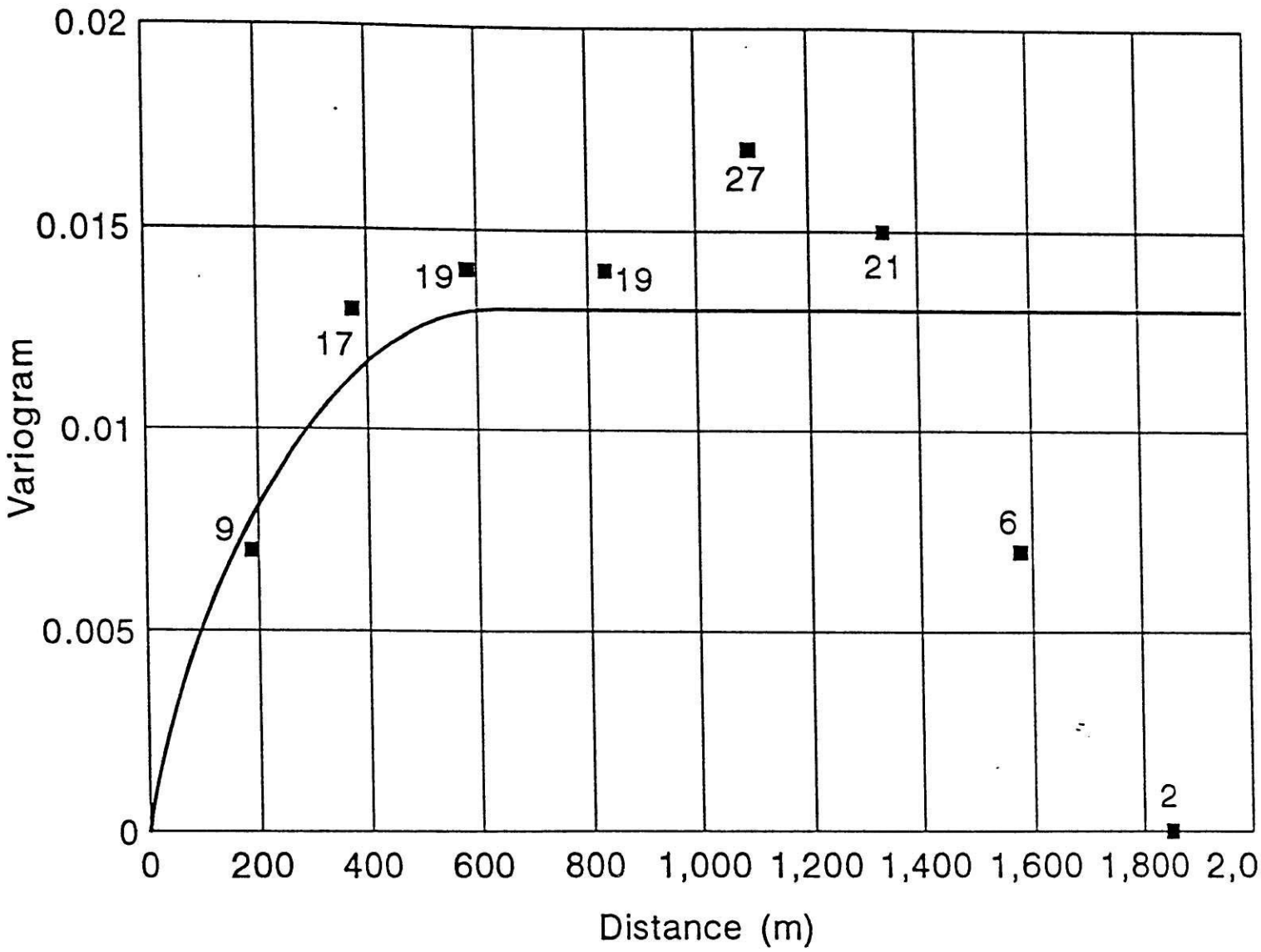

Fig. 23. Variogram for time-averaged vertical gradients at piezometer nests. Spherical model is shown. Values next to the points indicate the number of pairs used.

The nugget and range could easily be larger and smaller respectively, but the choices were conservative to give a smaller σ_k and a stricter calibration. Measured gradients ranged from 0.23 downward to 0.21 upward; kriged gradients at cells with piezometer nests ranged from 0.21 downward to 0.19 upward. For model cells encompassing piezometer nests, σ_k-values ranged from 0.024 to 0.059 and averaged 0.033. Since so few data were used, kriging results could not confidently be extended to estimate calibration values for model cells without piezometer nests. Model calibration with respect to vertical gradients is based on simulated Layer 1-2 gradients' being within 2 σ_k of the kriged value for cells in which a piezometer nest is located.

Flux into Sixmile Creek

For model calibration with respect to groundwater flux into Sixmile Creek, the simulated flux was compared to seepage metering data (Levy, 1993). Flux is calculated by the river package and occurs between the river reach and model cell that contains the reach. To estimate the Darcy flux, the volumetric leakage rates are divided by the length and width of the river reach in each model cell. Seepage metering was performed along a stretch of Sixmile Creek corresponding to model columns 27 to 40. The average simulated flux along this stretch was compared to the arithmetic mean measured flux of 4.1×10^{-6} cm/sec. The calibration target was derived from the measured mean's 95% confidence interval of 3.3×10^{-6} to 4.9×10^{-6} cm/sec.

CALIBRATION EVALUATION AND EXECUTION METHODS

During model calibration, model parameter values were adjusted so that simulated heads, gradients and fluxes would fall within the calibration targets defined above. The calibration process required 22 major model runs with frequent intermittent experimental runs. After each run, differences between simulated heads and gradients and their kriged calibration values were calculated with the goal

of every difference being less than 2 σ_k. For water-table elevations, comparisons were made for 25 cells with water-table wells. Comparisons within Sixmile Creek and Waunakee Marsh were not included since these heads were controlled by heads specified in the MODFLOW river package. For bedrock heads, comparisons were made at all 1,312 active cells in Layer 4. For vertical gradients, comparisons were made between Layers 1 and 2 at 17 cells with piezometer nests including creek piezometers. The one average simulated flux into Sixmile Creek in columns 27 through 40 was compared to the average measured flux. For each model run, the root mean square (RMS) errors between the kriged (or, for flux, the measured) and MODFLOW-simulated values were calculated and used as general measures of the goodness-of-fit of the calibration. (Since only one comparison was made for the groundwater flux into Sixmile Creek for each run, flux calibration was evaluated with the absolute difference, equal to the RMS error for one comparison.) Trends in these evaluations with major model runs are shown in Fig. 24. The bedrock head RMS error (Fig. 24a) does not decrease with model runs and even increases in the late model runs, unlike the other calibration evaluations. The increase reflects the trade-offs made during calibration. The RMS error for the bedrock heads was allowed to increase so that other calibration evaluations could decrease as long as simulated bedrock heads remained 2 σ_k of the kriged values.

Changes in model parameter values were made by changing the parameter-zone values or a model cell's zone. The type of change depended on the type of discrepancy that existed. When necessary adjustments were somewhat global (e.g., water-table elevations too low throughout the monitoring area), zone values were changed. Zone values representing the same medium were all changed by the same factor so that the relative conductivity distribution originally assigned remained unaltered. The amount of zone value change was restricted by the previously discussed 95% confidence intervals for the mean parameter values. Changes were limited so that a parameter's mean zone value remained roughly within its associated 95% confidence interval. By the final model run, K_h zone values for the till and bedrock were equal to 0.5 and 0.75 times their original values. The final mean till K_h was 6.0×10^{-5} cm/sec, i.e.,

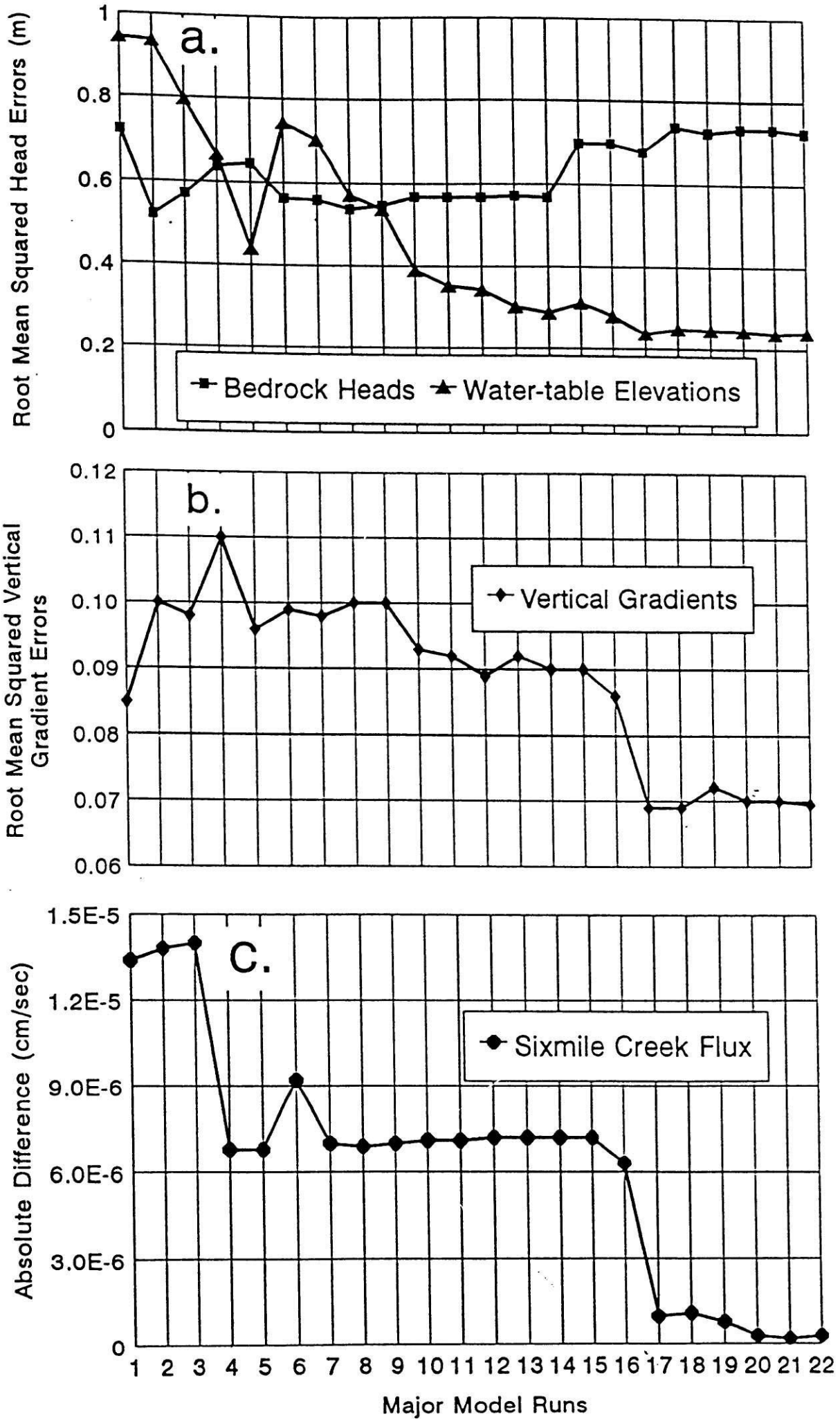

Fig. 24. Trend in calibration evaluation with major model runs of a) root mean squared hydraulic head errors, b) root mean squared vertical gradient errors and c) the absolute value of the Sixmile Creek-flux error.

just under the lower limit of the 95% confidence interval. The final mean bedrock K_h was 2.9×10^{-3} cm/sec, well within its 95% confidence interval. When changes were made to the K_h zone values, corresponding changes were made to K_v values so that the ratio of K_h to K_v did not change. If changes were made to all K_v values, they were made so that the usual till K_h:K_v remained within its 95% confidence interval of 1.7 to 4.6. The final till K_h:K_v was 4.6; the final sandstone K_h:K_v was 10, roughly twice the till value. To reach the calibration target for flux into Sixmile Creek, and simultaneously to match the vertical gradients measured between the creek and the underlying groundwater, two global adjustments were necessary. First, the creek bed K_v was multiplied by 0.25, still well within the measured mean's 95% confidence interval. Second, the specified head values in Layers 3 through 6 were adjusted to achieve consistency with respect to head differences between the specified values and the overlying creek elevations. Changes were generally < 0.3 m, except under Dorn Creek, where they did not exceed 1.5 m.

When finer adjustments were necessary at individual cells or in small areas, designated zones were changed only for cells in that area. The number of zones that an individual cell could change was also limited. For K_h, adjustments were generally limited to two zones, curtailing change to an average factor of 2.2 and a maximum of 4.2. Individual model cell zones for K_v generally were allowed to change by a maximum of three zones corresponding to a factor of 4.3.

Recharge was also used as a calibration parameter, but no field data were available for strict limits of allowable change. Greater recharge was added in the areas around K1, K2, R2, K6, K17 and on the drumlin just northeast of K17. Extra recharge was added to the septic field areas for all homes within the monitoring area. The majority of cells were assigned recharge values of either 2.8 cm/yr near observed and model-predicted discharge areas, or 22 cm/yr, for most of the recharge areas. Recharge rates of 27.8, 38.1 or 44.5 cm/yr were the final assigned values for septic fields, areas with ponding and areas where the Prairie du Chien dolomite is the uppermost bedrock unit.

CALIBRATION RESULTS

All differences between simulated and kriged water-table elevations were less than 2 σ_k. A plot of simulated versus kriged estimates for the comparison cells is presented in Fig. 25. The line with a slope and intercept of 1 and 0 is shown for comparison to the best-fit regression line through the data. The slope of the best-fit line is 1.2 indicating that the kriged values are somewhat smoother than the modeled values, i.e., modeled highs are a little higher and modeled lows a little lower than kriged estimates. Although not part of the calibration evaluation, kriged and simulated water-table elevations can be compared for every cell within the monitoring area (Fig. 26). Differences at each model cell within the monitoring area are in terms of the number of σ_k. In limited areas, differences exceed 2 σ_k, but in all cases, little reason exists to lend greater credence to the kriging than the MODFLOW results. In many cells in the southwest portion of the monitoring area, differences are greater than 2 σ_k because of the paucity of data in that area for kriging. While the kriged water table tends toward the local mean of the input data, the modeled water-table reflects the fact that the regional heads in the underlying model layers begin to rise toward the southwest. Here the modeled water-table elevations are probably more accurate than kriged values. The same type of discrepancy is found in the southeast portion of the monitoring area where data were insufficient for kriging while the modeled bedrock heads and water-table elevations are controlled by the Dorn Creek water levels, and therefore decline; Dorn Creek water-level data were not used in kriging. At cells just east of piezometer nest K2, simulated water-table elevations are higher than kriged values due to the simulation of perennially standing surface water. Since the water-table elevation was not measured under that water, there is no way to know if the model is correct. The lower simulated water-table elevation at cell row 20, column 28 results from the simulated pumping of private well PK1 in Layer 2 at that location, information not used in kriging. There are large discrepancies between piezometers at K1 and K2 and R2 in model rows 23 and 24 and columns 24

Page 102
(=Fig. 25?)
image missing/
not available

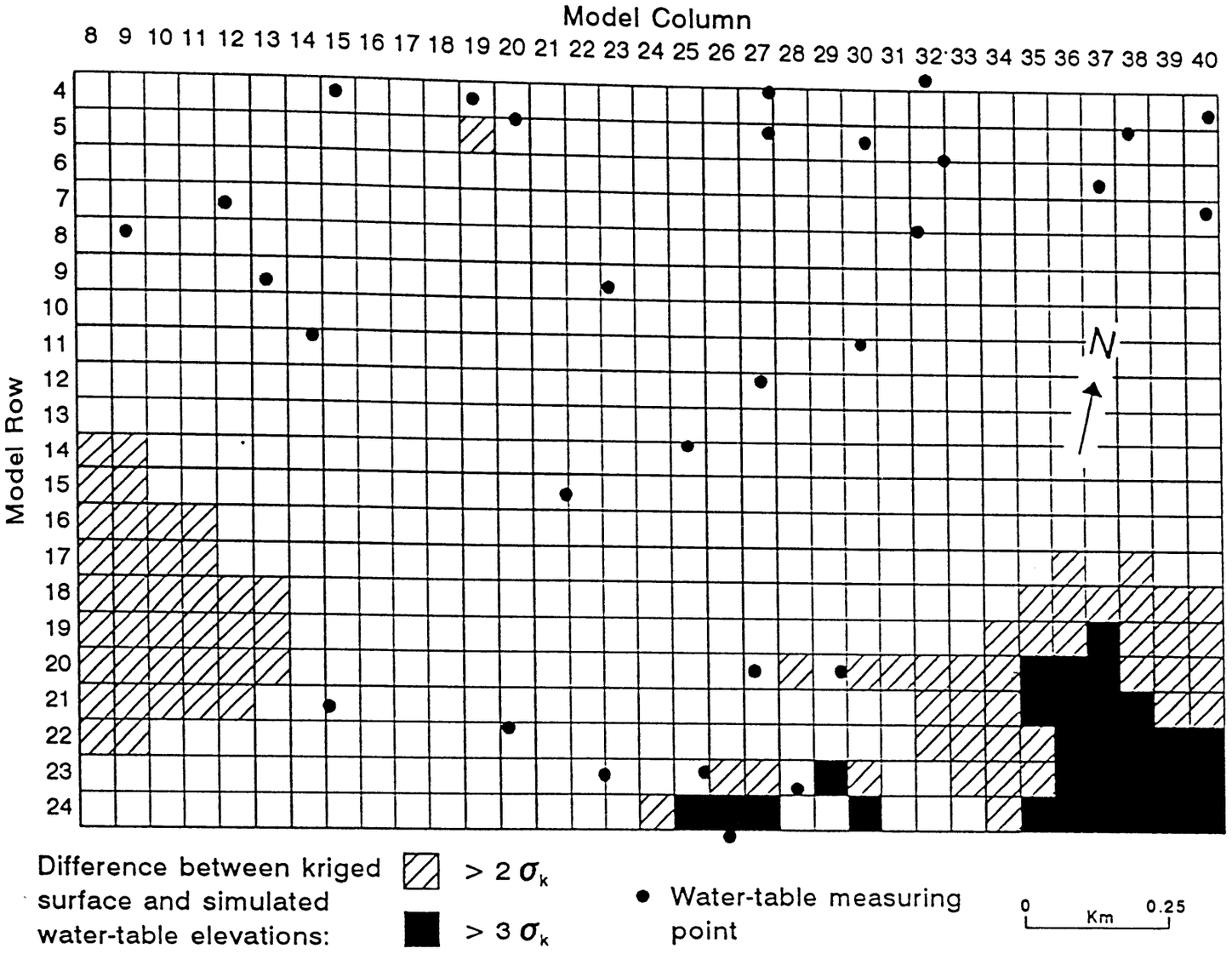

Fig. 26. Comparison of simulated and kriged water-table elevations in the monitoring area. Differences are in terms of σ_k.

through 27. Model-simulated water-table elevations at the cells with piezometers K1, K2 and R2, matched the measured values, but the simulated water table was lower than kriged surface between the wells. In the model the water-table was high at K2 and R2 due to nearby standing water and high at K1 due to the low hydraulic conductivity measured there. With kriging, a high water-table between piezometers was interpolated. Without additional piezometers, it is difficult to say which interpretation is correct. The final cell with a discrepancy greater than 2 σ_k was the cell at row 5, column 19 near Sixmile Creek where modeled water-table elevations are controlled in part by the specified surface-water elevations along the whole stretch of creek while only measured elevations at the stream gauges were used in kriging. Again the modeled elevations present a more likely portrayal of water-table elevations away from monitoring points than do kriged estimates.

Differences between the 1,312 simulated Layer 4 bedrock heads and the closest kriged estimates were all less than 2 σ_k. No strong spatial trends in the distribution of the discrepancies were apparent. The match between simulated and kriged heads is good because so much of the bedrock model boundaries comprised specified-head cells. The heads were specified based on the kriged surface and to a large extent control the interior heads. The plot of MODFLOW-simulated against kriged heads (Fig. 27) demonstrates the good match. Again the line of slope equal to 1 and intercept equal to 0 is shown in comparison to the best-fit line of slope 0.87. A slope less than 1 indicates that MODFLOW-simulated values are smoother than kriged values, i.e., the simulated values ignore variations in the model interior not related to specified values at the model boundaries.

All but three vertical gradients residuals were less than 2 σ_k. However, discrepancies at E6, CPM and CPW (Fig. 15) were 5.51, 6.59, and 2.75 σ_k, respectively. Measured and kriged vertical gradients at E6 are much higher than simulated values. Efforts to decrease the discrepancy by lowering hydraulic conductivity made the simulated water table too high. The cause of the discrepancy is unknown. More piezometers in that area would be needed to see if measured values at E6 are

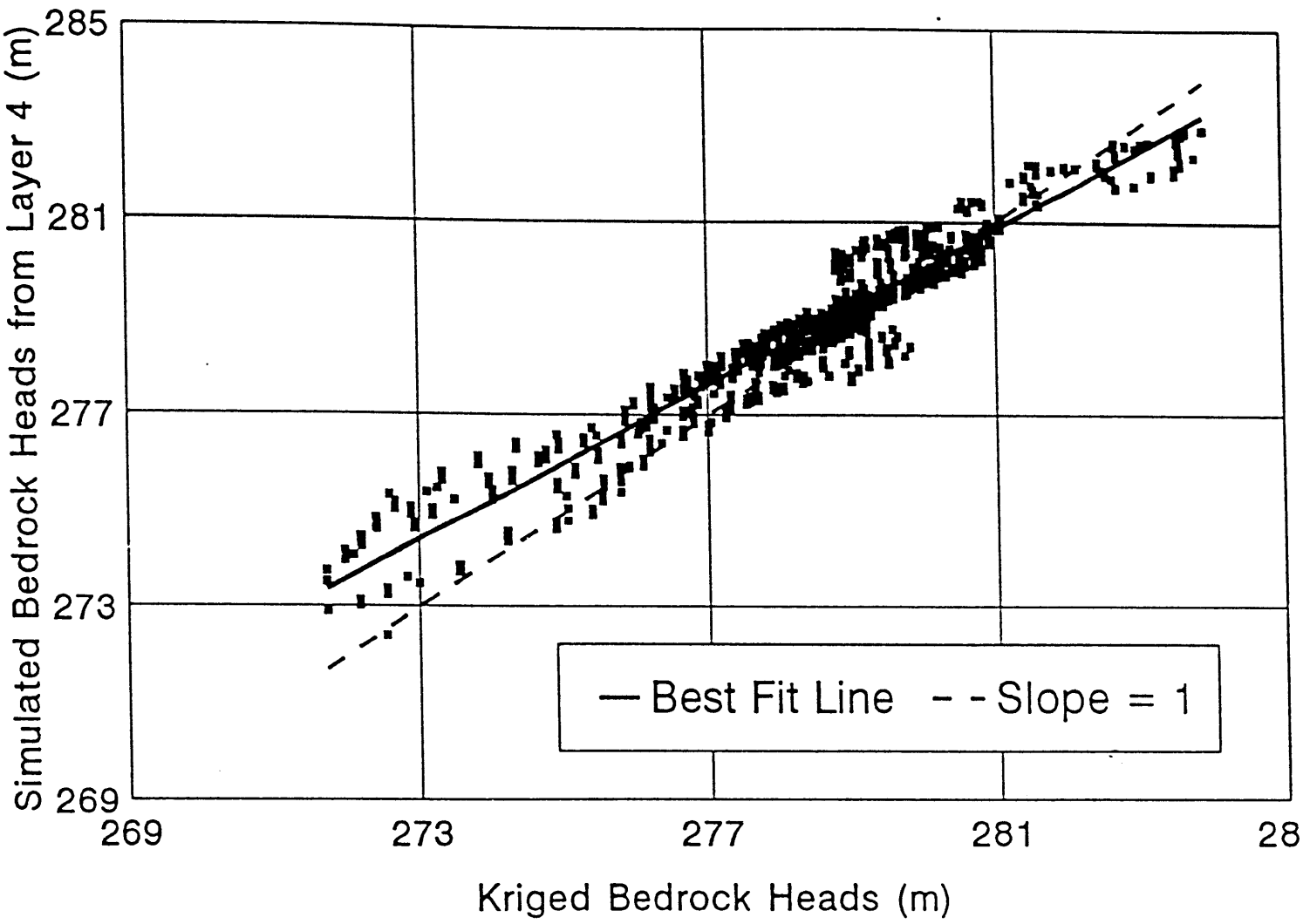

Fig. 27. MODFLOW-simulated hydraulic heads in model layer 4 versus kriged bedrock hydraulic heads (m above msl).

representative of the model-cell area. Because of its inaccessibility, gradients at CPM were only measured five times; values were unexpectedly low, and the discrepancy is due possibly to temporal error. MODFLOW simulated stronger upward gradients than were measured, but more frequent measurements at CPM and measurements at other locations within the marsh may be needed to dismiss the modeled gradients as incorrect. The match of kriged and simulated vertical gradients for each of the 16 cells or river nodes is shown in Fig. 28; on average, simulated gradients were smoother than kriged values.

The flux into Sixmile Creek averaged from columns 27 through 40 in the final model run was 4.0×10^{-6} cm/sec, compared to the mean measured value of 4.1×10^{-6} cm/sec.

SENSITIVITY ANALYSIS

A set of parameter values was found that satisfied most calibration criteria, but the question remains as to how sensitive the model calibration is to changes in the calibrated values. Sensitivity analysis helps quantify the uncertainty in the calibration caused by uncertainty in the estimates of the model parameters (Anderson and Woessner, 1992). The less sensitive the model calibration is to deviations from the calibrated parameter values, the smaller the impact of uncertainty on the model predictions. Conversely, very low sensitivity may imply that calibration is achieved with a non-unique set of parameter values and if model predictions depend on the values, those predictions may be erroneous.

Sensitivity analyses were performed for K_h, K_v and recharge, by changing parameter values of all parameter zones simultaneously and noting the change in RMS error. Sensitivity of the bedrock-head RMS error to changes in K_h, K_v and recharge are shown in Fig. 29a. Best-fit calibrations are indicated by the minimum RMS error. For bedrock heads, the sensitivity analysis indicates that the higher the K_h, the better the calibration. This is because bedrock boundaries are specified heads for much of model

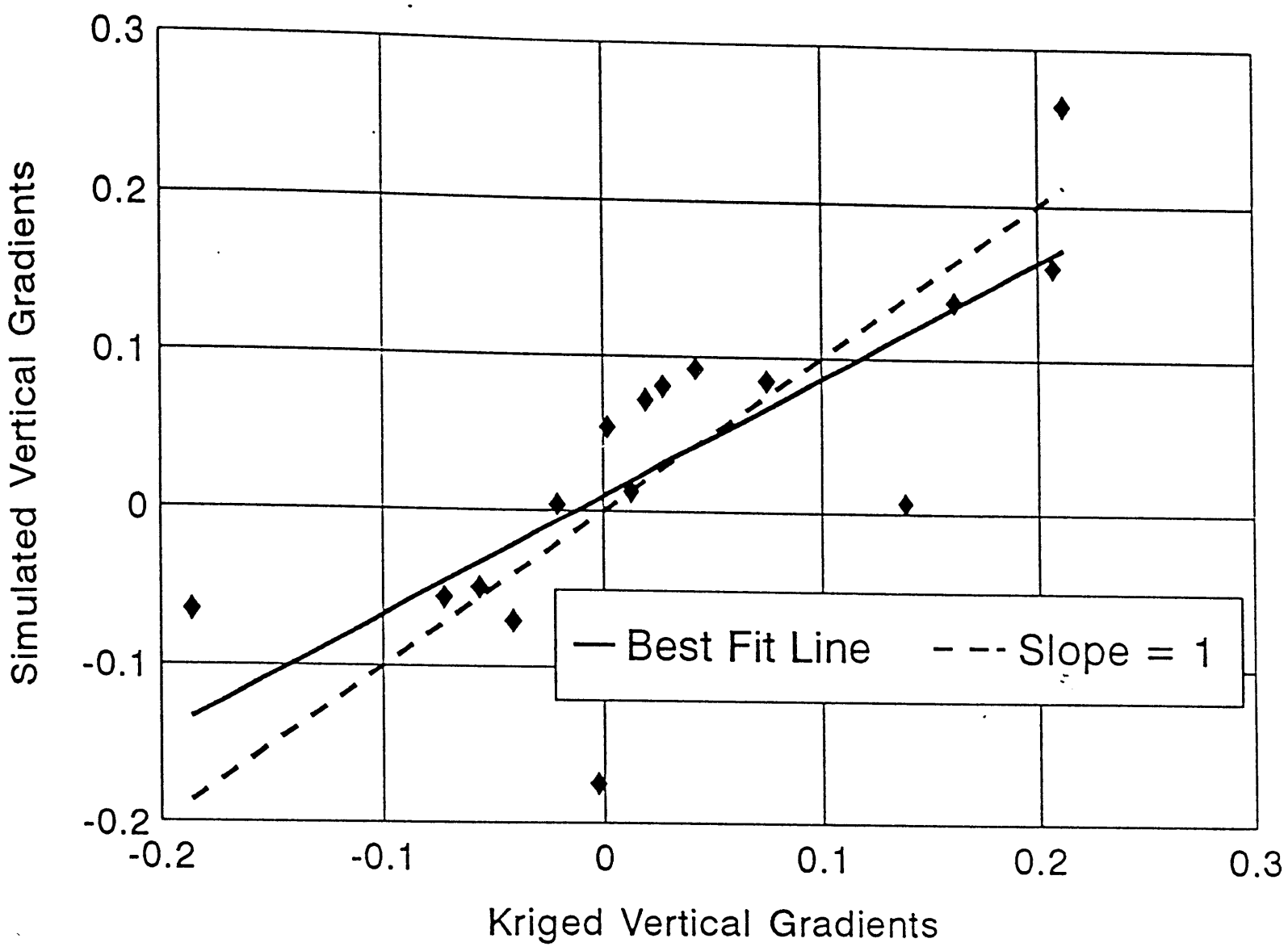

Fig. 28. MODFLOW-simulated versus kriged vertical gradients for model cells in which piezometer nests are located.

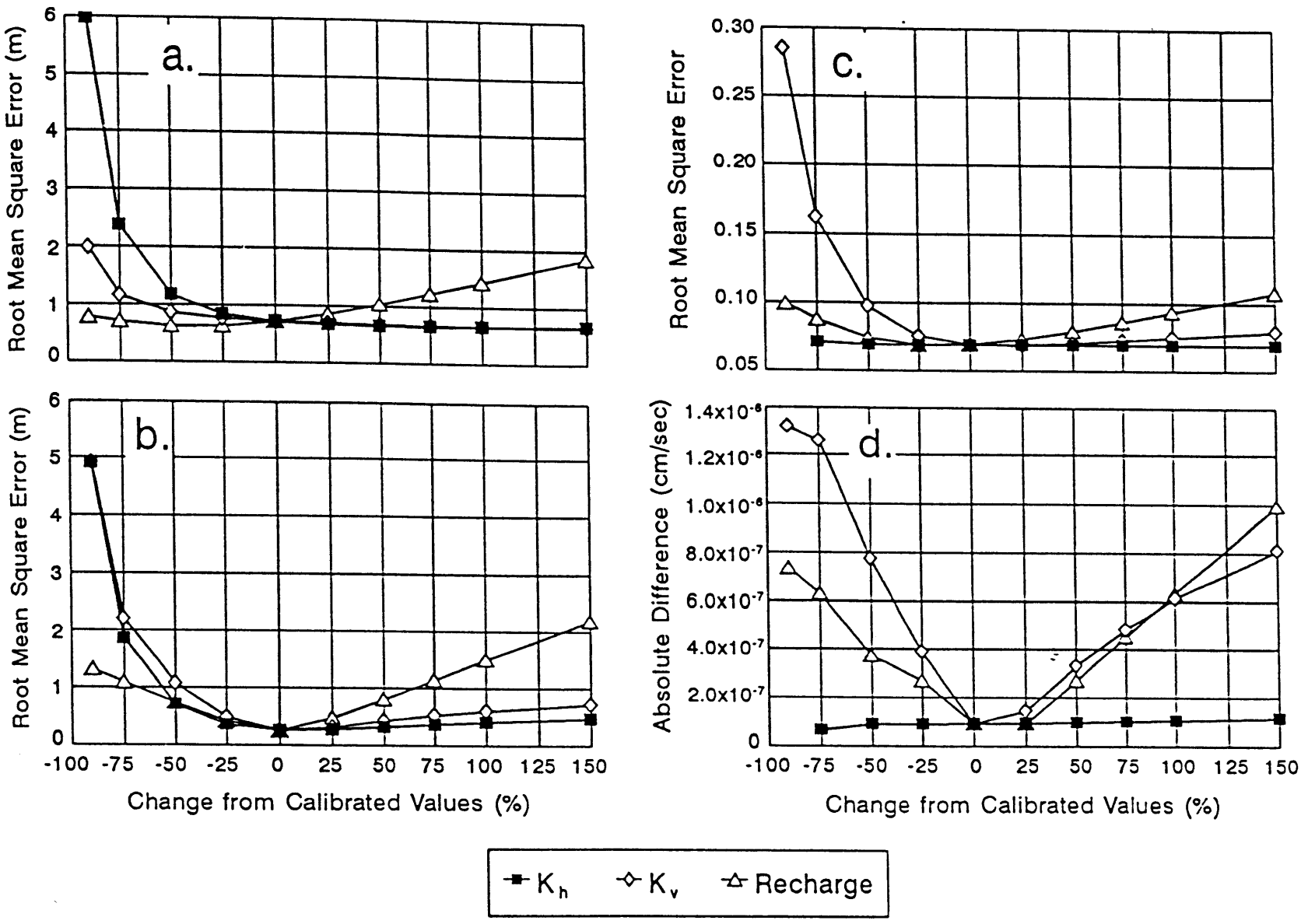

Fig. 29. Sensitivity of a) bedrock-head, b) water-table-elevation, c) vertical-gradient and d) Sixmile Creek-flux calibration measures to changes in model parameter values.

Layers 4, 5 and 6, and the higher the K_h-values, the more closely connected the interior heads are to the boundaries. The rate of calibration improvement decreases quickly at greater than 0% change, i.e., K_h-values are high enough at the calibrations levels and the bedrock heads decrease in sensitivity with increasing K_h. The bedrock-head calibration also continues to improve with increasing K_v values. Again, the marginal improvement decreases substantially after 0% change. Bedrock heads were improved most by about 50% less recharge.

The RMS error for heads at the water table is best at the calibrated values for all parameters (Fig. 29b). Improvements in bedrock heads at higher K_h and K_v values and lower recharge are made at the cost of worsening the calibration for water-table elevations. Given that the bedrock heads are well within their calibration targets at the calibrated values, the bedrock-head improvements with parameter changes are not justified. The preset calibration targets provide a guide for assessing how to balance the various calibration measures.

Vertical gradients are relatively insensitive to K_h (Fig. 29c). Increasing all K_h values lowers hydraulic heads in Layers 1 and 2 without changing the amount of hydraulic connection between them, keeping the gradient relatively constant. Vertical gradients are very sensitive to K_v: decreased K_v values lessen the hydraulic connections between layers and increase vertical gradients. The RMS error indicates that a 25 to 50% increase in K_v values slightly improves the fit as does a 25% decrease in recharge. The improvements are minimal and further analysis showed that the mean error was closest to zero at the calibrated K_v values.

For groundwater flux into Sixmile Creek, as noted, only one measured versus simulated comparison is made, and therefore, the RMS error is equivalent to the absolute difference (Fig 29d). Flux was negligibly affected by changes to K_h but increased with greater K_v values. Groundwater flux into Sixmile Creek is much more sensitive to creek-bed values of K entered in the MODFLOW river package than to K_h, K_v and recharge values. Doubling and halving the creek-bed K values resulted in

a 40% flux increase and a 36% decrease, respectively. The effect is slightly buffered because a decreased conductivity increases the hydraulic gradient between the creek and the aquifer, thereby increasing the flux. Groundwater flux is also sensitive to specified head values beneath the creek which have a direct influence on the gradients between the creek, the model cell containing the creek and the underlying cells. When specified heads in Layers 3 through 6 under creek cells 27 through 40 were raised only 0.06 m, there was a 36% reduction in average flux for those cells. Because of this sensitivity and the uncertainty in specified-head and creek-bed hydraulic conductivity values, flux into Sixmile Creek is not a useful calibration target parameter. The creek is a boundary without impact on most of the modeling area. Since the area in which groundwater discharges to the creek is small and most of the water flows downward and to the south, flow into the creek is not very sensitive to model parameter changes across the whole model area. Unfortunately, flux data for a major hydrologic boundary were not available.

The sensitivity analyses demonstrate that changes to model parameter values can cause improvements in some calibration measures while worsening others. With pre-set calibration targets, it is easier to balance such trade-offs to obtain the best overall calibration.

SUMMARY AND CONCLUSIONS

A three-dimensional groundwater-flow model constructed using MODFLOW incorporated all available hydrogeologic field data from a site in south-central Wisconsin, U.S.A. The model simulated the steady-state groundwater flow within the study area so that the model could be linked to a particle-tracking and contaminant-transport model to give insight into the atrazine contamination susceptibility of the bedrock aquifer.

An important part of the modeling effort was calibration of the groundwater-flow model using statistically-based calibration values and targets that reflect the uncertainty in the value estimation before beginning the calibration process. Variogram analyses and kriging aided in selection of calibration targets

for heads and vertical hydraulic gradients since kriging provides an estimate of the value and incorporates different souces of uncertainty to provide a standard deviation for the kriged value. The model was considered calibrated when the simulated heads and gradients were within 2 standard deviations of the kriged value. To achieve the calibration criteria, model parameter values were maintained within a predetermined, statistically based, plausible range. Although the MODFLOW-simulated values were sometimes quite different from the calibration values at specific model cells, differences were acceptable given the uncertainty of the calibration values.

Sensitivity analyses demonstrated that changes in model parameter values resulting in an improvement in one calibration measure might result in the worsening of another. Pre-set calibration targets help the model user balance such trade offs. Insufficient groundwater flux data for calibration brings into question the uniqueness of the calibrated parameter values, but the use of three other types of calibration targets and the limits placed on the model parameters lend credence to the final calibration and the subsequent simulation of groundwater flow.

In a trial-and-error calibration, model parameter values are adjusted in sequential model runs until simulated heads and flows match measured field conditions. The only way to judge the adequacy of such a match is in relation to the uncertainty of the measured values. Using statistically-determined, pre-set calibration targets based on this uncertainty eliminates much of the subjectivity from model calibration.

REFERENCES

Anderson, M. P. and W. W. Woessner, Applied groundwater modeling: simulation of flow and advective transport, 381 pp., Academic Press, Inc., Harcourt Brace Jovanovich, Publishers, San Diego, CA, 1992.

Birge, A. Professor of Dairy Science, University of Wisconsin-Madison, Madison, WI, Personal communication, 1992.

Bouwer, H. and R. C. Rice, R.C., A slug test for determining hydraulic conductivity of unconfined aquifers with completely or partially penetrating wells. Water Resour. Res., 12 (3), 423-428, 1976.

Bradbury, K. R. and E. R. Rothschild, A computerized technique for estimating the hydraulic conductivity of aquifers from specific capacity data. Ground Water, 23(2), 240-246, 1985.

Brockner, E. L. Superintendent of Waunakee Utilities, Waunakee, WI, Personal communication, 1992.

Cline, D. R., Geology and ground-water resources of Dane County, Wisconsin, 64 pp., Geological Survey Water-Supply Paper 1779-U, United States Government Printing Office, Washington, DC, 1965.

Cryer, J. D. Time series analysis, 286 pp., Duxbury Press, Boston, 1986.

Duffield, G. M. and J. O. Rumbaugh, III, AQTESOLV: aquifer test solver, version 1.00, 135 pp., Geraghty & Miller, Inc., Reston, VA, 1989.

Englund, E. and A. Sparks, Geostatistical environmental assessment software - User's guide. EPA 600/8-91/008, 129 pp. Environmental Monitoring Systems Laboratory, U.S. Environmental Protection Agency, Las Vegas, NV, 1991.

Gelhar, L. W., Stochastic subsurface hydrology from theory to applications. Water Resour. Res., 22(9), 135S-145S, 1986.

Harkin, J. M. Professor of Soil Science, University of Wisconsin-Madison, Madison, WI, Personal communication, 1993.

Levy, J., A field and modeling study of atrazine transport and fate in groundwater. Ph.D. Dissertation, 561 pp., University of Wisconsin-Madison, Madison, WI, 1993.

Levy, J., G. Chesters, H. W. Read and D. P. Gustafson, Distribution, sources and fate of atrazine in groundwater: a field study. J. Contam. Hydrol. In review, 1993.

Levy, J., G. Chesters, Simulation of atrazine and desethylated atrazine transport and fate in a sandy-till aquifer, J. Contam. Hydrol. In review, 1993.

McDonald, M.G. and A. W. Harbaugh, A modular three-dimensional finite-difference groundwater flow model, 528 pp., Open-file report 83-875, US Department of the Interior, US Geological Survey, Reston, VA, 1984.

Neuman, S. P., Analysis of pumping test data from anisotropic unconfined aquifers considering delayed gravity response. Water Resour. Res. 11(2), 329-342, 1975.

Ostrom, M. E. Paleozoic stratigraphic nomenclature for Wisconsin, 5 pp., Info. Circ. No. 8, Wisconsin Geological and Natural History Survey, Madison, WI., 1967.

Rayne, T., Variability of hydraulic conductivity in a sandy till: the effect of scale and method, 134 pp., Ph.D. Dissertation. University of Wisconsin-Madison, 1993.

Ryan, B. F., B. L. Joiner and T. A. Ryan, Jr., Minitab Handbook, Second Edition, 379 pp., Duxbury Press, Boston, 1985.

Stoertz, M. W. and K. R. Bradbury, Mapping recharge areas using a ground-water flow model - a case study, Ground Water, 27(2), 220-228, 1989.

IV. Using an Approximation of the Three-Point Gauss-Hermite Quadrature Formula for Model Prediction and Quantification of Uncertainty

ABSTRACT

Atrazine fate and transport for point- and nonpoint-source conditions is simulated in threedimensions using MT3D in conjunction with a steady-state MODFLOW simulation. Model predictions are combined with an approximation of the three-point Gauss-Hermite quadrature formula to quantify the uncertainty of the model predictions based on the collective uncertainties of the model parameter input values. This represents the first-time hydrogeologic application of this method. The approximation of the Gauss-Hermite method is a convenient substitute for the Monte Carlo approach since it requires fewer model runs and produces an immediate sensitivity analysis of parameter main effects and two-way interactions. The method is described in detail and simplified to facilitate future applications. Example model predictions are presented with their associated uncertainties and sensitivities to model parameters.

INTRODUCTION

The transport model MT3D [*Zheng*, 1990] was used to simulate point- and nonpoint-source atrazine contamination at a field site in south-central Wisconsin, U.S.A., exploring the range of expected concentrations at various depths, locations and times. Predicted answers to modeling questions can be obtained using the best estimates of the model input parameter values and running the model once. Missing from such an analysis is a measure of the uncertainty of the model predictions needed to make intelligent policy decisions based on those predictions. The uncertainty of the model predictions stems from the uncertainty of the model input parameter values.

A method of quantifying model prediction uncertainty is presented. The method is an approximation of the Gauss-Hermite three-point quadrature approach, derived by *Raftery and Zeh* [1993]. The approximation of the Gauss-Hermite method is a convenient substitute to a Monte Carlo approach since it requires fewer model runs and produces an immediate sensitivity analysis of parameter main effects and two-way interactions. The method is described in detail and simplified to facilitate future applications. Example model predictions are presented with associated uncertainties and sensitivities to model parameters. Estimating parameter probability density functions plays an integral role in the

Gauss-Hermite method. Three basic methods for doing so are demonstrated for the example model parameters.

The exemplified field study was conducted on a 4.1 km^2 area to evaluate the sources and distribution of atrazine and its metabolites in a shallow sandy-till aquifer (part of the Horicon Formation) overlying a Cambrian sandstone aquifer from which area residents get their drinking water. Of interest was evaluation of the long-term impact of atrazine use on groundwater quality at the field scale. For such an assessment, three-dimensional modeling is necessary to incorporate the spatial variability of depth to bedrock and account for the hydrologic effects of local surface water bodies. A groundwater-flow model was developed using MODFLOW [*McDonald and Harbaugh*, 1984] and all available hydrogeologic information [*Levy et al.*, 1993]. The chemical and transport parameter values used in the one-dimensional model were also used in MT3D [*Zheng*, 1990] with the calibrated groundwater flow simulation [*Levy*, 1993]. The uncertainties inherent in these chemical and transport parameters were incorporated into the approximation of the Gauss-Hermite method.

APPROACH TO THE ANALYSIS OF PREDICTION UNCERTAINTY

The Gauss-Hermite approach taken here stems from Bayesian methodology [*Press*, 1989], whose concepts are briefly reviewed. The fundamental notion of the Bayesian approach is that parameters and model predictions are uncertain, and this uncertainty can be characterized for each quantity by a probability density function (PDF). Assuming the PDFs are Gaussian, they can be completely described by their expected value and variance. Suppose $g(\theta)$ represents a model function dependent on the single parameter θ and that values of θ are determined by collection and analysis of field and/or laboratory data. The expected value of a model prediction, given the data, is defined as:

$$E[g(\theta)|data] = \int g(\theta)\, f(\theta|data)\, d\theta \qquad (35)$$

where f(θ | data) represents the model parameter value's PDF given the data. The prediction variance is defined as:

$$Var[g(\theta)|data] = \int g(\theta)^2 f(\theta|data)d\theta - \left(E[g(\theta)|data]\right)^2 \qquad (36)$$

In a formal Bayesian approach, f(θ | data) is a posterior PDF of the model parameter depending on a PDF based on information prior to the experiment, f(θ), and the PDF of collected data given the true distribution of parameter values, f(data | θ). Bayes' rule [*Press*, 1989] expresses the relationship as:

$$f(\theta|data) = \frac{f(data|\theta)\, f(\theta)}{\int f(data|\theta)\, f(\theta)\, d\theta} \qquad (37)$$

The PDF of collected data, f(data | θ), is known as the likelihood [*Press*, 1989]. Substituting the Bayesian formula for the posterior PDF into Eqs. 35 and 36, the expected value and variance become:

$$E[g(\theta)|data] = \frac{\int g(\theta)\, f(data|\theta)\, f(\theta)\, d\theta}{\int f(data|\theta)\, f(\theta)\, d\theta} \qquad (38)$$

and

$$Var[g(\theta)|data] = \frac{\int g(\theta)^2\, f(data|\theta)\, f(\theta)\, d\theta}{\int f(data|\theta)\, f(\theta)\, d\theta} - \left(E[g(\theta)|data]\right)^2 \qquad (39)$$

For complex models, the integrals in Eqs. 38 and 39 cannot be determined analytically. However, the difficulties can be avoided using a series of simplifications and assumptions. *Woodbury and Sudicky* [1992] use a formal Bayesian approach in their inverse stochastic simulation of plume migration at the Borden tracer test site in Ontario, Canada [e.g., *Freyberg*, 1986]. To handle the integrals in Eqs. 38, 39 and 40, *Woodbury and Sudicky* [1992] use Monte Carlo integration, which also could be applied to Eqs. 35 and 36. The Monte Carlo approach to Eq. 35, for example, approximates the integral with:

$$\frac{1}{N}\sum_{i=1}^{N} g(\theta_i) \tag{40}$$

where the θ_i are randomly sampled values from $f(\theta \mid \text{data})$. The Monte Carlo method typically requires hundreds to thousands of trials to accurately approximate the integral.

The simplifications and assumptions used here differ from those of *Woodbury and Sudicky* [1992]. Previously, sorption coefficients and dispersivities were derived from field data and regression models based on literature data [*Levy and Chesters*, 1993]. Informally, these parameter-value estimates can be considered posterior estimates because they are based on literature values, regression models and field data. Estimates of degradation rates were based on calibration of the one-dimensional transport model to observed average atrazine and atrazine metabolite concentrations [*Levy and Chesters*, 1993]. The calibration process is one in which subjective information is combined with field data to produce posterior estimates. Thus, the first simplification is to adopt the approach of *Raftery and Zeh* [1993] by sidestepping the formal Bayesian approach in Eqs. 38 and 39 and assuming that the carefully chosen parameter value estimates are posterior and are independent since their estimation comes from different analyses and data sets. With the assumption that estimates of the parameter values represent posterior estimates, the only integrals to be solved are in Eqs. 35 and 36.

The second simplification adopted is to approximate the integrals using the three-point Gauss-Hermite quadrature formula [*Raftery and Zeh*, 1993; *Press et al.*, 1989]. In the Gauss-Hermite method, the integral is approximated by carefully selecting specific θ_i values from $f(\theta \mid \text{data})$ and summing them with appropriate weights. If θ represents a single parameter, the Gauss-Hermite formula is:

$$E[g(\theta)\,|\,data] = \int g(\theta)\, f(\theta\,|\,data)\, d\theta = \frac{1}{6}g(\theta_1) + \frac{2}{3}g(\theta_2) + \frac{1}{6}g(\theta_3) \tag{41}$$

where θ_1, θ_2 and θ_3 are the 0.042, 0.5 and 0.958 quantiles of $f(\theta \mid \text{data})$. The Gauss-Hermite formula is

exact if f(θ | data) is equal to a normal density times any polynomial of degree ≤ 5 [*Press et al.*, 1989]. With only one model parameter, the Gauss-Hermite method requires only three model runs to estimate the expected value of the model prediction. Similarly, estimating variance requires only three model runs:

$$Var[g(\theta)|data] = \frac{1}{6}g(\theta_1)^2 + \frac{2}{3}g(\theta_2)^2 + \frac{1}{6}g(\theta_3)^2 - \left[\frac{1}{6}g(\theta_1) + \frac{2}{3}g(\theta_2) + \frac{1}{6}g(\theta_3)\right]^2 \qquad (42)$$

In the case of two parameters, θ and ϕ:

$$E[g(\theta,\phi)|data] = \int g(\theta,\phi)\, f(\theta|data)\, f(\phi|data)\, d\theta\, d\phi \qquad (43)$$

which is evaluated using all possible combinations of the three specific quantile values and the appropriate coefficients:

$$\begin{aligned} E[g(\theta,\phi)|data] = {} & \frac{1}{6}\cdot\frac{1}{6}g(\theta_1,\phi_1) + \frac{1}{6}\cdot\frac{2}{3}g(\theta_1,\phi_2) + \frac{1}{6}\cdot\frac{1}{6}g(\theta_1,\phi_3) \\ & + \frac{2}{3}\cdot\frac{1}{6}g(\theta_2,\phi_1) + \frac{2}{3}\cdot\frac{2}{3}g(\theta_2,\phi_2) + \frac{2}{3}\cdot\frac{1}{6}g(\theta_2,\phi_3) \\ & + \frac{1}{6}\cdot\frac{1}{6}g(\theta_3,\phi_1) + \frac{1}{6}\cdot\frac{2}{3}g(\theta_3,\phi_2) + \frac{1}{6}\cdot\frac{1}{6}g(\theta_3,\phi_3) \end{aligned} \qquad (44)$$

where the parameter subscripts 1, 2 and 3 refer to the 0.042, 0.5 and 0.958 quantiles, respectively. Eq. 44 can be written more simply as:

$$E[g(\theta,\phi)|data] = \sum_{i=1}^{3}\sum_{j=1}^{3} w_i\, w_j\, g(\theta_i,\phi_j) \qquad (45)$$

where $w_1 = w_3 = 1/6$, $w_2 = 2/3$; and by analogy:

$$Var[g(\theta,\phi)|data] = \sum_{i=1}^{3}\sum_{j=1}^{3} w_i\, w_j\, g(\theta_i,\phi_j)^2 - \left(E[g(\theta,\phi)|data]\right)^2 \qquad (46)$$

Calculation of the expected value and variance for two model parameters requires nine model runs.

Writing out the expected value and variance for the case of more than two model parameters can become unwieldy. For brevity (using the notation of *Raftery and Zeh* [1993]) let θ represent the set of all the model parameters with $\theta_{i,j,k,\ldots n}$ indicating the quantile level assigned to the individual parameters; n applies to the N^{th} parameter. For example, $\theta_{1,2,2,\ldots 3}$ represents the first parameter at the 0.042 quantile, the second and third parameters at the 0.5 quantile, and so on up to the N^{th} parameter at the 0.958 quantile. Eqs. 45 and 46 can be expanded to the general case of N parameters:

$$E[g(\theta)|data] = \sum_{i,j,k,\ldots n=1}^{3} w_i w_j w_k \ldots w_n\, g(\theta_{i,j,k,\ldots n}) \qquad (47)$$

and:

$$Var[g(\theta)|data] = \sum_{i,j,k,\ldots n=1}^{3} w_i w_j w_k \ldots w_n\, g(\theta_{i,j,k,\ldots n})^2 - \left(E[g(\theta)|data]\right)^2 \qquad (48)$$

Calculation of the expected value and variance requires 3^N model runs. With more than four model parameters, application of Eqs. 47 and 48 is computationally demanding because of the time needed to perform each model run.

To save this considerable effort, *Raftery and Zeh* [1993] adopt a further simplification. In their treatment, running the model at the three quantile values of a parameter is akin to investigating the effect of that parameter by considering model runs at the low, mean and high values. For more than one parameter, running the model at all quantile combinations investigates parameter main effects and all

possible parameter interactions. To reduce the number of total model runs, *Raftery and Zeh* [1993] assume that $g(\theta)$ can be approximated by a linear model consisting of the "grand mean", and only the "main effects" and the "two-way interactions" of the parameters.

To exemplify their approximation to the Gauss-Hermite method, the case of three parameters is presented. Using the notation of *Raftery and Zeh* [1993], let g_{ijk} equal $g(\theta_{i,j,k})$ and let u be the "grand mean" equal to g_{222}, i.e., g evaluated with all the parameters at the 0.5 quantile value. The main effect of, for example, the first parameter at the i^{th} level is $u_{1(i)} = g_{i22} - u$, i.e., the model result with the first parameter at the i^{th} level (i = 1, 2 or 3) and the other parameters at the 0.5 quantile level minus the grand mean. The main effect of the second parameter at the j^{th} level is $u_{2(j)} = g_{2j2} - u$. Two-way interactions are represented by u terms with two subscripts. The two-way interaction of the first and second parameters at the i^{th} and j^{th} levels, respectively, is $u_{12(ij)} = g_{ij2} - u_{1(i)} - u_{2(j)} - u$. The two-way interaction of the first and third parameters at the i and k values, respectively, is $u_{13(ik)} = g_{i2k} - u_{1(i)} - u_{3(k)} - u$. The model result for any particular combination of levels for the three parameters can be approximated by the sum of the grand mean, the main effects and the two-way interactions [*Raftery and Zeh*, 1993]:

$$g_{ijk} \approx u + u_{1(i)} + u_{2(j)} + u_{3(k)} + u_{12(ij)} + u_{13(ik)} + u_{23(jk)} \tag{49}$$

Eq. 49 is substituted into Eqs. 47 and the expected value of the model function is evaluated by performing the sums in Eqs. 47 on each of the terms from the right hand side of Eq. 49. Interactions of higher order than two are ignored because they are likely to be small and have low weights in Eq. 47 [*Raftery and Zeh*, 1993]. Because $w_1 + w_2 + w_3 = 1$, the equation can be simplified. For example:

$$\sum_{i,j,k=1}^{3} w_i w_j w_k \, u = u \tag{50}$$

and:

$$\sum_{i,j,k=1}^{3} w_i w_j w_k \, u_{1(i)} = \sum_{i=1}^{3} w_i \, u_{1(i)} \tag{51}$$

For all the terms in Eq. 49, Eq. 47 simplifies to:

$$\begin{aligned} E[g(\theta)\,|\,data] \approx\; & u + \sum_{i=1}^{3} w_i \, u_{1(i)} + \sum_{j=1}^{3} w_j \, u_{2(j)} + \sum_{k=1}^{3} w_k \, u_{3(k)} \\ & + \sum_{i,j=1}^{3} w_i w_j \, u_{12(ij)} + \sum_{i,k=1}^{3} w_i w_k \, u_{1,3(ik)} + \sum_{j,k=1}^{3} w_j w_k \, u_{2,3(jk)} \end{aligned} \tag{52}$$

Eq. 52 represents the approximation of the Gauss-Hermite method for three parameters and requires fewer model runs than the full method in Eq. 47. The full Gauss-Hermite approach would require 27 model runs to account for all possible combinations of parameters at the three quantile levels. The approximation requires only model runs that are components of the grand mean, the main effects and the two-way interactions. The eight model runs with more than two parameter not at the 0.5 quantile level (g_{111}, g_{113}, g_{131}, g_{133},g_{311}, g_{313}, g_{331} and g_{333}) play no part in the analysis. In essence, by ignoring three-way interactions, these runs have been approximated with linear combinations of other model runs. Therefore, only 19 model runs are required to evaluate all terms in Eq. 52: one run is for the grand mean; six model runs are required in which exactly one parameter is not at the 0.5 quantile value -- g_{122}, g_{322}, g_{212}, g_{232}, g_{221} and g_{223}; and twelve model runs are required in which exactly two parameters are not at the 0.5 quantile value, i.e., 4 runs for each of the three combinations of two parameters:

g_{112}, g_{312}, g_{132}, g_{332},
g_{121}, g_{321}, g_{123}, g_{323},
g_{211}, g_{231}, g_{213}, g_{233}.

Each of the terms in Eqs. 52 can be expressed in terms of the component model runs. For example, since $u_{1(i)} = g_{i22} - g_{222}$, then:

$$\sum_{i=1}^{3} w_i\, u_{1(i)} = \frac{1}{6}\,(g_{122} - g_{222}) + \frac{2}{3}\,(g_{222} - g_{222}) + \frac{1}{6}\,(g_{322} - g_{222})$$

$$= \frac{1}{6}\,g_{122} + \frac{1}{6}\,g_{322} - \frac{1}{3}\,g_{222} \qquad (53)$$

or, for example, since $u_{12(ij)} = g_{ij2} - u_{1(i)} - u_{2(j)} - u = g_{ij2} - g_{i22} - g_{2j2} + g_{222}$, then:

$$\sum_{i,j=1}^{3} w_i w_j\, u_{12(ij)} = \frac{1}{6}\cdot\frac{1}{6}\,(g_{112} - g_{122} - g_{212} + g_{222}) + \frac{1}{6}\cdot\frac{1}{6}\,(g_{132} - g_{122} - g_{232} + g_{222})$$
$$+ \frac{1}{6}\cdot\frac{1}{6}\,(g_{312} - g_{322} - g_{212} + g_{222}) + \frac{1}{6}\cdot\frac{1}{6}\,(g_{332} - g_{322} - g_{232} + g_{222})$$

$$= \frac{1}{36}\,(g_{112} + g_{132} + g_{312} + g_{332}) - \frac{1}{18}\,(g_{122} + g_{322} + g_{212} + g_{232}) + \frac{1}{9}\,g_{222} \qquad (54)$$

When i or j = 2, all individual components cancel. By similarly expanding each term in Eq. 52 and simplifying, the expected value can be expressed a weighted average of each of the 19 required model runs:

$$E[g(\theta)|data] \approx \frac{1}{3}g_{222} + \frac{1}{18}g_{122} + \frac{1}{18}g_{322} + \frac{1}{18}g_{212} + \frac{1}{18}g_{232} + \frac{1}{18}g_{221} + \frac{1}{18}g_{223}$$
$$+ \frac{1}{36}g_{112} + \frac{1}{36}g_{312} + \frac{1}{36}g_{132} + \frac{1}{36}g_{332}$$
$$+ \frac{1}{36}g_{121} + \frac{1}{36}g_{321} + \frac{1}{36}g_{123} + \frac{1}{36}g_{323} \qquad (55)$$
$$+ \frac{1}{36}g_{211} + \frac{1}{36}g_{231} + \frac{1}{36}g_{213} + \frac{1}{36}g_{233}$$

and the weights sum to 1. Since $\mathrm{Var}[g(\theta) \mid \mathrm{data}] = E[g(\theta)^2 \mid \mathrm{data}] - (E[g(\theta) \mid \mathrm{data}])^2$, Eq. 55 can be adapted also to determine variance:

$$
\begin{aligned}
Var[g(\theta)|data] \approx\ & \frac{1}{3}g_{222}{}^2 + \frac{1}{18}g_{122}{}^2 + \frac{1}{18}g_{322}{}^2 + \frac{1}{18}g_{212}{}^2 + \frac{1}{18}g_{232}{}^2 + \frac{1}{18}g_{221}{}^2 + \frac{1}{18}g_{223}{}^2 \\
& + \frac{1}{36}g_{112}{}^2 + \frac{1}{36}g_{312}{}^2 + \frac{1}{36}g_{132}{}^2 + \frac{1}{36}g_{332}{}^2 \\
& + \frac{1}{36}g_{121}{}^2 + \frac{1}{36}g_{321}{}^2 + \frac{1}{36}g_{123}{}^2 + \frac{1}{36}g_{323}{}^2 \\
& + \frac{1}{36}g_{211}{}^2 + \frac{1}{36}g_{231}{}^2 + \frac{1}{36}g_{213}{}^2 + \frac{1}{36}g_{233}{}^2 \\
& - \left(E[g(\theta)|data]\right)^2
\end{aligned}
\tag{56}
$$

Note that model runs with equal numbers of parameters at the 0.5 quantile level (i.e., i, j or k = 2) have equal weights. For the case of three parameters, all runs with exactly 2 parameters not at the 0.5 quantile level have weights of 1/36; runs with exactly one parameter not at the 0.5 quantile level have weights of 1/18; the only run with all three parameters at the 0.5 quantile level (the grand mean) has a weight of 1/3.

Eqs. 55 and 56 depict the approximation of the Gauss-Hermite method for the case of three parameters. For the general case of N parameters, the model result for any particular combination of quantile levels can be approximated as:

$$
\begin{aligned}
g_{i,j,k,\ldots n} \approx\ & u + u_{1(i)} + u_{2(j)} + \ldots + u_{N(n)} \\
& + u_{12(ij)} + u_{13(ik)} + \ldots + u_{1N(in)} \\
& + u_{23(jk)} + u_{24(jl)} + \ldots + u_{2N(jn)} + \ldots \\
& + u_{N-2,N-1(n-2,n-1)} + u_{N-2,N(n-2,n)} + u_{N-1,N(n-1,n)}
\end{aligned}
\tag{57}
$$

where n is the quantile level (1, 2 or 3) for the N^{th} parameter. Substituting Eq. 57 into Eq. 48 results in the expected value representation for N parameters:

$$
\begin{aligned}
E[g(\theta)|data] \approx\ & u + \sum_{i=1}^{3} w_i\, u_{1(i)} + \sum_{j=1}^{3} w_j\, u_{2(j)} + \ldots + \sum_{n=1}^{3} w_n\, u_{N(n)} \\
& + \sum_{i,j=1}^{3} w_i w_j\, u_{12(ij)} + \ldots + \sum_{n-1,n=1}^{3} w_{n-1} w_n\, u_{N-1,N(n-1,n)}
\end{aligned}
\tag{58}
$$

For one or two parameters, the application of Eq. 58 and subsequent calculation of the variance is exactly equal to the application of the full Gauss-Hermite formulas in Eqs. 47 and 48 since there are no interactions of order three or higher. As the number of parameters increases above two, the savings in required model runs offered by approximating the Gauss-Hermite formula increases dramatically. For N parameters one run is required for the grand mean and 2xN runs are required for the main effects, i.e., each parameter evaluated at the 0.042 and 0.958 quantiles. (Each parameter evaluated at the 0.5 quantile has already been made in the model run for the grand mean.) For the two-way interactions, four runs are required for each pair of parameters, i.e., evaluation of each parameter in a pair at the 0.042 and 0.958 quantile. For N parameters, there are N(N-1)/2 pairs to consider requiring 2N(N-1) two-way interaction runs in all. For N parameters, the total number of required model runs is $1+2N^2$. The savings in required model runs with increasing numbers of parameters is shown in Table 9.

TABLE 9. Number of Model Runs Required for the Gauss-Hermite Full Method and Approximation

No. of Parameters	Required Number of Model Runs	
	Full Gauss-Hermite	Approximation
1	3	3
2	9	9
3	27	19
4	81	33
5	243	51
6	729	73
7	2,187	99
8	6,561	129

As with the case of three parameters, Eq. 58 can be simplified algebraically and expressed in terms of the weighted sums of the model predictions from each of the required model runs rather than the weighted sums of the main effects and interactions. For a given number of model parameters, the

model-run weights depend on how many parameter values for that run are not at the 0.5 quantile level. The algebraic simplifications have been performed and the appropriate weights have been calculated for up to eight parameters (Table 10) so that the user can refer to this table alone rather than work through Eq. 58. The "class" of a model run referred to in Table 10 is defined by the number of parameter values

TABLE 10. Weights for Each Class of Model Run Given the Number of Model Parameters

	Model-run Class: No. of Parameter Values ≠ 0.5 Quantile Level					
No. of	Class-0		Class-1		Class-2	
Parameters	Weight	# runs	Weight	# runs	Weight	# runs
1	2/3	1	1/6	2	not applicable	
2	4/9	1	1/9	4	1/36	4
3	1/3	1	1/18	6	1/36	12
4	1/3	1	0	8	1/36	24
5	4/9	1	-1/18	10	1/36	40
6	2/3	1	-1/9	12	1/36	60
7	1	1	-1/6	14	1/36	84
8	13/9	1	-2/9	16	1/36	112

≠ 0.5 quantile. The only class-0 run is the grand mean, u. Main effects involve class-0 and class-1 runs; two-way interactions involve all three classes. For a given number of model parameters, the number of required runs falling into each class is shown in Table 10. The total number of model runs for a given number of parameters equals the number of runs shown in Table 9. For example, for three parameters, there are 1, 6 and 12 model runs that are of class-0, class-1 and class-2, respectively (Table 10). Those runs total 19 (Table 9). Eqs. 55 and 56 demonstrate the application of Table 10 to the case of three parameters. Note also from Table 10 that, for a given number of parameters, the sum of all the weights multiplied by the number of associated runs equals 1. For three parameters:

$$\left[(1\ \text{"class-0" run})\times\frac{1}{3}\right] + \left[(6\ \text{"class-1" runs})\times\frac{1}{18}\right] + \left[(12\ \text{"class-2" runs})\times\frac{1}{36}\right] = 1 \quad (59)$$

The expected value is evaluated by multiplying each required model run by the appropriate weight in Table 10 and summing the results. In a fashion directly analogous to Eq. 56, the variance is calculated by applying the same procedure to the squares of the model run results and then subtracting the square of the expected value.

APPLICATION OF THE APPROXIMATION OF THE GAUSS-HERMITE METHOD TO THE MT3D SIMULATIONS

The approximation of the Gauss-Hermite method was applied to predictions made using the three-dimensional chemical-transport model, MT3D [*Zheng*, 1990]. Seven MT3D parameters were included in the analysis. For each parameter, a PDF that depends on the parameter-estimate uncertainty had to be defined so that the 0.042, 0.5 and 0.958 quantile values could be determined.

Parameter Value and PDF Estimation

Three methods for determining PDFs and the appropriate quantile values are exemplified. The method applied depends on the way in which the parameters values are estimated: regression models, a simple collection of values (from either literature or field data) or a guess of a probable range in lieu of other information. In all methods, the PDF is first defined by a mean (the 0.5 quantile value) and an appropriate 95% confidence interval (CI). Knowing the 95% CI of a normal distribution allows computation of the 0.042 and 0.958 quantile values. Specifically, the extreme values of the 95% CI are 1.96 standard deviations from the mean value while the 0.042 and 0.958 quantiles are approximately 1.73 standard deviations from the mean. The differences between the mean and the limits of the 95% CI are

thus multiplied by 1.73/1.96. The 0.042 and 0.958 quantile values are obtained by subtracting and adding the adjusted differences from and to the mean, respectively.

The seven chemical and transport parameter values considered were the Freundlich coefficient and exponent (K_f and a), the dissolved- and sorbed-phase degradation rates (k_1 and k_2), the effective porosity (n_e), longitudinal dispersivity (A_l) and the ratio of longitudinal to transverse dispersivity (A_l:A_t). (Only one ratio is required with the assumption of isotropy. Since the dominant flow direction in the till aquifer being simulated is vertical, the assumption of isotropy in the orthogonal, horizontal directions seems reasonable.) The aquifer was considered homogenous to these parameters. Groundwater velocities were calculated from conductivities and gradients from the MODFLOW solution. Selection of those conductivities and calibration of the MODFLOW simulation are described in detail in *Levy* [1993]. The PDFs for A_l and K_f were based on multiple regression analyses of literature data. Literature-value dependence on site characteristics was examined using multiple linear and log-transformed linear regression models. Once a regression model was found, the site characteristics from this study were used in the regression models as predictors of appropriate MT3D parameter values [*Levy and Chesters*, 1993]. The regression models were used to estimate parameter mean values, and the uncertainty in the estimates of the means stems from the uncertainty of the regression models and the uncertainty of the regression model predictor values. Both sources of uncertainty are incorporated in the design of the MT3D-parameter PDFs. Regression analyses were performed using the computer software package Minitab [*Ryan et al.*, 1985]. For a given set of regression predictor values, Minitab calculates the regression estimate and the 95% CI associated with that estimate, quantifying the uncertainty associated with the regression model itself. The regression predictor value estimates are based on field measurements, and are themselves uncertain. The uncertainty of the predictor values is combined with the uncertainty of the regression model by using the CI extreme values of each predictor to generate the widest possible range

of plausible estimates. For example, in the regression model for the K_f of atrazine, K_f depends on three predictors: pH and organic matter (OM) and clay contents of the medium. Based on field measurements, OM and clay contents and pH have 95% CIs of between 0.17 and 0.21%, 7.3 and 9.3%, and 7.14 and 7.32, respectively. Their average values of 0.19%, 8.3% and 7.23 produced an estimated K_f of 0.37 $\mu g^{1-a} mL^a/g$ (units depend on the Freundlich exponent -- a --) with a 95% CI of 0.054 to 0.68 $\mu g^{1-a} mL^a/g$. Using the 95% CIs of the predictors, the lowest K_f value plausible with the regression model is with 0.17% OM, 7.3% clay and a pH of 7.32. These values produce a mean estimate of 0.30 with a 95% CI of -0.026 (assumed = 0 since K_f cannot be negative) to 0.63 $\mu g^{1-a} mL^a/g$. The highest possible K_f estimate is with 0.21% OM, 9.3% clay and a pH of 7.14, which produces a mean estimate of 0.44 $\mu g^{1-a} mL^a/g$ and a 95% CI of 0.13 to 0.74 $\mu g^{1-a} mL^a/g$. The final PDF for K_f is constructed using the mean predictors, which yield a mean K_f of 0.37, and the extremes of the predictor 95% CIs, which produce an assumed 95% CI of 0 to 0.63 $\mu g^{1-a} mL^a/g$. This final PDF is not symmetrical, but still reflects the uncertainty associated with K_f. As mentioned, the 0.042 and 0.958 quantile values are determined using the 95% CI extremes. The 0.042 quantile value = 0.37-(1.73/1.96)(0.37-0) = 0.043 $\mu g^{1-a} mL^a/g$; the 0.958 quantile value = 0.37+(1.73/1.96)(0.74-0.37) = 0.69 $\mu g^{1-a} mL^a/g$. The PDF for A_l was designed similarly to that for K_f. A regression model was developed from the collection of literature values in *Gelhar et al.* [1992] using only those considered to be of high and moderate reliability. In this regression model, the log of A_l depends on n_e and the log of the scale of the experiment. The n_e was estimated to be 0.15 with an assumed plausible range of 0.07 to 0.25 [*Levy*, 1993]. The scale of interest of the MT3D modeling is approximately 5 to 35 m with a mean of 20 m. In the regression model, these means and ranges yield a mean of 1.38 m and a log-based 95% CI of 0.15 to 10.4 m. To compute the 0.042 and 0.958 quantile values, the differences between the log of 1.38 m (the mean value) and the logs of 0.15 and 10.4 m are multiplied by 1.73/1.96 and subtracted from and

added to the log of the mean. The resulting antilog 0.042 and 0.958 quantile values are 0.19 and 9.8 m.

No significant regression model was found relating the Freundlich exponent -- a -- to sorbent characteristics. Its PDF estimation was therefore more straightforward and is based on a subset of the collection of literature values. For 15 mineral soils with clay contents < 27%, the mean Freundlich exponent is 0.894 with a 95% CI of 0.865 to 0.922. The 0.042 and 0.958 quantile values of this PDF are 0.868 and 0.920. A similar method was used for the PDF of A_l:A_t. Several dispersivity studies summarized by *Gelhar et al.* [1992] provide estimates of transverse horizontal and transverse vertical dispersivity along with longitudinal (in these cases horizontal) dispersivity. Bedding is minimal or nonexistent in the Horicon till, flow is predominantly vertical and isotropy in the horizontal direction was assumed. Therefore, the appropriate estimate of transverse dispersivity is made from the ratios of longitudinal to horizontal transverse dispersivities provided by *Gelhar et al.* [1992]. Ten such estimates of high or intermediate reliability are approximately log-normal and yield a mean A_l:A_t of 8.0 and a 95% CI of 3.6 to 17.8. The 0.042 and 0.958 quantile values are 3.95 and 16.2 and these values were used in the Gauss-Hermite analysis.

Pumping-test data were used to calculate the aquifer specific yield [*Levy*, 1993] and based on that estimate, n_e was assumed to be 0.15 with a plausible range of 0.07 to 0.25. That range was informally assumed to be the 95% CI leading to a PDF estimation with 0.042 and 0.958 quantile values of 0.088 and 0.21.

The parameter values with the most associated uncertainty are dissolved- and sorbed-phase atrazine degradation rates (k_1 and k_2). Mean values were based on calibration of the one-dimensional transport model presented by *Levy and Chesters* [1993]. Since little information exists with which to assign a CI, the calibrated pseudo-first-order degradation rates of 0.00035 day^{-1} (corresponding to half-lives of 2000

d) are assumed to be good to within one-half an order of magnitude. The corresponding 95% CI would be based on a log-normal distribution with a standard deviation of 0.821. The resulting 0.042 and 0.958 quantile values are 0.0000846 and 0.00145 day^{-1}, corresponding to half-lives of 8,200 and 480 d.

The 0.042, 0.5 and 0.958 quantile values for the seven transport parameters involved in the MT3D Gauss-Hermite analysis are summarized in Table 11. The coefficient of molecular diffusion and bulk density of the till were not included in the Gauss-Hermite analysis, but their values are user-specified as $1x10^{-5}$ cm^2/sec and 1.6 g/cm^3, respectively.

TABLE 11. Summary of Parameter Quantile Values Used in the MT3D/Gauss-Hermite Analysis

Parameter	Units	Quantile Value		
		0.042	0.5	0.958
K_f	$\mu g^{1-a} mL^a/g$	0.043	0.37	0.69
a	unitless	0.87	0.89	0.92
A_l	m	0.19	1.4	9.8
$A_l:A_t$	unitless	4.0	8.0	16
n_e	unitless	0.088	0.15	0.21
k_1	day^{-1}	$8.5x10^{-5}$	$3.5x10^{-4}$	$1.4x10^{-3}$
k_2	day^{-1}	$8.5x10^{-5}$	$3.5x10^{-4}$	$1.4x10^{-3}$

MT3D Simulation Objectives

The objective of the MT3D modeling was to simulate atrazine movement and fate within an area of focus given contamination scenarios. The simulations addressed questions of regulatory significance dealing with the expected spatial extent of atrazine contamination, the maximum concentrations expected over time and the rate of concentration dissipation given the best-case outcome of implementation of atrazine-use restrictions and prohibitions. A nonpoint- and a point-source contamination scenario were

examined in detail [*Levy*, 1993]. Concentration distributions were examined horizontally, vertically and temporally. Of interest were: How long is it before steady-state concentrations are reached? What are the ranges of expected concentrations at various depths due to the spatial variability of hydraulic conductivities and gradients? What are the expected concentrations in area private wells that are mostly finished in the bedrock aquifer? After 35 years of simulation, the contamination sources were cut off, i.e., the recharge was given a concentration of 0 ppb. The question was addressed as to how long contamination would be a problem if atrazine use were prohibited and no leaching occurred through the unsaturated zone. (This is a best-case scenario, for in reality, leaching may continue for many years after application.) To address all these questions, the Gauss-Hermite approach was applied to predicted concentrations at many model cells and at many simulated times. To demonstrate the Gauss-Hermite approach, only a subset of those predictions and their uncertainties is presented here. Specifically, given the nonpoint-source contamination scenario, what is the expected 35-year concentration in the location with the maximum simulated concentration, and what happens to those concentrations over time after contamination ceases? Predictions are noted in the shallowest model layer (Layer 1) and the layer corresponding to the uppermost bedrock layer throughout much of the area of focus (Layer 4).

Model Predictions: Expected Values, Variances and Grand Means

The approximation of the Gauss-Hermite method is now applied to the subset of MT3D model predictions using the quantile values presented in Table 11. The examples demonstrate the method as well as its usefulness in the assessment of certain aspects of complex groundwater contamination problems. Estimating the expected values and variances of the MT3D predictions using the approximation requires 99 model runs when seven parameters are involved (Table 9). Results are presented in Table 12. Model-Layer 1 extends from the water table to an average depth of 3.1 m below

the water table. Layer 4 extends an average of 17 to 26 m below the water table. The "grand mean" results are included for comparison. The grand mean model run is the one in which all parameters are at their 0.5 quantile values [*Raftery and Zeh*, 1993] and is equal to the expected value only if model results for the other quantile values are equally distributed about the grand mean. The grand mean is the conventional deterministic prediction based on the best parameter-value estimates.

TABLE 12. Prediction of the Maximum Atrazine Concentrations at Various Depths and Times Given Nonpoint-Source Contamination

Prediction	Expected value (ppb)	Variance (ppb^2)	2 x Stnd Error (ppb)	95% Confidence Interval (ppb)	Grand mean (ppb)
Layer 1, 35 yr	1.32	2.89×10^{-1}	1.08	0.241 to 2.39	1.35
Layer 1, 40 yr	0.339	6.47×10^{-2}	0.509	0 to 0.847*	0.325
Layer 1, 45 yr	0.142	2.55×10^{-2}	0.319	0 to 0.461	0.109
Layer 1, 50 yr	0.0730	1.25×10^{-2}	0.224	0 to 0.297	0.0414
Layer 1, 55 yr	0.0418	6.24×10^{-3}	0.158	0 to 0.200	0.0169
Layer 1, 60 yr	0.0262	3.32×10^{-3}	0.115	0 to 0.141	0.00710
Layer 4, 35 yr	0.0896	4.16×10^{-2}	0.408	0 to 0.498	0.0137
Layer 4, 40 yr	0.0792	3.10×10^{-2}	0.352	0 to 0.432	0.0137
Layer 4, 45 yr	0.0544	1.23×10^{-2}	0.222	0 to 0.276	0.0113
Layer 4, 50 yr	0.0387	5.80×10^{-3}	0.152	0 to 0.191	0.00810
Layer 4, 55 yr	0.0278	3.23×10^{-3}	0.114	0 to 0.141	0.00510
Layer 4, 60 yr	0.0215	2.28×10^{-3}	0.0955	0 to 0.117	0.00300

*Negative concentrations have been replaced by 0 ppb.

Some of the 95% CIs are quite large, reflecting the large uncertainty in the parameter input values. The large 95% CI for the maximum Layer 1 concentrations at 35 years covers the majority of the possible range of concentrations. Deeper in the system, however, the 95% CIs are narrower. At > 17.8 m below the water table (Layer 4 and below), concentrations are unlikely to ever exceed 0.5 ppb no matter how enduring the contamination (Table 12). Analyses indicate that under the given scenario,

the bedrock aquifer is relatively safe from violations of the Wisconsin groundwater standards -- the preventive action limit of 0.3 ppb and the enforcement standard of 3.0 ppb -- when the depth to bedrock is > 20 m. If all leaching to the water table were to abruptly cease, the expected Layer 1 maximum concentration falls to < 0.3 ppb in about 6 years after the contamination input stops, but the 95% CI high concentration falls to < 0.3 ppb only after 15 years.

The approximation of the Gauss-Hermite method was applied to the MT3D runs for the cases of one through seven parameters, progressively. Preliminary analysis indicated the order of model parameter sensitivity, and parameters were added in that order. An example of the trend in expected value and variance with additional model parameters included in the analysis is shown (Figure 30). In this example, the Layer 1 concentration at a cell with intermediate groundwater velocity is predicted. Based on marginal increases in the variance, most of the prediction uncertainty is explained by parameters K_f and k_2. Additional parameters do not increase prediction variance, but have some impact on the expected values. The impact of parameters K_f and k_2 on prediction variance can be demonstrated by excluding them from the Gauss-Hermite analysis. Their exclusion from the analysis applied to the maximum Layer 1 concentration prediction results in a much smaller 95% CI (Table 13).

TABLE 13. Prediction of Layer 1 Maximum Atrazine Concentrations at Various Times Given Nonpoint-Source Contamination --Analysis Excludes the Sorption Coefficient and the Sorbed-Phase Degradation Rate Constant

Prediction	Expected value (ppb)	Variance (ppb^2)	2 x Stnd Error (ppb)	95% Confidence Interval (ppb)	Grand mean (ppb)
Layer 1, 35 yr	1.28	3.50×10^{-2}	0.374	0.902 to 1.65	1.35
Layer 1, 40 yr	0.302	3.98×10^{-3}	0.126	0.176 to 0.429	0.325
Layer 1, 45 yr	0.101	6.10×10^{-4}	0.0494	0.051 to 0.150	0.109
Layer 1, 50 yr	0.0383	1.17×10^{-4}	0.0216	0.017 to 0.0599	0.0414
Layer 1, 55 yr	0.0156	2.43×10^{-5}	0.0099	0.006 to 0.0255	0.0169
Layer 1, 60 yr	0.0066	5.10×10^{-6}	0.0045	0.002 to 0.0111	0.0071

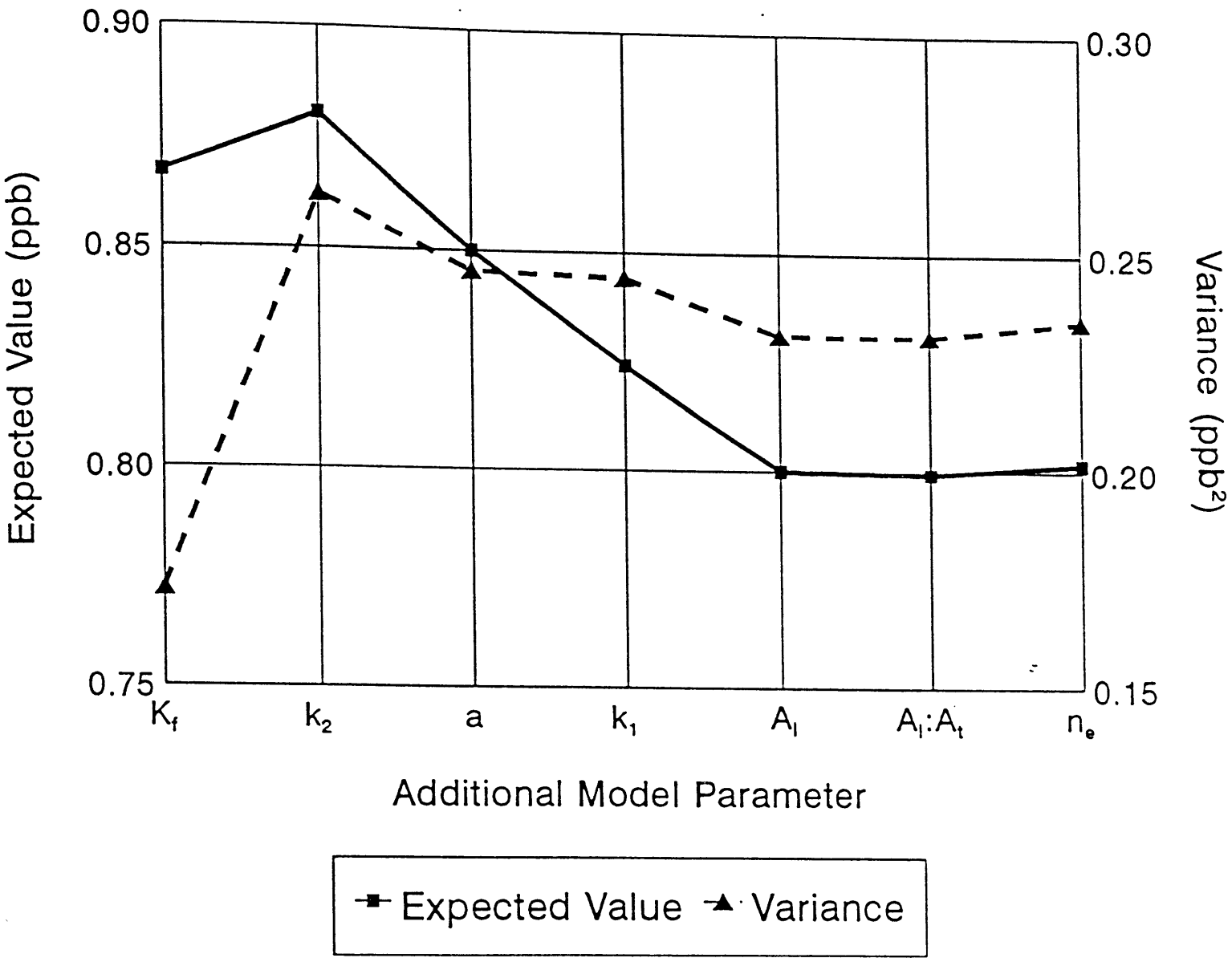

Fig. 30. Change in a cell's predicted concentration expected value and variance with additional model parameters included in the Gauss-Hermite analysis.

USING THE GAUSS-HERMITE APPROACH IN A SENSITIVITY ANALYSIS

A benefit of the Gauss-Hermite procedure is that the sensitivity of model predictions to the parameters is easily quantified. The measure of sensitivity applies not to an arbitrary percent change in parameter value, but to the parameter PDF as defined by the 0.042 and 0.958 quantile values. Also quantifiable is a measure of the interactive effects of any two parameters. In some cases, a single parameter may not have a large impact on model predictions, but its interaction with another parameter can be dramatic. Quantifying the two-way interactions is difficult using a deterministic or Monte Carlo modeling approach.

Prediction sensitivity to model parameters and parameter-pair interactions is quantified using the definitions of parameter main effects and interactions presented earlier. For example, the main effect of the first of seven parameters at the i^{th} level is $u_{1(i)} = g_{i222222} - u$, where u is the grand mean. To evaluate the total main effect of the first parameter throughout its PDF, this quantity is evaluated by summing the component main effects at the 0.042, 0.5 and 0.958 quantile values. The main effect at the 0.5 quantile value is always 0. Since the sign of each main effect component is not relevant in assessing sensitivity, the total parameter main effect is defined as the sum of the squares of the 0.042 and 0.958 quantile components, so for the N^{th} model parameter:

$$\textit{Total Main Effect of } N^{th} \textit{ Parameter} = u_{N(1)}^{\ 2} + u_{N(3)}^{\ 2} \qquad (60)$$

where $u_{N(1)}$ and $u_{N(3)}$ are the 0.042 and 0.958 quantile component main effects. To compare the relative sensitivity of various predictions to the model parameters, the quantity derived in Eq. 60 is standardized by taking the square root and dividing by the expected value of the prediction.

As defined earlier, two-way interactions are the model predictions minus the individual main effects minus the grand mean. For example, the interaction between the first two of seven parameters, both at level 1 (the 0.042 quantile value) is:

$$u_{12(11)} = g_{11\underline{2}\underline{2}\underline{2}\underline{2}} - u_{1(1)} - u_{2(1)} - u \tag{61}$$

which simplifies to:

$$u_{12(11)} = g_{11\underline{2}\underline{2}\underline{2}\underline{2}} - g_{1\underline{2}\underline{2}\underline{2}\underline{2}} - g_{21\underline{2}\underline{2}\underline{2}} + u \tag{62}$$

For evaluation of the complete interactive effect of the first two parameters, the value in Eq. 62 is considered one of nine components representing all combinations of the three quantile values (i.e., 1-1, 1-2, 1-3, 2-1, 2-2, etc.). All components with combinations involving the second quantile level equal 0, leaving four components. As in the case of total main effects, the total two-way interactions are evaluated by taking the sum of the squares of the individual components. For the first two parameters, the total interaction is:

$$\begin{aligned} \textit{Total Parameter } 1\text{-}2 \textit{ Interaction} = {} & \left(g_{11\underline{2}\underline{2}\underline{2}\underline{2}} - g_{1\underline{2}\underline{2}\underline{2}\underline{2}} - g_{21\underline{2}\underline{2}\underline{2}} + u\right)^2 \\ & + \left(g_{13\underline{2}\underline{2}\underline{2}\underline{2}} - g_{1\underline{2}\underline{2}\underline{2}\underline{2}} - g_{23\underline{2}\underline{2}\underline{2}} + u\right)^2 \\ & + \left(g_{31\underline{2}\underline{2}\underline{2}\underline{2}} - g_{3\underline{2}\underline{2}\underline{2}\underline{2}} - g_{21\underline{2}\underline{2}\underline{2}} + u\right)^2 \\ & + \left(g_{33\underline{2}\underline{2}\underline{2}\underline{2}} - g_{3\underline{2}\underline{2}\underline{2}\underline{2}} - g_{23\underline{2}\underline{2}\underline{2}} + u\right)^2 \end{aligned} \tag{63}$$

Again, this quantity is standardized by taking its square root and dividing by the expected value of the prediction.

Application of the Gauss-Hermite Sensitivity Analysis to the MT3D Simulations

The model sensitivity to single or paired parameters was evaluated using Eqs. 60 and 63 for various model predictions. Table 14 presents the standardized total main effects for four of the 12 model predictions presented in Table 12. Predictions of the 35- and 50-year maximum concentrations are shown for Layers 1 and 4. In general, model predictions are most sensitive to K_f and k_2. This is not surprising, since it was shown that most of the model prediction uncertainty resulted from uncertainty associated with these parameters. The magnitudes of the sensitivities usually drop substantially for other parameters.

TABLE 14. Sensitivity of Maximum Concentration Predictions to Single Parameters -- Total Main Effects

Layer 1, 35 yr		Layer 1, 50 yr		Layer 4, 35 yr		Layer 4, 50 yr	
Parameter	Total Main Effect	Parameter	Total Main Effect	Parameter	Total Main Effect	Parameter	Total Main Effect
k_2	8.2×10^{-1}	k_2	4.1	K_f	4.9	k_2	3.8
K_f	7.5×10^{-1}	k_1	3.4×10^{-1}	k_2	1.2	K_f	2.0
A_l	3.0×10^{-1}	K_f	1.7×10^{-1}	A_l	2.2×10^{-1}	a	1.9×10^{-1}
k_1	1.7×10^{-1}	A_l	1.5×10^{-1}	a	1.5×10^{-1}	A_l	1.7×10^{-1}
a	1.1×10^{-1}	a	5.0×10^{-2}	k_1	8.4×10^{-2}	k_1	1.5×10^{-1}
n_e	3.8×10^{-2}	n_e	1.2×10^{-2}	n_e	2.3×10^{-2}	n_e	3.5×10^{-2}
$A_l:A_t$	2.4×10^{-2}	$A_l:A_t$	7.0×10^{-3}	$A_l:A_t$	9.5×10^{-3}	$A_l:A_t$	1.7×10^{-2}

Generally, the parameters with the third and fourth largest main effects are k_1 and A_l. A more complete sensitivity analysis for many model predictions [*Levy*, 1993] revealed that the relative sensitivities depend on what is being predicted. As time increases, sensitivity to the sorption coefficients decreases while sensitivities to the degradation rates increase. Sorbed-phase degradation plays a larger role than dissolved-phase because even with the small sorption coefficients used, the majority of the contaminant is in the sorbed phase. Model predictions are quite insensitive to porosity because it plays a controlling role in groundwater velocity and contaminant retardation. Velocity and retardation both increase with decreasing porosity. With high sorption rates, the increase in velocity is almost completely cancelled by the increase in retardation. The dispersivity ratio $A_l:A_t$ plays a negligible role in the nonpoint-source scenario simulations, since the contamination input was simulated over a large horizontal area and groundwater movement is predominantly vertical.

With seven model parameters, there are 21 possible parameter pairs and associated total two-way interactions for every model prediction. Table 15 presents the 10 largest interactions for the same four predictions presented in Table 14. The most prominent interactions are between K_f and k_2, K_f and k_1, k_1 and k_2, and K_f and a. The relative importance of the degradation rate of a phase depends on how much compound is sorbed and how much is dissolved, explaining the strong interactions between sorption and degradation. The interaction between degradation rates arises because the dissolved-phase degradation rate is only important when the sorbed-phase degradation rate is low. Similarly, when sorption is low, dispersivity plays a relatively minor role. The most important interactions involving degradation rates increase with time and depth and decrease with velocity. The interaction between the sorption coefficient and exponent decreases with time and velocity and increases with depth.

TABLE 15. Sensitivity of Predicted Maximum Concentrations Parameter-Pair Interactions -- Values are the Standardized Total Two-Way Interactions

Layer 1, 35 yr		Layer 1, 50 yr		Layer 4, 35 yr		Layer 4, 50 yr	
Parameter Pair	Total 2-Way Interact	Parameter Pair	Total 2-Way Interact	Parameter Pair	Total 2-Way Interact	Parameter Pair	Total 2-Way Interact
K_f, a	6.8×10^{-1}	K_f, k_2	3.5	K_f, k_1	5.8	K_f, k_1	4.8
K_f, k_2	4.8×10^{-1}	k_2, k_1	3.1	K_f, a	4.9	k_1, k_2	3.4
$A_l{:}A_t, n_e$	3.2×10^{-1}	k_2, A_l	9.4×10^{-1}	K_f, k_2	4.8	K_f, k_2	3.4
K_f, k_1	3.0×10^{-1}	k_2, n_e	7.1×10^{-1}	K_f, n_e	2.2	K_f, a	2.0
k_2, A_l	2.8×10^{-1}	K_f, k_1	5.3×10^{-1}	k_1, k_2	9.0×10^{-1}	a, k_2	1.5
k_2, k_1	2.2×10^{-1}	K_f, a	3.7×10^{-1}	$k_2{:}A_l$	7.8×10^{-1}	k_2, n_e	1.2
K_f, A_l	1.6×10^{-1}	K_f, A_l	2.3×10^{-1}	a, k_2	6.4×10^{-1}	k_2, A_l	8.8×10^{-1}
K_f, n_e	7.8×10^{-2}	a, k_2	1.7×10^{-1}	K_f, A_l	5.7×10^{-1}	$K_f{:}A_l$	7.9×10^{-1}
k_1, n_e	7.7×10^{-2}	k_1, n_e	1.3×10^{-1}	k_2, n_e	4.1×10^{-1}	$A_l{:}A_t, n_e$	2.9×10^{-1}
A_l, n_e	6.8×10^{-2}	K_f, n_e	1.3×10^{-1}	$A_l{:}A_t, n_e$	2.2×10^{-1}	$k_2, A_l{:}A_t$	2.0×10^{-1}

COMPARISON OF THE FULL AND APPROXIMATE GAUSS-HERMITE ANALYSES

As in *Raftery and Zeh* [1993], one of the simplifications made in this study was to ignore all interactions of order three and higher. The effect of higher order interactions on expected values and variances were assumed negligible because the interactions are likely to be small and their weights are small in Eqs. 47 and 48. This assumption was tested using the case of three parameters. With three parameters, the full Gauss-Hermite analysis (Eqs. 47 and 48) requires only eight additional runs over the approximation (Eqs. 55 and 56), representing the three-way interactions. In each additional run, all three parameters involved are at either the 0.042 or 0.958 quantile levels. For the nonpoint-source scenario, 96 concentration predictions were made spanning four locations, four layers and six times [*Levy*, 1993]. The parameters involved in the analyses were K_f, k_2 and a. For the 96 predictions, the expected values and variances of the full and approximate analyses were nearly identical. The ratios of approximate:full analysis expected values ranged from 0.957 to 1.007 and averaged 0.985. Ratios for the variances ranged from 0.967 to 1.02 and averaged 0.995. For the point-source scenario, concentration predictions were made at five private wells at six times [*Levy*, 1993]. Expected value ratios ranged from 0.997 to 1.006 and averaged 1.000. Variance ratios ranged from 0.996 to 1.017 and averaged 1.005. Based on the analyses, third and higher order interactions can safely be ignored.

SUMMARY AND CONCLUSIONS

Simulations of three-dimensional atrazine transport within an area of focus were made using MT3D [*Zheng*, 1990]. The simulations combined a calibrated, steady-state three-dimensional groundwater flow model [*Levy et al.*, 1993] with estimates of atrazine transport parameter values [*Levy and Chesters*, 1993]. One simulated scenario assumed spatially constant nonpoint-source contamination in which the recharge reaching the water table everywhere is contaminated with 3.0 ppb atrazine. Contamination continues for 35 simulated years and then abruptly stops. The scenario was simulated to

examine the effects of long-term contamination and the nature of the subsequent dissipation.

The uncertainty of the model predictions resulting from uncertainty in the input parameter values was quantified using the approximation of the Gauss-Hermite method [*Raftery and Zeh*, 1993]. Model predictions are considered probability density functions (PDFs) with expected values that are integrals of the products of the complex model function performed on model parameter values and the individual PDFs of those parameter values. The variance is the same integral with the model function squared minus the square of the expected value. The approach is essentially Bayesian, in which the parameter PDFs represent the posterior PDFs based theoretically on field and laboratory data and prior information. In this approach, a number of simplifications and assumptions are made to allow approximation of the required integrals. The first is to estimate the parameter PDFs based on literature values, regression analyses and previous modeling [*Levy and Chesters*, 1993] and to consider the parameter PDFs to be posterior PDFs based on the analyses and vague prior information. The second simplification is to use the Gauss-Hermite approach to solve the integral, providing an exact solution assuming the parameter PDFs are equal to normal density functions times any polynomial of degree ≤ 5. The third simplification is to approximate the Gauss-Hermite solution ignoring parameter interactions of order three and higher. For quantifying uncertainty, the approximation of the Gauss-Hermite method represents a significant computational saving over such alternatives as the Monte Carlo approach. For the case of three parameters, the approximation was shown to be accurate compared to the full method.

The Gauss-Hermite analysis was performed with seven MT3D parameters. Certain model predictions were used to exemplify the approximation of the Gauss-Hermite approach. The uncertainty of the model predictions mostly stemmed from the uncertainty associated with the sorption coefficient and sorbed-phase degradation rate. The resulting 95% CIs for concentration predictions in shallow groundwater were quite large indicating, for example, that, given recharge entering the system at 3.0 ppb atrazine, maximum Layer 1 (the water table to 3.1 m below the water table) concentrations are not likely

to exceed 2.4 ppb. Deeper concentration predictions had smaller 95% CIs; for example, concentrations at > 8.2 and 17.8 m below the water table are unlikely to exceed 0.9 and 0.5 ppb given the nonpoint-source contamination scenario. The expected maximum shallow concentration, 5 years after contamination ceases, is about 0.3 ppb (the Wisconsin preventive action limit), but it takes about 15 years before it becomes very unlikely (i.e., outside the 95% CI) for concentrations to exceed 0.3 ppb.

The approximation of the Gauss-Hermite approach provides a simple method of quantifying prediction sensitivity to the parameter PDFs and their interactions. For example, predictions are generally most sensitive to the Freundlich sorption coefficient and the sorbed-phase degradation rate, and their interaction is quite strong. Dissolved-phase degradation rate and longitudinal macrodispersivity play a secondary role, as do their interactions with other model parameters. Model predictions are very insensitive to porosity and the macrodispersivity anisotropy ratio. Such sensitivities can signify needed areas of future research. In the case presented here, for example, more research is needed to differentiate and quantify atrazine degradation rates for the sorbed and dissolved phases.

Acknowledgments. These investigations were supported in part by grants from the University of Wisconsin-System, the Wisconsin Departments of Agriculture, Trade and Consumer Protection, and of Natural Resources and the U.S. Geological Survey. Our sincerest appreciation is extended to Daniel P. Gustafson and Harry W. Read for atrazine-residue determination and their help in the collection of hydrogeologic field data.

REFERENCES

Freyberg, D. L., A natural gradient experiment on solute transport in a sand aquifer. 2. Spatial moments and the advection and dispersion of nonreactive tracers. *Water Resources Res.* 22(13):2031-2046. 1986

Gelhar, L. W., C. Welty and K. R. Rehfeldt, A critical review of data on field-scale dispersion in aquifers. *Water Resour. Res.*, 28(7):1955-1974, 1992.

Levy, J., A field and modeling study of atrazine transport and fate in groundwater. Ph.D. Dissertation, 561 pp., University of Wisconsin-Madison, Madison, WI, 1993.

Levy, J., G. Chesters, Simulation of atrazine and desethylated atrazine transport and fate in a sandy-till aquifer, *J. Contam. Hydrol.* In review, 1993.

Levy, J., M. K. Clayton, M. P. Anderson and G. Chesters, Simulation of groundwater flow with the use of geostatistical methods for model calibration. *Water Resour. Res.* In review, 1993.

McDonald, M.G. and A. W. Harbaugh, A modular three-dimensional finite-difference groundwater flow model, 528 pp., *Open-file report 83-875*, US Department of the Interior, US Geological Survey, Reston, VA, 1984.

Press, S. J. *Bayesian statistics: Principles, models and applications*, 237 pp., John Wiley, New York, 1989.

Press, W. H., B. P. Flannery, S. A. Teukolsky and W. T. Vetterling. *Numerical Recipes: The Art of Scientific Computing*, Cambridge University Press, Cambridge, 1989.

Raftery, A. E. and J. E. Zeh, Estimation of bowhead whale, *Balaena mysticetus*, population size. In: Gatsonis, C., Hodges, J., Kass, R. and Singpurwalla, N. (eds) *Case Studies in Bayesian Statistics in Science and Technology*, Springer-Verlag, Berlin, 1993.

Ryan, B. F., B. L. Joiner and T. A. Ryan, Jr., *Minitab Handbook, Second Edition*, 379 pp., Duxbury Press, Boston, 1985.

Woodbury, A. D. and E. A. Sudicky, Inversion of the Borden tracer experiment data: Investigation of stochastic moment models, *Water Resour. Res.*, 28(9):2387-2398, 1992.

Zheng, C., *MT3D: a modular three-dimensional transport model for simulation of advection, dispersion and chemical reactions of contaminants in groundwater systems*, S.S. Papadopulos & Associates, Inc., Rockville, MD, 1990.

V. Assessing Aquifer Susceptibility to and Severity of Atrazine Contamination at a Field Site in South-central Wisconsin

ABSTRACT

A 33-month field study was conducted on a 4.1 km^2 area encompassing three dairy farms in south-central Wisconsin, USA to study the sources and distribution of atrazine and atrazine metabolites in groundwater and to relate the contaminant distribution to the groundwater-flow system. A modeling approach was used to assess deep aquifer susceptibility to contamination as well as the potential long-term impact of atrazine contamination on area drinking water quality. A particle-tracking program, PATH3D, was used in conjunction with a calibrated MODFLOW simulation to estimate groundwater travel paths and times throughout the monitoring area. The estimated travel time from the water table to the bedrock surface was used as an indication of the susceptibility of the bedrock aquifer to contamination. Spatial distribution of the estimates demonstrates that in addition to depth to bedrock and hydraulic conductivity, shallow surface-water bodies can have a dramatic influence on travel time to bedrock. The range of estimates illustrates the difficulty of determining susceptible areas on a state- or even county-wide scale. Travel times to private wells in the area were estimated and are related to atrazine residue concentrations found in water from those wells.

The potential impact of long-term atrazine use and leaching to groundwater on aquifer water quality was investigated with nonpoint- and point-source scenario simulations of atrazine fate and transport using MT3D in conjunction with the MODFLOW simulation. The predictions integrate predicted flow-paths and estimated chemical parameter values to detail the aquifer's susceptibility to atrazine contamination. A modeling approach was used in which predicted concentrations at various depths and times are presented with their associated uncertainties. The regulatory implications of the modeling results were considered.

INTRODUCTION

A field study was conducted on a 4.1 km^2 area in Dane County, Wisconsin, USA (Fig. 31), to investigate sources and distribution of atrazine and its metabolites in a shallow sandy-till aquifer overlying a Cambrian sandstone aquifer from which area residents get their drinking water. One objective was to relate contaminant distribution to the groundwater-flow system. Relationships between atrazine and metabolite concentrations and the groundwater-flow system are described in Levy et al. (1993a), which provide insights into atrazine and metabolite degradation processes and rates. Atrazine transport and fate was simulated in one dimension at individual piezometer-nest sites (Levy and Chesters, 1993) where hydraulic gradients and predicted flow paths were predominantly downward. Freundlich sorption coefficients and dispersivity were estimated using site characteristics and multiple linear regression models

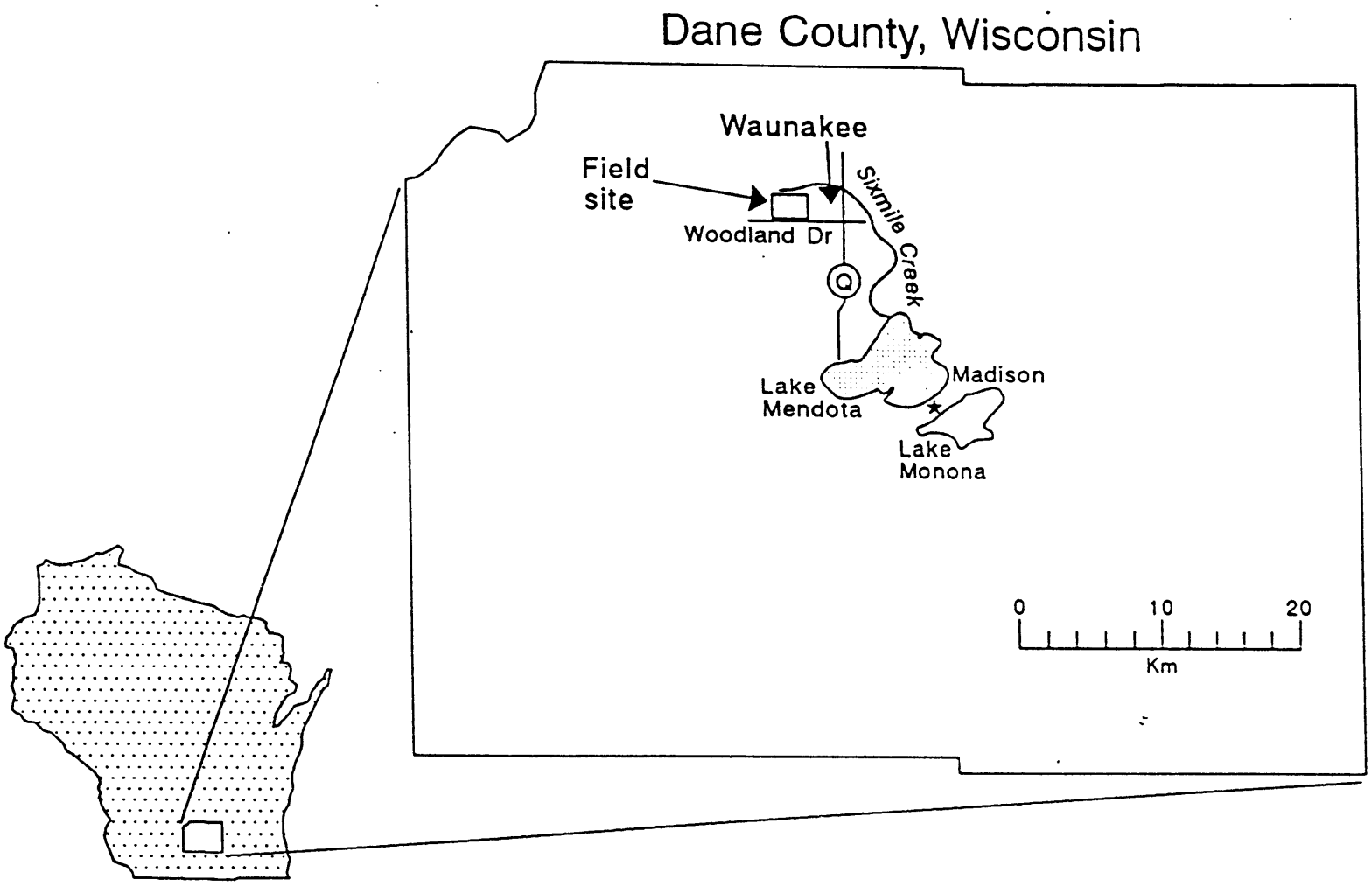

Fig. 31. Field site location.

based on literature data. The one-dimensional simulations were calibrated to match relationships between time-averaged atrazine concentrations at individual sampling-point locations and estimates of groundwater travel-time to those points. The calibration allowed the estimation of pseudo-first-order atrazine degradation rates.

The distribution of atrazine in shallow groundwater and the relationships of the concentrations to the local groundwater-flow system allow an assessment of the potential long-term impact of atrazine leaching to groundwater. Such assessments are useful to regulatory agencies trying to evaluate the severity and future threat of contamination problems. The Wisconsin Department of Agriculture, Trade and Consumer Protection currently regulates atrazine use by establishing maximum application rates for atrazine of outright prohibition. To assess the effectiveness of such actions, regulators must know the longevity of atrazine in groundwater. The assessment of susceptibility, long-term threat and potential dissipation is presented in detail for the specific case of atrazine at the Wisconsin field site, but the general strategy has universal applicability. A two-pronged approach is employed. The first component estimates groundwater travel times from the water table to the bedrock surface and to area domestic wells using a particle-tracking program, PATH3D (Zheng, 1991) in conjunction with a three-dimensional simulation of groundwater flow using MODFLOW (McDonald and Harbaugh, 1984). Since only advection is considered, the first component is not compound-specific. The second component is a contaminant-transport model of specific compounds using MT3D (Zheng, 1990) in conjunction with the MODFLOW simulation. In lieu of actual contaminant-input information, nonpoint- and point-source contamination scenarios are simulated and predicted concentrations are noted at various depths and times. The scenarios include eradication of the contaminant to address atrazine dissipation. The MT3D simulations incorporate sorption, degradation and dispersivity estimated by the one-dimensional contaminant-transport modeling (Levy and Chesters, 1993) into the calibrated flow model (Levy et al.,

1993b). Because much uncertainty is associated with estimation of those parameter values, a modeling approach is employed by which predicted concentrations are presented with associated uncertainties.

SITE DESCRIPTION AND HYDROGEOLOGY

Within a 4.1 km^2 area, monitoring wells were installed at 25 locations and included water-table wells, piezometer nests, creek piezometers and multilevel sampling units (Fig. 32); the area comprises two hydrostratigraphic units. The upper sandy till unit is part of the Horicon Formation of undifferentiated Quaternary deposits; no bedding planes were observed in split-spoon samples. Typical grain-size distribution is 65 to 75% sand, 15 to 30% silt and 1 to 15% clay with pebbles and cobbles up to 20 cm in diameter. In the monitored area, till thickness ranges from < 7 m overlying a bedrock drumlin to > 40 m overlying a bedrock valley near Waunakee Marsh. For most of the monitored area, bedrock comprises various Cambrian sandstones containing dolomite and shale (Cline, 1965; Ostrom, 1967). The sandstone aquifer extends to the Precambrian bedrock surface at about 47 m above mean sea level (msl), a thickness of 190 to 235 m.

Hydraulic conductivity of the till aquifer was measured using piezometer slug tests (Bouwer and Rice, 1976). Conductivities were distributed approximately log-normally with a mean of 1.2×10^{-4} cm/sec and a 95% confidence interval of 6.7×10^{-5} to 2.3×10^{-4} cm/sec. Bedrock hydraulic conductivities were calculated based on specific capacity data from private well logs using the computer program TGUESS (Bradbury and Rothschild, 1985). Bedrock conductivities were log-normally distributed with a mean of 3.5×10^{-3} cm/sec and a 95% confidence interval of 2.5×10^{-3} to 4.9×10^{-3} cm/sec. Vertical hydraulic conductivities were estimated from measured horizontal hydraulic conductivities and a horizontal to vertical hydraulic conductivity anisotropy ratio (K_h:K_v). Estimates of K_h:K_v can be obtained from time-drawdown curves from aquifer pumping tests. Although no pumping tests were performed at this site, Rayne (1993) conducted two pumping tests in the Horicon Formation at a site 22 km to the southeast.

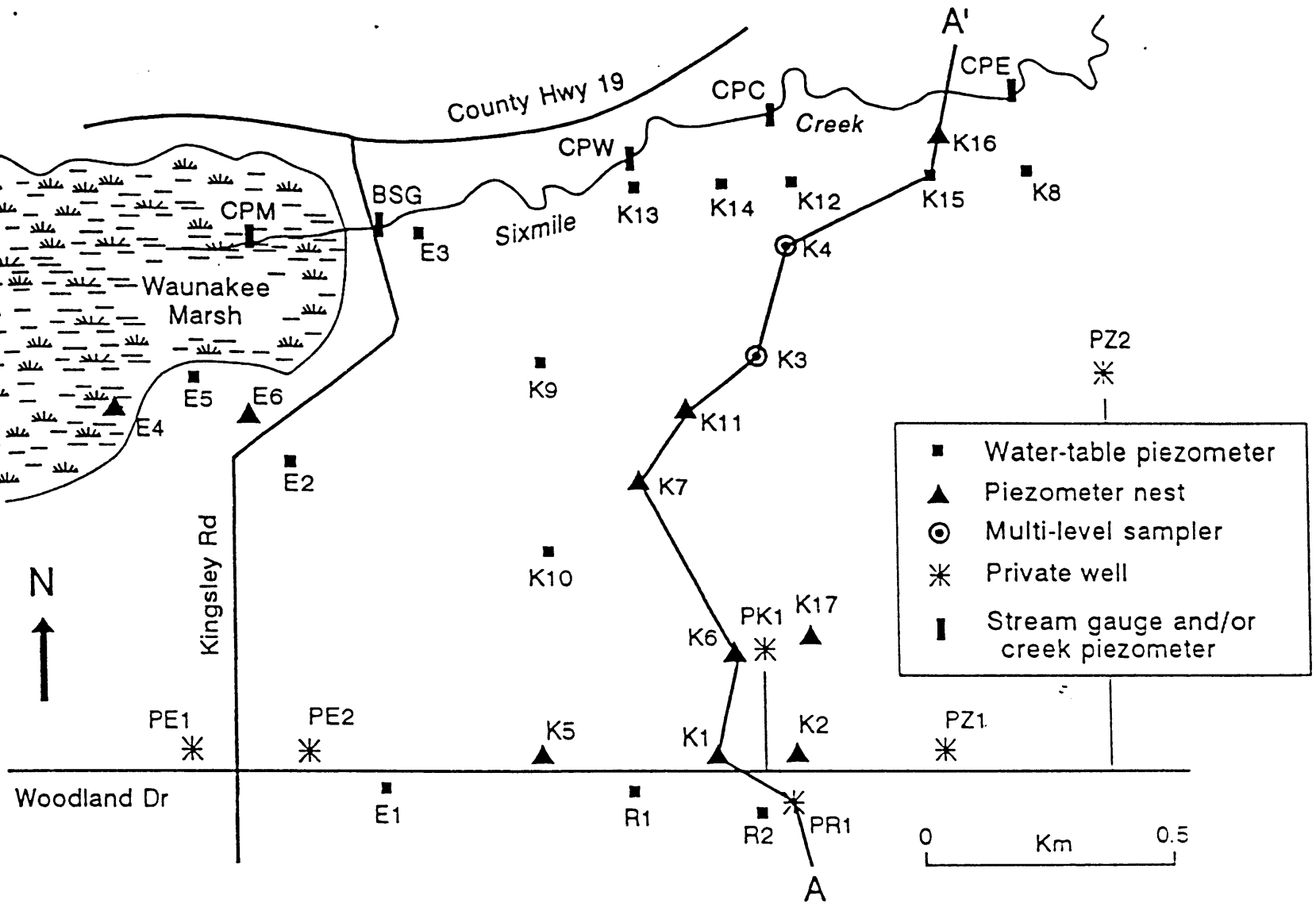

Fig. 32. Monitoring area and well locations. The transect A-A' corresponds to the geologic cross section shown in Fig. 33.

Time-drawdown data were analyzed to estimate likely K_h:K_v-values. Analyses were performed with a computer program, AQTESOLV (Duffield and Rumbaugh, 1989), according to the method for delayed yield in unconfined aquifers with partially penetrating pumping and observation wells (Neuman, 1975). K_h:K_v estimates for 19 observation wells were distributed approximately log-normally with a geometric mean of 2.8 and a 95% confidence interval between 1.7 and 4.6. The pumping-test analyses allowed estimation of specific yield from which effective porosity of the till was estimated at 0.15.

Potentiometric surface maps constructed with 217 private well-drilling logs and 11 private-well head measurements show a regional groundwater divide located 5 to 7 km northwest of the study site which separates groundwater flowing east and south to the Yahara River basin and north and west to the Wisconsin River. Regional flow through the bedrock aquifer in the monitoring area is southeasterly with a gradient of 0.0033.

Water-table mapping shows a complex, shallow flow system affected by surface topography, drainage features, recharge patterns and variations in hydraulic conductivity. In areas of bedrock highs, the water table is in the sandstone and the sandstone aquifer is unconfined. A representative cross-sectional potentiometric-surface maps is shown for August 1991 (Fig. 33). Water recharges most of the study area as indicated by downward gradients at most piezometer nests; vertical hydraulic gradients are much greater than horizontal gradients. Flow direction is predominantly downward eventually joining the southeasterly regional flow. Upward hydraulic gradients are found near and in Sixmile Creek and Waunakee Marsh, signifying groundwater discharge areas. Based on the equipotential contours (Fig. 33) and measured groundwater seepage rates into Sixmile Creek, the discharge area to Sixmile Creek and Waunakee Marsh may extend only 100 to 150 m to each side. Within that area, water from the till discharges into the surface-water bodies. It is unlikely that Sixmile Creek, Waunakee Marsh or Dorn Creek (1.6 km to the south of Woodland Drive) are hydrologic boundaries to regional flow within the

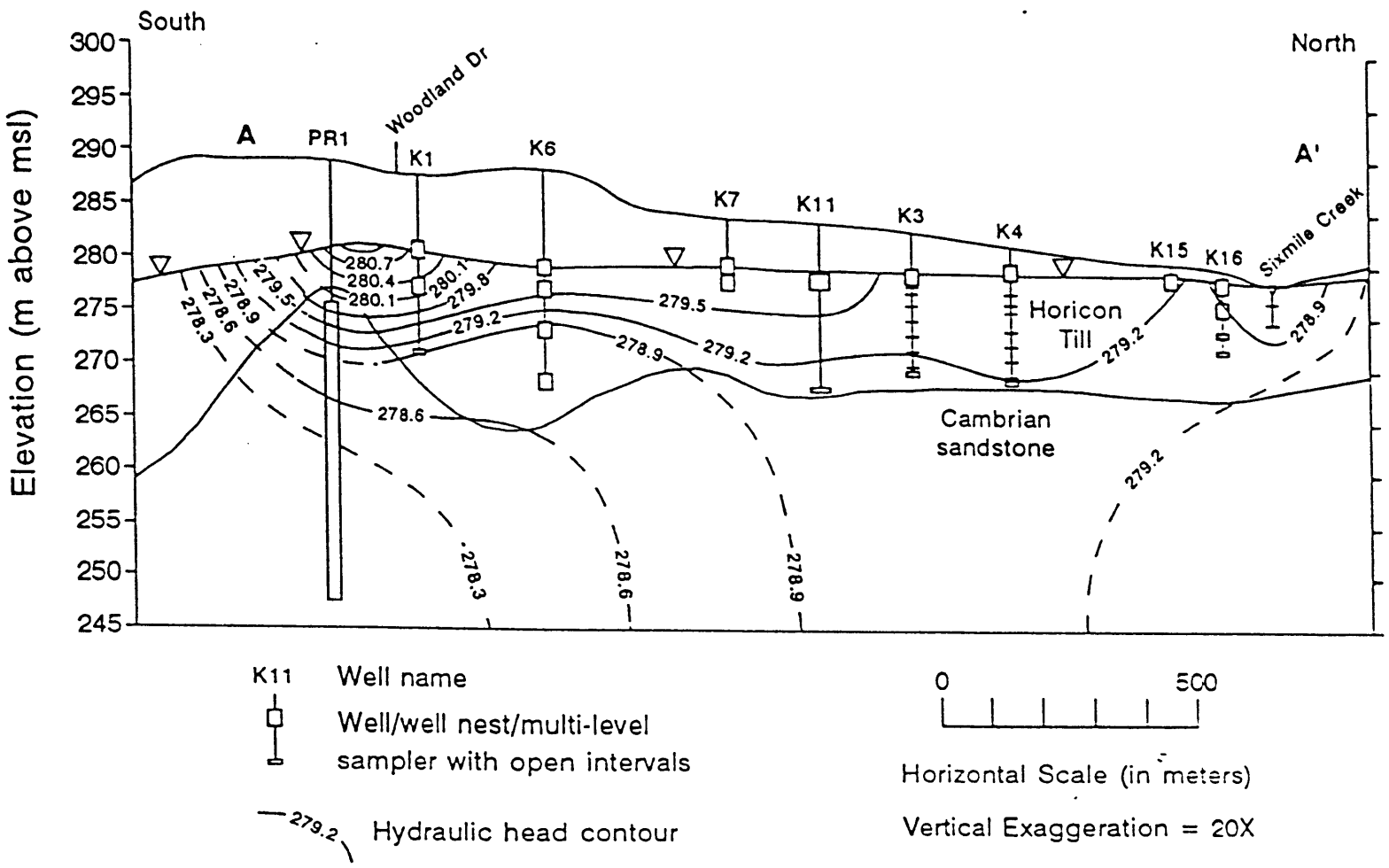

Fig. 33. Generalized geology and hydraulic head along cross section A-A' (transect shown in Fig. 32) in August 1991. Contour interval is 0.3 m. Dashed contours indicate greater uncertainty.

sandstone. Lake Mendota and associated creeks and marshes 6 to 7 km to the southeast are the likely discharge areas for the regional flow.

Recharge is likely to be spatially variable due to surface drainage and ponding patterns; irrigation is not used. Three municipal wells finished in the Cambrian sandstone serve the village of Waunakee, about 2 km east of the monitoring area. There are seven private wells within the monitoring area, two serving private residents and five serving dairy farms.

GROUNDWATER-FLOW MODEL

Groundwater flow was modeled assuming steady-state and using all available hydrogeologic information. Selection of model boundaries, grid discretization, parameter-value selection and model calibration are described in detail in Levy (1993) and Levy et al. (1993b). The MODFLOW simulation incorporates the spatial variability of depth to bedrock and accounts for the hydrologic effects of local surface water bodies. The groundwater flow system was modeled assuming steady-state conditions; cell size within the monitoring area was 61 m^2. The distance between the water table and the Precambrian bedrock surface was divided into six model layers. The number of layers representing the till and bedrock was spatially variable. For most of the monitoring area, the till-bedrock interface was between either Layers 2 and 3 or 3 and 4. The model was calibrated to water-table elevations, bedrock hydraulic heads, shallow vertical gradients and groundwater flux into Sixmile Creek.

PARTICLE TRACKING

PATH3D (Zheng, 1991) is a particle tracking model that calculates groundwater paths and travel times in transient and steady-state three-dimensional flow fields. It is run in conjunction with MODFLOW simulations and used to calculate the advection-controlled component of pesticide movement

in groundwater. PATH3D numerically solves the governing equation for advective movement of particles in the groundwater flow system:

$$\overline{p} = \overline{p}_0 + \int_{t_1}^{t_2} \overline{v}\,(x,y,z,t)\ dt \qquad (64)$$

where $\overline{p}$ is the particle position vector (x,y,z), $\overline{p}_0$ is the starting position, t_1 and t_2 are starting and ending times and $\overline{v}$ (x,y,z,t) is the seepage velocity vector. PATH3D uses MODFLOW predictions of potentiometric head to calculate velocities at every point in space and time. (In this case the MODFLOW simulation is steady-state and velocities are constant in time.) Flow paths and travel times calculated with PATH3D neglect dispersion and chemical reactions of groundwater contaminants, reflecting only advective movement. To predict flow paths and travel times with PATH3D, the user places hypothetical groundwater particles anywhere in the flow system. Particle movement can be tracked forward and (for steady-state simulations) backward through time.

General description of groundwater-flow paths and travel times in the monitoring area

PATH3D-predicted groundwater flow paths agree closely with the conceptual model of groundwater flow (Levy et al., 1993b). Particles were placed at the water table throughout the monitoring area and their progress was tracked forward in time. At most locations, particles moved almost straight down until they reached the more conductive bedrock aquifer. On entering the bedrock, their movement became mostly horizontal and they flowed with the regional gradient to the southeast. Flow within the monitoring area is demonstrated with 12 particle paths displayed in the plan view in Fig. 34. Numbers shown at stars along the paths represent travel time (TT), in years, to that point. A profile views of particle paths F through J are displayed along with equipotential lines (dashed) in Fig. 35; the path labels, stars and adjacent numbers represent the same labels, locations and TTs as in Fig. 34. Although all particle paths except one go from northwest to southeast, the potentiometric profiles run

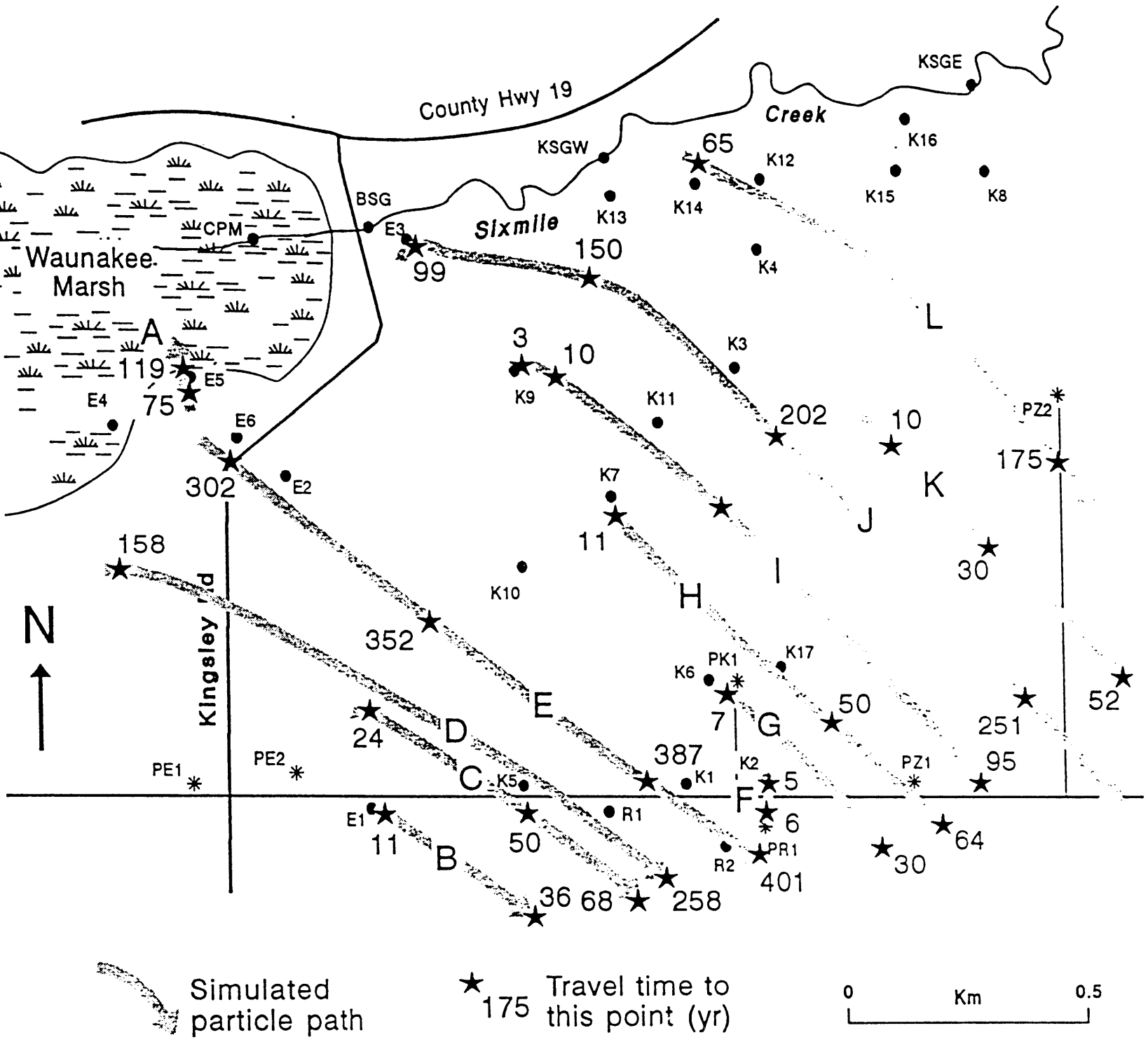

Fig. 34. Plan view of particle paths A through L. Stars and numbers indicate travel time to that point in years.

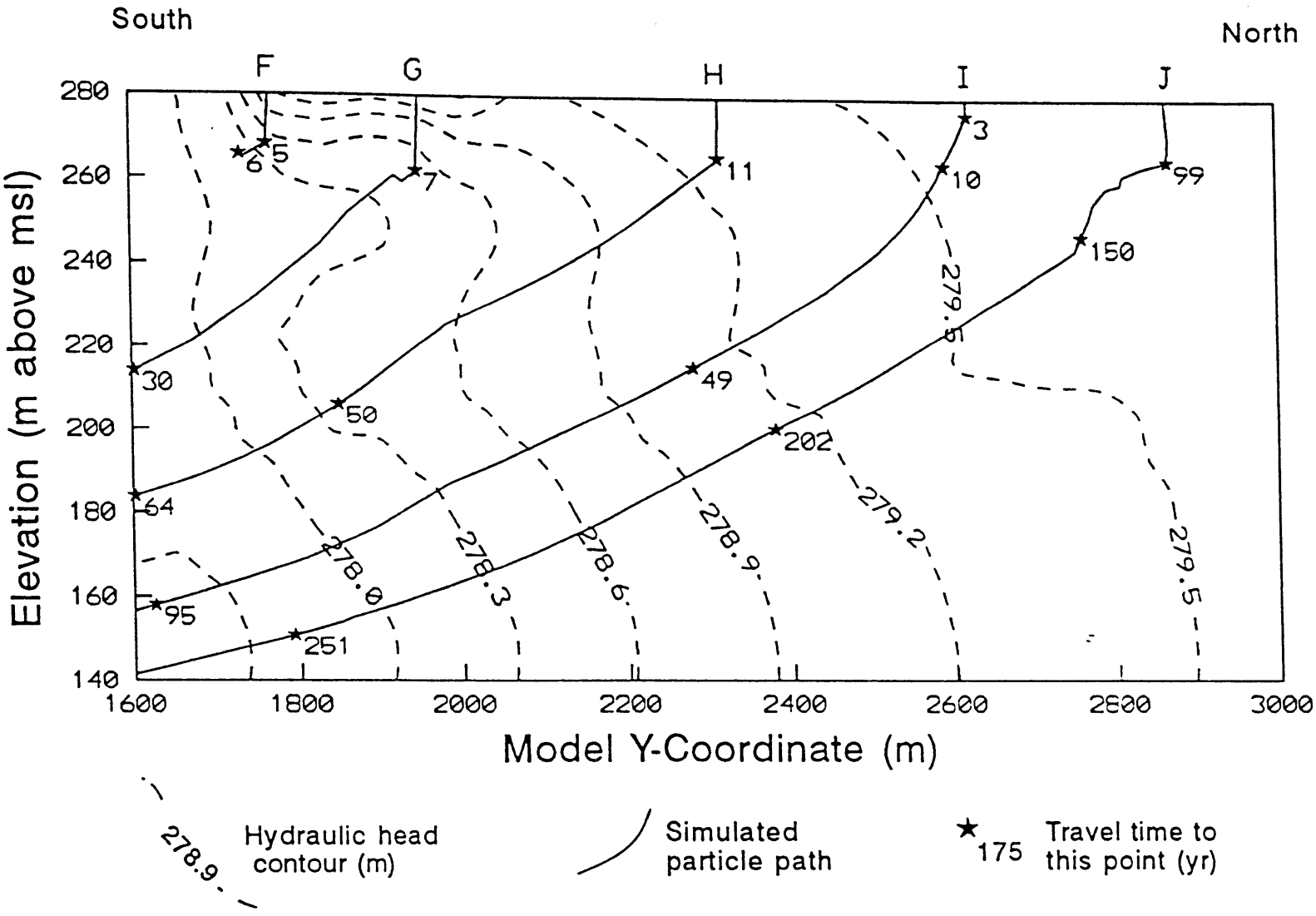

Fig. 35. Profile view of particles paths F through J (see Fig. 34). Stars and numbers indicate travel time to that point in years.

along the model columns aligned 13° west of north. The model y-coordinates of the particle paths (distance along model rows) are used to superimpose the paths on the column profiles. Particle distances traveled are therefore longer than they appear in Fig. 35. The top boundary of Fig. 35 approximates the water table, but is not meant to be an exact representation. Strictly speaking, equipotential lines meet the water table at the elevation equal to the heads they represent, which is not the case in Fig. 35.

Path A (Fig. 34) starts one cell south of the southern edge of Waunakee Marsh. The particle flows down and slightly to the north for 75 yr and then makes its way upward, reaching the adjacent marsh cell in 119 yr. Usually particles beginning one cell from the marsh eventually end up in the marsh. Particle path E (Fig. 34) begins in the next cell to the south and escapes capture by the marsh. A divide is simulated between the two cell centers indicating that the marsh's capture distance is about 60 m. Hydraulic gradients near the divide are minuscule, causing a small stagnation area and accounting for long TTs. Most particle paths (e.g., G through J in Fig. 35) flow down to the bedrock (the first marked TTs) in times that reflect depth to bedrock, model hydraulic conductivities, and proximity to the marsh. After reaching the bedrock, flow is more horizontal than it appears due to the five-fold vertical exaggeration. The particle paths presented in Fig. 35 are superimposed on the potentiometric surface along model column 27. Although they do not represent identical cross sections, the modeled heads can be compared with those in Fig. 33. The profiles compare favorably, providing the same general heads, gradients and projected flow paths. Particle path F begins near piezometer nest K2 (Fig. 34), reaches the bedrock surface at an elevation of 268 m above msl in 5 yr and is trapped the following year by private well PR1 (Fig. 34) in the cell immediately to the south. Bedrock elevations corresponding to paths G, H, and I are 262, 265 and 276 m above msl and predicted TTs to bedrock are 7, 11 and 3 yr, respectively. Note that particle path G goes up for a short distance after about 7 yr. This slight deviation is caused by private well PK1 modeled in Layer 2 from 268 to 276 m above msl. A particle in path G escapes capture by well PK1, however, and joins the regional groundwater flow. Particle path J begins

one cell south of simulated Sixmile Creek. The path still goes down and joins the southeasterly regional flow. Although depth to bedrock is the same as at piezometer K7 (path H), TT to the bedrock surface for path J is nine times greater. The long TT to bedrock is due to lower hydraulic conductivity and to the hydrologic influence of the creek. Downward gradients are much smaller in cells next to the creek and are reversed in the creek cells themselves. Generally, particles had to be placed in the cell in which the creek was modeled to be captured by the creek. Model estimates of the capture distance of the creek are 25 to 60 m. Although small, these values are in the range estimated from seepage metering data (Levy, 1993).

Spatial distribution of groundwater travel times from the water table to the bedrock surface

Given a contaminant whose concentrations tend to decrease with groundwater TT (as is the case for atrazine and a principle atrazine metabolite), the estimated TT from the water table through the till to the bedrock surface provides a measure of the contamination susceptibility of the bedrock aquifer. Water table to bedrock TTs were estimated with PATH3D by placing one particle in the center of each model cell at the bedrock surface and tracking its movement backward through time to its point of origin at the water table. Some particles close to the model boundaries were trapped in boundary cells and were not included in the analysis. In some areas, the water table is in bedrock and there is no TT to the bedrock surface.

The TTs to the bedrock surface are approximately log-normally distributed with a geometric mean of 10.8 yr and a range of < 0.25 to > 512 yr; spatial distribution of TTs is presented in Fig. 36 with contours of equal time in years. The contours are in intervals corresponding to the geometric progression of powers of two. The 0-yr contour is included to designate areas where the water table is in the bedrock. TTs greatly increase close to the creek (along the top edge of the figure) and marsh due to decreased vertical gradients and formation of stagnation areas. Immediately adjacent to the creek and

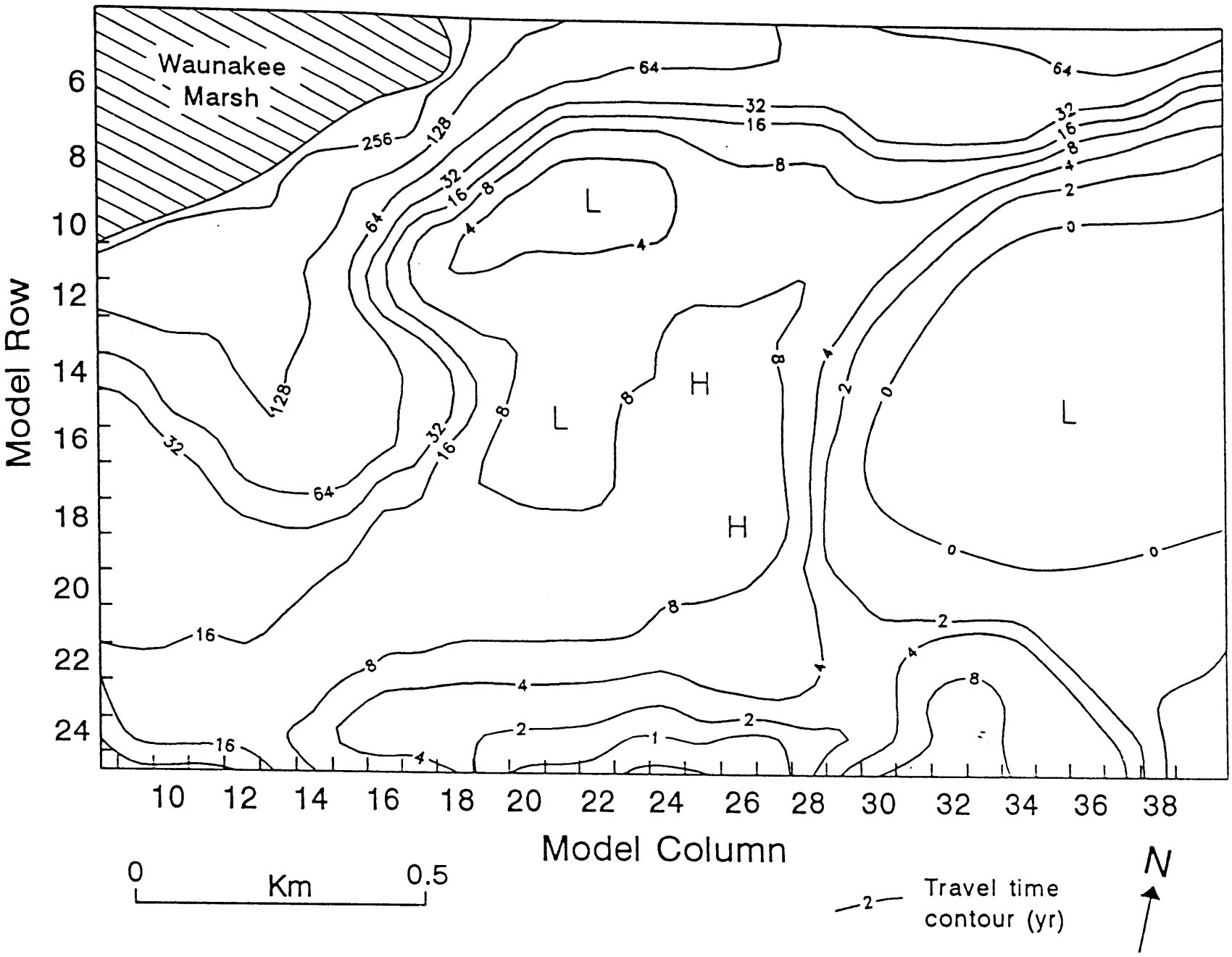

Fig. 36. Simulated travel time from the water table to the bedrock for the calibrated model. Contour intervals are a progression using powers of 2 yr. The 0 contour indicates the water table is in the bedrock.

marsh, water does not flow to bedrock, but discharges to those bodies. Patterns elsewhere generally reflect depths to bedrock and the variability of hydraulic conductivity. Bedrock is relatively shallow in the south central portion of the figure, (e.g., row 24, column 24) and deep in the western portion. The low TT area enclosed by the 4-yr contour in the north-central portion (e.g., row 9, column 21) is due to a bedrock high.

Travel Times and Zones of Contribution for Private Domestic Wells

The spatial distribution of TT to bedrock surface was of interest since most area residents have private wells finished in the sandstone. Of the seven private wells in the area, water from six was analyzed at least twice for atrazine and metabolite concentrations. Of particular interest were the PATH3D-calculated groundwater TTs to those wells and whether they did, in fact, bear a relationship to atrazine and metabolite concentrations in water. A pumping well forms a cone of depression in the water table or potentiometric surface, creating an area in which hydraulic heads are lower than in the ambient state. The cone of depression induces flow towards the well so that even groundwater downgradient of the well in the ambient flow field might be drawn into the well. The induced area of capture for a well projected up to the land surface is known as the zone of contribution (ZOC) and represents the area in which aquifer recharge will eventually be drawn into a well. TTs and ZOCs were delineated by tracking particles from the well backward to the water table. In MODFLOW, wells are simulated throughout entire cells. Using PATH3D, 100 particles were randomly distributed in each cell with simulated pumping. Particles with different starting coordinates within a cell take different paths as they move backward in time. The aggregate of all particle paths delineates the ZOC. ZOCs for six private wells in the monitoring area are shown in Fig. 37. The ZOC orientation reflects the horizontal hydraulic gradient in the bedrock aquifer. The horizontal extent of the ZOCs is mainly controlled by the

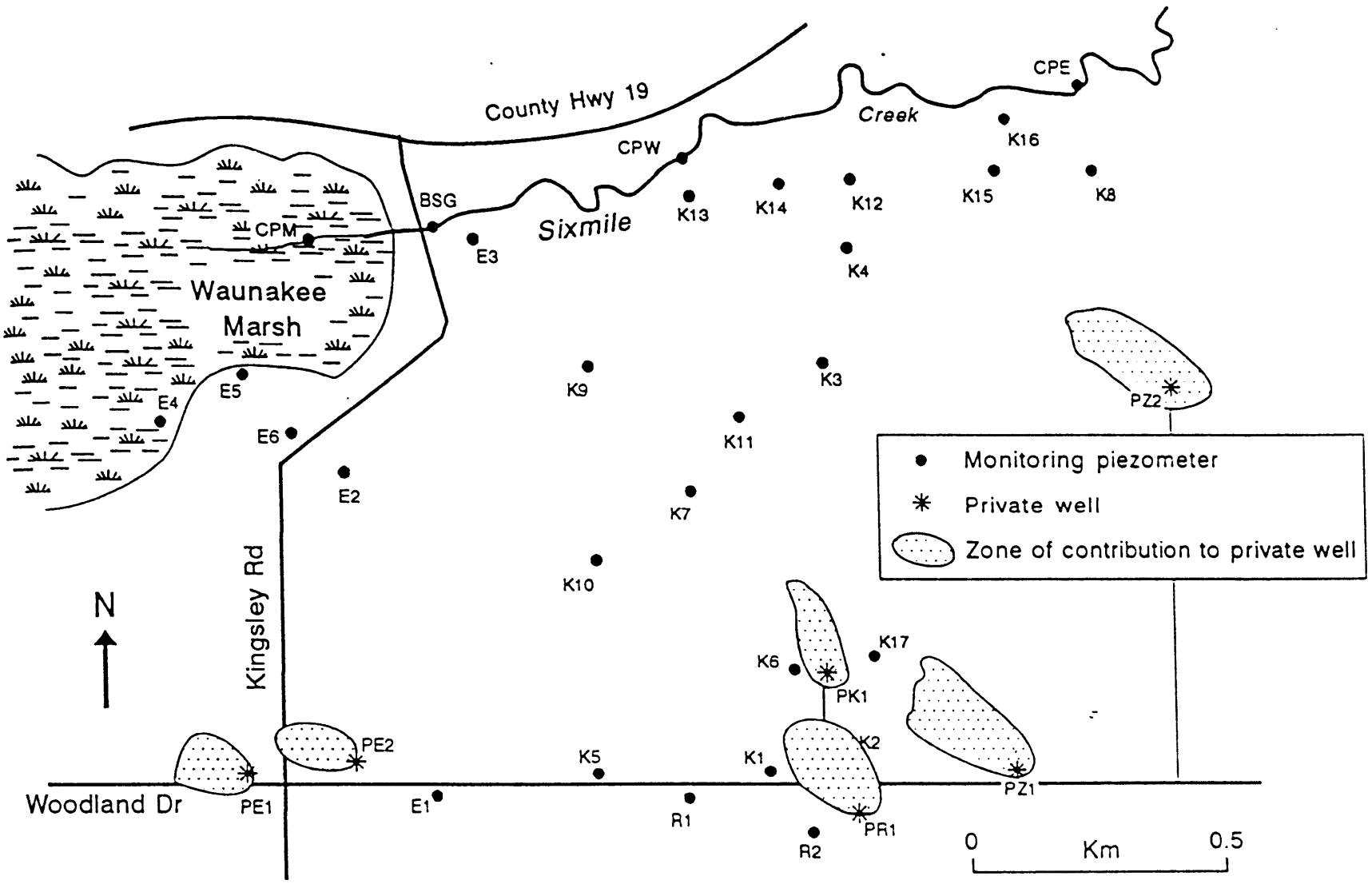

Fig. 37. PATH3D-derived zones of contribution for privates wells within the monitoring area.

time the water spends in the bedrock aquifer since flow through the till is predominantly vertical and to a lesser degree by the simulated pumping rates. ZOCs range from 0.9 ha at PE2 to 2.6 ha at PZ2.

Each particle path contributing to the ZOC delineation has an associated TT to the well, and the aggregate of the TTs from many simulated particles provides a good estimate of typical TTs for most water entering the well. TT distributions and the average for each well are shown in Fig. 38. The TTs reflect the MODFLOW-simulated horizontal and vertical hydraulic conductivities and gradients, depth to bedrock and depth of the well's open interval. Water reaching PK1 is the youngest since it is the shallowest well and depth from the water table to bedrock in that vicinity is 11 m. TTs to PR1 were small since the bedrock is only 3 m below the water table; 31 yr was the longest time for water to travel from the water table to any well.

As was previously done with many of the monitoring wells (Levy et al., 1993a) regression analyses were used to explore relationships between average particle TTs and average atrazine residue concentrations determined in water sampled from the private wells. Atrazine and desethylated atrazine (a principal metabolite of atrazine) concentrations decreased log-linearly with increased logs of average TT to the well (Fig. 39):

$$\ln(Avg\ Atra) = 19 - 2.4 \ln(TT), \qquad R^2 = 0.77\ on\ 4\ df \tag{65}$$

$$\ln(Avg\ DEAT) = 16 - 2.0 \ln(TT) \qquad R^2 = 0.75\ on\ 4\ df \tag{66}$$

where Avg Atra and Avg DEAT are atrazine and desethylated atrazine concentrations averaged over the sampling period and TT the average particle travel time in days. No data were available for other metabolite concentrations at the private wells other than PK1. Given the uncertainties inherent in TT estimates and the fact that the private wells -- other than PK1 -- were sampled only two or three times, the relationships are speculative. The regression equations have slopes and intercepts different from those

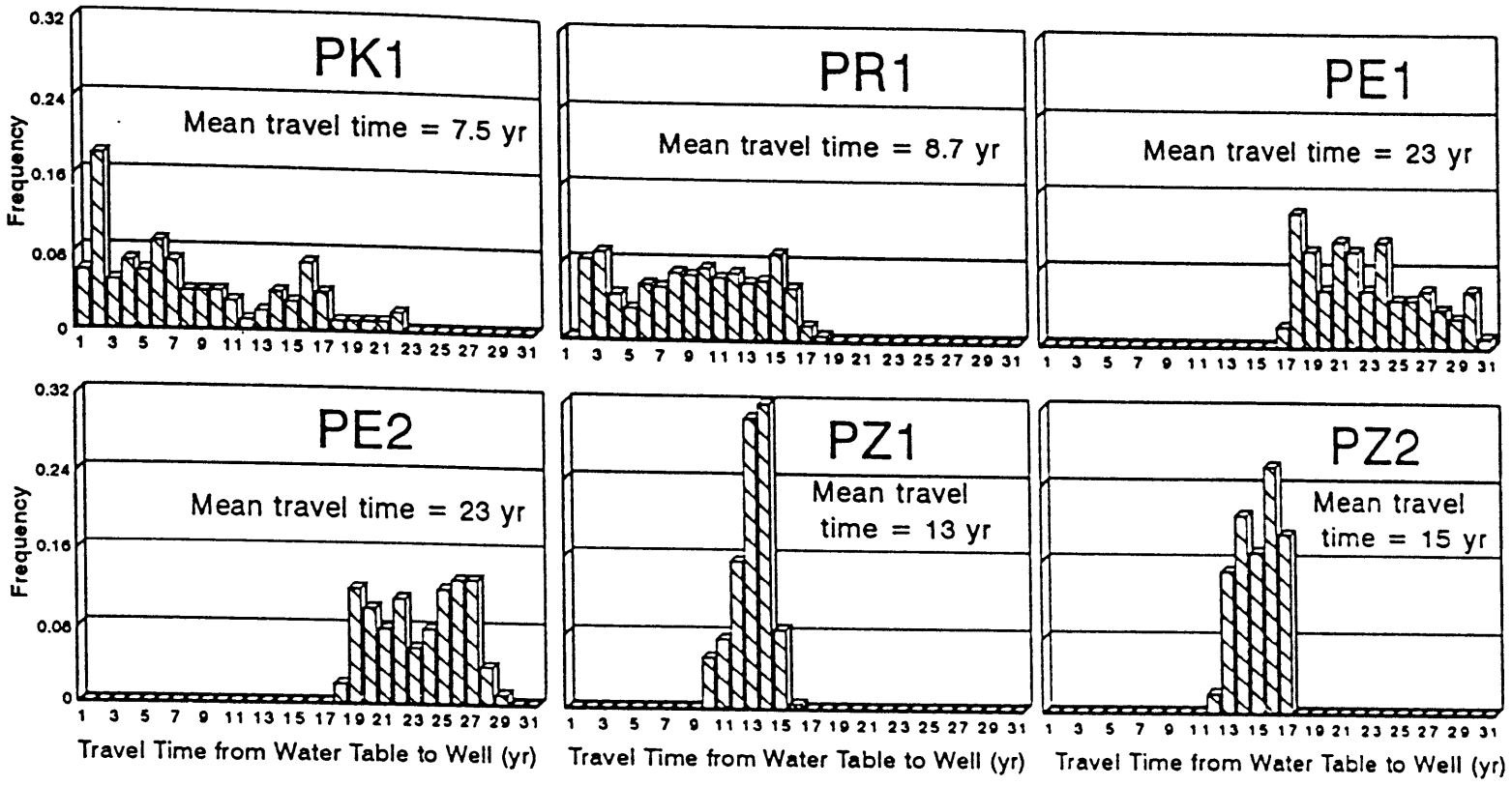

Fig. 38. Distributions of PATH3D-estimated groundwater travel times from the water table to private wells.

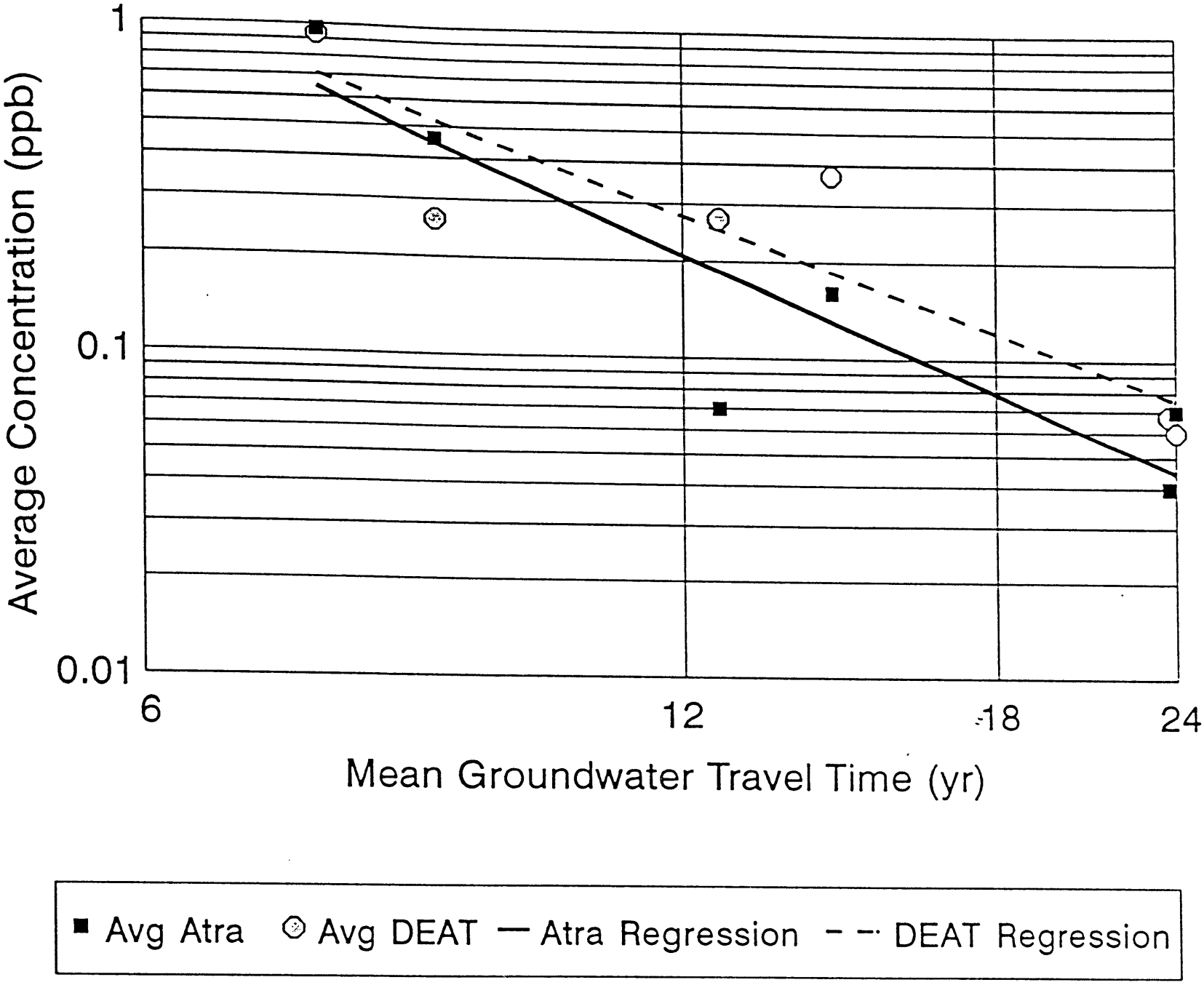

Fig. 39. Time-averaged atrazine and desethylated atrazine (DEAT) concentrations (in ppb) in water from six area private wells versus the mean PATH3D-estimated travel times to the wells.

established with the monitoring wells (Levy et al., 1993a). The differences result from the high concentrations found at PK1 and PR1 and may be caused by the ZOCs encompassing areas of pesticide handling. Concentrations at the water table in those areas may be substantially higher than in most of the field area.

THREE-DIMENSIONAL SIMULATIONS OF ATRAZINE TRANSPORT AND FATE

Previously, the distribution of atrazine and desethylated atrazine concentrations at monitoring piezometers and their relationship to the groundwater TTs to those piezometers were used in combination with literature-based estimates of sorption coefficients and aquifer dispersivity in a one-dimensional transport model, simulating atrazine fate and transport at piezometer nests (Levy and Chesters, 1993). Estimates of atrazine and desethylated atrazine degradation rates were made by model calibration. While the PATH3D simulations provide an assessment of aquifer susceptibility to contamination in general, incorporation of transport-parameters (dispersion, sorption and degradation) into a contaminant-transport model allows a more specific and detailed examination of the future threat posed by atrazine. The three-dimensional transport model, MT3D (Zheng, 1990), is used with the calibrated groundwater-flow model to simulate point- and nonpoint-source contamination and explore the range of expected concentrations at various depths, locations and times. The prediction uncertainty, caused by inherent uncertainties in model parameter value estimates, is investigated using the approximation of the three-point Gauss-Hermite Quadrature formula (Raftery and Zeh, 1993; Press, 1989). The Gauss-Hermite method is explained in detail and simplified in Levy et al. (1993c). In addition to quantifying uncertainty, the method provides a sensitivity analysis of single model parameters and parameter pair interactions.

Description of MT3D

MT3D is a modular computer model that uses a mixed Eulerian-Lagrangian approach to the solution of the three-dimensional advection-dispersion equation (Zheng, 1990). The modular structure is similar to that of MODFLOW, with separate packages for simulating advection, dispersion, sources and sinks and chemical reactions. MT3D can be used in conjunction with MODFLOW, by directly utilizing the MODFLOW simulated flow field and finite-difference grid. As with PATH3D, the velocity term in the advection-dispersion equation is calculated from the MODFLOW simulation using hydraulic conductivity inputs and simulated heads to calculate hydraulic gradients. MT3D calculates a dispersion tensor based on groundwater velocities and user-specified estimates of longitudinal and transverse dispersivities and the molecular diffusion coefficient. MT3D allows simulation of sorption with a linear, Freundlich or Langmuir isotherm and simulates degradation assuming pseudo-first order kinetics with a separate degradation rate for sorbed and dissolved phases. The Freundlich isotherm was chosen for this study. The contaminant concentration of the recharge was specified; its entry into the system is analogous to the third-type boundary used in the one-dimensional model.

Simulation objectives and approach to the uncertainty analysis

The objective of MT3D modeling is to simulate atrazine movement and fate across the monitoring area given contamination scenarios which address questions of regulatory significance; two are examined. The first is nonpoint-source contamination in which, for 35 yr (the period of atrazine use in Wisconsin) the recharge entering the groundwater system everywhere has a concentration equal to the Wisconsin enforcement standard (ES) for atrazine of 3 ppb. Wisconsin has a two-tiered groundwater standard system. The higher level -- the ES -- is similar to the U.S. EPA maximum contaminant level. For pesticides, an ES violation requires a pesticide-use prohibition in the area of violation. The lower level -- the preventive action limit (PAL) -- which for possible carcinogens like atrazine is 10% of the ES.

When a certain number of atrazine PAL violations occur in a specific area, atrazine management areas are created in which maximum allowable atrazine applications rates are reduced. In 1992, three atrazine metabolites as well as the parent were included in the standards so that violations are based on the sum of the concentrations. Simulation of only the parent compound is considered here and concentration distribution is examined horizontally and vertically. Specific questions are: How long before steady-state concentrations are reached? What are the ranges of expected concentrations at various depths due to the geologic configuration and spatial variability of hydraulic conductivities and gradients? What are the expected concentrations in area private wells finished in the bedrock aquifer? After 35 simulated years, the contamination source is cut off, i.e., recharge is given a concentration of 0 ppb. This addresses how long contamination will be a problem if atrazine use is prohibited and no leaching occurs through the unsaturated zone. In reality, leaching may continue for many years after prohibition. Therefore, a best-case is examined. The second case represents minor point-source contamination, similar to that at K6 and PK1 (Fig. 32). One model cell within each private well ZOC is assigned recharge with an atrazine concentration of 8 ppb for 35 yr, after which time it is optimistically assumed that the unsaturated zone is entirely cleansed of atrazine residues. Thus, how long does it take for the contaminant front to arrive, what are the expected peak concentrations and what kind of dissipation is expected to occur once the source is removed?

Predicted answers to the posed questions can be obtained by using best estimates of the model input parameter values in MT3D and running the model once. Missing from such an analysis is a measure of the uncertainty of the model predictions needed to make intelligent policy decisions based. Uncertainty of model predictions stems from uncertainties in the input parameter values. In the analysis described here, it is assumed that model predictions are not single deterministic quantities, but are probability density functions (PDFs) dependent on the model parameters. Those parameters are, in turn, represented by their own PDFs which characterize the random uncertainty associated with them (Levy

et al., 1993c). In the Gauss-Hermite approach, the expected value and variance of the model prediction is calculated by running the model once for every combination of three specific quantile values for each parameter PDF: the 0.042, 0.5 and 0.958 quantile values. In this study, seven parameters are included. The full Gauss-Hermite method would therefore require 3^7 or 2,187 model runs. Raftery and Zeh (1993) present an approximation of the full Gauss-Hermite method that ignores third- and higher-order interactions between parameters. The approximation is simplified and explained in Levy et al. (1993c). For seven parameters, 99 model runs are required for the approximation, (a significant savings over the Monte Carlo approach). The seven parameters and their 0.042, 0.5 and 0.958 quantile values are presented in Table 16.

TABLE 16

Summary of parameter quantile values used in the MT3D/Gauss-Hermite analysis.

Parameter	*Units*	*Quantile Value*		
		0.042	*0.5*	*0.958*
Freundlich coefficient	$\mu g^{1-a} mL^a g^{-1}$ *	0.043	0.037	0.69
Freundlich exponent	unitless	0.87	0.89	0.92
Longitudinal dispersivity	m	0.19	1.4	9.8
Longitudinal:transverse dispersivity ratio	unitless	4.0	8.0	16
Effective porosity	unitless	0.088	0.15	0.21
Dissolved-phase degradation rate	day^{-1}	8.5×10^{-5}	3.5×10^{-4}	1.4×10^{-3}
Sorbed-phase degradation rate	day^{-1}	8.5×10^{-5}	3.5×10^{-4}	1.4×10^{-3}

* Units depend on the Freundlich exponent, a.

"Grand mean" MT3D model runs

The model run in which all parameters are at their 0.5 quantile values is the "grand mean" (Raftery and Zeh, 1993) and equals the expected value only if model results for the other quantile values

are equally distributed about the grand mean. The grand mean is the conventional deterministic prediction based on the best parameter value estimates. Whereas it is computationally impractical to evaluate the expected value and variance of the concentration of every model cell at different times, this is easily done with the grand mean. Therefore, grand mean results allow examination of spatial and temporal variability of concentrations due to the geologic configuration and the spatial variability of hydraulic conductivities and gradients -- parameters not considered in the Gauss-Hermite analysis.

In the first simulation, nonpoint-source contamination is simulated using recharge contaminated with an atrazine concentration of 3.0 ppb entering the groundwater system everywhere within the monitoring area. Actual concentrations as high as 3.0 ppb were determined only in water from one piezometer. This simulation is a "bad-" if not "worst-case". Contaminated recharge continues for a period of 35 yr, when recharge is assumed free of atrazine. This case assumes that the monitoring area has been placed in an atrazine prohibition area and atrazine leaching to the water table ceases. Such a condition represents a "best-case", because leaching may continue for many years after application. For this simulation, the MT3D modified method of characteristics technique is used. Although this technique may produce some numerical dispersion, it is free of the numerical instabilities associated with other MT3D options. The coefficient of molecular diffusion and bulk density of the till are not included in the Gauss-Hermite analysis, but their values are specified as 1×10^{-5} cm^2/sec and 1.6 g/cm^3.

Fig. 40 shows spatial distribution of simulated 35-yr atrazine concentrations in model Layers 1, 2 and 3. Layer 1 extends from the water table to an average depth of 3.1 m below the water table. Layer 1 simulated concentrations (Fig. 40a, with contour intervals of 0.10 ppb) range from < 0.1 to > 1.2 ppb, and the distribution is closely connected to the PATH3D TT estimates (Fig. 36). Highest simulated concentrations occur where bedrock surface elevation is high and Layer 1 is bedrock rather than till (as in the east-central portion of Fig. 40). Concentrations are lowest near the creek and marsh (along the northern edge of Fig. 40) where vertical hydraulic gradients are weakest and hydraulic conductivities

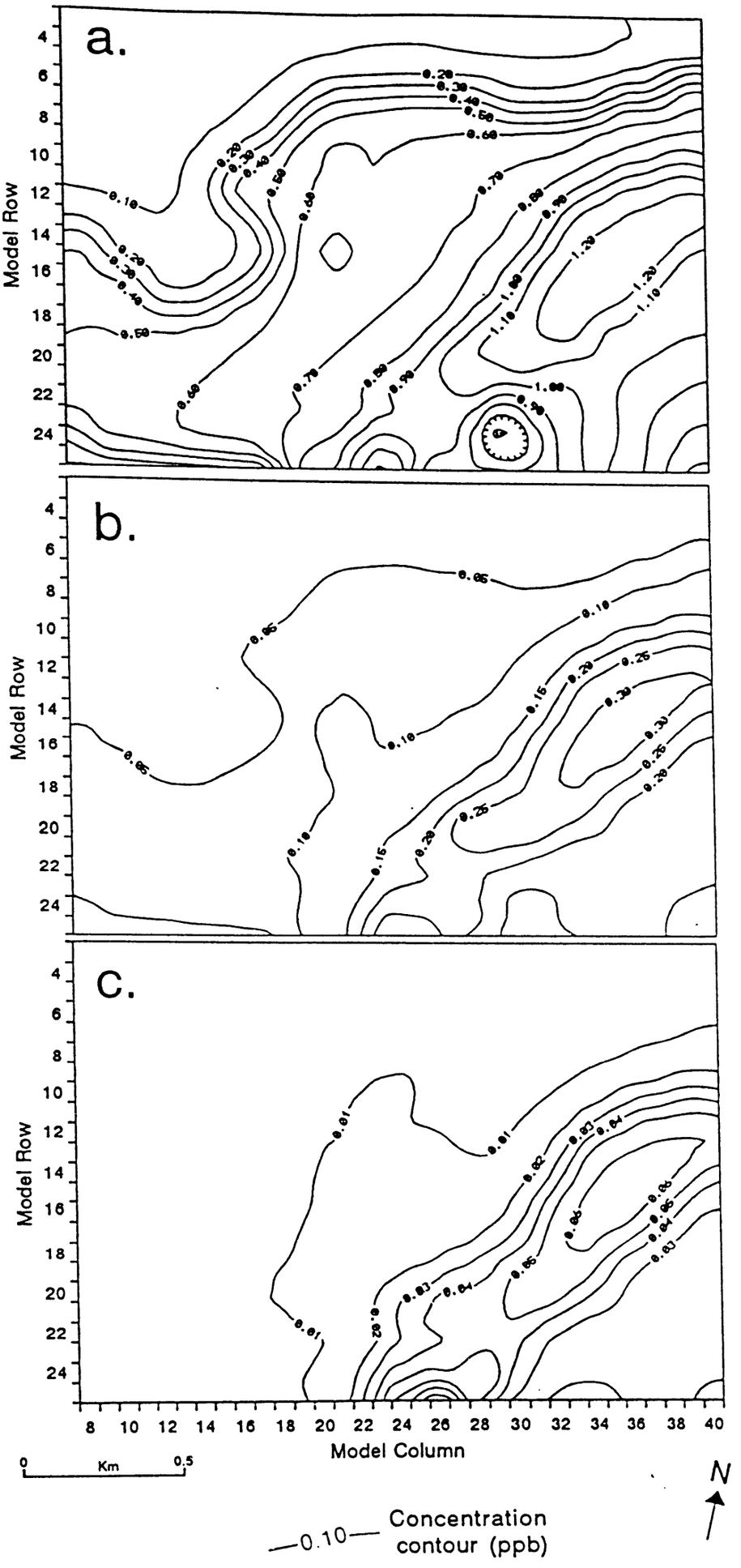

Fig. 40. MT3D nonpoint-source contamination scenario, grand-mean atrazine concentration (in ppb) after 35 years of steady-state, 3.0 ppb recharge in (a) model Layer 1, (b) model Layer 2 and (c) model Layer 3.

are low. Another controlling factor is the calibrated MODFLOW distribution of hydraulic conductivities. Simulated concentrations throughout most of Layer 1 violate Wisconsin's PAL of 0.3 ppb. While concentrations right at the water table would be closer to the input concentration of 3.0 ppb, the effect of averaging concentrations through the 3.1-m thickness of Layer 1 is that maximum concentrations are well below the ES (again assuming that no metabolites are present). The predicted Layer-1 concentrations are greater than those expected at the water table and less than those expected at the layer bottom. Layer 2 extends from an average of 3.1 to 8.2 m below the water table. The 35-yr concentration distribution in Layer 2 (Fig. 40b, with contour intervals of 0.05 ppb) is similar to that of Layer 1, but concentrations are only 10 to 25% of those in Layer 1. Simulated Layer 2 concentrations in violation of the PAL are restricted to the east-central area of high bedrock surface elevation. Layer 3 extends from an average of 8.2 to 17.8 m below the water table. Maximum 35-yr simulated concentrations (Fig. 40c, in contour intervals of 0.01 ppb) are < 0.06 ppb and concentrations > 0.01 ppb are limited in extent. Simulated concentrations > 0.01 ppb were not found in model Layer 4 (> 17.8 m below the water table).

For model Layers 1, 2 and 3, Fig. 41 shows the contamination distribution 5 yr after contaminant additions to the groundwater system stops. In Layer 1 (Fig. 41a, with contour intervals of 0.05 ppb) maximum concentrations declined from 1.3 to 0.35 ppb; the area violating the PAL is limited. Most of the monitoring area has concentrations < 0.3 ppb. Maximum simulated concentrations in Layers 2 and 3 are 0.20 and 0.05 ppb (Figs. 41b and 41c with contour intervals of 0.05 and 0.01 ppb, respectively). Ten years after the end of contaminated recharge, maximum Layer 1 concentrations are 0.10 ppb (Fig. 42a). With advection, Layer 2 concentrations are similar to those in Layer 1 and are half to equal those in Layer 1 and do not exceed 0.12 ppb (Fig. 42b). Layer 3 concentrations are all < 0.05 ppb. Five years later, concentrations in all layers are <0.05 ppb, and Layer 2 concentrations are slightly greater than those in Layer 1 in some areas.

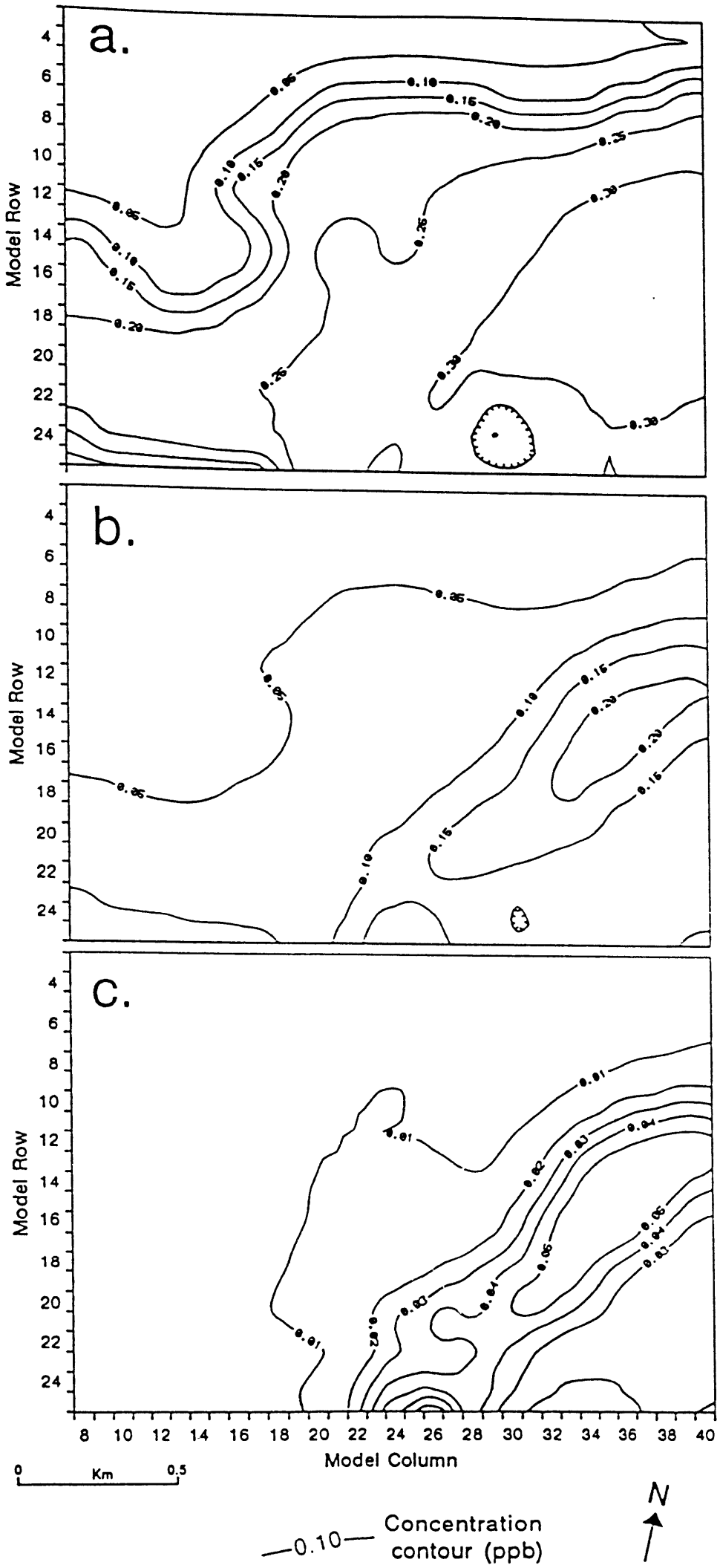

Fig. 41. MT3D nonpoint-source contamination scenario, grand-mean atrazine concentration (in ppb) 5 yr after stopping contaminated recharge in (a) model Layer 1, (b) model Layer 2 and (c) model Layer 3.

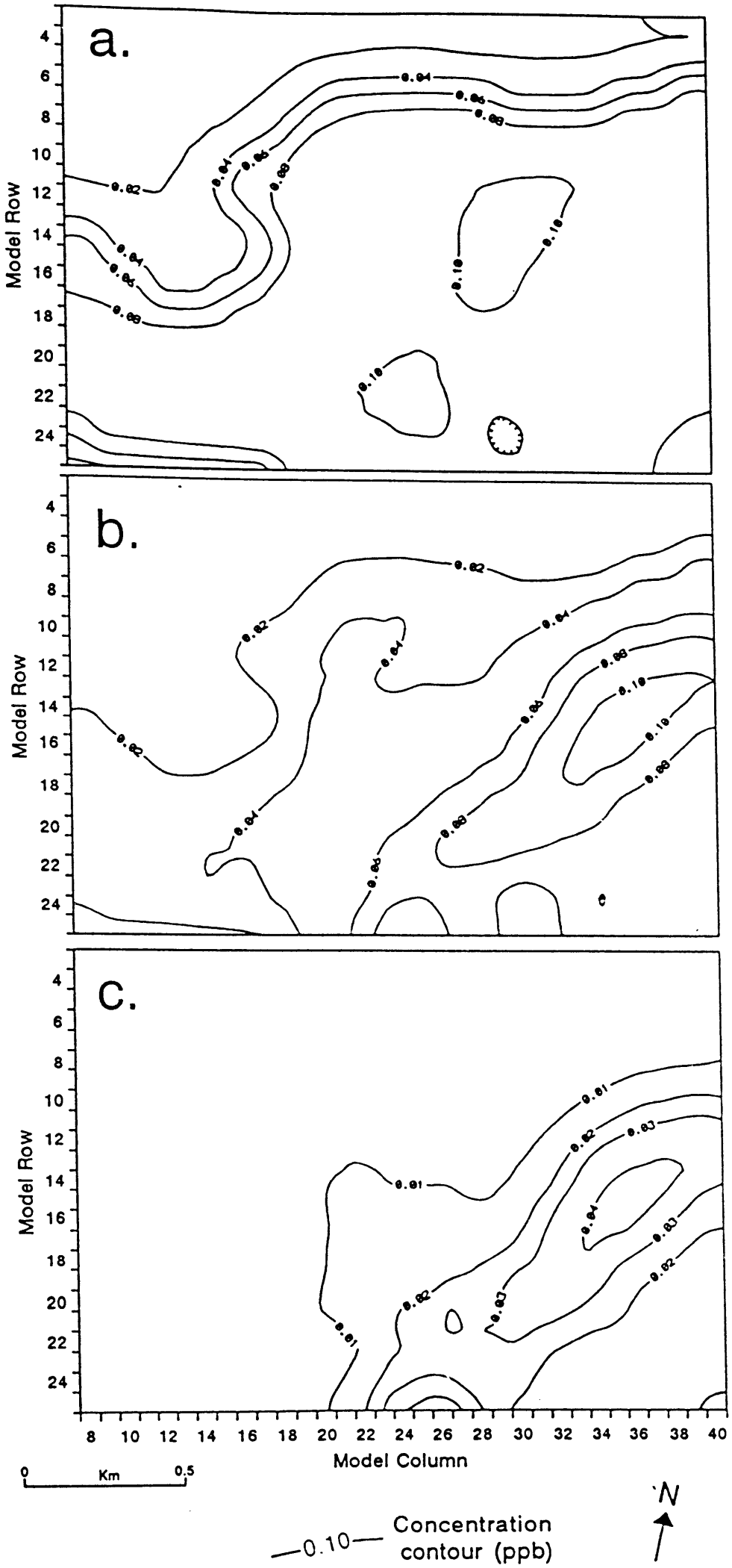

Fig. 42. MT3D nonpoint-source contamination scenario, grand-mean atrazine concentration (in ppb) 10 yr after stopping contaminated recharge in (a) model Layer 1, (b) model Layer 2 and (c) model Layer 3.

Concentration breakthrough curves for individual model cells (Fig. 43) demonstrate the simulated changes in concentration over time more clearly. Model cells which include piezometer nests K7 and K17 are selected since they represent cells with some of the lowest and highest simulated hydraulic conductivities. For both piezometer nest locations, the breakthrough curves for Layers 1 through 4 are shown. At K7 (Fig 43a), concentrations in Layer 1 increase to almost the maximum concentration of 0.59 ppb in 15 to 20 yr. After the contamination ceases, dissipation to < the PAL and approximately one-half the maximum concentration, takes 3 yr. Concentrations in Layers 2 and 3 increase to a maximum and dissipate more slowly, but remain < 0.1 ppb for the entire simulation. At piezometer nest K17 (Fig. 43b), concentration patterns are similar. The maximum Layer 1 concentration of 1.2 ppb is practically reached within 15 to 20 yr. Even though the concentration is about twice that at K7, dissipation to one-half the maximum and to 0.3 ppb takes only 3 and 5 yr, respectively. Maximum concentration in Layer 2 of 0.17 ppb is practically reached in 20 yr, and dissipation to one-half the maximum takes about 7 yr. The Layer 3 concentration remained < 0.05 ppb through the entire period of simulation. Simulated Layer 4 concentrations were negligible at both piezometer locations.

For the point-source scenario, the recharge is specified to be at a concentration of 8 ppb atrazine (parent compound) for just the one cell directly above each of the private wells PK1, PR1, PE1, PE2 and PZ1. The cells in which the contaminated recharge falls are all within the ZOCs. In each case, the recharge covers a 61x61 m^2 area. As in the nonpoint-source scenario, the simulated contamination continues for 35 yr and then stops. Simulating concentration breakthroughs at model cells containing simulated private wells required use of the finite-difference Eulerian (FD) solution technique to avoid numerical instabilities. Most private wells are simulated in more than one model cell. Therefore, concentrations for each private well are the weighted averages from the component cells with weights proportional to simulated pumping rates of the cells. Point-source grand mean results are presented in Fig. 44. As for measured concentrations, highest and second highest simulated concentrations are found

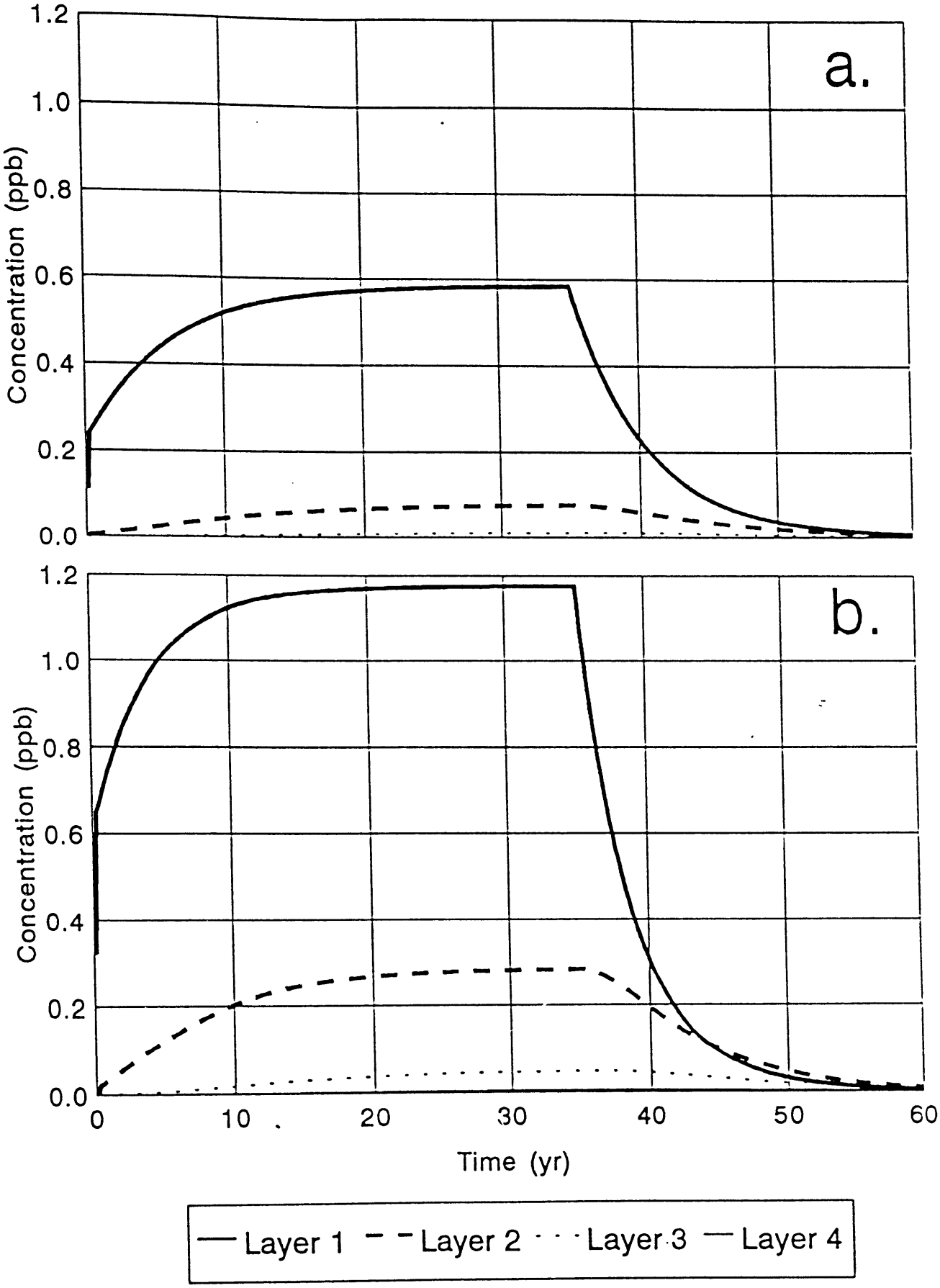

Fig. 43. MT3D, nonpoint-source scenario grand-mean results for model cells in which are located piezometer nests (a) K7 (where groundwater velocities are relatively slow) and (b) K17 (where groundwater velocities are relatively fast).

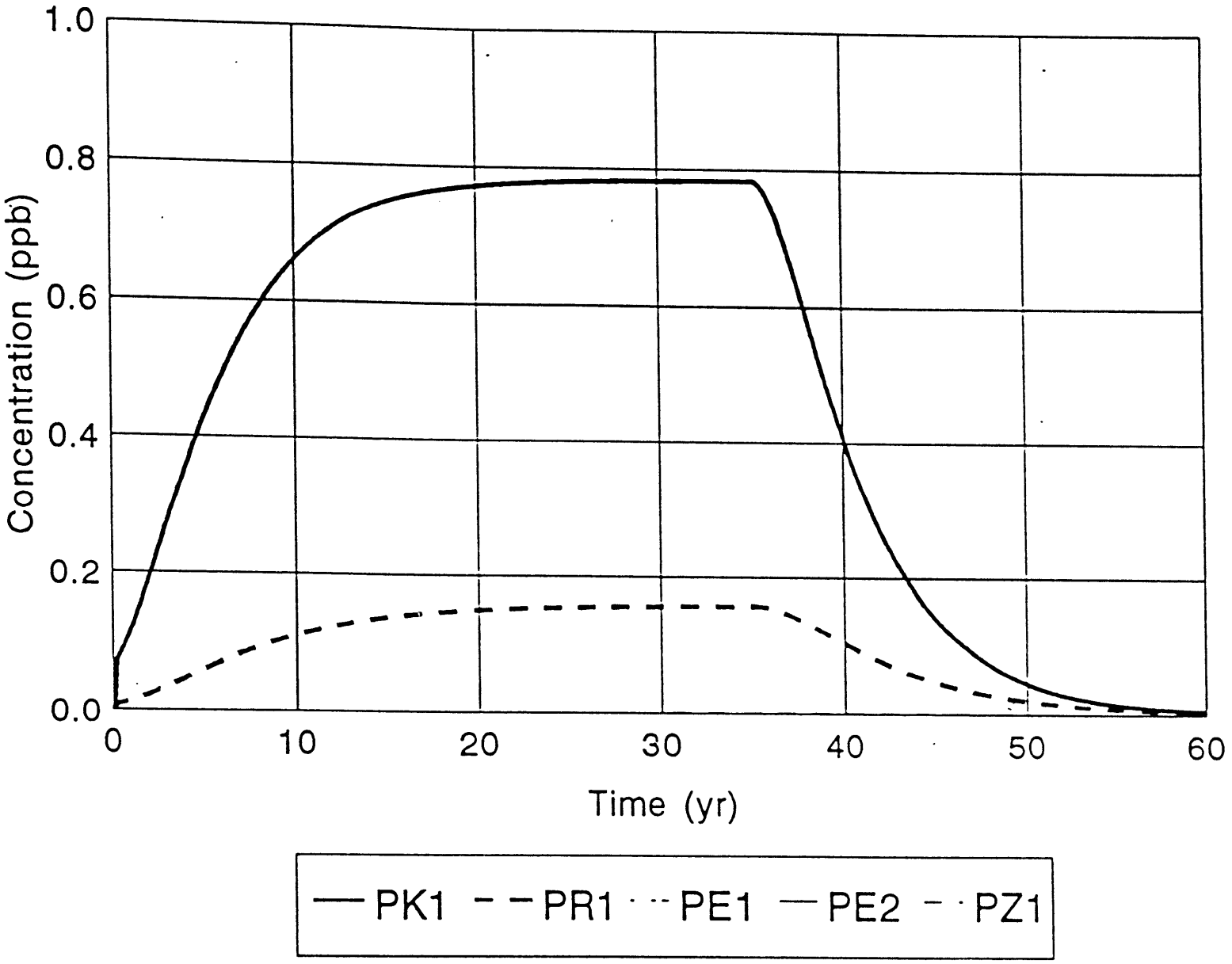

Fig. 44. MT3D, point-source scenario grand-mean results for five area private wells. PE1, PE2 and PZ2 simulated concentrations are negligible.

at PK1 and PR1, respectively. Simulated concentrations at PK1 and PR1 reach maximums of 0.78 and 0.16 ppb. Concentrations at PE1, PE2 and PZ1 never exceed zero. Concentrations at PK1 take 5 and 6 yr to decrease below 50% of the maximum concentration and the PAL of 0.3 ppb. Average predicted PATH3D TTs to PK1 and PR1 are 7.5 and 8.7 yr for particles starting at the water table anywhere within the ZOCs (Fig. 38). However, for particles starting at the water table just in the cell directly above the well, average TTs to the wells are 298 and 534 days for PK1 and PR1. The midpoint of the breakthrough curve (50% of the maximum concentration) is used to estimate average contaminant TT. The arrival times for the 50% of the maximum concentration at PK1 and PR1 are 1,660 and 2,410 days, respectively, corresponding to effective retardation factors of 5.6 and 4.5. With the Freundlich isotherm, the actual retardation factor at each time step depend on the concentration.

Expected values and variances of the model predictions

The Gauss-Hermite approximation analysis for the nonpoint case included predictions at many locations of concentrations in Layers 1 through 4 at 35, 40, 45, 50, 55 and 60 yr. To cover a range of conditions, examples are presented graphically for the predictions for the model cells in which piezometer nest K7 is located (Fig. 45), where modeled groundwater velocities and simulated concentrations are relatively small, and for the model cell in each layer with the maximum simulated concentrations (Fig. 46). Expected values shown differ from the grand mean results since they incorporate information regarding not only the 0.5 quantile values, but the entire PDFs of the transport parameters. The Gauss-Hermite analysis yields an approximation of the estimate variance. The 95% confidence intervals shown in Figs. 45 and 46 are approximated by twice the standard error, which is the square root of the variance. Some of the 95% confidence intervals are quite large, reflecting the uncertainty in the parameter input values. Expected Layer 1 concentrations at location K7, for example, are < 0.7 ppb, but the 95% confidence interval goes from 0 to 1.6 ppb (Fig. 45a). (The upper limit is always the recharge

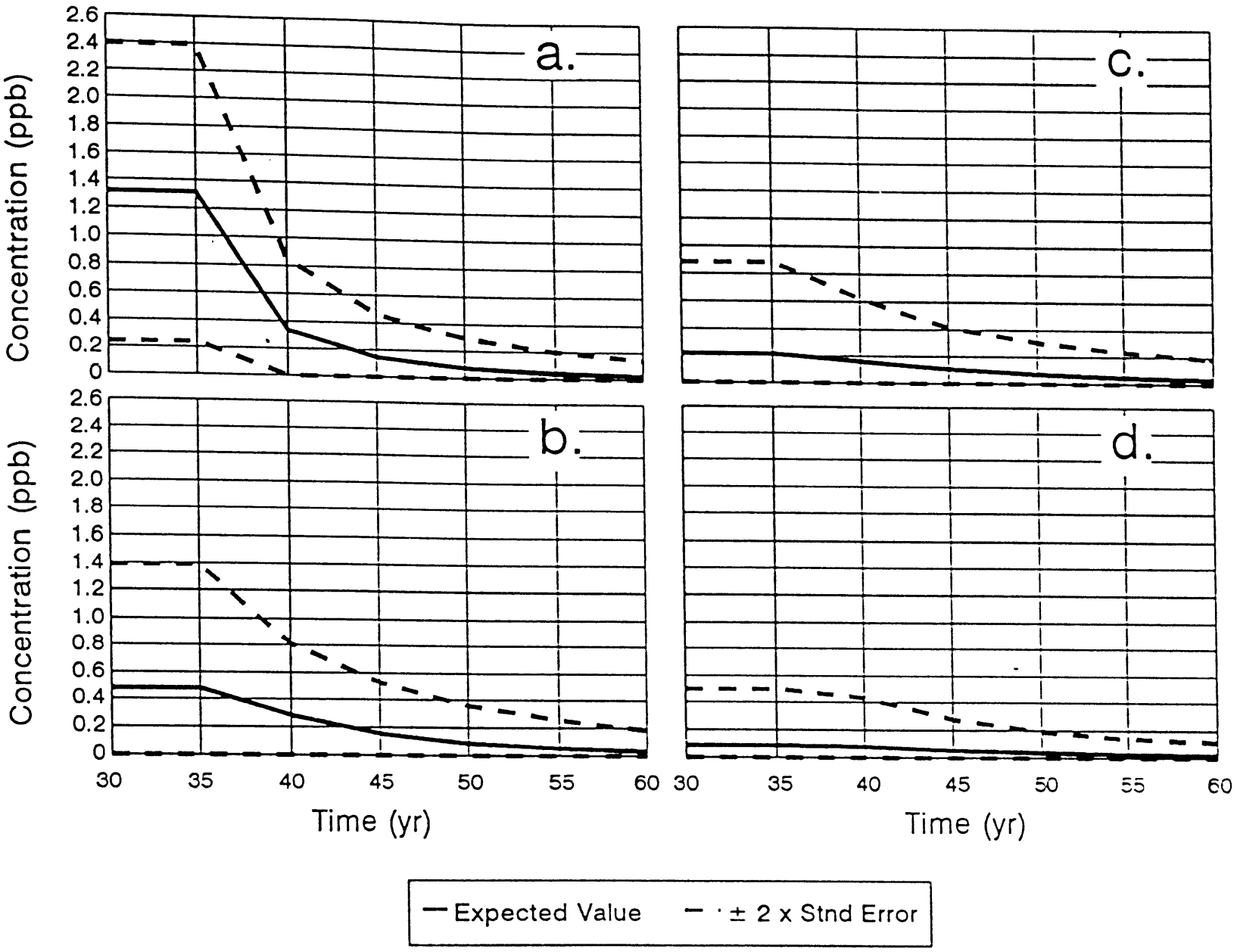

Fig. 45. Expected value and 95% confidence interval for the nonpoint-source scenario simulated concentrations at model cells with the maximum concentrations in model Layers (a) 1, (b) 2, (c) 3 and (d) 4.

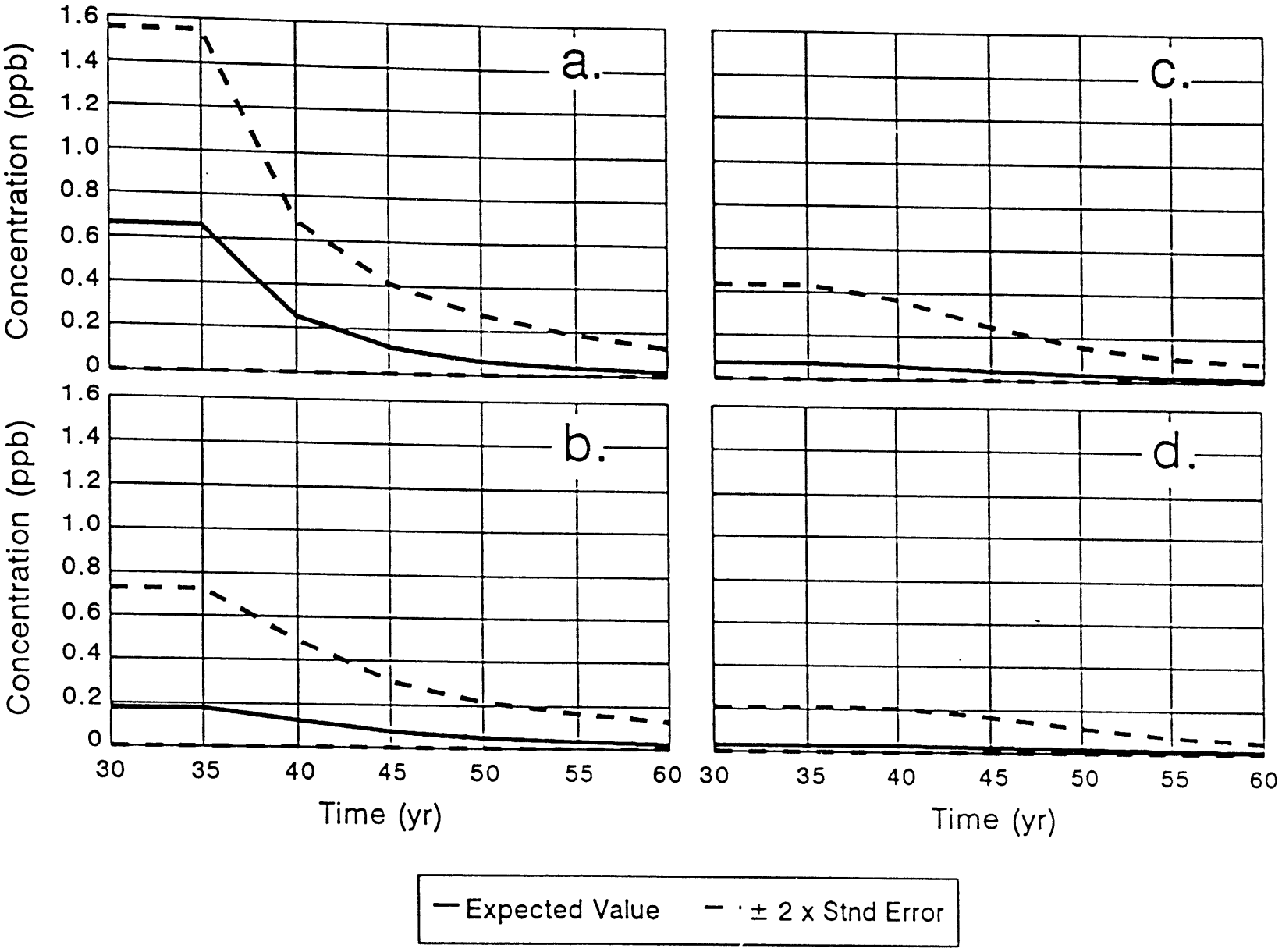

Fig. 46. Expected value and 95% confidence interval for the nonpoint-source scenario simulated concentrations at piezometer nest K7 in model Layers (a) 1, (b) 2, (c) 3 and (d) 4.

concentration of 3.0 ppb.) The large 95% confidence interval for the maximum Layer 1 concentrations at 35 yr covers the majority of the entire range of concentrations. Deeper in the system, however, the uncertainty analyses become more informative. Fig. 46d indicates that > 17.8 m below the water table (Layer 4 and below), concentrations are unlikely to ever exceed 0.5 ppb, no matter how enduring the contamination. The bedrock aquifer is relatively safe from violations of the PAL and ES when the depth to bedrock is > 20 m. The expected Layer 1 maximum concentration falls to < 0.3 ppb in about 6 yr after contaminant input stops, but the 95% confidence interval high concentration falls to < 0.3 ppb only after 15 yr.

The results for the point-source scenario are presented for four private wells (those with the two highest and lowest predicted concentrations) in the monitoring area in Fig. 47. The results indicate that given leaching of atrazine at 8 ppb in a limited area within the ZOCs, concentrations in the wells are unlikely to exceed 2, 0.6, 0.2 and 0.1 ppb at PK1, PR1, PE2 and PE1, respectively (based on the 95% confidence intervals). The expected concentrations are all much lower. At PK1 (Fig. 47a) it takes 15 yr after contamination ceases before the likelihood of exceeding 0.3 ppb becomes very small. At PR1, it takes a little over 5 yr.

Sensitivity Analysis

A benefit of the Gauss-Hermite procedure is that the sensitivity of model predictions to the parameters is easily quantified. The measure of sensitivity applies not to an arbitrary percent change in parameter value, but to the parameter PDF as defined by the 0.042, 0.5 and 0.958 quantile values. Also quantifiable is the interactive effects of any two parameters. In some cases, a single parameter may not have a large impact on model predictions, but its interaction with another parameter can be dramatic. The sensitivity analysis method is fully described in Levy et al. (1993c).

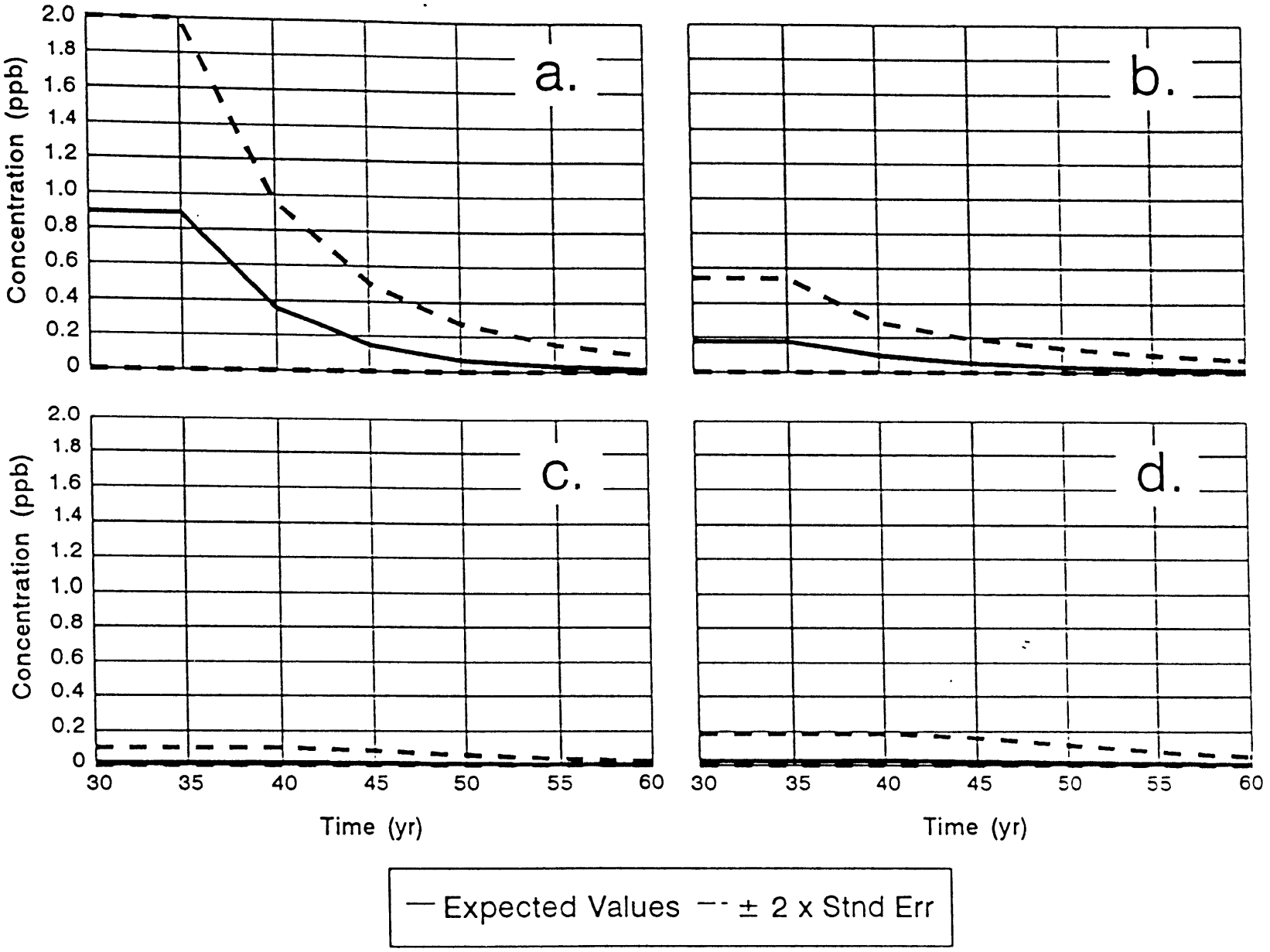

Fig. 47. Expected value and 95% confidence interval for the point-source scenario simulated concentrations at private wells (a) PK1, (b) PR1, (c) PE1 and (d) PE2.

In general, model predictions are most sensitive to sorption coefficient and the sorbed-phase degradation rate. The magnitudes of the sensitivities drop substantially after these parameters. Generally, the parameters with the third and fourth largest main effects are dissolved-phase degradation rate and longitudinal dispersivity. The relative sensitivities depend on what is being predicted. As time increases, sensitivity to sorption coefficients decreases while sensitivity to the degradation rates increases. Sorbed-phase degradation plays a larger role than dissolved-phase because even with small sorption coefficients, the majority of the contaminant is in the sorbed phase. For example, given a dissolved concentration of 1 ppb and the 0.5 quantile values for the Freundlich coefficient and exponent, 89% of the compound would be sorbed. Through the range of K_f- and a-values used in this analysis, the compound in the sorbed phase ranges from 34 to 95% when the dissolved phase concentration is at 1 ppb. At lower concentrations, the percent sorbed increases. Model predictions are insensitive to porosity because it plays a controlling role in both groundwater velocity and contaminant retardation. Both velocity and retardation increase with decreasing porosity. With high sorption rates, the increase in velocity is almost completely cancelled by the increase in retardation. The longitudinal to transverse dispersivity ratio plays a negligible role in the nonpoint source simulations since the contamination input was simulated over a large horizontal area and groundwater movement is predominantly vertical. Likewise, in the point-source scenario, contamination was input directly above the wells in question.

With seven model parameters, there are 21 possible parameter pairs and associated total two-way interactions for every model prediction. The most prominent interactions are those between Freundlich coefficient and the degradation rates, between the sorbed- and dissolved-degradation rates and between Freundlich coefficient and exponent. The relative importance of sorbed- or dissolved-degradation rate depends on how much is sorbed and dissolved, thereby explaining the strong interactions between sorption and degradation. The interaction between degradation rates is because the dissolved-phase degradation rate is only important when the sorbed-phase degradation rate is low. Similarly, when sorption is low,

dispersivity plays a relatively minor role. As with the main effects, the interaction between degradation rates increases with time and depth and decreases with velocity as do most other interactions involving degradation rates. The interaction between sorption coefficients decreases with time and velocity and increases with depth. There were no strong unexpected interactions.

CONCLUSIONS AND REGULATORY IMPLICATIONS

Pesticide-use restrictions in recent rules issued by the Wisconsin Department of Agriculture, Trade and Consumer Protection (WDATCP) are based largely on results of large-scale groundwater quality monitoring surveys. In 1988, WDATCP's Grade A Dairy Farm Well Survey indicated statewide atrazine contamination and, along with subsequent groundwater monitoring, led to the creation of Chapter AG 30 of the Wisconsin Administrative Code. AG 30, which first took effect in time for the 1991 growing season, imposed statewide and area-specific rules including areas of atrazine-use prohibition (APAs) and areas of reduced maximum atrazine application rates (AMAs). They are not determined by such methods as susceptibility mapping or predictive computer modeling, since the surveys could not demonstrate clear associations between atrazine residue concentrations and the environmental variables believed to affect those concentrations. From In models reported here, concentrations of atrazine at specific locations are largely controlled by TTs to those locations. Relationships between average TTs to area private wells and measured atrazine and atrazine metabolite concentrations indicate that groundwater-flow modeling and particle tracking have potential for evaluating relative contamination susceptibility. Particle tracking indicated that TTs to the bedrock surface varied widely across the monitoring area (< 0.25 to > 512 yr) due to spatial variations in depth to bedrock and hydraulic conductivity and gradients. While these factors are often incorporated in susceptibility mapping or computer modeling, the particle tracking also demonstrated that TTs to bedrock were partially controlled by proximity to Sixmile Creek and Waunakee Marsh. While the effect pertained to only a small area,

the relationship points out that there are complex and often subtle hydrogeologic factors controlling groundwater movement and velocity that can easily be overlooked when assessing the susceptibility of an aquifer to contamination. Even without the effects of the surface-water bodies, the range of expected bedrock contaminant concentrations can vary considerably in response to variations of hydraulic conductivity, gradient and depth to bedrock that are of too small a scale to incorporate into a regulatory framework. Continuing to regulate according to groundwater standards violations is the only reasonable alternative.

The chemical transport modeling predicted the range of expected long-term atrazine concentrations at various depths given constant inputs at the water table, thus allowing an assessment of the potential severity of present and future contamination of the bedrock aquifer based on an observed contaminant distribution in the shallow groundwater. The simulations combined the calibrated, steady-state three-dimensional groundwater flow model with estimates of atrazine transport parameter values derived for previous one-dimensional contaminant-transport modeling (Levy and Chesters, 1993). 95% confidence intervals for concentration predictions in shallow groundwater were large but indicated that, given 3.0 ppb entering the system, maximum Layer 1 concentrations are not likely to exceed 2.4 and 1.6 ppb in areas of relatively large and small Horicon till groundwater velocities. Deeper concentrations had smaller confidence intervals that suggested that concentrations at $>$ 8.2 and 17.8 m below the water table are unlikely to exceed 0.9 and 0.5 ppb given the nonpoint-source contaminant case. For the point-source case (based on the highest atrazine concentrations actually detected throughout the study period), the 95% confidence intervals suggest that concentrations in private wells PK1, PR1, PE2 and PE1 are unlikely to exceed 2, 0.6, 0.2 and 0.1 ppb, respectively.

AG 30 is updated annually in response to new groundwater monitoring data and the number and density of atrazine standards violations. Section AG 30.40 of the original 1991 atrazine rule called for a review of the atrazine provisions in 1996 by evaluating the success of AG 30 in attaining and

maintaining compliance with the groundwater standards. Obviously, APAs will eventually reduce atrazine contamination of groundwater. Depending on aquifer characteristics, however, immediate beneficial results are not expected. The contaminant-transport simulations performed here suggest that under similar hydrogeologic conditions, given an atrazine concentration resulting from long-term steady leaching to the water table, it can take 5 to 10 yr after contaminant movement to the water table ceases before the groundwater concentration is reduced by half at relatively shallow depths. For example, it takes > 10 yr before it becomes very unlikely (i.e., outside the 95% confidence interval) for concentrations in Layer 1 will exceed 0.3 ppb. It takes about 15 yr before it becomes very unlikely for concentrations in PK1 to exceed 0.3 ppb. At greater depths, expected concentrations are likely to be less, but dissipation takes longer. The amount of leaching that may occur after atrazine application stops was not accounted for by any analysis or modeling in this study. The "best-case" assumption was always made, i.e., when application stopped, leaching stopped. Some leaching of atrazine residues is likely to occur in AMAs and perhaps APAs, even if at reduced rates. Continued input to the water table will lengthen the time of dissipation to a predetermined benchmark such as the PAL or ES. Large-scale surveys will be an essential component for a critical review of the atrazine rules, but in many pedologic and geologic settings 2 to 4 yr may be insufficient to make an accurate assessment of the long-term effects of altered application rates. Such complications need to be taken into account by regulators and legislators.

The Gauss-Hermite analysis pointed out the great uncertainty inherent in some model predictions. The uncertainty was mostly due to the uncertainty of the sorption coefficient and sorbed-phase degradation rate estimates. Laboratory studies quantifying such transport model parameter values under aquifer conditions are rare. Especially rare are studies differentiating the sorbed-phase from dissolved-phase degradation rates. Such studies are recommended for accurate prediction of pesticide movement and fate. Continued long-term groundwater monitoring is also recommended, especially in AMAs and APAs to

assess atrazine and metabolite dissipation rates and improve the evaluation of the threats they pose to groundwater quality in the future.

REFERENCES

Bouwer, H. and Rice, R.C., 1976. A slug test for determining hydraulic conductivity of unconfined aquifers with completely or partially penetrating wells. Water Resour. Res., 12: 423-428.

Bradbury, K.R. and Rothschild, E.R., 1985. A computerized technique for estimating the hydraulic conductivity of aquifers from specific capacity data. Ground Water, 23: 240-246.

Cline, D.R., 1965. Geology and ground-water resources of Dane County, Wisconsin. Geological Survey Water-Supply Paper 1779-U, United States Government Printing Office. Washington, DC, 64 pp.

Duffield, G.M. and Rumbaugh, J.O. III, 1989. AQTESOLV: aquifer test solver, version 1.00. Geraghty & Miller, Inc., Reston, VA, 135 pp.

Levy, J., 1993. A field and modeling study of atrazine transport and fate in groundwater. Ph.D. Dissertation, University of Wisconsin-Madison, Madison, WI, 561 pp.

Levy, J., Chesters, G., 1993. Simulation of atrazine and desethylated atrazine transport and fate in a sandy-till aquifer, J. Contam. Hydrol. In review.

Levy, J., Chesters, G., Read H.W. and Gustafson, D.P., 1993a. Distribution, sources and fate of atrazine in groundwater: a field study. J. Contam. Hydrol. In review.

Levy, J., Clayton, M.K., Anderson M.P. and Chesters, G., 1993b. Simulation of groundwater flow at a field site in south-central Wisconsin with the use of geostatistical methods for model calibration. Water Resour. Res. In review.

Levy, J., G. Chesters and Clayton M.K., 1993c. Three-dimensional stochastic simulation of atrazine transport and fate in groundwater using an approximation of the three-point Gauss-Hermite quadrature formula. Water Resour. Res. In review.

McDonald, M.G. and Harbaugh, A.W., 1984. A modular three-dimensional finite-difference groundwater flow model. Open-file report 83-875, US Department of the Interior, US Geological Survey, Reston, VA, 528 pp.

Neuman, S.P., 1975. Analysis of pumping test data from anisotropic unconfined aquifers considering delayed gravity response. Water Resour. Res. 11: 329-342.

Ostrom, M.E. Paleozoic stratigraphic nomenclature for Wisconsin. *Info. Circ. No. 8*, Wisconsin Geological and Natural History Survey, Madison, WI., 5 pp.

Rayne, T., 1993. Variability of hydraulic conductivity in a sandy till: the effect of scale and method. Ph.D. Dissertation. University of Wisconsin-Madison, 134 pp.

Press, S.J., 1989. Bayesian statistics: Principles, models and applications. John Wiley, New York, 237 pp.

Raftery, A.E. and Zeh, J.E., 1993. Estimation of bowhead whale, *Balaena mysticetus*, population size. In: Gatsonis, C., Hodges, J., Kass, R. and Singpurwalla, N. (eds) Case Studies in Bayesian Statistics in Science and Technology, Springer-Verlag, Berlin.

Zheng, C., 1990. MT3D: a modular three-dimensional transport model for simulation of advection, dispersion and chemical reactions of contaminants in groundwater systems. S.S. Papadopulos & Associates, Inc., Rockville, MD.

Zheng, C., 1991. PATH3D 3.0 - a ground-water path and travel-time simulator. S.S. Papadopulos & Assoc., Inc., Rockville, MD.